Mechanisms of action and resistance to anti-angiogenic small-molecule tyrosine kinase inhibitors in preclinical breast cancer and pancreatic neuroendocrine tumor mouse models

Inauguraldissertation

zur

Erlangung der Würde eines Doktors der Philosophie

vorgelegt der

Philosophisch-Naturwissenschaftlichen Fakultät

der Universität Basel

von

Ruben Michael Bill

aus Münchenbuchsee, Bern

Basel, 2015

Genehmigt von der Philosophisch-Naturwissenschaftlichen Fakultät
auf Antrag von:

Prof. Dr. Gerhard Christofori
Prof. Dr. Markus Affolter

Basel, den 13. Oktober 2015

Prof. Dr. Jörg Schibler

Dekan

Für Euch meine Töchter, Leona und Lilja

Summary

„Cancer" – this one term is used to name a large spectrum of different syndromes, ranging from the relatively indolent chronic lymphocytic leukemia to highly lethal cancer types such as glioblastoma multiforme with a median survival of about 15 months even when treated with upfront treatment schedules. Based on the notion that tumors critically rely on their own blood supply, targeting the tumor blood vasculature by anti-angiogenic therapeutics has been implemented as an important treatment modality for certain cancer types.

Pancreatic neuroendocrine tumors (PNETs) are rare but represent a deadly disease when detected at a metastatic stage. Importantly, PNETs have proven to respond especially well to the anti-angiogenic compound sunitinib – however, not without a significant amount of side effects. To increase the treatment options for PNET patients, we performed a preclinical evaluation of nintedanib, a small-molecule anti-angiogenic tyrosine kinase inhibitor (TKI), in the Rip1Tag2 PNET mouse model. Our work revealed that nintedanib exerted a strong anti-angiogenic and thus anti-tumor effect translating into improved animal survival. Based on our data we therefore suggest the clinical evaluation of nintedanib as a new treatment modality in PNET patient care.

In contrast, numerous large clinical trials in breast cancer patients treated with compounds targeting tumor angiogenesis only resulted in improved progression-free survival (PFS) at best, without increasing overall survival (OS). This observation suggests the rapid establishment of therapy resistance. We therefore set out to investigate mechanisms of resistance to nintedanib and sunitinib in a murine syngeneic transplantation model of breast cancer. Similar to the clinical observations, targeting tumor angiogenesis in this mouse model resulted in the rapid development of resistance. Interestingly however, tumor re-growth was occurring despite a sustained reduction of the number of tumor blood vessels (*i.e.* microvessel density; MVD) and increased hypoxia. Mechanistically, this tumor re-growth was enabled by the upregulation of glycolysis and the establishment of a metabolic symbiosis between hypoxic and normoxic tumor areas. Interestingly, similar mechanisms might be also responsible for re-growing tumors occasionally observed in nintedanib-treated Rip1Tag2 mice.

Taken together, our data provide a preclinical basis for the evaluation of nintedanib as a new treatment modality for PNET patients. Furthermore, we describe the upregulation of glycolysis as a mechanism how tumor cells can escape the action of anti-angiogenic therapies allowing them to survive and proliferate in a detrimental environment of low oxygen tension, acidic pH and nutrient deprivation.

Table of contents

1   General Introduction

1.1   Systemic cancer therapy

1.1.1   The past[1]

At the end of the 19th and beginning of the 20th century, attempts to cure cancer were based on surgical resection. Before the area of anesthetics, aseptic procedures and antibiotics, these painful procedures were accompanied by high peri- and postoperative mortality. Motivated by local and distant recurrences, surgeons began to increase the amount of tissue being resected. A leading figure in the field of breast surgery at this time was William Stewart Halsted. His eagerness to cure a systemic disease "with the knife" resulted in a technique to surgically treat breast cancer patients, known as radical mastectomy, which involved the resection of bones, muscles and lymph nodes neighboring the affected breast [2]. Despite well-advanced surgical techniques, physicians sooner or later realized that only the resection of small and mobile tumors eventually cured the patients. The rest of the patients, which was a significant fraction, could not be saved even with the most aggressive surgery. The identical caveat was faced when radiotherapy was introduced into anti-cancer treatment strategies. Patients with localized tumors were cured, but not when the cancer had already systemically spread. Willy Meyer, a German surgeon who spent the second part of his career in New York and who developed the technique of radical mastectomy in parallel to Halsted, stated shortly before his death in 1932 that cancer would be a systemic disease [3].

The concept of cancer as a systemic disease is older than maybe anticipated. More than two millennia ago, the Greek philosopher and physician Hippocrates established the theory of the balance of the four humors as being the basis for the state of the individual's health. According to him, and later to Galen, cancer is caused by an excessive abundance of black bile. Since the excess of black bile would be a systemic problem, the simple extirpation of a tumor would therefore not cure the patient, Galen hypothesized [1]. It became apparent that a systemic disease needs a systemic treatment and cancer patients would most likely benefit from an adjuvant systemic treatment – unfortunately none of these substances were yet identified in the first half of the 20th century [1]. Shortly after the Second World War, the first two chemotherapeutic substances were tested in cancer patients. Nitrogen mustard gas injections resulted in transient responses in several malignancies of the hematopoietic system [4, 5]. Ironically, nitrogen mustard gas, used as chemical weapons in both World

---

[1] The subchapter „the past" is primarily based on the book from Siddharta Mukherjee "The Emperor of All Maladies: A Biography of Cancer" [1].

1

Wars and has thus caused untold suffering to soldiers and civilians, represents one of the bases of systemic chemotherapy.

Shortly thereafter, a pathologist named Sidney Farber reported cases of temporary remission in children suffering from childhood leukemia upon treatment with the antifolate 4-aminopteroyl-glutamic acid (aminopterin) [6]. In the following years, the list of chemotherapeutic agents was continuously growing and to date many of these agents or derivatives of them are still in clinical use [1].

The New England
Journal of Medicine

Copyright, 1948, by the Massachusetts Medical Society

| Volume 238 | JUNE 3, 1948 | Number 23 |

TEMPORARY REMISSIONS IN ACUTE LEUKEMIA IN CHILDREN PRODUCED BY FOLIC ACID ANTAGONIST, 4-AMINOPTEROYL-GLUTAMIC ACID (AMINOPTERIN)*

SIDNEY FARBER, M.D.,† LOUIS K. DIAMOND, M.D.,‡ ROBERT D. MERCER, M.D.,§
ROBERT F. SYLVESTER, JR., M.D.,¶ AND JAMES A. WOLFF, M.D.‖

BOSTON

Figure 1. The first successful treatment for childhood leukemia.
In 1948 Sidney Farber reported in The New England Journal of Medicine that some of his patients treated with aminopterin achieved temporary remission (adapted from [6])

1.1.2   Current systemic treatment modalities in oncology

Modern evidence based systemic cancer therapy is complex and as such treatment guidelines are rapidly changing based on the myriad of clinical trials that are continually being published. Different treatment modalities administered via the systemic blood circulation are being combined with each other, are administered prior to (*i.e.* neoadjuvant), shortly after surgery (*i.e.* adjuvant) in a curative intention or are administered to prolong life span and reduce morbidity when there is no reasonable chance of cure (*i.e.* palliative) [7]. What adds additional layers of complexity are the rapidly changing (sub)classification systems by clustering tumors based on gene expression, the mutational landscape or chromosomal aberrations [8, 9]. This refined classification is splitting up tumors from a given organ, which were traditionally mainly classified based on histopathological criteria, into almost distinct cancer entities.

Despite the rapid development of innovative therapeutics, systemic cancer therapy is still heavily based on traditional chemotherapy [7]. Other than that, therapeutic antibodies have improved treatment of certain cancer types. The monoclonal antibody trastuzumab (Herceptin®) against HER2 leads to anti-proliferative effects but also antibody-dependent cytotoxicity against HER2 overexpressing tumor cells [10]. Trastuzumab, together with an antibody against CD20 (rituximab/MabThera®) in CD20$^+$ lymphoma and the anti-angiogenic antibody neutralizing vascular endothelial growth factor (VEGF)-A (bevacizumab/Avastin®) are among the pioneers of this class of drugs [11]. Recently, antibodies were coupled with chemotherapeutic agents, called antibody-drug conjugates, to allow a more specific drug delivery. As an example, an antibody against CD30, which is expressed by Hodgkin lymphoma cells, was coupled to the cytostatic agent monomethyl auristatin E (brentuximab vedotin/Adcetris®) allowing this agent to specifically be delivered to lymphoma cells. Similarly, instead of chemotherapeutics, toxins or radioisotopes can also be linked to antibodies [12].

Antibodies are also the backbone of another relatively new and highly promising strategy to boost the anti-cancer immune response mainly mediated by T cells, *i.e.* the so called "immune checkpoint inhibitors". One unique feature of T cell mediated anti-tumor therapy lies in the tremendous variety of epitopes T cells can recognize. Calculations suggest that every individual possesses a repertoire of T cell receptors (TCR) against as many as 10^9 different epitopes, thereby being sufficiently armed to fight against intratumoral heterogeneity as well as recurring tumors [13]. As an example, the anti-cytotoxic T-lymphocyte-associated protein (CTLA)-4 monoclonal antibody ipilimumab (Yervoy®) significantly improved the survival of melanoma patients with a significant fraction of long-term survivors in phase III trials [14, 15]. CTLA-4 is upregulated by T cells upon activation to control and prevent an overshooting immune response [16]. Therefore, blocking CTLA-4 "releases the break" and increases the T cell activation and subsequent proliferation. More recently, the immune checkpoint regulator PD-1 (on activated T cells) and its ligand PD-L1 (on many cell types including tumor cells) became successful targets for anti-cancer therapy [17-19]. Interestingly, combining antibodies against PD-1 (nivolumab) and CTLA-4 (ipilimumab) further increased the clinical benefit with a manageable safety profile [20, 21].

Besides local radiotherapy, radioactive isotopes are systemically administered for certain indications. In the case of thyroid cancer, adjuvant iodine-131 treatment is used to ablate residual thyroid tissue and microscopic carcinoma lesions [22, 23].

The growth of certain tumor subtypes of breast and prostate cancer critically depend on female and male sex hormones respectively. Breast cancers with ≥1% of cancer cells expressing estrogen receptors benefit from therapeutics interfering with estrogen signaling either via modulating the estrogen receptor such as with tamoxifen or via inhibiting estrogen production by the administration of aromatase inhibitors [7]. Men with prostate cancer, where treatment is indicated (low-risk localized disease can be left with watchful waiting) can benefit from androgen deprivation therapy [24].

Most funding, research and publications are currently related to compounds targeting the cancer kinome [13, 25]. Since the present MD-PhD thesis is mainly based on kinase inhibitors, the following sections are dedicated to this class of cancer therapeutics – with a special emphasis on the anti-angiogenic tyrosine kinase inhibitor nintedanib.

1.1.3   Targeted therapy by targeting the cancer kinome

The human kinome encodes approximately 518 kinases that represent about 1.7% of all protein coding genes [26]. Protein kinases are enzymes able to catalyze the addition of an ATP-derived phosphate to the hydroxy-group of the amino acids serin, threonine and tyrosine. An integral component of the catalytically active kinase domain is the ATP-binding pocket (for a detailed description please see below). Kinases are essential for integrating extracellular and intracellular signals into a wide spectrum of meaningful cellular activities. Several kinases appear as interesting targets for cancer therapy (as well as in non-malignant diseases), since their functions have been shown to be essential for cancer cell survival, proliferation, migration and invasion [27].

Since the first kinase inhibitor imatinib was approved by the Food and Drug Administration (FDA) in 2001 for the treatment of chronic myelogenous leukemia (CML), 27 additional compounds have been added to this list (valid at time of writing, [25]). In addition, a tremendous amount of new inhibitors are in various stages of preclinical and clinical development. Most small-molecule kinase inhibitors inhibit the catalytic function of its target kinase by interfering with the normal function of the ATP-binding pocket. The usually well-conserved kinase domains are characterized by an N-terminal lobe with a β-sheet secondary protein structure and a C-terminal lobe with an α-helical structure flanking a central ATP-binding pocket. The access to the central ATP-binding pocket is controlled by a flexible activation loop containing the conserved amino acid sequence Asp-Phe-Gly (DFG) [25, 28]. To date, most kinase inhibitors act in a reversible manner. ATP-competitive compounds can target the active conformation (type I inhibitors; e.g. sunitinib) or bind to and thus stabilize the inactive conformation of kinases (type II inhibitors; e.g. sorafenib, imatinib). Interestingly,

targeting the inactive conformation facilitates the design of more selective inhibitors, since the inactive conformations of kinases display more structural heterogeneity than kinases in the active conformation [28]. A smaller group of compounds allosterically influences the kinase activity by binding outside of the ATP-binding pocket (*e.g.* CI-1040 inhibiting MEK1 and MEK2). These inhibitors usually display a higher target selectivity compared to ATP-competitive drugs due to their interaction with less conserved residues than are present inside the ATP-binding pocket [27]. Allosteric inhibitors either bind to an allosteric pocket neighboring the ATP-binding pocket (type III inhibitors) or to an allosteric site distant to the ATP-binding pocket (type IV inhibitors) [25].

In addition to reversible inhibitors, compounds are being developed, which irreversibly inhibit their target by forming covalent interactions usually with a cystein residue located in immediate vicinity to the important DFG sequence in the kinase activation loop. This covalent interaction prevents the access of ATP to the ATP-binding pocket [27]. With the exception of a lipid kinase inhibitor (idelalisib), all kinase inhibitors approved by the FDA are protein kinase inhibitors, most act in a reversible manner, their targets mainly belong to the tyrosine kinase group (*i.e.* tyrosine kinase inhibitors; TKI) and most are approved for the treatment of malignant diseases [25]. Notably, there is a certain redundancy regarding the kinases, which are currently targeted. This can be seen by the fact that 18 out of the 27 FDA approved compounds either have BCR-ABL, epidermal growth factor receptor (EGFR) or vascular endothelial growth factor receptors (VEGFRs) as one of their targets (Table 1).

Name	Targets[a]	Approved indications in Switzerland[b]	Key References
Imantinib	BCR-ABL, c-KIT	Ph+ CML; Ph+ ALL; Hypereosinophilia syndrome; atypical MDS/MPS; aggressive systemic mastocytosis;GIST; dermatofibrosarcoma protuberans	[29-31]
Dasatinib	BCR-ABL, SRC	Ph+ CML (first or second-line); Ph+ ALL (second-line)	[32, 33]
Nilotinib	BCR-ABL	Ph+ CML (first or second-line)	[34, 35]
Bosutinib	BCR-ABL, SRC	Ph+ CML (second-line)	[36, 37]
Ponatinib	BCR-ABL	Ph+ CML and Ph+ ALL (with T315I mutation)	[38, 39]
Ruxolitinib	JAK1/2	MPS	[40-43]
Tofacitinib	JAK3	RA	[44, 45]
Gefitinib	EGFR	NSCLC (Adenocarcinoma, *EGFR* activating mutation)	[46, 47]

Name	Targets[a]	Approved indications in Switzerland[b]	Key References
Erlotinib	EGFR	NSCLC (second-line; first-line with activating *EGFR* mutation)	[48-50]
Lapatinib	EGFR, ERBB2, ERBB4	Her2+ BC (after failure to trastuzumab)	[51, 52]
Vandetanib	EGFR, VEGFR1-3, RET	medullary thyroid carcinoma	[53, 54]
Afatinib	EGFR, ERBB2, ERBB3, ERBB4	NSCLC (with activating *EGFR* mutation)	[55, 56]
Sorafenib	VEGFR1-3, B-/C-RAF, p38α, c-KIT, PDGFRβ, FLT3	HCC, RCC, thyroid carcinoma	[57-60]
Sunitinib	PDGFRα/β, VEGFR1-3, c-KIT, FLT3, CSF-1R, RET	GIST, RCC, PNET	[61-64]
Axitinib	VEGFR1-3	RCC	[65, 66]
Regorafenib	VEGFR1-3, TIE2, c-KIT, RET, RAF-1, BRAF, BRAFV66E, PDGFR, FGFR	CRC, GIST	[67-69]
Nintedanib	VEGFR1-3, FGFR1-3, PDGFRα/β, SRC, LCK, LYN, FLT3[c]	IPF[d]	[70-72]
Lenvatinib	VEGFR1-3, FGFR1-4, PDGFRα, RET, c-KIT	thyroid carcinoma[d]	[73, 74]
Pazopanib	VEGFR1-3, PDGFRα/β, c-KIT	RCC, soft tissue sarcoma	[75-77]
Crizotinib	ALK, ROS1, MET	NSCLC (ALK[+])	[78-80]
Ceritinib	ALK	in clinical testing for NSCLC (ALK[+])	[81, 82]
Cabozantinib	MET, VEGFR2, TIE2, FLT3, RET, c-KIT, AXL	unknown status	[83, 84]
Ibrutinib	BTK	mantle cell lymphoma, CLL	[85-87]
Vemurafenib	mut BRAF (V600E/K)	melanoma (V600 mutations)	[88-91]
Dabrafenib	mut BRAF (V600E)	melanoma (V600E mutation)	[92]
Trametinib	MEK1/2	status unknown	[93-95]
Palbociclib	CDK4/6	status unknown	[96, 97]
Idelalisib	PI3K∂	B-CLL, follicular lymphoma	[98-100]

Table 1. The status of FDA approved kinase inhibitors in Switzerland.
FDA approved compounds inhibiting kinases and their current status in Switzerland for the treatment of malignant and non-malignant diseases are shown (valid at time of writing; adapted from [25]).
[a] based on original articles cited in "Key References" and on of the Swiss Drug Reference Book [101]
[b] based on the Swiss Drug Reference Book [101]
[c] see Table 2
[d] orphan drug indication [102]

1.1.4 Nintedanib

Nintedanib is a relatively new small-molecule anti-angiogenic TKI that warrants a more detailed desription since it was an integral part of this thesis. Nintedanib (formerly known as BIBF1120; brand names Ofev® in pneumology and Vargatef® in oncology) was developed and selected by Boehringer Ingelheim GmbH out of a panel of indolinone derivatives synthesized and screened for VEGFR-2 inhibition within the scope of a chemical lead optimization program. This 6-Methoxycarbonyl substituted indolinone was chosen out of a number of similar compounds because of its low-nanomolar inhibition of kinases implicated in angiogenesis (angiokines), *i.e.* VEGFRs 1-3, platelet-derived growth factor receptors (PDGFRs)-α and β as well as fibroblast growth factor receptors (FGFRs) 1-3. Importantly, it lacks significant inhibitory action ($IC_{50} > 10\mu M$) on a panel of other kinases, such as EGFR, HER2, CDKs and IGF1R, and therefore reduces the risk of potential adverse effects caused by off-target effects. In addition to the angiokines, nintedanib inhibits FLT-3 and SRC-family members (SRC, LCK, LYN) [70, 103] (Table 2).

Cell-based assays revealed a half-maximal effective concentration (EC_{50}) for nintedanib of 9nM for VEGF and 290nM for basic FGF (bFGF) stimulated human umbilical vein endothelial cell (HUVEC) proliferation, respectively [103]. It induced apoptosis in a dose-dependent manner, accompanied by a reduction of phosphorylated AKT and MAPK [70]. In addition, probably due to its strong inhibitory effect on PDGFRβ, PDGFB-driven proliferation of bovine retinal pericytes (BRP) and human umbilical artery smooth muscle cells (HUASMC) was inhibited by nintedanib at an EC_{50} of 79 and 69 nM. These data highlight an important feature of nintedanib, *i.e.* its ability to target both endothelial cells and perivascular cells (pericytes, smooth muscle cells). This approach has been suggested to be superior to targeting endothelial cells alone [104]. In contrast, proliferation of several carcinoma cell lines was not inhibited at clinically meaningful concentrations (>3.5-4μM [2] [70]). Evidence for relevant direct anti-tumor cell effects are rare. Most cancer cell lines assessed in *in vitro* proliferation assays apparently did not depend on signals derived from kinases primarily targeted by nintedanib [70]. Notable exceptions were ALL cell lines with *PAX5* translocations that have shown to be critically dependent on survival signals mediated by the SRC-kinase

---

[2] Peak plasma concentrations do not exceed 1μM in mice when being treated with 50mg/kg daily [70, 103].

family member LCK[3] [105]. In addition, the colon carcinoma cell line LS174T displayed an half-maximal inhibitor concentration (IC_{50}) of about 600nM in an *in vitro* MTT cell viability assay [106]. Recently, nintedanib was shown to exert anti-hepatocellular carcinoma (HCC) cell activity *in vitro* and *in vivo* independent of its anti-angiokinase activity but by directly activating SH2 domain-containing phosphatase 1 (SHP-1), which led to a reduction of pSTAT3 and consequently cell death [107].

Kinase	IC_{50} (nmol/L)
VEGFR-1	34
VEGFR-2	21
VEGFR-2 (mouse)	13
VEGFR-3	13
PDGFRα	59
PDGFRβ	65
FGFR-1	69
FGFR-2	37
FGFR-3	108
FGFR-4	610
FLT-3	26
SRC	156
LCK	16
LYN	195
TGFβRI (ALK5)	505

Table 2: *In vitro* kinase inhibitory profile of nintedanib.
The following kinases were inhibited at nintedanib concentrations >1µM: InsR, IGF1R, EGFR, HER2, CDK1, CDK2, CDK4GSK3B, ROCKII, DYRK1A, TGFβRII, PKCA, MAPK2ERK2, HGFR, MSK1, PDK1, CHK1, MAPKAPK2, SAPK2AP38, S6K1, SGK, CK1, CK2, PKA, SAPK2BP38B2, SAPK3P38G, JNK1A1, SAPK4P38D, PHK, PKBA, CSK, CDK2/CYCLINA, PRAK, PP2A (adapted from [70] and Meyer-Schaller *et* al., unpublished data).

Comparing pharmacodynamic and pharmacokinetic studies in cells culture experiments and in mice has pointed towards interesting features of nintedanib. Whereas nintedanib is promptly metabolized by methylester cleavage to the metabolite BIBF1202 and is almost completely cleared from the plasma within 24 hours (single *per os* treatment with 50mg/kg), target inhibition can be detected for at least 32 hours [70, 108]. Since co-crystal structure analysis suggested that nintedanib reversibly binds the ATP-binding pocket, the sustained target inhibition is most likely mediated by the metabolite BIBF1202 that inhibits VEGFR-2 phosphorylation in the low-nanomolar range [70].

---

[3] The SRC-kinase family member LCK represents a low-nanomolar target of nintedanib (Table 2; [70]).

In vivo preclinical studies aiming to determine the antitumor activity of nintedanib to date have mainly been based on xenograft transplantation assays of human cancer cell lines into heterotopic subcutaneous sites of immunodeficient mice. Tumor growth reduction was observed by nintedanib monotherapy in the following subcuatenous xenograft carcinoma models: FaDu (head and neck squamous cell), Caki-1 (renal cell), HT-29 (colon), SKOV-3 (ovarian), PAC-120 (prostate); A549, Calu-6, H1993 (lung); HepG2 (hepatoblastoma), PLC5 (HCC) and AsPC-1 (pancreatic) [70, 106, 107, 109, 110]. In addition, significant growth reduction achieved by nintedanib monotherapy was shown in orthotopic xenograft models with the pancreatic adenocarcinoma cell lines HPAF-II, MIA PaCa-2 and AsPC-1 [111]. Interstingly, despite a marked increase in hypoxia in the A549 xenograft model of lung cancer, nintedanib treatment did not induce an epithelial to mesenchymal transition (EMT). In contrast, the epithelial adherens junction protein E-cadherin was upregulated and the mesenchymal marker vimentin showed a trend towards lower expression in nintedanib-treated tumors [111]. In line with this finding, the Thiery laboratory reported upregulation of E-cadherin expression when the mesenchymal human ovarian cancer cell line SKOV3 was treated with nintedanib *in vitro*, albeit in micromolar concentrations [112]. Future work will have to elucidate if nintedanib's promotion of an epithelial phenotype can be attributed to inhibition of FGFRs and PDGFRs, both of which are primary targets of nintedanib and previously implicated in EMT [113, 114]. Alternatively, this could also be due to inhibition of yet unknown targets of nintedanib. Unpublished data in our laboratory derived from an *in vitro* kinase assay suggest that nintedanib inhibits TGFβRI (ALK5) with an IC_{50} of 505nM (Meyer-Schaller *et* al., unpublished results). This finding is partially supported by cellular assays showing inhibitory effects of nintedanib on TGFβ signaling – although in the micromolar range [115]. Therefore, it has yet to be elucidated, whether inhibition of TGFβRI can be achieved by clinically relevant concentrations of nintedanib.

Based on phase I clinical trials, the recommended nintedanib dose for subsequent phase II clinical trials for cancer patients was set to 200mg twice daily *per os (p.o.)*, both for monotherapy and for combined schedules with the chemotherapeutic agents paclitaxel plus carboplatin, docetaxel or pemetrexed [116-119]. Importantly, the combination of nintedanib with chemotherapeutic agents was well tolerated and the chemotherapeutics could be administered at standard doses. In one study, nintedanib 150mg twice daily in combination with paclitaxel for the treatment of HER2-negative breast cancer was recommended [120]. The main dose-limiting side effect was the reversible elevation of liver enzymes. Other than that, nausea, vomiting and diarrhea were frequently observed. Interestingly though, nintedanib only rarely caused hypertension and skin abnormalities, both of which are two "classical" side effects of other anti-angiogenic compounds [119]. The etablished anti-

angiogenic TKIs sunitinib and sorafenib in general lead to increased toxicity when co-administered with chemotherapeutic agents resulting in the requirement of sub-standard dosing. In contrast, nintedanib seems to contain superior features, as it can be combined with chemotherapy at standard dosing [120-122]. In pharmacokinetic studies, nintedanib reached steady-state plasma levels after 8 days of twice daily administration. Peak plasma concentrations reached 67.6ng/ml (≈104nM), levels that should be sufficient to inhibit their primary targeted angiokine receptors ([70, 123] Table 2). Subsequent phase II clinical trials were conducted in different solid tumor types with nintedanib as monotherapy. A randomized, double-blind, placebo-controlled phase II clinical trial for recurrent ovarian cancer with nintedanib monotherapy directly adjoining a line of chemotherapy with the aim to prolong the time until progression, showed encouraging responses in a subgroup of patients [124]. Strikingly, one patient was treated with nintedanib maintenance therapy for more than 4.5 years and was disease free at the time her case was published [125]. In late stage non-small cell lung cancer (NSCLC), nintedanib monotherapy led to tumor stabilization in 46% of the patients [126]. In contrast to the trials in ovarian and lung cancer, nintedanib monotherapy in patients with recurrent high-grade glioma, persistent or recurrent endometrial cancer and castration-resistant prostate cancer did not lead to a relevant response [127-130]. The encouraging activity of nintedanib in ovarian cancer and NSCLC led to subsequent phase III clinical trials. AGO-OVAR 12/LUME-OVAR 1 investigates the addition of nintedanib to a carboplatin and paclitaxel combination regimen and results will be available soon [131].

In advanced NSCLC that recurred after a first line of platinum-based chemotherapy, nintedanib plus docetaxel versus docetaxel alone (LUME-Lung 1) significantly improved progression-free survival (PFS), whereas overall survival (OS) was only increased in NSCLC with adenocarcinoma histology [71]. In a second phase III clinical trial investigating the addition of nintedanib to pemetrexed *versus* pemetrexed alone in advanced NSCLC (LUME-Lung 2) was stopped prematurely, because it appeared unlikely that the primary endpoint (PFS) could be met. However, despite the premature conclusion of the study, the following analyses showed that PFS was significantly increased by the addition of nintedanib [132].

Of note, nintedanib monotherapy displayed an encouraging result in a phase II clinical trial for the treatment of idiopathic pulmonary fibrosis (IPF), which was recently confirmed by a double blind, randomized, controlled phase III clinical trial [72, 133].

Taken together, nintedanib has shown promising results as monotherapy in early clinical trials in certain tumor types. In addition, the co-treatment with classical chemotherapy did not increase adverse events. Currently, nintedanib is approved by the FDA for IPF and in the European Union for the treatment of advanced NSCLC with adenocarcinoma histology

after first-line chemotherapy [134]. In the future, it will be interesting to see how nintedanib performs in cancer types that have been shown to be especially sensitive to anti-angiogenic therapies, such as pancreatic neuroendocrine tumors (PNETs), renal cell carcinoma (RCC) or HCC [59, 63, 64].

1.1.5 *Excursus*: A global perspective on cancer therapy

A PhD thesis built around the preclinical validation of new compounds for targeted anti-cancer therapy, which upon potential approval by regulatory authorities will cost a certain amount of money, cannot stand without some brief thoughts about the global economic impact and accessibility of medical interventions to prevent and to treat cancer.

Since the first clinical trials with the chemotherapeutic agents nitrogen mustard and antifolate over half a decade ago, the field of medical oncology has tremendously developed [1]. Much has been learned about the etiologies, molecular characteristics, intertumoral heterogeneity (cancer subtypes) and resistance mechanisms to conventional chemotherapeutic agents and newer targeted kinase inhibitors. The end of the tunnel in changing cancer from a deadly into a chronic or even curable disease might be in sight, one might think. This might be true for some cancers, as in the case of CML with the discovery of imatinib and second and third line treatments (dasatinib, nilotinib, bosutinib, ponatinib), which greatly increase the survival of CML patients [31, 33, 34, 36, 38]. It seems therefore contra-intuitive, when Dr. Franco Cavalli, a Swiss politician, medical oncologist and former president of the Union for International Cancer Control (UICC) stated: „Current strategies to control cancer are demonstrably not working" [135]. What he addressed with this statement was the increase of 40% of people dying of cancer worldwide since 1990 [135, 136]. Most of this increase takes place in low- and middle income countries because of three reasons: Economic development is paralleled by adaptation to western lifestyle with exaggerated calorie intake resulting in obesity, which is a well established risk factor for breast, prostate and colorectal cancer [137]. Secondly, the incidence of cancer types remain high that would potentially be preventable by screening or immunization: Papanicolau smear to detect cervical dysplasia; hepatitis B virus immunization eradicating one etiologic agent of hepatocellular carcinoma or immunization against human papillomavirus most likely preventing cervical, penile and anal carcinoma – to name just a few [135, 138]. Third, patients in low-income countries have a higher risk to die once diagnosed with cancer compared to western countries. One reason is the reduced access to effective treatments. In addition, inadequate access to diagnostics when first symptoms are present delays a proper diagnosis. Therefore, cancer patients in low-income countries often present with further advanced tumors than in high-income countries [136, 138].

What are the strategies advocated by the experts? The primary problem is obviously limited resources in developing countries. Since this will most likely not substantially change within a reasonable time frame, the primary aim has to be the usage of the existing resources as effectively as possible. Primary prevention (*i.e.* prevent a disease before it occurs) and secondary prevention (*e.g.* screening programs) have to be directed to the right population and have to be as cost-effective and targeted as possible. To our knowledge, many cancers are not preventable, neither in low-income countries nor with the most sophisticated screening techniques and expensive primary prevention campaigns of the western world. However, early detection of symptomatic cancers followed by appropriate treatments was mainly responsible for the reduction in cancer mortality in high-income countries. This approach can be translated to developing countries in the sense that health care professionals should receive better training in order to recognize cancer related symptoms earlier. This would facilitate diagnosis of tumors in early and possibly still curable stages. When it comes to treatment, it has been suggested that simple treatments with inexpensive chemotherapeutics would still be better than no treatment [138].

Inaccessibility to cancer therapeutics is simply an obstacle in low- and maybe also middle-income countries - one could erroneously assume. Recent reports about drug shortage in the United States showed that even conventional chemotherapeutics can become limited in high-income countries. Essential generic chemotherapeutic agents such as cisplatin, etoposide or doxorubicin were repeatedly in short supply in the United States in 2011 and before. Various reasons were responsible, including that after expiring of patents, pharmaceutical companies lose large parts of their financial incentive to continue producing these drugs because generic drugs contain smaller margins than patented drugs [139]. Probably influenced by the public awareness for the shortage of generic drugs, the "Preserving Access to Life Saving Medications Act" was implemented in the United States in 2011. The consequence of this new act was that pharmaceutical companies have to inform the FDA if a prescription drug is going to be in short supply [140]. However, the problem of essential chemotherapeutic drug shortage still remains [139, 141]. The result of this shortage - also in Switzerland - is that generic chemotherapeutics are substituted with newer brand-name drugs which are equally effective, but much more expensive. For example, the widely used chemotherapeutic agent doxorubicin can be replaced by liposomal doxorubicin that is 48.2 times more expensive and paclitaxel can be replaced by abraxane (protein-bound paclitaxel) which is 18.7 times more expensive [142, 143].

One day, molecular medicine might be able to provide curative solutions to most cancer patients. For the majority of the world's population this does not help at all, since

people living in low-income countries do often not even benefit from simple screening and treatment regimens, simply because they do not have access or cannot afford it. In high-income countries, the development of extremely expensive new compounds (mostly more than $5000 per month [144]), which are more and more being combined with each other, will sooner or later result in a financial burden, which cannot be covered by the general public anymore. It is extrapolated that direct annual costs in the United States for cancer patient care will rise from $104 billion to $173 billion between 2006 and 2020 [145]. On this way, if researchers and health care professionals stay away from discussions regarding health policies and leave it to people influenced by parties allowed to gain financial benefit from the diseases of other people, this curative solutions will only be available for those who can afford it, even in Switzerland as one of the richest countries in the world.

1.2 Tumor angiogenesis

1.2.1 Important ligand-receptor systems in angiogenesis

Physiological and pathological angiogenesis are highly complex processes orchestrated by a variety of pro- and anti-angiogenic factors. In the following section, I will provide a brief overview over the characteristics of the VEGF/VEGFR, PDGF/PDGFR and FGF/FGFR family members. With differing selectivity, the receptors of these families represent the main anti-angiogenic targets of nintedanib and related anti-angiogenic TKIs such as sunitinib and sorafenib [60, 62, 103].

VEGFs and their receptors

The VEGF family in mammals consists of VEGF-A, -B, -C, -D and placental growth factor (PlGF) [146]. Furthermore, the family is extended by the Orf virus-encoded VEGF-E, which exclusively acts via binding to VEGFR-2 [147]. In addition, the venom of a snake living in Southeast Asia, *Trimeresurus flavoviridis,* contains a VEGF-like protein (*Tf*svVEGF) that mainly induces vascular permeability [148].

VEGF-A is considered to be the predominant angiogenic molecule of the VEGF family. Remarkably, both *VEGFA* alleles are required during embryonic development, as mice deficient for even only one allele of *VEGFA* die *in utero*[4] [149, 150]. Several isoforms with the length of 121 to 206 amino acids are encoded by the *VEGFA* gene and are the products of

---

[4] The phenomenon when the deletion of one allele is enough to lead to a phenotype differing from the wild-type situation is called „haploinsufficiency".

alternative splicing. VEGF-A$_{121}$, VEGF-A$_{165}$ and VEGF-A$_{189}$ are the most abundant isoforms[5]. In general, the length of the VEGF-A isoform correlates with its the ability to bind to heparan sulfate proteoglycans (HSPG). Consequently, VEGF-A$_{165}$ can be found soluble and HSPG-bound, whereas VEGF-A$_{121}$ is freely diffusible [151]. VEGF-A binds to the tyrosine kinase receptors VEGFR-1 (VEGFR-1/FLT-1) and VEGFR-2 (FLK-1/KDR), representing two of the three VEGFRs. Since VEGFR-1 has a higher binding affinity to VEGF-A, but lower signaling capabilities than VEGFR-2, and a soluble VEGFR-1 isoform acts as VEGF-A-trap, VEGFR-1 is considered to be a negative regulator of VEGF-A signaling in certain situations [146, 152].

VEGF-B and PlGF solely bind to VEGFR-1 and NRP-1. VEGF-B exerts important physiological functions in the heart and in other metabolically active tissues such as skeletal muscle and adipose tissue [153]. A role for VEGF-B in regulating fatty acid transport into endothelial cells has been shown [154]. PlGF displays highest expression in the placenta. VEGF-B and PlGF-deficient mice develop normally [153]. Mainly VEGF-C, but also VEGF-D promote lymphangiogenesis via signaling through VEGFR-3. Upon proteolytic processing, VEGF-C and D are capable of binding to VEGFR-2 as well. Interestingly, during embryogenesis and tumor angiogenesis, VEGFR-3 can also be found on blood vessel endothelial cells [155]. The neuropilins (NRP)-1 and 2 act as co-receptors for several VEGF family members, which bind with isoform-specific affinities [156]

---
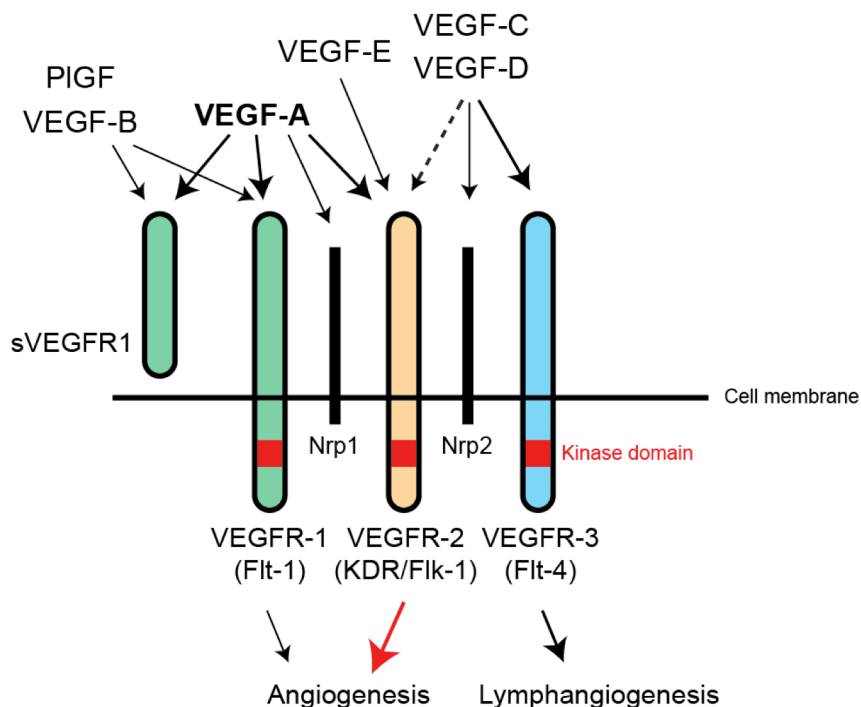
[5] The indicated isoform lengths apply to human VEGF-A isoforms as the lenght of the isoforms slightly vary among species

Figure 2. VEGF family members and their receptors.
VEGF-A represents a central driver of physiological and pathological angiogenesis. Its pro-angiogenic signals are mainly transduced via VEGFR-2, as VEGFR-2 contains higher kinase activity compared to VEGFR-1. Soluble VEGFR-1 (sVEGFR-1) exerts anti-angiogenic activity by sequestering its ligands PlGF, VEGF-B and VEGF-A. VEGF-C and D primarily stimulate lymphangiogenesis through VEGFR-3. The VEGF co-receptors Nrp-1 and 2 increase the binding between VEGFs and VEGFRs and thus stimulate VEGFR signaling (for further details see main text; modified from [157]).

PDGFs and PDGF receptors

Four genes encode the PDGF family members. Their products form five biologically active homo- or heterodimers (PDGF-AA, PDGF-AB, PDGF-BB, PDGF-CC, PDGF-DD)[6]. Two genes are encoding the two subunits of the PDGF tyrosine kinase receptors (PDGFRα and PDGFRβ). The assembly to homo- or heterodimeric receptors (PDGFR$\alpha\alpha$, PDGFR$\alpha\beta$ or PDGFR$\beta\beta$) is determined by the affinity of each of the subunits present in the ligand. Notably, the PDGF-B subunit contains high affinity for both receptor subunits; hence PDGF-BB can bind and activate all three receptor dimers [158].

PDGFs act on several mesenchymal cells such as fibroblasts. However regarding angiogenesis, their action on pericytes is of predominant interest. Mice deficient for *Pdgfb* die perinatally due to the impaired ability to recruit pericytes resulting in microaneurysms, hemorrhages and edema [159]. A similar phenotype has already earlier been observed in mice deficient for *Pdgfrb* [160]. The general view is that endothelial cells recruit PDGFRβ-expressing pericyte progenitor cells by producing PDGF-B in order to stabilize newly formed blood vessels with a tight pericyte coverage [161].

FGFs and FGF receptors

Of the 22 genes encoding FGF ligands, *FGF1* (acidic FGF, aFGF) and *FGF2* (basic FGF, bFGF) are thought to play a predominant role in angiogenesis [162]. In contrast to the tremendous number of FGF ligands, only 4 genes encoding FGF receptors are described (*FGFR 1-4*). Importantly however, *FGFR 1-3* undergo extensive alternative splicing resulting in a panel of isoforms with differing specificity to FGF ligands. Endothelial cells have been reported to mainly express FGFR-1, rarely also FGFR-2, but lack the expression of FGFR-3 and FGFR-4 [163]. Interestingly, a synergistic action of FGF-2 and VEGF-A has been observed [164, 165].

---

[6] For the sake of simplicity, homodimeric ligands and receptors are described by PDGF-B instead of PDGF-BB for instance. However, the heterodimeric PDGF is written as PDGF-AB.

1.2.2 Historical overview

Before the field of research on tumor angiogenesis was founded in the 1970's and in the following decades heavily influenced by the Bostonian surgeon Judah Folkman, the research community was well aware that tumors contain blood vessels. However, the general assumption was that these blood vessels are a bystander effect caused by some non-specific inflammation [166]. In his seminal review published in The New England Journal of Medicine in 1971, Judah Folkman proposed that tumor cells and endothelial cells "constitute a highly integrated ecosystem" where the "mitotic index of the two cell populations may depend on each other" [167]. In this review, he further discussed recent results of his laboratory and proposed ideas which are largely still valid today: 1) tumors have to acquire new blood vessels in order to grow beyond the size of 2 to 3 mm (*i.e.* the angiogenic switch); 2) tumor cells do so by secreting (a) diffusible factor(s) which stimulate endothelial cells to form new capillaries; 3) they identified and purified a factor from tumors (*i.e.* tumor angiogenesis factor, TAF) that is able to stimulate endothelial cell proliferation *in vitro* and *in vivo* without the evidence of accompanying inflammation; 4) anti-angiogenesis as a new anti-tumor strategy to (i) prevent the outgrowth of yet unvascularized tumors, (ii) antibodies could be used to neutralize circulating pro-angiogenic factors such as TAF, (iii) anti-angiogenesis could synergize with cellular anti-tumor immunity; 5) the dependence of a certain tumor type on angiogenesis based on its capillary density could be used to stratify patients prior to anti-angiogenesis therapy [167].

The first pro-angiogenic molecule to be purified and sequenced, bFGF, was already described in 1976 by Gospodarowicz and colleagues as a survival factor and mitogen for endothelial cells [168]. It was subsequently purified in 1984 by the Folkman laboratory followed by its sequencing 1985 by Esch et al. [169, 170]. In 1983, Donald Senger and Harold Dvorak identified and purified a factor from tumor ascites of laboratory animals, which induced permeability of vessels without causing damage to endothelial cells (vascular permeability factor; VPF). Remarkably, a part of this publication described how an antibody against VPF was able to abrogate its permeability inducing action [171]. Subsequent research identified VPF as being identical to VEGF-A [172]. It was first sequenced in 1989 in the Ferrara and Connolly laboratories and shortly thereafter by the Folkman laboratory as well [173-175]. In the following years, more pro-angiogenic, but also endogenous anti-angiogenic factors, such as endostatin, thrombospondin-1 and angiostatin, have been identified and characterized [176].

1.2.3 Mechanisms of tumor angiogenesis

Blood vessels provide tumor cells with oxygen and nutrients necessary for their proliferation and facilitate the removal of accumulating waste products. Tumors hijack programs that normally drive blood vessel formation under a variety of physiological conditions, *e.g.* embryonic development, wound healing, remodeling of the endometrium during the menstruation cycle, and placental growth during a pregnancy [177, 178]. Several mechanisms have been described to be involved in the vascularization of tumors (Figure 3) [179, 180]. The term angiogenesis refers to the formation of new vessels based on existing vessels and involves sprouting and non-sprouting angiogenesis (intussusception) [181].

Sprouting angiogenesis

Sprouting angiogenesis represents most likely the prototypical mode how tumors acquire new blood vessels. Tumor cells residing in regions of insufficient oxygenation orchestrate a hypoxia program, which is built around the stabilization of the transcription factors hypoxia-inducible factor (HIF)-1 and 2. HIF-1, a dimer consisting of HIF-1α and HIF-1β, stimulates the expression of a plethora of genes including angiogenic factors such as VEGF-A and various enzymes implicated in glycolysis. HIF-2 is formed by the dimerization of HIF-2α with HIF-1β and shares a number of target genes with HIF-1 such as VEGF-A, but not glycolysis enzymes [182]. VEGF-A, signaling via VEGFR-2 expressed by endothelial cells, is an important first trigger leading to endothelial cell activation of previously quiescent mature blood vessels. This includes the acquisition of migratory, invasive and proliferative endothelial cell-phenotypes and increased permeability of the endothelial layer [183]. In order to enable sprouting from existing blood vessels, the basement membrane (BM) lining the vessel wall and the underlining extracellular matrix (ECM) has to be degraded. This degradation is mainly mediated by increased abundance of proteases of the matrix metalloproteinase family (*e.g.* secreted MMP-2 and MMP-9, membrane-type MT1-MMP/MMP-14), which are secreted by endothelial cells, tumor cells and other cells of the tumor microenvironment. Increased protease activity is also achieved by the downregulation of protease inhibitors [184-186]. Besides BM and ECM degradation providing physical space for endothelial sprouts, MMPs contain two additional angiogenesis modulating properties. Namely, the release of ECM- bound growth factors, such as bFGF or VEGF and the activation of latent transforming growth factor (TGF)-β, and the generation of endogenous angiogenesis inhibitors such as endostatin and angiostatin, representing cleavage products of the ECM components collagen XVIII and plasminogen, respectively [186]. As an example, the growth factor-releasing property of MMP-9 is responsible for the angiogenic switch in the Rip1Tag2 transgenic mouse model of neuroendocrine carcinoma of the pancreas (see below) by liberating ECM-bound VEGF-A, whereas VEGF-A expression is not differentially

regulated during the stepwise Rip1Tag2 tumorigenesis [184, 187]. Importantly, angiogenesis initiation seems to be less dependent on the expression levels of one single pro- or anti-angiogenic factor but rather on the net balance between the sums of pro- and anti-angiogenic factors [188].

Growing vascular sprouts are characterized by leading tip cells and a following cord of stalk cells. Tip cells are thought to mainly migrate and invade without substantial proliferation, whereas stalk cells represent the pool of proliferating cells. Tip *versus* stalk cell specification is mainly based on Notch signaling regulating VEGFR-2 expression: Delta-like ligand 4 (DLL4) expression is stimulated by VEGF-A in tip cells and reduces VEGFR-2 levels on neighboring stalk cells via its receptor NOTCH1, thus resulting in differential responses to VEGF-A gradients [189, 190]. In addition, a role of VEGFR-3 in sprouting angiogenesis has been demonstrated as tumor blood vessels express VEGFR-3 in addition to VEGFR-2 on filopodia of tip cells [191, 192]. Recently, the Augustin laboratory has proposed a role for angiopoietin-2 (ANG-2) in stimulating migration of TIE-2-low tip cells by binding to and signaling via integrins (classically, ANG-2 is a context dependent antagonist of the receptor TIE-2) [193]. In order to form mature vessels lined by the so-called phalanx cells, vascular sprouts have to fuse, form a lumen and to differentiate into a quiescent monolayer which is paralleled and influenced by the acquisition of a tight pericyte coverage at the abluminal surface [161, 194, 195]. Pericyte coverage is induced by endothelial cells, which express PDGF-B and thereby attract PDGFRβ-expressing pericytes. Attracted pericytes in turn promote growth arrest of endothelial cells and their differentiation into a quiescent state [196]. In addition to PDGF-B/PDGFRβ signaling, TGFβ, NOTCH, S1P and ANG/TIE-2 are part of the paracrine and juxtacrine crosstalk between endothelial cells and pericytes [161].

The aforementioned stepwise model of sprouting angiogenesis resulting in mature and perfused vessels with tight perivascular coverage mainly takes place during physiological angiogenesis. During tumor angiogenesis, similar pathways might be employed, however in a much more disorganized manner. Tumor blood vasculature is characterized by overshooting angiogenesis resulting in immature and leaky vessels with a significant fraction of non-perfused (non-patent) vessels [197, 198]. A more detailed description of the features of the abnormal tumor vasculature will be provided when discussing the concept of vessel normalization.
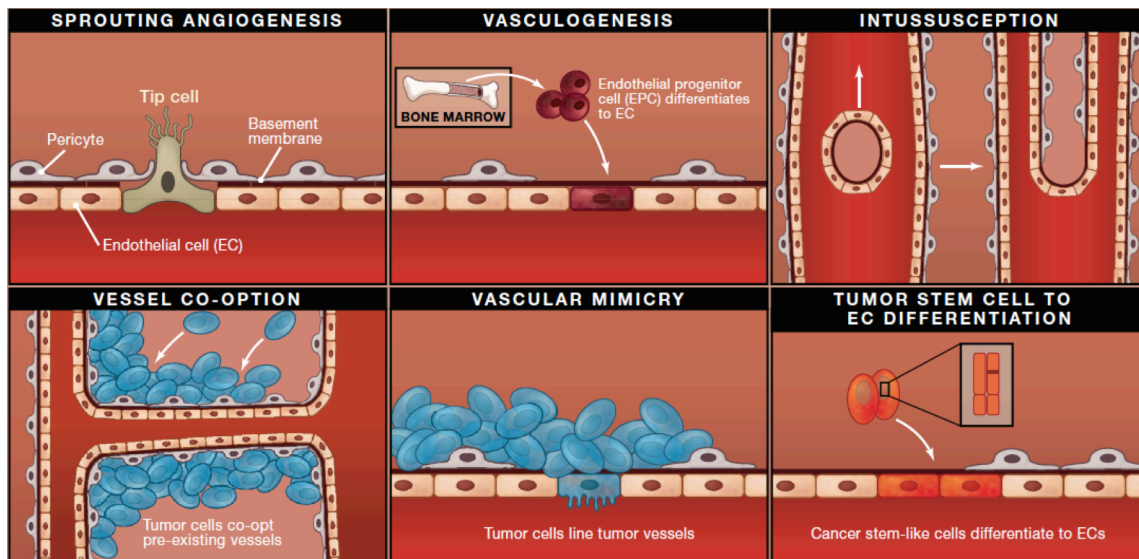
Figure 3. The different mechanisms of tumor angiogenesis.
Tumors ensure their supply with essential factors delivered by the systemic circulation via several mechanisms: angiogenesis by sprouting, vasculogenesis by bone marrow-derived cells, intussusception (non-sprouting angiogenesis), vessel co-option, vascular/vasculogenic mimicry or tumor stem cell to endothelial cell differentiation (Figure adapted from [179]).

Vasculogenesis

Vasculogenesis, i.e. the *de novo* formation of vessels, is a well established process during embryogenesis leading to the first blood vessels in the embryo and the primary vascular plexus in the yolk sac [199]. Postnatal vasculogenesis has long thought to be absent. However, newer but controversial data suggest its contribution to the vascularization of tumors [181, 200]. Besides the pool of mature circulating endothelial cells (CEC), which are thought to be scaled off from existing blood vessels, a rare bone marrow-derived cell population, termed endothelial progenitor cells (EPC), circulates in the peripheral blood. EPCs can differentiate into mature endothelial cells and incorporate into the endothelial monolayer of blood vessels (*i.e.* vasculogenesis) [201]. The marker expression of EPCs is however not yet clearly defined. Immature EPCs seem to commonly express CD133, CD34 and VEGFR-2, and the more they undergo differentiation, the more lineage-specific markers, such as CD31, CD146 and VE-cadherin, are expressed [201]. Nolan and colleagues have elegantly demonstrated that bone marrow-derived EPCs incorporate into the endothelium of sprouting neovessels preferentially in early phases of tumor angiogenesis by employing fluorescent tracing [202]. This and other reports, including the observation that EPC homing to tumors peaks after the administration of vascular disrupting agents [203], suggests to what extent vasculogenesis is implicated in the formation of the tumor vasculature is context dependent [203-207].

It is noteworthy that work in our laboratory has failed to indentify the incorporation of bone marrow-derived cells into the endothelial layer of tumor blood vessels in the Rip1Tag2 transgenic mouse model. In contrast, bone marrow-derived cells from the myeloid lineage were found to incorporate into peritumoral lymphatic vessels and to express *bona fide* lymphatic endothelial cell markers such as LYVE-1 [208].

Instussusception

Intussusception (non-sprouting or splitting angiogenesis) is described as the mechanism by which new microvessels are formed by the insertion of transcapillary pillars into existing vessels and subsequent division into two "daughter vessels". This phenomenon was first described by the Bernese anatomy professor Peter Burri [209-211]. Discovered in lung development, subsequent work has shown the occurrence of intussusceptive microvascular growth (IMG) of capillaries, small arteries and veins in other organs such as the kidney [212, 213]. The mechanisms inducing and regulating intussusception are not well understood. Increased blood flow and blood pressure, VEGF-A overexpression and direct actions of erythropoietin have been suggested to induce IMG in non-malignant experimental models [212, 214, 215]. Importantly, IMG has been observed in several mouse models of cancer, including the transgenic breast cancer model driven by the *NeuT* oncogene and in human melanoma tissues [213, 216, 217]. Interestingly, IMG could represent a mechanism of how tumors induce revascularization and thus escape anti-angiogenic therapy by switching from sprouting angiogenesis to IMG [218].

Vessel co-option

Vessel co-option means the (ab)use of pre-existing host vessels. Vessel co-option represents a possibility how tumors, when occurring in well vascularized tissues, can start proliferating in a very early stage, even before the angiogenic switch occurs. Since by definition co-opted vessels do not multiply, initial tumor cell proliferation will only lead to tumor expansion until the diffusion distance for oxygen becomes limiting – unless the angiogenic switch occurs (Holash, Science99). Vessel co-option also seems to be important for metastatic colonization in lung and brain [219, 220].

Vasculogenic mimicry

Vasculogenic mimicry defines the process when tumor cells line the vascular lumen replacing endothelial cells, but without transdifferentiation into endothelial cells. First reported in 1999 in uveal melanoma by the Hendrix laboratory, the significance and even the existence of vasculogenic mimicry was immediately doubted [221, 222]. In the meanwhile,

numerous publications demonstrated vasculogenic mimicry in other solid cancer types and its presence was often correlated to poor prognosis [223, 224]. In a recent study by Wagenblast and colleagues, the potential of vasculogenic mimicry was greatest in 4T1 murine breast cancer cell line subpopulations with the highest capacity to form distant metastasis. Mechanistically, the two endogenous anticoagulants SERPINE2 and SLPI enabled vasculogenic mimicry and thereby brought cancer cells into a optimal position for intravasation [225].

It is clear that the controversy regarding the existence and significance of vasculogenic mimicry remains high. In line with this, Karl Plate, Alexander Scholz and Daniel Dumont concluded in an article that in the case of glioblastoma multiforme, the significance of vasculogenic mimicry might be rather small, since, if existing at all, most blood vessel would still be lined with endothelial cells [180].

Transdifferentiation into endothelial cells

Tumor stem cell to endothelial cell differentiation describes a process whereby tumor cells – often with stem cell characteristics – transdifferentiate into cells with endothelial cell marker expression and function. The consequences of this process stand in sharp contrast to the literature precedent often stating that tumor-associated endothelial cells are genetically stable [226, 227]. Tumor to endothelial cell transdifferentiation has been heavily investigated in glioblastoma multiforme. In one report, a significant proportion glioblastoma-derived endothelial cells that expressed the endothelial cell marker CD105^{+} (ENDOGLIN) contained *EGFR* and chromosome 7 amplifications comparable to tumor cells, suggesting a tumor-derived origin of these endothelial cells. These glioblastoma-derived endothelial cells were the progeny of a CD133^{+} cancer stem cell-like population [228]. In another set of experiments, more than half of the glioblastoma associated endothelial cells displayed the same genomic alterations that were found in the respective tumor cells [229]. Endothelial cells with the same genomic aberrations as in the respective tumor cells have also been discovered in neuroblastoma and lymphoma samples [230, 231]. In contrast to this, other groups failed to detect a relevant proportion of tumor cell-derived endothelial cells in glioblastoma samples [232, 233]. Similarly, recent evidence derived from lineage tracing experiments revealed a glioblastoma cell origin of a high proportion of tumor blood vessel associated pericytes but not of endothelial cells [234].

Bridging the concepts of vasculogenic mimicry and endothelial transdifferentiation, it has been hypothesized that vasculogenic mimicry might represent an incomplete step in differentiation along the way to cells expressing endothelial cell markers [229].

21

Taken together, several mechanisms how tumors ensure their supply with essentials delivered via the systemic circulation by the generation of vessels or vessel-like structures co-exist. However, their relative significance between different cancer types and subtypes and even within a certain tumor, and molecular mechanisms mediating these vascularization types have to be further investigated. In addition, what type of tumor vascularization is most affected by anti-angiogenic therapies has remained largely elusive.

1.2.4 New avenues in angiogenesis research – the important role of endothelial cell metabolism

In parallel to the renaissance of the tumor metabolism field, angiogenesis researcher became interested in the metabolism of endothelial cells. This parallel rapid evolution of the two "hot topics" culminated in a joint Keystone symposium in Whistler, Canada, in spring 2014. Glycolysis is central to endothelial cell metabolism and only a small proportion of ATP is generated by oxidative phosphorylation. It has been shown that already quiescent endothelial cells lining mature vessels display a high glycolytic flux, which is approximately doubled when endothelial cells are activated [235]. VEGF-A promotes the tip cell phenotype and at the same time increases phospho-fructokinase-2/fructose-2,6-bisphosphatase 3 (PFKFB3) levels, as does FGF-2. The product of the reaction catalyzed by PFKFB3, fructose-2,6-bisphosphate, strongly stimulates glycolytic flux via allosteric activation of phosphofructokinase-1 (PFK-1) [235]. Abrogating PFKFB3 levels in endothelial cells reduced microvessel sprouting *in vitro* and *in vivo* in a neonatal mouse retina assay by affecting both, migration of tip cells and proliferation of stalk cells. In line with this finding, overexpression of PFKFB3 increased endothelial cell sprouting by increasing sprout numbers and length. The migration phenotype can be explained by the observation that in PFKFB3-deficient endothelial cells lamellipodia formation was impaired, which is a critical structure for endothelial cell migration. Interestingly, PFKFB3 knockdown reduced, whereas overexpression increased the fitness to compete for the tip cell position in a mosaic spheroid assay. In addition to this genetic evidence, partial and transient inhibition of glycolysis by a small molecule inhibitor of PFKFB3, 3-(3-pyridinyl)-1-(4-pyridinyl)-2-propen-1-one (3PO), reduced vascular sprouting by affecting endothelial cell migration and proliferation [236].

Recently, it was found that endothelial cell proliferation but not migration critically relies on carnitine palmitoyltransferase 1 (CPT1A), which is a rate-limiting enzyme of fatty acid oxidation because it transports long-chain fatty acids into the mitochondria and thereby supplies β-oxidation. Consistent with the notion that most ATP of endothelial cells is glucose derived, CPT1A knock-down did not affect cellular ATP levels. Instead, in isotope labeling studies, fatty acid-derived carbons could be retrieved in tricarboxylic acid (TCA) cycle

intermediates and TCA cycle-derived amino acids such as aspartate. The authors could finally link the proliferation defect upon CPT1A deficiency to a diminished *de novo* deoxyribonucleotide (dNTP) biosynthesis presumably via reducing the aspartate pool, which is a carbon source for dNTP synthesis [238].
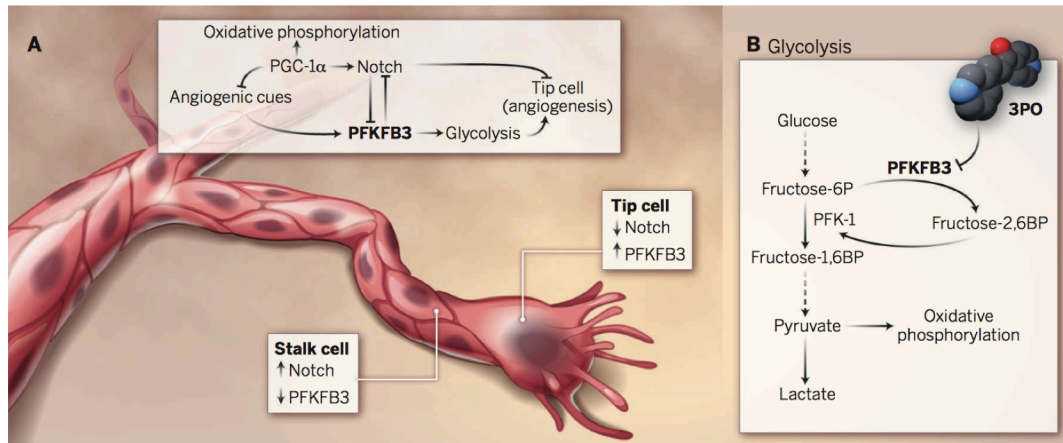
Figure 4. Glycolysis controls vascular sprouting.
Endothelial cell metabolism is heavily based on glycolysis, both in the quiescent and activated states. (A) PFKFB3 is highly expressed in endothelial tip cells and produces fructose-2,6-bisphosphate, which is a strong positive regulator of glycolysis. (B) PFKFB3 is inhibited by the small molecule 3PO. Therefore, 3PO is exerting anti-angiogenic effects (adapted from [237]).

Taken together, it is relatively obvious that endothelial cells would adapt their metabolism during angiogenic sprouting. However, even though research on endothelial cell metabolism is still in its infancy, first hallmark papers suggested that endothelial cell metabolism does not appear to be simply a passive consequence of angiogenic processes, but can rather actually regulate them [239].

1.3 Anti-angiogenic therapy

1.3.1 Targeting tumor angiogenesis

The first drug being identified with anti-angiogenic properties was interferon α/β [240]. In the subsequent years, a number of synthetic or endogenous angiogenesis inhibitors such as thalidomide, TNP-470 or thrombospondin-1 have been discovered – a substantial fraction of them in the Folkman laboratory [176]. Based on encouraging evidence derived from various preclinical experiments, the monoclonal anti-VEGF-A antibody bevacizumab (Avastin®) was introduced into the clinics as the first "pure"[7] angiogenesis inhibitor and

---

[7] it should be kept in mind that VEGF-A not only acts on endothelial cells, but also directly on e.g. certain cancer cells or cells of the hematopoietic system [241].

received FDA approval in 2004 for the treatment of metastatic colorectal cancer in combination with chemotherapy [200, 242]. Since then, numerous clinical trials with various classes of angiogenesis inhibitors for the treatment of a number of different cancer types have been conducted. This is highlighted with the resulting 1489 hits (on 23.08.2015) when performing a search of clinical trials on Pubmed with the MeSH terms "angiogenesis" and "cancer". Current FDA approved *sensu stricto* anti-angiogenic therapeutics either neutralize VEGF-A (*e.g.* bevacizumab, or the VEGF-trap aflibercept, which traps also VEGF-B and PlGF) or are tyrosine kinase inhibitors that block the signaling of all 3 VEGFRs and display differing selectivity to PDGFRs and FGFRs (*e.g.* sunitinib, sorafenib, axitinib, regorafenib, lenvatinib, pazobanib; Table 1) [243]. Considering the sheer amount of data, reviewing the preclinical and clinical data of anti-angiogenic therapy in cancer in general clearly lies beyond the scope of this thesis. Therefore, the following section is restricted to the two tumor entities mainly used in the present MD-PhD thesis, namely PNETs and breast cancer. In addition, I have restricted the discussion to strategies directly targeting the VEGF family and thus ignoring attemps of therapies with endogenous angiogenesis inhibitors such as endostatin, MMP-inhibiting agents or interfering with integrin function [244, 245].

Anti-angiogenic treatment of PNETs: preclinical and clinical aspects

In 1985, the Rip1Tag2 PNET mouse model, one of the first transgenic mouse models of cancer ("oncomice"), was published by Douglas Hanahan [246, 247]. Rip1Tag2 transgenic mice express the oncogene simian virus 40 large T-antigen (*SV40 Tag*) under the control of the rat insulin promoter (*Rip*) and represent a prototypical multi-step model of hormone positive β-cell carcinogenesis (insulinoma) [248, 249]. Several other transgenic or transplantation PNET mouse models have subsequently been generated and characterized [250]. Nevertheless, most studies investigating tumor angiogenesis or evaluating anti-angiogenic therapies in the context of PNETs have employed the Rip1Tag2 model, not least because of its dependence on angiogenesis and rapid and reproducible multistep carcinogenesis [251]. The angiogenesis-dependence of the Rip1Tag2 tumors quickly became evident when it was noted that the angiogenic switch occurring in hyperplastic islets preceded the progression into a neoplasia [249]. This was later supported by genetic evidence showing that the conditional knock-out of VEGF-A in β-cells of the pancreas prevented tumorigenesis to a large extent in a non-redundant manner [252]. Furthermore, anti-angiogenic compounds without direct anti-tumor cell effects significantly reduced tumor volumes [251, 253-255]. Conversely, the overexpression of the 165 amino acid isoform of VEGF-A under the control of the rat insulin promoter (*Rip1-VEGFA165*) in the Rip1Tag2 model led to an earlier occurrence of the angiogenic switch, accelerated tumor development, and a shortened life span. This was likely due to early onset hypoglycemia, since metastases

were absent [256]. Overexpression of another VEGF-family member, PIGF1, showed anti-angiogenic properties by reducing intratumoral microvessels (but not larger intratumoral vessels) and reduced tumor burden by forming low-angiogenic heterodimers with VEGF-A [257].

In summary, the repetitively observed correlation between microvessel density and tumor volumes has demonstrated that tumor growth in the Rip1Tag2 model is extremely angiogenesis dependent. Because of this, it appears intuitive that anti-angiogenic therapy strongly inhibits tumor burden. But how predictive is this model for future successful therapeutic applications of compounds in the clinics? In fact, compounds successfully tested in the Rip1Tag2 model have proven to be highly active in PNET patients [258]. Although the tumor initiating viral oncogene is not present in human PNETs, SV40 large T antigen inhibits the tumor suppressor proteins p53 and retinoblastoma (RB), two tumor suppressor genes that often dysregulated in human PNETs [259, 260].

With an annual incidence of 0.32/100'000 in the United States (male 0.38/100'000, female 0.27/100'000), PNETs in humans are rare [261]. But this does not detract from their importance as a life threatening cancer entity. Whereas the majority of pancreatic tumors are affecting the exocrine pancreas (pancreatic ductal adenocarcinoma), PNETs account for a small minority of all pancreatic tumors [261]. Like other neuroendocrine tumors, NETs originating in the pancreas displayed an increased incidence over the last few decades. This is in part due to improved classification and diagnosis. However, a "true" increase in incidence cannot be excluded [262]. Although patients with localized disease have an excellent prognosis, metastatic disease displays a 5-year survival rate of only about 30-40% [263]. PNETs are treated with multiple modalities including surgery, somatostatin analogues, radiotherapy and conventional chemotherapy [264]. In addition, everolimus and sunitinib are indicated for the treatment of non-resectable well differentiated, advanced or metastatic PNETs [101]. To reiterate the predictive power of the Rip1Tag2 model for successful translation into clinics, it is useful to consider the examples of everolimus and sunitinib. In a phase III clinical trial, the mammalian/mechanistic target of rapamycin (mTOR) inhibitor everolimus increased PFS in PNET patients [265]. This was predicted by the successful treatment of the Rip1Tag2 model with rapamycin, the first mTOR inhibitor discovered, leading to a transient tumor stasis [266]. Unlike in the human clinical trial, whereby everolimus failed to increase OS, a single agent treatment with rapamycin in Rip1Tag2 mice increased survival. However, an initial response phase was rapidly followed by tumor regrowth [265, 266]. In the case of sunitinib, single agent treatment prolonged survival of Rip1Tag2 mice for about 7 weeks, which was translating into an OS benefit in PNET patients

[64, 267]. Regarding the encouraging response of PNET patients to sunitinib monotherapy, it seems that this heterogeneous group of cancers is especially sensitive to anti-angiogenic therapy [64]. Since sunitinib therapy has been accompanied by a number of side effects and PNET therapy often involves long-term treatments, it is mandatory to develop additional anti-angiogenic compounds with similar anti-tumor actions but with a different or a reduced side-effect profile [263]. To this end, pazopanib, a multi-TKI targeting similar to sunitinib blocking VEGFRs, PDGFRs and KIT [75] was evaluated in two separate phase II clinical trials. In one trial, pazopanib monotherapy resulted in encouraging disease control rate [268]. In the second trial, pazopanib was combined with octreotid, a somatostatin analog, and displayed objective responses in a proportion of PNET patients (but not in patients with carcinoid tumors) [269]. Last but not least, a phase III trial is planned in which pazopanib *versus* best supportive care in advanced PNET patients after failure to targeted therapies will be evaluated [269].

Resistance to therapies targeting mainly the VEGF/VEGFR signaling axes can be mediated by compensatory FGF/FGFR mediated signaling. Therefore, TKI inhibiting FGFRs in addition to VEGFRs and PDGFRs might provide additional benefit (for details see section 1.4.1 Ref [162, 270]). The group of Douglas Hanahan has therefore evaluated the anti-tumor action of brivanib, which blocks FGFRs in addition to VEGFRs and PDGFRs, in the Rip1Tag2 model. Consistent with the aforementioned hypothesis, brivanib increased mouse survival in a superior manner compared to sorafenib, which lacks FGFR-inhibiting activity [253]. Despite promising preclinical evidence, a clinical trial currently evaluating brivanib in PNET patients has not been initiated so far (webpage "clinicaltrials.gov" [271]).

In summary, anti-angiogenic therapy appears to be a successful strategy for the treatment of NETs of pancreatic origin. The availability of similar anti-angiogenic TKIs with slight differences in the target spectrum and side-effect profile will hopefully improve personalized treatment regimens in the future.

The significance of anti-angiogenic therapy in breast cancer: preclinical and clinical aspects

Since breast cancers are highly prevalent, they represent a huge market for pharmaceutical companies. It is therefore not surprising that anti-angiogenic therapeutics have been and are still being busily tested (and marketed) for their efficacy in breast cancer patients. Preclinical assessments employing breast cancer xenograft models showed that interfering with the VEGF-A/VEGFR-2 axis resulted in encouraging repressive effects on MVD and tumor growth [272-274]. Similarly, sunitinib reduced primary tumor growth as a monotherapy in the MMTV-v-Ha-ras transgenic breast cancer mouse model and in a

carcinogenesis-induced breast cancer model in rats [275]. Furthermore, sunitinib in combination with various standard chemotherapeutic agents displayed synergistic effects on primary tumor growth and bone metastasis in the MX-1 and MDA-MB-435 human xenograft models, respectively [275]. In line with this, the small-molecule anti-angiogenic TKI vandetanib (which inhibits EGFR in addition to VEGFRs and RET) strongly reduced primary tumor growth of the triple-negative MDA-MB-231 human breast cancer cell line [53]. Based on these preclinical results, the evaluation of bevacizumab and sunitinib in breast cancer patients in large phase III clinical trial was optimistically awaited.

Four large phase III clinical trials (GeparQuinto, CALGB 40603, NSABP B-40, ARTemis) investigating the addition of bevacizumab to standard chemotherapy regimens in the neoadjuvant setting have been published to date [276-279]. Neoadjuvant treatments aim to decrease the rate of complete axillary lymph node dissection and facilitate breast-conserving surgery [280, 281]. In all four clinical trials, the addition of bevacizumab significantly increased the rate of complete pathological responses (cPR) compared to chemotherapy alone (Table 3; [276-279]). cPR has proven to be a valid surrogate endpoint for neoadjuvant clinical trials when evaluating chemotherapeutic agents [282]. However, the numerical increase in cPR was relatively small, and as such it has to be seen if this translates into longer breast cancer specific survival, disease-free survival (DFS) and OS when following up the patients. To date, data addressing this question is only available from the GeparQuinto study, which showed that the 3-year DFS and OS was not improved by the use of bevacizumab [283].

study identifier	absolute increase in pCR rate (%)	References
GeparQuinto (GBG44)	3.5	[279]
NSABP B-27	6.3	[276]
ARTemis	5	[277]
CACGB 40603	11	[278]

Table 3. Neoadjuvant treatment with bevacizumab in breast cancer.
The four currently published phase III clinical trials evaluation the addition of bevacizumab to standard chemotherapy regimens in the neoadjuvant treatment setting are displayed. Indicated is the absolute increase of pCR (in %) per study when bevacizumab was added.

In the adjuvant setting (*i.e.* post-operative treatments to increase the rate of cured patients), the addition of bevacizumab failed to improve clinical outcome. In the BEATRICE

trial, invasive disease-free survival was not significantly improved in the patient cohort of triple-negative breast cancer receiving bevacizumab in addition to chemotherapy [284]. This negative result was rather surprising, since preclinical evidence pointed towards an important role of neovascularization in the outgrowth of micrometastases – the putative target in the adjuvant setting [285].

Bevacizumab in combination with chemotherapy had initially received FDA approval for first-line treatment of metastatic breast cancer based on the E2100 study. In this study, an increase in PFS of 5.9 months when patients were treated with paclitaxel in combination with bevacizumab compared to treatment with paclitaxel alone was reported. However, OS was not significantly changed [286]. The increase in PFS without OS benefit was a recurrent observation in numerous phase III trials evaluating the addition of bevacizumab to chemotherapy in metastatic breast cancer (Table 4 and references therein). In addition, the gain in PFS was smaller in the follow-up studies compared to the original E2100 study. Employing PFS survival as primary endpoint, as it was the case in all the bevacizumab trials in advanced breast cancer, was causing some controversy [287]. On the other hand, the alternative OS as primary endpoint, when evaluating first-line treatments in advanced breast cancer, is potentially confounded by crossing-over after progression[8] (as in the case of the RIBBON-1 study [289]). An additional confounding could be caused by subsequent lines of treatment after progression, as metastatic breast cancer patients often receive up to six lines of chemotherapy [290]. Despite a tremendous amount of large phase III clinical trials mainly investigating the therapeutic efficacy of bevacizumab in advanced breast cancer, diverging conclusions were drawn by two important regulatory authorities, the FDA and the European Medicines Agency (EMA). Whereas the FDA retracted the approval for bevacizumab in HER2-negative metastatic breast cancer, it remains approved in Europe when administered in combination with paclitaxel or capecitabine [291, 292].

Based on the finding that simultaneous targeting of pericytes in addition to endothelial cells might be superior to targeting endothelial cells only, sunitinib and sorafenib were evaluated as monotherapy or in combination with chemotherapy in breast cancer patients [104]. Disappointingly, second-line sunitinib single-agent therapy of advanced breast cancer as compared to capecitabine monotherapy was inferior with regards to PFS and no statistical significant difference in OS was observed [293]. Similarly, the addition of sunitinib to capecitabine or docetaxel displayed unchanged PFS and OS as compared to either chemotherapy alone [122, 288]. In another study, sunitinib plus paclitaxel was compared to bevacizumab plus paclitaxel as first-line therapy of metastatic breast cancer, clearly favoring

---

[8] „crossing-over" can be part of a study protocol and allows patients of the control arm to receive the investigational compound after progression. In this case, it does therefore not affect PFS [288].

bevacizumab over sunitinib based on PFS, 2-year survival rate and tolerability [294]. One potential influence regarding the failure of sunitinib in combination with chemotherapy was the increased rate of adverse events observed in several trials [122, 288, 294]. This led to deviation from the study protocol in a proportion of patients and it led to reduction of chemotherapy dosing already in the study protocol for the combination group as compared to the chemotherapy only group [288]. Sorafenib, an oral multi-target TKI, showed promising results by increasing PFS (but not OS) in two phase II clinical trials in combination with chemotherapy in advanced or metastatic breast cancer [121, 295]. At least one phase III clinical trial is ongoing evaluating the efficacy of adding sorafenib to capecitabine [296].

Taken together, anti-angiogenic treatment approaches have largely failed to influence endpoints in large phase III clinical trials in a relevant manner with regards to a risk-cost-benefit evaluation. Whereas bevacizumab in combination with chemotherapy slightly but significantly increased cPR in the neoadjuvant setting and PFS in metastatic disease, it did not influence OS in metastatic situation or invasive DFS in the adjuvant therapy situation. Sunitinib completely failed clinical evaluation in breast cancer and appeared to be even inferior to bevacizumab. These disillusioning notions stand in sharp contrast to promising data of derived from preclinical evaluation of several anti-angiogenic compounds [297, 298]. Mainly led by Robert Kerbel, attempts are ongoing to better model clinical situations in mouse cancer models in order to improve clinical translatability of new compounds in the future [299, 300].

A full chapter of this thesis is dedicated to discuss the potential reasons why anti-angiogenic therapy of breast cancer displayed disappointing results. A special emphasis was laid on biological mechanisms of resistance to anti-angiogenic therapy, whereas reasons derived from clinical study designs were largely ignored since these aspects clearly lie beyond the scope of this thesis.

study identifier	study design	median PFS gain (months)	ORR gain (%)	OS gain (months)	References
E2100	Paclitaxel ± BEV (1st)	5.9 (5.5/ 5.6[a])	15.7	n.s.	[286, 301]
AVADO	Docetaxel ± BEV (1st)	n.s./1.9[b]	n.s./18[b]	n.s.	[302]
RIBBON-1	Capecitabine or Tax/Anthra ± BEV[e] (1st)	2.9[c]/1.2[d]	11.8[c]/13.4[d]	n.s.	[294]
E2100, AVADO, RIBBON-1[f]	CHT ± BEV (1st)	2.5	17	n.s.	[291]
AVF2119	Capecitabine ± BEV (2nd+)	n.s.	10.7	n.s.	[303]
RIBBON-2	CHT[g] ± BEV (2nd)	2.1	n.s.	n.s.	[304]
AVAREL	Docetaxel plus Trastuzumab ± BEV (1st)	n.s./ 2.9[h]	n.s.	n.s.	[305]
LEA	Endocrine therapy[i] ± BEV (1st)	n.s.	19	n.s.	[306]
TANIA	CHT ± BEV (2nd) after CHT + BEV[k]	2.1	n.s.	immature[l]	[307]

Table 4. Phase III clinical trials evaluating bevacizumab in advanced or metastatic breast cancer
The clinical efficacy of bevacizumab (BEV) when added to chemotherapy (CHT) regimen in advanced or metastatic breast cancer is shown. If not a specific chemotherapeutic agent is indicated, several alternative chemotherapeutic agents have been used in the same study. ORR= objective response rate; n.s.= non-significant; Tax= taxane; Anthra= anthracycline
[a] independent review by independent review facility (IRF) and ECOG investigators (based on the criteria of the IRF), respectively
[b] BEV 7.5mg/kg every 3 weeks / BEV 15mg/kg every 3 weeks
[c] BEV in combination with capecitabine
[d] BEV in combination with taxane/anthracycline
[e] investigators were free to choose a taxane-based (Tax; nab-paclitaxel or docetaxel) or a anthracycline-based (Anthra; epirubicin or doxorubicin based combinations) chemotherapy
[f] Metaanalysis
[g] investigators free to choose CHT before randomization (capecitabine, taxane (paclitaxel, nab-paclitaxel, docetaxel), gemcitabine or vinorelbine
[h] investigator assessed/ Independent Review-Committee
[i] letrozole or fulvestrant
[k] third-line therapy after progression was identical to the randomized second-line therapy (CHT ± BEV)
[l] interim analysis of overall survival reavealed no relevant numerical difference

1.3.2 Anti-angiogenesis extended

Metronomic chemotherapy

Metronomic chemotherapy is defined as "frequent administrations of chemotherapeutic drugs at doses significantly below the maximum tolerated dose (MTD) with no prolonged drug-free breaks" [308]. Whereas conventional chemotherapy is often administered at MTD and scheduled in intervals of 1-3 weeks, Browden et al. first reported that when treating mice bearing cyclophosphamide-resistant Lewis lung carcinoma more often (6 days vs. 21 days) and with lower doses of cyclophosphamide (170 mg/kg vs. 450 mg/kg) than in conventional

cytotoxic chemotherapy treatment regimens, it resulted in a superior anti-tumor effects [309]. With both treatment regimens, endothelial cell apoptosis occurred before secondary tumor cell apoptosis. The waves of apoptosis were found to be more frequent in the metronomic than with the conventional chemotherapy schedule leading to a sustained anti-angiogenic effect [309]. Similarly, continuous vinblastin administrations at doses below those known to cause direct anti-tumor cell effects inhibited angiogenesis and tumor growth in a neuroblastoma mouse model [310]. Interestingly, in both studies the addition of *bona fide* angiogenesis inhibitors to metronomic chemotherapy resulted in improved anti-tumor effects [309, 310].

It is well established that a number of frequently used chemotherapeutics induce endothelial cell and tumor cell apoptosis. However, the novelty in the metronomic treatment schedule was that tumor cells resistant to a certain agent would still be forced into apoptosis solely by the anti-angiogenic, cytotoxic effect on endothelial cells. In addition, more frequent dosing might lead to a sustained anti-angiogenic effect and the reduced doses would reduce drug-induced side effects [226, 309-311]. Since its first thorough description, the mechanistical knowledge behind the significant anti-tumor impact of metronomic chemotherapy treatment regimens has been extended from a pure anti-angiogenesis mediated effect to a mode with multiple targets [308]. Metronomic chemotherapy has shown positive effects on multiple levels of anti-tumor immunity [312], it reduced the frequency of cancer stem cell-like cells [313, 314], induced vessel normalization and thus increased tumor oxygenation [315, 316] and inhibited HIF-1 activity [317].

Clinical experience about the efficacy of metronomic chemotherapy in patients – to the best of our knowledge – is so far restricted to encouraging data derived from phase II clinical trials, but several phase III trials are ongoing. In addition, clinical trials are underway or have already been completed that translate hypotheses derived from preclinical experiments by combining metronomic chemotherapeutics with radiotherapy, immunotherapy or targeted agents including bevacizumab, sorafenib and erlotinib into the clinic [308]. But again, large phase III trials will finally tell us how valid these hypotheses are.

Metronomic chemotherapy regimens are low-cost and reduce the occurrence of drug-related side effects. Therefore, it was hypothesized that this treatment mode could ameliorate treatment accessibility in low and middle income countries [318].

Vessel normalization

The rational behind targeting the tumor vasculature was based on the assumption that tumors need to acquire new blood vessels to be able to grow beyond the size of 2-3mm [167]. Reducing MVD would therefore result in the starvation of the tumor and would thus induce tumor shrinkage or at least dormancy. An alternative phenomenon induced by anti-angiogenic therapy has in the meantime been proposed by Rakesh Jain. He suggested that in certain circumstances "normalization" of the typically aberrant and disorganized tumor microvasculature would provide benefits to the patients [319].

Tumor angiogenesis often "overshoots" and results in immature, dilated and hyperpermeable/leaky vessels leading to increased intratumoral fluid pressure and hypoxic areas. Increased intratumoral fluid pressure can diminish delivery of therapeutic compounds into the tumor. Therefore, a "mild" anti-angiogenic treatment could result in a transient window with a normalized vasculature and thus in improved delivery of chemotherapeutic agents and reduced hypoxia, possibly ameliorating radiation therapy [319, 320].

Vessel normalization has been defined as the process when immature vessels are pruned, but the residual vessels become more mature. In contrast, "vessel blocking" means when besides immature also mature vessels are depleted [320]. The sole neutralization of VEGF-A by bevacizumab is thought to cause such a "vessel normalization window". In contrast, TKIs like sunitinib, due to its additional targeting of pericyte coverage via inhibition of PDGFRβ, rather results in vessel blocking and therefore reduced perfusion with increased hypoxia, but without a significant normalization window [320, 321]. It is often hypothesized that vessel normalization would be the major cause for the beneficial outcome when adding bevacizumab to chemotherapy. In addition, it can explain why bevacizumab alone had no impact in clinical trials as single-agent therapy in solid tumors except in renal cell carcinoma [322, 323]. Furthermore, the disappointing results, when evaluating sunitinib in combination with chemotherapy in metastatic breast cancer, could be explained by the rapid blood vessel pruning without the establishment of a "normalization window". Even when solely targeting the VEGF-A/VEGFR-2 signaling axis, vessels normalization does not seem to be indefinite, as a prolonged VEGFR-2 blockade eventually leads to extensive pruning of the transiently normalized vasculature [324]. Treatment of orthotopic human xenograft GBM mouse models with DC101, a blocking antibody against VEGFR-2, resulted in a normalization window in the first week after the first administration and was followed by the restoration of hypoxia [324].

In addition to approaches interfering with VEGF-A/VEGFR2 signaling, additional mechanisms worth mentioning have been described to induce tumor blood vessel

normalization [320]. Heterodeficiency in tumor endothelial cells of the prolyl hydroxylase domain protein 2 (PHD2), an oxygen sensor targeting HIFs for degradation in normoxia, induced normalization of the endothelial layer and vessel maturation [325]. The resulting increased perfusion and decreased interstitial fluid pressure resulted in improved chemotherapy delivery and synergistic anti-tumor effect [326]. Similarly, the anti-malaria drug chloroquine induced vessel normalization and thus enhanced chemotherapy delivery in tumor mouse models, independent of its known capacity to inhibit autophagy [327].

Some controversy regarding the vessel normalization hypothesis exists. In a report providing a time course of perfusion and oxygenation in the MDA-MB-231 xenograft mouse model, the Kerbel laboratory detected impaired vascular perfusion after 2 days when treating with DC101 [328]. Strikingly, the same authors have previously reported a synergism of combining DC101 with chemotherapy in the very same model [329]. Since a vessel normalization window was not detected at the time points investigated, the synergism observed was likely not dependent on vessel normalization [328]. In line with this, a single administration of bevacizumab impaired the perfusion of NSCLC tumors in patient as early as a 5 hours post-bevacizumab injection that was detected by positron emission tomography and the diffusible tracer $[^{15}O]H_2O$. In parallel, the net influx rate of radiolabeled $[^{11}C]$docetaxel was decreased already at 5 hours post-bevacizumab injection and endured until at least day 4 [330].

Besides improving drug delivery, vessel normalization is also thought to influence metastatic spread and anti-tumor immunity. Since metastatic cancer cells intravasate more easily into immature vessels, vessel normalization has also been shown to reduce metastatic spread [325]. Furthermore, an antibody against VEGF-A increased homing of adoptively transferred T cells into experimental tumors and displayed improved anti-tumor immunity [331]. In addition, single-agent bevacizumab therapy reduced neurological symptoms caused by glioblastoma associated edema probably due to a vessel normalizing effect [332].

The divergent reports in favor or against the vessel normalization hypothesis most likely reflect heterogeneity of different tumor subtypes in responding to different anti-angiogenic approaches. Furthermore, the in depth knowledge about the kinetics of the normalization window might guide the proper scheduling of chemotherapies in relation to the infusion with bevacizumab to take advantage of this synergistic interaction.

1.4 Resistance to anti-angiogenic therapy

"Resistance to cancer therapy" can be defined as the period, during which malignant lesions progress despite an ongoing appropriate therapy. More specifically, the term "evasive" resistance is used when the resistance phase was preceded by a transient phase of tumor regression or stasis. In contrast, "intrinsic" resistance describes the process when no signs of initial response could be detected. Technically though, to distinguish between evasive resistance with a short response phase versus intrinsic resistance with no response phase is challenging [333]. However, these simple phenotypic definitions underline complex mechanistic processes.

Currently, existing concepts about resistance to anti-angiogenic approaches are mainly based on studies with drugs interfering with VEGF/VEGFR signaling and are based on mechanisms to re-assure oxygen and nutrient supply (Figure 5): Revascularization occurs after a transient phase of reduced MVD, mature vessels are intrinsically more resistant to VEGF inhibition and increasing pericyte coverage is an escape mechanism; or cancer cells emigrate from hypoxic areas into regions with secured blood supply, *i.e.* by migration to perivascular location with subsequent metastasis to distant organs [243].

The following section gives an overview over the complexity of resistance to drugs that are mainly interfering with VEGF/VEGFR signaling, and of attempts how these escape mechanisms have already been targeted by combinatorial treatments.

1.4.1 Revascularization

Resistance to interference with the VEGF-A/VEGFR2 signaling axis was reported to occur on the level of endothelial cells, obviously the primary target of anti-angiogenic therapy. After an initial phase of tumor blood vessel pruning, leading to increased hypoxia and inhibition of tumor growth (mostly stasis rather than regression), tumor MVD was increased again to baseline levels [270, 333]. Mechanistically, the hypoxia-induced upregulation of alternative pro-angiogenic pathways in the tumor or the recruitment of pro-angiogenic growth factors providing bone marrow-derived cells (BMDCs) have been implicated in this mode of resistance [243, 333, 334].
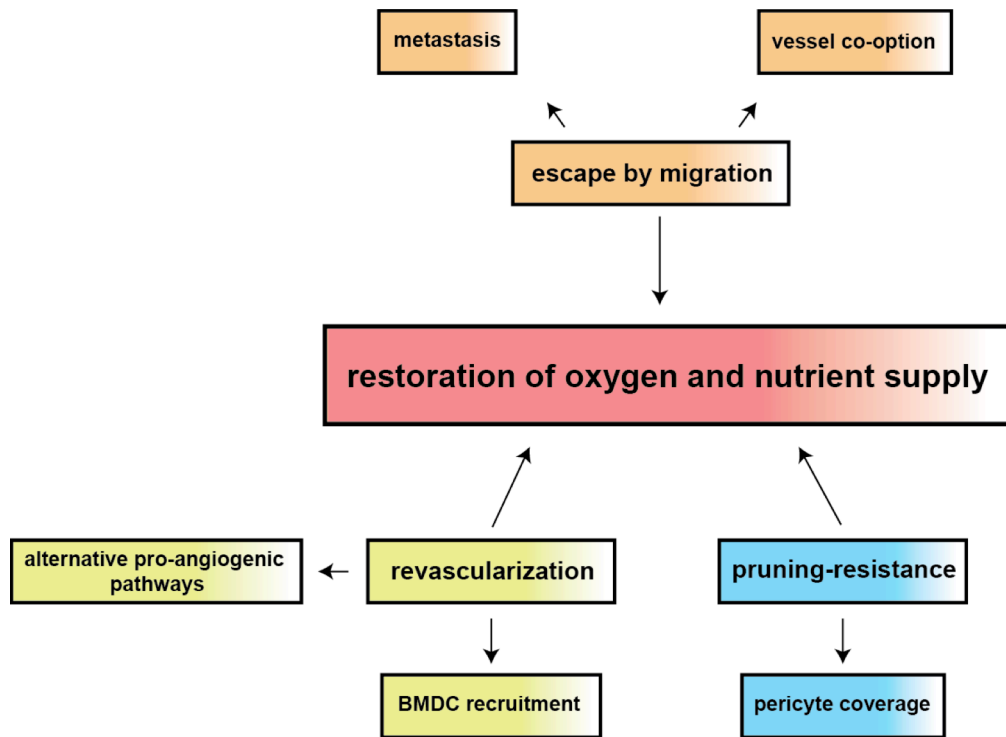
Figure 5. Mechanisms of resistance to anti-angiogenic therapies.
Traditional concepts are built around the notion that resistance to anti-angiogenic therapy is based on mechanisms aiming for the restoration of oxygen and nutrient supply. This is achieved by revascularization or by protecting existing vessels from the action of anti-angiogenic compounds by tight pericyte coverage. Alternatively, tumor cells utilize pre-existing vessels (vessel co-option) or migrate towards oxygen-rich perivascular location, which facilitates systemic dissemination.

Revascularization and restoration of tumor growth upon prolonged blockade of VEGFR-2 by the monoclonal rat antibody DC101 in the Rip1Tag2 transgenic mouse model was attributed to a hypoxia-driven upregulation of various pro-angiogenic factors such as FGF-1, FGF-2, FGF-7, EphrinA1, EphrinB2 and ANG-1, thereby potentially providing alternative signals driving angiogenesis [270]. In metastatic CRC patients treated with the combination of chemotherapy and bevacizumab, FGF-2 levels rose shortly before and during the progression phase [335]. Consequently, tumor re-growth could be halted with the co-administration of a FGF decoy receptor in addition to DC101 starting when tumors became resistant to DC101 treatment [270]. A similar result had previously been reported when a combined trapping of VEGF-A and FGF-1 by soluble forms of VEGFR-1 and FGFR-2 IIIb, respectively, resulted in a synergistic reduction of primary tumor growth of an allograft of a Rip1Tag2-derived β tumor cell line [162][9]. Pharmacological proof of principle was obtained

---

[9] The same adenoviral construct with an FGF-trap has been used in the study of Casanovas et al. [270]. The FGF-trap consisted of a soluble form of FGFR-2 IIIb which was stabilized by fusion to a mouse immunoglobulin heavy chain and trapped FGF-1, FGF-3, FGF-7 and FGF-10 [162].

by the preclinical evaluation of the dual VEGFR/FGFR inhibitor brivanib in the Rip1Tag2 model. A head-to-head comparison of DC101 and brivanib revealed suppression of tumor growth after 4 weeks of treatment with brivanib, whereas at this point considerable tumor regrowth in the DC101 treated animals was observed. Similarly, switching from sorafenib, a TKI inhibiting VEGFRs and PDGFRβ but not FGFRs, at the timepoint of treatment failure to brivanib, increased survival. Notably, at the end point of the survival trial, brivanib treated tumors did not show signs of revascularization [253].

The observed correlation between upregulation of ANG-1 during resistance to VEGFR-2 blockade was subsequently investigated on a functional level. However, due to the context dependent action of angiopoietins many questions are only partially answered [270]. These questions are: is ANG-1 alone sufficient to promote revascularization during VEGF inhibition, or does it rather support the proangiogenic activity of other factors such as FGFs? What is the role of ANG-2, the context dependent antagonist of ANG-1, in revascularization during sustained VEGF inhibition?

Tumor cell-specific overexpression of ANG-1 in the Rip1Tag2 model did neither influence tumor volume nor tumor vascularization [336]. In contrast, ANG-1 overexpression in a rat glioma model increased tumor vascularization and tumor growth [337]. In the context of anti-VEGF therapy, elevated levels of Ang-1 rendered tumor blood vessels largely intrinsically resistant to VEGF inhibition, reduced hypoxia and was involved in vessel normalization [324, 338]. In the process of revascularization during interference with VEGF signaling, the role of ANG-1 could therefore lie in directly promoting maturation and stabilization of new blood vessels induced by other pro-angiogenic factors. Alternatively, ANG-1 in this context could directly stimulate angiogenic sprouting.

The main sources of ANG-2 are endothelial cells and its levels are increased in the tumor vasculature upon activating stimuli and by hypoxia. The role of ANG-2 in tumor angiogenesis and its impact on tumor growth is based on a plethora of contradictory literature [339]. As a "rule of thumb" it appears that ANG-2 destabilizes vessels and leads to regions in the vasculature with enhanced plasticity resulting in vessel sprouting when sufficient levels of other pro-angiogenic factors are present. Conversely, ANG-2 leads to vessel regression in situations of an insufficient net-amount of pro-angiogenic factors [340]. The recently reported role of a TIE-2-independent function of ANG-2 by stimulating tip cell migration and thus vascular sprouting added another layer of complexity [193]. Work by Brown and colleagues has shown that combined inhibition of ANG-2 and VEGF signaling in various xenograft models resulted in superior effects compared to either treatment alone.

Unfortunately, it was not reported if this effect was due to an additive reduction in MVD [340]. This was specifically addressed in publication by the groups of Donald McDonald and Michele De Palma, who demonstrated that inhibition of ANG-2 alone inhibited vessel sprouting but not regression. In contrast, the combined inhibition of ANG-2 and VEGF-A resulted both in inhibition of vascular sprouting and vessel regression. This was accompanied by an additive anti-tumor effect [341, 342]. Based on observations that combined blockade of ANG-2 together with VEGF-A could lead to an improved anti-tumor action, a bispecific antibody against ANG-2 and VEGF-A (ANG-2-VEGF CrossMab) was developed by Roche. It displayed superior inhibition of tumor growth over targeting either ANG-2 or VEGF-A alone and is currently in clinical evaluation [343]. Although the additional targeting of ANG-2 to VEGF-A has shown anti-angiogenic synergism when both treatments were initiated at the same time, formal proof is still missing demonstrating that ANG-2 blockade can counteract revascularization when ANG-2 blocking starts after the initiation of anti-VEGF-A treatment. Actually, this experiment has been performed in the Rip1Tag2 model, when an anti-ANG-2 antibody combination therapy with DC101 was started after 1.5 weeks of DC101 monotherapy. Results showed a comparable tumor burden when initiating the treatment with both antibodies at the same time or when initiated sequentially. Unfortunately, the effects on MVD were not reported in this publication [342].

In addition, VEGF-C, VEGF-D, PlGF and PDGF-C have been implicated in revascularization during anti-VEGF-A therapy [243, 344]. However, in the case of PlGF contradictory results exist [345-347].

Besides compensatory upregulation of pro-angiogenic factors in "tumor resident cells" upon anti-angiogenic therapy, pro-angiogenic factors can also be provided by recruited bone marrow-derived cells (BMDCs). A variety of myeloid cells with pro-angiogenic capabilities have been described [334]. $CD11b^+Gr-1^+$ myeloid-derived suppressor cells (MDSCs), a heterogeneous population composed of early myeloid cells, immature dendritic cells, monocytes and neutrophils [334]; TIE-2-expressing monocytes (TEMs) [348], T regulatory cells (T_{regs}) [349], plasmacytoid dendritic cells [350] and T helper type 17 (T_{H17}) cells [351] have been reported to directly or indirectly promote angiogenesis. Some of these cell types promote VEGF-A-dependent, whereas others promote VEGF-A-independent angiogenesis. Mainly the latter group contains candidates that could mediate revascularization despite ongoing inhibition of VEGF signaling. The Ferrara lab has worked out an interesting cascade of events over the last decade. Tumor-infiltrating T_{H17} cells stimulate via IL-17A the production of granulocyte colony stimulating factor (G-CSF) in tumor-associated fibroblasts. G-CSF in turn acts systemically by stimulating the expression of the pro-angiogenic protein

Bv8 (prokineticin 2) in CD11b$^+$Gr-1$^+$ MDSCs in the bone marrow. Both, Bv8 and G-CSF, subsequently promote mobilization and homing of these cells to the tumor site where Bv8 can induce revascularization independent of VEGF-A. In line with these findings, co-administration of anti-VEGF-A and anti-Bv8 or anti-G-CSF antibodies exerted additive anti-tumor effects [152, 347, 352, 353]. In clear cell RCC (ccRCC) xenograft models, resistance to sunitinib therapy was associated with enhanced MVD compared to sensitive tumors and was paralleled by increased interleukin (IL)-8 levels [10] . Interestingly, ccRCC patients intrinsically resistant to sunitinib displayed higher pre-treatment tumor IL-8 expression levels compared to responding patients. Consequently, combined anti-IL-8 and sunitinib treatment counteracted resistance development and suppressed revascularization [354].

1.4.2 Pericytes as bodyguards of endothelial cells

Tumor microvessels do not respond uniformly to approaches targeting the VEGF-A/VEGFR-2 axis [355]. Tight coverage by pericytes is a hallmark of mature blood vessels. Pericytes induce quiescence and promote survival of endothelial cells, and reduce the dependency on VEGF signaling. This notion led to the hypothesis that targeting pericytes by interfering with the PDGF-B/PDGFRβ signaling axis and thus counteracting the intimate contact between endothelial cells and pericytes would render the tumor vasculature more vulnerable to VEGF inhibition [333]. Indeed, Bergers and colleagues had previously demonstrated that combined targeting of VEGFRs and PDGFRs exerted superior anti-tumor effects by a stronger reduction of the functional tumor vasculature in established tumors, compared to targeting of VEGFRs alone. In this report, sole inhibition of PDGFRβ signaling by imatinib had no effect [104]. In contrast, the McDonald laboratory showed that neutralization of the PDGFRβ ligand PDGF-B was sufficient to induce regression of tumor blood vessels as a secondary effect following detachment of pericytes [356]. Not surprisingly, given the important role of pericytes in promoting the structural and functional integrity of tumor blood vessel endothelial cells, intact pericyte coverage was demonstrated to be a mediator of intrinsic resistance to VEGF pathway inhibition [357].

Of note, most anti-angiogenic small-molecule TKI used in the clinics (sunitinib, sorafenib, nitendanib, pazopanib) or in late-stage clinical development contain significant inhibitory action against PDGFRβ (Table 1).

---

[10] In contrast to this model, survival studies with sunitinib in the Rip1Tag2 model did not reveal resistance based on revascularization [253].

1.4.3 Migration to areas richer in oxygen

Metastasis involves a cascade of multiple steps during which cancer cells leave the primary tumor and colonize distant organs (for a more detailed description of the metastasis cascade, see [358], section 5). In brief, cancer cells reach the systemic circulation either by different modes of active migration and invasion (EMT-derived mesenchymal or amoeboid single-cell migration or by collective migration) or by passive shedding. A fraction of the cells survive the harsh conditions in the blood stream and successfully leave the vasculature at distant sites. In well-vascularized tissues such as the lung and brain, arriving cancer cells can co-opt the preexisting vasculature for initial proliferation. Subsequently, the preexisting host vasculature regresses and causes tumor cell death, unless VEGF-A and ANG-2-mediated angiogenesis[11] provides the metastases with an own vasculature [219]. It was hypothesized that similar to the primary tumor, targeting the metastatic switch in metastases would induce dormancy by preventing colonization (*i.e.* the outgrowth from micro- to macrometastases) [188]. Indeed, a number of experimental evidence point towards an anti-metastatic effect of anti-angiogenic therapy [359]. However, this optimistic picture is scrutinized since some years. In preclinical models of brain tumors, hypoxia caused by interfering with angiogenesis induced an infiltrative migration pattern towards and along preexisting blood vessels [267, 360, 361]. Supporting evidence comes from infiltrative perivascular growth of tumor cells observed in glioblastoma patients following treatment with bevacizumab [362]. In cancer models where the tumors arise outside of the central nervous system, increased local tumor invasiveness following anti-angiogenic therapy has been repeatedly demonstrated – including a number of publications involving the Rip1Tag2 mouse model [267, 363-365]. In line with the notion that local tumor invasiveness is a direct cause or at least a surrogate for the ability of a tumor to form distant metastases, several groups have demonstrated that anti-angiogenic therapies can also increase lymph node and distant metastasis [267, 358, 363-368]. However, whereas for TKIs such as sunitinib, which target multiple pro-angiogenic receptors, the pro-metastatic effect has been repeatedly observed, a controversy exists regarding the effects on metastasis of antibodies targeting the VEGF-A/VEGFR-2 axis [267, 363-367]. Namely, Rigamonti and Singh *et* al. failed to detect increased local invasiveness and liver metastasis upon anti-VEGFR-2 and anti-VEGF-A treatments in Rip1Tag2 mice, respectively [342, 365]. These class-specific differences in the pro-metastatic effect raise interesting hypotheses regarding potential underlying mechanisms.

It seems that the mechanistic basis for the pro-metastatic effect of certain anti-angiogenic drugs in certain model systems is based on "passive" and "active" components (Figure 5). "Passive" drivers of metastasis involve effects of the drugs antagonizing an intact

---

[11] this process can be seen as an angiogenic switch in metastases

vascular barrier, promoting both intravasation (by active migration or passive shedding) at primary tumor site and extravasation at metastatic site simply by means of reduced physical barriers. "Active" promoters of dissemination signify the gain of migratory/invasive properties induced by hypoxia-dependent and -independent mechanisms. As we will see below, experimental manipulation of metastasis models often affect both conceptual aspects, as increasing the vascular integrity is often accompanied by reduced hypoxia – a well described driver of cancer cell migration and invasion – and *vice versa* [369]. Therefore, the two aspects of passive and active promoters of metastasis cannot be discussed separately.

Pericytes, the master regulators of vascular integrity, have shown to contain gate-keeping functions for cancer cell dissemination. Interference with blood vessel pericyte coverage caused by reduced NCAM levels or by using knock-in mice lacking the ECM-retention motif of PDGF-B, led to increased lymphatic and hematogenous metastasis in the Rip1Tag2 model [370]. Similarly, depletion of pericytes in established tumors (late-depletion) resulted in hypoxia, EMT and elevated metastatic dissemination [321]. The contrary was observed when pericytes were depleted shortly after tumor cell implantation (early-depletion). This difference was attributed to increased ANG-2 levels in the late-depletion setting leading to distorted vascular integrity, whereas the elevated ANG-1 levels present in the early-depletion setting preserved an intact vessel structure and functionality limiting metastatic spread. Furthermore, anti-ANG-2 antibody treatment paralleling pericyte depletion in the late-depletion setting reverted the pro-metastatic phenotype by increasing tight-junctions of endothelial cells resulting in reduced vessel leakiness, hypoxia and EMT [371]. This data highlight the putative therapeutic potential of a dual targeting of VEGF signaling and Ang-2 neutralization, as discussed before [343]. In contrast, Fagiani and colleagues observed decreased pericyte coverage but failed to detect increased lymph node, lung or liver metastasis in Rip1Tag2 mice overexpressing ANG-2 in a β-cell specific manner [336].

Similar to intravasation, a distorted vascular barrier facilitates extravasation into the target organ. "Supra-therapeutic" dosing of sunitinib (120mg/kg) resulted in increased permeability of the lung vasculature in mice and enhanced cancer cell extravasation after pretreating the animals with this concentration of sunitinib. This translated into increased metastatic burden when a lung colonization assay was performed in sunitinib (120mg/kg) pretreated mice. However, pretreatment with lower sunitinib doses (40 and 60 mg/kg) did not affect lung metastasis [372]. These results may explain previous work from the Kerbel laboratory, which observed shortened survival of i.v. injected MDA-MD-231 (LM2 clone with lung tropism) cells after sunitinib pretreatment at 120mg/kg [367]. Paradoxially, in the same

experimental setting, a shorter survival was recently observed when the animals were pretreated with 60mg/kg [373].

As pointed out before, reduced pericyte coverage not only facilitates metastatic dissemination by reducing physical restrains, but is also often paralleled by vessel leakiness and hypoxia [321]. Hypoxia induces HIF-driven transcriptional programs able to induce EMT and thus, the upregulation of a number of pro-metastatic genes such as protein-lysin-6-oxidase (LOX), c-MET and AXL [374-376]. In addition, hypoxia induced by anti-angiogenic therapy enriched for cancer cells with stem cell-like phenotype and function [377]. Experimentally, administration of anti-angiogenic compounds with therapeutics targeting pro-invasive escape pathways could counteract invasion and metastasis induced by anti-angiogenic therapies. Co-therapy with c-MET inhibitors prevented increased local invasiveness, lymph node and distant metastasis induced by anti-angiogenic compounds in the Rip1Tag2 mouse model [364, 368]. Regarding this data, the small-molecule kinase inhibitior cabozantinib is of interest, since it displays inhibitory actions against VEGFR2, c-MET and AXL and in contrast to sunitinib it did not enhance lung metastasis in a breast cancer xenograft model [84]. In addition to hypoxia-induced invasion programs, interesting work from the Bergers laboratory has recently demonstrated a hypoxia-independent mechanism of increased invasiveness upon anti-angiogenic therapy. In GBM mouse models, VEGF-A induced VEGFR-2 phosphorylation and recruited the phosphatase PTP1B to VEGFR-2/c-MET heterdimeric receptors expressed on cancer cells. PTP1B in turn inhibited hepatocyte growth factor (HGF) induced c-MET phosphorylation and downstream signaling. In this line, anti-angiogenic therapy interfering with the VEGF-A/VEGFR-2 pathway counteracted VEGFR-2 mediated c-MET inhibition and increased invasiveness along with the induction of an EMT-like process [378].

At last, despite the availability of an overwhelming amount of literature investigating a potential pro-invasive effect of anti-angiogenic therapies, data addressing this question in patients are limited. As pointed out before, in GBM patients this pro-invasive phenotype has been demonstrated [362]. Outside the CNS, however, pro-invasive effects in terms of accelerated tumor progression or reduced survival has not been observed when following up patients with RCC after sunitinib treatment [379]. Considering the plethora of contradictory results, research evaluating potential pro-invasive actions of this class of drugs should therefore accompany large clinical trials. This would potentially shed light on the relevance of these preclinical findings.

2   Aim of the study

Targeting tumor angiogenesis has been shown to provide clinical benefit to patient with certain types of solid tumors. PNETs belong to a group of tumor types, which seems to respond remarkably well to anti-angiogenic therapeutics. Nevertheless, sunitinib, the current anti-angiogenic compound of choice for the treatment of advanced PNETs, induces a considerable rate of side effects. In addition, the combination of sunitinib with standard chemotherapy is often hampered due to adverse events leading to discontinuation of the treatment. In contrast, the relatively new anti-angiogenic TKI nintedanib showed high efficacy in xenograft transplantation models and a remarkable positive side effect profile, even when combined with chemotherapy.

Whereas anti-angiogenic therapy in general increases PFS, OS benefits are only observed in a subset of tumor types. This observation suggests the development of mechanisms rendering tumors resistant to angiogenesis inhibition. A better understanding of these resistance mechanisms might lead to meaningful combination treatments and thus will eventually improve patient care in oncology.

In my MD-PhD thesis, I have employed preclinical mouse models of PNET and breast cancer to:

- In depth characterize nintedanib's efficacy *in vivo*

- Unravel mechanisms of resistance to nintedanib (and sunitinib) *in vivo*

- Interfere with the identified resistance mechanisms by performing combination treatments together with nintedanib *in vivo*

3   Results

3.1   The Rip1Tag2 transgenic mouse model

Ruben Bill and Gerhard Christofori

Department of Biomedicine, University of Basel, 4058 Basel, Switzerland

- in preparation -

Invited book chapter for the edition of "Tumor angiogenesis assays" of the lab protocol series "Methods in Molecular Biology"

3.1.1 Abstract

The Rip1Tag2 transgenic mouse model of β-cell carcinogenesis has been instrumental in studying various aspects of tumor angiogenesis and in investigating the response to anti-angiogenic therapeutics. Thereby, the in depth assessment of blood and lymphatic vessel phenotypes and functionality represent key experiments. In this chapter, we describe protocols to assess tumor blood vessel morphology (pericyte coverage), functionality (perfusion, leakiness and hypoxia), lymphatic tumor coverage and tumor cell proliferation and apoptosis based on immunofluorescence analysis.

3.1.2 Introduction

Generated in 1985, the Rip1Tag2 transgenic mouse model of PNETs has ever since served as a versatile tool to study various aspects of tumor angiogenesis. In this model, the oncogene simian virus 40 large T-antigen (*Tag*) is expressed under the control of the rat insulin promoter (*Rip*) leading to multifocal development of insulin-producing β-cell carcinoma (insulinoma) in the islets of Langerhans of the pancreas [246]. Whereas all β-cells present in the approximately 400 islets of Langerhans contain the property to express the *Tag* oncogene at birth, stochastically occurring additional genetic and epigenetic events are required for successful stepwise carcinogenesis. Such an event important for tumor progression is for example the acquired capability to express insulin-like growth factor 2 (IGF2). Only about 1-2% of all islets eventually progress into highly vascularized solid tumors [248]. Finally, Rip1Tag2 mice start to die at around week 12 due to the tumors' excessive production of insulin resulting in fatal hypoglycemia (see **Notes** 1 and 2, [380]).

It became quickly apparent that primary tumor growth in the Rip1Tag2 mouse model is highly angiogenesis dependent. The acquisition of new blood vessels (*i.e.* the angiogenic switch) has been shown to be a critical event in order to progress from hyperplastic lesions to adenoma, which is a prerequisite for further development into invasive tumors (carcinoma) [249]. Furthermore, tumor growth was prevented in Rip1Tag2 mice with a β-cell specific deletion of the major pro-angiogenic molecule VEGF-A [252]. In the following years, the Rip1Tag2 model has revealed important insights into the functions of key angiogenesis-mediators by their β-cell specific deletion or overexpression [184, 256, 257, 267, 336, 381, 382]. In addition, this PNET mouse model has proven to be highly instrumental for preclinical validation of eligible compounds, which were subsequently successfully implemented into clinical practice [258].

Tumor angiogenesis is generally considered to be overshooting, resulting in abnormal vessels with poor pericyte coverage and a fenestrated endothelial monolayer resulting in leakiness and, thus, increased interstitial fluid pressure. Intriguingly, despite an abundance of pro-angiogenic factors, regional differences in blood vessel perfusion can result in hypoxic areas with low pH [320]. The delivery of chemotherapeutic agents to tumors is hampered because of hypo-perfused areas and increased interstitial fluid pressure caused by an abnormal vasculature. Vessel-normalizing interventions have been shown to increase chemotherapy availability in tumors [319, 325]. Key to the identification of quantitative and qualitative (*i.e.* vessel functionality) tumor blood vessel characteristics are methods based on immunofluorescence (IF) analysis.

In the present chapter, we aim to provide a simple workflow for routine assessment of the most important parameters of tumor blood vessel characteristics. Analysis of blood vessel MVD (*i.e.* the number of CD31^{+} vessels per tumor area) provides quantitative insights into the extent of angiogenesis. This can be further complemented by injecting fluorescently labeled Lectin (typically Fluorescein/FITC or Texas Red) into the mice prior to euthanization to label the vessel lumen and to assess the percentage of actually patent (*i.e.* perfused) tumor blood vessels. Similarly, leaky vessels are identified by extravasation of FITC-labeled Dextran. Pericytes are perivascular cells sitting on the abluminal site of endothelial cells, sharing a common basement membrane and stabilizing the vessel tube. To date, a marker exclusively expressed by pericytes has not been identified [161]. However, the marker neuron-glia antigen 2 (NG2) known to be expressed by pericytes is commonly used in our laboratory to assess pericyte coverage of tumor blood vessels in the Rip1Tag2 model when combined with a staining for CD31 [380]. In contrast, staining for α-smooth muscle actin, a marker often used to visualize perivascular cells, in our hands only results in a strong staining around large blood vessels, but not capillaries. To estimate the consequences of an experimentally altered MVD on tumor oxygenation, the aforementioned characterization of the tumor vasculature can be complemented with the assessment of tumor hypoxia. Intraperitoneally (i.p.) injected pimonidazole hydrochloride (HCl) is chemically reduced in hypoxic areas, and the resulting pimonidazole adducts can be visualized by IF staining.

Lymphatic vessels represent an alternative route for metastatic spread in addition to tumor blood vessels. Indeed, employing the Rip1Tag2 mouse model, it has been shown that tumor cell specific overexpression of the lymphangiogenesis inducing VEGF-family member VEGF-C massively increased peritumoral lymphatic coverage and promoted lymph node metastasis [382]. Assessing peritumoral lymphatic coverage therefore provides insights into lymphangiogenesis-promoting or -inhibiting mechanisms (see **Note** 3).

The ultimate read out of most experimental manipulations in the Rip1Tag2 mouse model is the impact on tumor volumes (see **Note** 4). In parallel to this, analysis of proliferation by staining for phospho-histone H3 (pH3) and of apoptosis by staining for cleaved caspase 3 (cCasp3) can give first mechanistic insights into reasons underlying a potentially altered tumor burden. In addition, performing a combination staining for CD31 and cCasp3 reveals the amount of dying endothelial cells.

The methods presented in this chapter should allow a routine workflow as a basis for further morphological, biochemical and molecular biology experiments.

3.1.3   Materials

Rip1Tag2 mice

Rip1Tag2 mice start to die at the age of 12 weeks. Due to this short survival, the mouse colony has to be constantly bred to prevent loss of the colony. Additionally, due to ethical reasons, only heterozygous transgenic males can be used for breedings. Rip1Tag2 mice should be strictly kept in a C57Bl/6 background, since the genetic background of the mice significantly affects tumorigenesis [383]. Therefore, heterozygous transgenic males are bred with wild-type C57Bl/6 females. Both, heterozygous females and males are used for experiments. Although no striking gender-dependent phenotypic differences in terms of tumor development have been observed, it is recommended to stratify experimental groups based on sex. Genotyping is performed by employing the primers Tag1 5'GGACAAACCACAACTAGAATGCAG and Tag2 5'CAGAGCAGAATTGTGGAGTGG. The resulting PCR product has a size of 449kb.

Lectin or Dextran injection and mouse perfusion

1. Fluorescein Lycopersicon Esculentum (Tomato) Lectin (FITC-Lectin), Vector Laboratories/ Reactolab (FL-1171), dilute in sterile PBS to 1mg/ml
2. Dextran Fluorescein (FITC-Dextran), Life technologies, anionic, Lysine fixable, 70'000MW, (D-1822), dilute in sterile PBS to 1.25mg/ml
3. Pimonidazole Hypoxyprobe TM-1 Omni Kit, pimonidazole HCl plus rabbit antisera, (HP3-100 Kit), dilute in sterile PBS to 6mg/ml.
4. Ethanol 70% spray
5. Surgical scissors
6. Forceps
7. Insulin syringe, BD Micro-Fine, 29G (324824)

8. Anesthetic, according to the licensed compounds for terminal anesthesia (e.g. Pentobarbital)

9. "Butterfly", BD Valu-Set, 25G (387425)

10. Syringe, 10ml

11. PBS (sterile for diluting Lectin, Dextran and Pimonidazole; non-sterile for mouse perfusion and tissue processing)

12. PBS/4% PFA

Tissue fixation and cryopreservation

1. PBS/4% PFA

2. PBS/20% sucrose

3. Optimal cutting tempterature (OCT) compound, Tissue-Tek (4583)

4. Embedding Mold for frozen tissues

5. Dry ice pellets

6. Ethanol 100%

Cryosectioning and immunofluorescence staining

1. Cryotome

2. Microscope slides

3. Cover slips

4. Liquid blocker, Super Pap Pen, Daido Sangyo Co., Ltd. Tokyo, Japan

5. PBS (non-sterile)

6. PBS/0.2% Triton X-100

7. PBS/5% or 20% normal goat serum (ngs)

8. DAPI 1:10'000, Sigma, D9542

9. Dako Fluorescent Mounting Medium, Dako, S3023 (see **Note** 5)

10. primary antibodies, dilution:

   CD31, rat, BD Pharmingen, 550274, 1:50

   Cleaved Caspase-3 (cCasp3), Cell Signaling, 9664, 1:50

   Insulin, guinea pig, Dako, A0564, 1:200

   LYVE-1, rabbit, RELIATech, 103-PA50S/0412P02-2, 1:200

   NG2, rabbit, Chemicon, AB5320, 1:100

   Phospho Histone H3 (pH3), rabbit, Millipore, 06-570, 1:200

   Pimonidazole, rabbit, Hypoxyprobe Inc., antibody included in "Pimonidazole Hypoxyprobe TM-1 Omni Kit", 1:25

   SV40 Large T antigen, rabbit, Santa Cruz, sc-20800, 1:50

11. Secondary antibodies, Alexa labeled, Molecular probes/Life technologies

3.1.4 Methods

*Injections, systemic perfusion and harvest of pancreas (*see **Note** 6*)*

1. Inject all animals with pimonidazole 60mg/kg (inject 100µl per 10g mouse body weight of a 6mg/ml solution) intraperitoneally 1-2 hours prior to euthanization (see **Note** 7).

2. If the anesthetic licensed for terminal anesthesia provides fast narcosis, the intravenous (i.v.) injection of FITC-Lectin or FITC-Dextran can be performed in non-anesthetized animals, followed by anesthesia (methods adapted from refs [325, 363, 384]).

3. For the injection with FITC-Lectin continue with step 3a, for FITC-Dextran with step 3b.

   a. Inject 100µl of FITC-Lectin i.v. into the tail vein (=0.1mg/mouse, perfuse after 10 minutes)

   b. Inject 200µl of FITC-Dextran i.v. into the tail vein (=0.25mg/mouse, perfuse after 5 minutes)

4. For the perfusion, anaesthetize the mouse with ultra-deep (terminal) isoflurane anesthesia (see **Note** 8). Pin the extremities of the animal on a dissection pad, spray it with ETOH 70% and incise the skin and the underlying peritoneum with a horizontal cut immediately *caudal* of the costal arch using scissors. Now, the *caudal* surface of the diaphragm should be visible. Grab the *processus xiphoideus* with forceps and induce a pneumothorax by incision of the diaphragm. The resulting collapse of the lungs prevents them from damage potentially caused during the dissection procedure. Introduce the scissors carefully along the interior surface of the ribs in direction of the axilla and cut the ribs. Repeat this on the other side. Free the resulting flap containing the cut ribs and the *sternum* from remaining caudal attachments to the diaphragm, fold it and pin it over one of the shoulders on the surface. Now, a free look on the collapsed lungs and the heart should be possible. Introduce the needle of the butterfly into the left ventricle of the heart (due to the arterial blood it shows a lighter red color than the right ventricle) and cut into the right atrial auricle to open the circulation and provide an opening for the perfused solution (For the perfusion of FITC-Lectin injected animals continue with step 4a., for FITC-Dextran with step 4b.)

   a. Perfuse the FITC-Lectin injected animal slowly with 10ml ice-cold PBS/4% PFA for immediate fixation

   b. Perfuse the FITC-Dextran injected animals slowly first with 10ml ice-cold PBS to wash out the intravascular Dextran, immediately followed by the perfusion with 10ml ice-cold PBS/4% PFA for fixation (see **Notes** 9 and 10)

5. In order to dissect the pancreas (and other abdominal organs such as the liver), widen the existing abdominal incision to have free access to the abdominal organs. Move the intestine to the right side of the animal and identify the spleen. Pull the spleen carefully. This helps to identify the pancreas, which is the fatty tissue containing the reddish insulinoma and is connected via the *ligamentum pancreato-lienale* to the spleen. Dissect the pancreas, rinse it briefly in PBS to get rid of blood, measure the diameter of the macroscopic tumors using a ruler and fix the tissue as soon as possible in cold PBS/4% PFA. Incubate the tissue in PBS/4% PFA for 2 hours while rotating at 4°C, followed by over-night incubation at 4°C in PBS/20% sucrose.

6. On the next day, prepare a bath with dry ice pellets covering the floor of a Styrofoam container and add Ethanol 100% (see **Notes** 11 and 12). Snap-freeze the tissues in optimal cutting temperature (OCT) freezing solution in the ethanol/ dry ice bath. Store samples at -80°C.

Cryosectioning and IF staining

1. Put frozen OCT blocks at -20°C (into cryotome or freezer) >30 min before starting sectioning (see **Notes** 13, 14 and 15).

2. Cut 7-10µm thick sections (see **Note** 16).

3. Let it dry for at least 30 minutes.

4. Encircle the sections with a liquid blocker and let it dry for some additional minutes.

5. Rehydrate in PBS 3 x 5 minutes (see **Note** 17).

6. Permeabilize in PBS/0.2% Triton X-100 for 20 minutes.

7. Wash in PBS 3 x 5 minutes.

8. Block with blocking buffer (PBS/5% ngs) for 1 hour in a humid chamber. For stainings with the anti-cCasp3 antibody perform the blocking with PBS/20% ngs.

9. Replace the blocking buffer with the desired antibodies diluted in blocking buffer. Incubate in a humid chamber over night at 4°C (see **Note** 18).

10. On the next morning, wash the specimen 3x 5 minutes in PBS at room temperature

11. Incubate for 1 hour at room temperature with secondary antibodies directed against the species of the corresponding primary antibodies and labeled with Alexa fluorochroms suitable for the filters of the fluorescence microscope available.

12. Wash in PBS 3 x 5 minutes.

13. Incubate with DAPI diluted 1:10'000 in PBS at room temperature for 10 minutes in a humid chamber.

14. Wash in PBS 3 x 5 minutes.

15. Mount slides with cover slips using DAKO mounting medium (see **Note** 19). Avoid air bubbles.

16. Let slides dry (in the dark) for some hours at room temperature. Then transfer them to 4°C and analyze the slides within few days.

17. We recommend acquiring the images using a 20x magnification.

18. For image analysis we routinely employ ImageJ image processing and analysis software.

3.1.5 Notes

1. Although the Rip1Tag2 mice used in different laboratories around the globe stem from the same founder line, breeding in isolation over years has led to interesting phenotypic differences even when kept in a pure C57Bl/6 background. Notable differences in survival, lymph node and liver metastasis at baseline and upon anti-angiogenic therapy, and the extent of intra- and peritumoral lymphangiogenesis can be detected when screening the literature [267, 342, 363-366, 368, 380].

2. Rip1Tag2 mouse survival can be extended by the administration of food pellets consisting of 60% glucose starting from the age of around 9 weeks.

3. Insulinoma in the Rip1Tag2 model only rarely display intratumoral lymphatic vessels. Instead, they can be found at peritumoral location. Whereas peritumoral lymphatic vessels in Rip1Tag2 single transgenic mice only cover less than 10% of the tumor circumference, almost complete lymphatic coverage can be achieved by intercrossing Rip1Tag2 mice with Rip1-VEGF-C transgenic mice [380, 382].

4. Tumor volumes of macroscopic tumors (≥1mm diameter) are assessed by measuring the diameter of each tumor, calculate the volume assuming a spherical shape (volume = $(4/3)*\pi*(diameter/2)^3$) and summing up the resulting volumes per mouse.

5. DAKO mounting medium can be replaced with Mowiol.

6. Blood vessel perfusion and leakiness can in principle be analyzed in the same mouse by co-injecting FITC-Dextran and Texas-Red labeled Lectin. However, this reduces the possibilities of future IF co-stainings, since the "green" and the "red" channel are occupied in this setting. Additionally, please note that DAPI is always accompanying the stainings. Therefore, we usually split the mouse cohorts into 3 groups. All the animals receive an injection of pimonidazole, one-third of the animals FITC-Lectin or FITC-Dextran, respectively, and one-third pimonidazole only. Furthermore, tissues from the latter group can be conveniently used for RNA or protein isolation, since the pimonidazole injection alone does only require a (immediate) post-dissection fixation in PBS/4% PFA, but not a systemic PBS/4% PFA perfusion prior to organ dissection, as it is the case for FITC-Lectin and FITC-Dextran injected animals.

7. Pimonidazole HCl displays a half-life of about 0.25 h in mice. To avoid artifacts introduced by hypoxia/anoxia during the euthanization and dissection procedure, pimonidazole levels in the systemic circulation should therefore be sufficiently low at time of euthanization. Therefore, the manufacturer recommends to dissect the mice 1-2 h (the chosen timepoint should be strictly kept for all the animals in the same experiment) after injection, using a fast euthanization technique (cervical dislocation rather than CO_2 suffocation) [385].

8. In principle, mice could also be perfused shortly after death by CO_2 suffocation. If mice are co-injected with pimonidazole however, CO_2-suffocation should be avoided (see **Note** 7). In this case, any terminal anesthesia method licensed by the relevant veterinary office can be employed to obtain a humane perimortal perfusion.

9. Changing from the syringe containing 10ml PBS to the 10ml syringe containing PBS/4% PFA should ideally be performed by a second assisting person. Like this, the needle can remain in the exact same position in the left ventricle preventing the creation of holes in the myocardium of the left ventricle that could reduce the perfusion quality.

10. If the perfusion with PBS is incomplete, remaining intravascular FITC-Dextran can be distinguished from extravascular (*i.e.* leaking) FITC-Dextran by visualizing the blood vessels with a staining for the endothelial cell marker CD31.

11. Styrofoam containers, which are often used to ship laboratory materials, can easily be recycled for the purpose of freezing tissues. Please make sure that you take a container that does not leak.

12. To prevent vanishing of markings made on the embedding molds, use an alcohol resistant lab marker and fill the ethanol only to a level below the markings.

13. Prevent prolonged handling of OCT blocks at room temperature because the OCT solution should not thaw. If rapid transfer from the -80°C freezer to the cryotome or -20°C freezer is not possible, transport the OCT blocks cooled.

14. Short term storage of OCT blocks at -20°C for a few days is possible, although not recommended. In addition, avoid leaving the OCT blocks in the cryotome over night, since some machines display temperature fluctuations.

15. Protect sections from light throughout the whole experiment, especially if FITC-Lectin or FITC-Dextran ist present in the respective tissue.

16. Since cutting sections of larger experiments containing numerous OCT blocks often takes some hours, the time the different sections are drying may vary. To account for potential "batch effects", the order of the OCT blocks processed should not be according to the experimental groups, but random instead.

17. All washing and the permeabilization steps (if not otherwise indicated) can be performed by putting the sections as a batch in one container gently shaking on a tumbling table at room temperature.

18. Alternatively to over night incubation with the primary antibodies, the incubation can also be shortened to 1 hour at room temperature in a humid chamber (do not forget to protect the specimen from light).

19. Insulinoma can be easily distinguished from the surrounding exocrine pancreas based on the more dense distribution pattern of the DAPI stained nuclei. Pancreatic lymph nodes display a densely packed nuclei distribution pattern as well, but nuclei are more densely distributed and smaller than observed in insulinoma. However if required, tumor cells can be specifically visualized by staining for insulin or SV40 Large T antigen. Importantly, it has been described that a subpopulation of insulinoma in the Rip1Tag2 mouse model lose insulin expression but remain positive for SV40 Large T antigen expression [386]. Therefore, SV40 Large T antigen appears to be a more sensitive marker to detect tumors (and metastases) in this model. On the other hand, the quality of the IF staining on cryosections for insulin is significantly better than that for SV40 Large T antigen.

3.2 Nintedanib is a highly effective therapeutic for neuroendocrine carcinoma of the pancreas (PNET) in the Rip1Tag2 transgenic mouse model

Ruben Bill[1*], Ernesta Fagiani[1*], Adrian Zumsteg[1#], Helena Antoniadis[1], David Johansson[1], Simon Haefliger[1], Imke Albrecht[1#], Frank Hilberg[2], and Gerhard Christofori[1]

[1]Department of Biomedicine, University of Basel, 4058 Basel, Switzerland
[2]Boehringer Ingelheim Austria RCV GmbH & Co KG, Vienna, Austria
[#]Current addresses: (A.Z.) Covagen AG, 8952 Schlieren, Switzerland; (I.A.) Drug Discovery Biology, Actelion Pharmaceutical Ltd, Allschwil, Switzerland

*These authors contributed equally to this work

3.2.1 Statement of Translational Relevance

Pancreatic neuroendocrine tumors are often diagnosed at an advanced stage and thus remain a deadly disease with restricted systemic treatment options. Nevertheless, this group of cancers in advanced stages has proven to be sensitive to the anti-angiogenic tyrosine kinase inhibitor sunitinib – yet with considerable side effects. On the other hand, the broad-spectrum anti-angiogenic tyrosine kinase inhibitor nintedanib has displayed an encouraging anti-cancer and safety profile in preclinical cancer models and in cancer patients. We have employed the Rip1Tag2 transgenic mouse model of hormone-positive neuroendocrine carcinoma of the pancreas to test the efficacy of nintedanib in treating insulinoma in a preclinical setting. This mouse model recapitulates multistage neuroendocrine carcinogenesis and the co-evolution of the tumor microenvironment with the tumor cells. Notably, it has been shown highly predictive in translating preclinical drug evaluation into successful clinical application, e.g. as demonstrated in the cases of sunitinib and mTOR inhibition.

3.2.2 Abstract

PNETs represent a rare but challenging heterogeneous group of cancers with an increasing incidence over the last number of decades. Herein, we report an in depth evaluation of the new anti-angiogenic small-molecule TKI nintedanib in the preclinical Rip1Tag2 transgenic mouse model of neuroendocrine carcinoma of the pancreas (insulinoma). We have assessed the anti-angiogenic and anti-tumor activity of nintedanib, in comparison to other anti-angiogenic TKI, by treating Rip1Tag2 transgenic mice with different treatment schedules complemented with histopathological, cell biological and biochemical analyses. Prolonged nintedanib treatment of Rip1Tag2 mice has led to a strong suppression of angiogenesis, accompanied by a reduced tumor burden, which translated into a significant prolongation of survival. Despite nintedanib's inhibitory action on perivascular cells, the blood vessels remaining after therapy displayed a considerably mature phenotype with tight perivascular cell coverage and preserved perfusion. Nintedanib treatment did not increase local tumor invasiveness or metastasis to the liver and pancreatic lymph nodes - a phenomenon which has been observed with anti-angiogenic treatments of Rip1Tag2 transgenic mice in other laboratories. In contrast to the strong reduction in blood microvessel densities, nintedanib did not have any impact on tumor lymphangiogenesis. Based on our findings we propose the clinical evaluation of the anti-angiogenic drug nintedanib as a new treatment modality of PNET patients, notably in a direct comparison to already established therapeutic regimen such as sunitinib.

3.2.3 Introduction

PNETs, although representing a minority of pancreatic tumors, remain a therapy-challenging heterogeneous group of tumors with increasing incidence over the last decades [262]. Whereas 45-60% of PNETs are non-functional, 40-55% produce a variety of hormones leading to different clinical presentations, e.g. hypoglycemic syndrome in the case of insulin-producing PNETs (insulinoma) [264]. Aside from cytoreductive surgery, somatostatin analogs, peptide receptor-targeted radiotherapy and systemic chemotherapy, management of advanced PNETs involves targeted therapies, such as the mTOR inhibitor everolimus or the anti-angiogenic small-molecule tyrosine kinase inhibitor sunitinib [264]. In a phase III clinical trial, sunitinib was shown to be highly effective and significantly prolonged progression-free and overall survival of PNET patients. This study even had to be discontinued early, because of a significantly worse clinical outcome in the placebo group. However, a number of patients experienced treatment-related side effects, such as grade 3 or 4 hypertension and neutropenia in 10 and 12% of patients respectively [64]. Reducing adverse events is of particular importance in this cancer entity, since patients usually undergo long-term therapy and usually experience good quality of life even without treatment until late in the course of the disease [263].

Despite the encouraging results derived from numerous preclinical studies, anti-angiogenic therapies targeting mainly the VEGF/VEGFR axis have widely failed to substantially increase patient survival in a large number of cancer types [297]. In mouse models, the upregulation of alternative pro-angiogenic factors, such as FGFs, PDGFs, Bv8 and others, has been shown to mediate the resistance to blocking the VEGF-A/VEGFR-2 axis. Hence, a simultaneous targeting of the VEGF and the FGF receptor families and other alternative signaling pathways may lead to an improved clinical outcome [162, 270, 333, 334]. Nintedanib (BIBF1120), a small-molecule kinase inhibitor that targets not only VEGFRs and PDGFRs but also FGFRs and c-SRC [70, 103], has recently been shown to yield significant anti-cancer effects in a variety of preclinical cancer models and in NSCLC patients [70, 71, 110]. In a recent phase III clinical trial of nintedanib in NSCLC patients (LUME-Lung 1), the majority of side effects ascribed to nintedanib were of gastrointestinal origin (diarrhea, nausea, vomiting) and reversible elevations in liver enzymes. Hypertension and white blood cell alterations were not pronounced in the cohort treated with nintedanib plus standard chemotherapy versus the cohort treated with chemotherapy alone [71]. Moreover, treatment of IPF in a randomized, double-blind phase III trial has not resulted in any severe adverse effects [72].

The apparent discrepancies between the efficacies of anti-angiogenic therapies in

preclinical models and in patients may be attributed to the altered stromal microenvironment that human tumor cells encounter in immunodeficient mice, frequently aggravated by an inadequate subcutaneous (heterotopic) implantation of cancer cells of other organs. Especially when evaluating drugs that mainly target the tumor microenvironment, as is the case with anti-angiogenic therapies, these artefacts might be of significant importance [70, 298]. A solution to this problem is the use of transgenic animal models that stochastically develop endogenous tumors in a robust and reproducible manner. For example, the Rip1Tag2 transgenic PNET mouse model expresses the oncogenic SV40 Large T-antigen (*Tag*) under the control of the rat insulin promoter (*Rip*) and reproducibly elicits multi-stage tumorigenesis of the insulin-producing β-cells of the pancreas [246, 254]. The stochastic and stepwise development enables the tumor microenvironment to co-evolve with the cancer cells, thus recapitulating the patient situation. Indeed the RipTag2 transgenic model has proven a versatile and robust preclinical model that reliably mimics human insulinoma. For example, SV40 Tag binds and inactivates the retinoblastoma (RB) and the p53 tumor suppressor gene products, which are found dysregulated in a large subset of human PNETs as well (18, 19). Rip1Tag2 mice develop PNETs in a multistep fashion. Although SV40 Large-T antigen serves as the initial oncogenic driver presumably in all β-cells present within the islets of Langerhans of the pancreas, stochastically occurring additional genetic alterations lead to hyperplastic lesions in only some of the islets. A proportion of these preneoplastic lesions further progress and induce the formation of new blood vessels (angiogenic switch). Only few of these angiogenic hyperplastic islands progress first to adenoma and subsequently become invasive (carcinoma) [259, 260]. The Rip1Tag2 transgenic mouse model has been used for the testing of numerous experimental therapies and has been instrumental in predicting the successful application of novel therapies in clinical trials [258]. For example, preclinical results derived from combined anti-VEGFR and anti-PDGFRβ treatments of the Rip1Tag2 transgenic PNET mouse model have paved the way for the successful clinical application of sunitinib in PNET patients [64, 104, 267]. Finally, the use of Rip1Tag2 transgenic mice has led to the use of radio- labeled Exendin-IV to non-invasively image insulinoma in patients, a method that is now in clinical use [387].

Here, we report an in-depth preclinical characterization of nintedanib in the Rip1Tag2 transgenic mouse model of neuroendocrine carcinoma of the pancreas. We report a strong anti-angiogenic response, which translates into significantly reduced tumor growth and prolonged survival. Despite a vast reduction in microvessel density upon extended nintedanib treatment, only a slight increase in tumor hypoxia is observed. In addition, the remaining tumor blood vessels displayed mature characteristics. Furthermore, we did not find increased local invasiveness or metastases in the liver and lymph nodes in any of

thetreatment regimens assessed. Based on the results we propose that nintedanib should be evaluated in clinical trials as a new treatment modality of PNET.

3.2.4 Results

3.2.4.1 *Nintedanib efficiently reduces tumor burden and prolongs survival*

We first investigated the gross effects of nintedanib on tumor growth in Rip1Tag2 transgenic mice. Mice were stratified (in a 1:1 ratio) according to sex and age, and littermates were balanced between the nintedanib and the vehicle-treated control group and then treated with 50mg/kg nintedanib daily *p.o.* beginning at the age of 9 weeks for 3 weeks, a time period in which tumor angiogenesis and tumor growth are highly active [255]. Nintedanib- treated mice showed a strong reduction in the total tumor burden per mouse, as well as less macroscopically detectable tumors (Figure 1A, B). In addition, the few macroscopically detectable tumors in nintedanib-treated animals were white, in contrast to the red, highly vascularized appearance of the tumors in vehicle-treated control animals, indicating decreased vascularization (Figure 1C). Next we assessed whether this dramatic reduction of primary tumor growth translated into a prolongation of survival of Rip1Tag2, as it has been observed for sunitinib with this mouse model [267]. Treatment with nintedanib (50mg/kg, 1x/d, *p.o.*) or placebo was initiated at the age of 10 weeks and continued open end. Animals were euthanized before suffering of hypoglycemia, by fulfilling the termination criteria as described in Materials and Methods. We observed a significant (log-rank test, P < 0.001) increase in the survival of the nintedanib-treated group (median survival 55 days on treatment) as compared to the vehicle-treated control group (median survival 24 days on treatment) (Figure 1D). Interestingly, tumors of nintedanib-treated animals displayed a white color even at the terminal stage (data not shown). Together, these results demonstrate an efficient anti- tumor effect of nintedanib in Rip1Tag2 mice by reducing primary tumor burden and significantly extending survival time.

3.2.4.2 *Reduced tumor blood vessel density correlates with increased tumor cell apoptosis*

To determine the anti-angiogenic capabilities of nintedanib, we quantified MVD by IF staining with the endothelial cell marker CD31 on 3 weeks nintedanib and placebo-treated tumors. Nintedanib treatment significantly reduced MVD by more then 50 percent (Figure 2A).
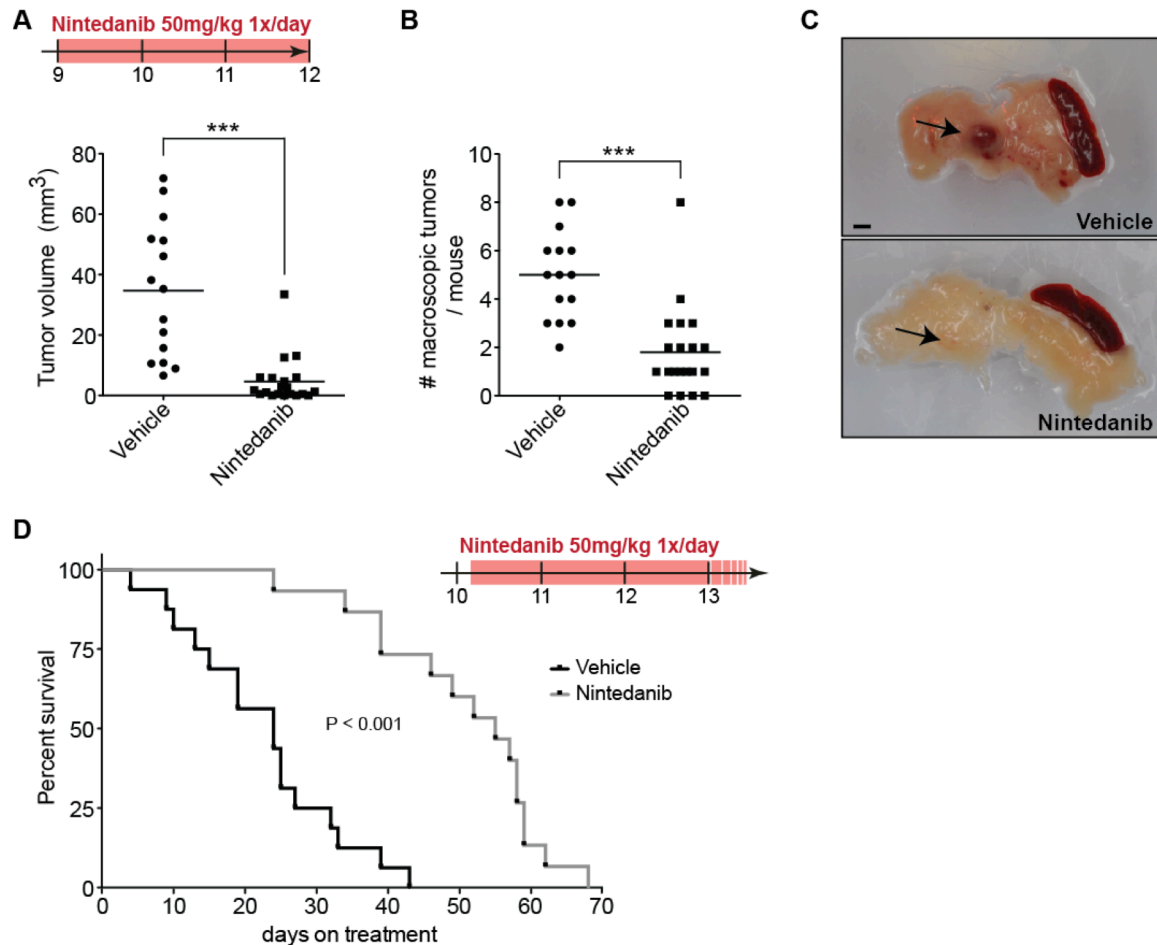
Figure 1. Reduced tumor volume and improved survival upon nintedanib treatment of Rip1Tag2 transgenic mice.
(A, B) Shown are total tumor volumes (A) and number of macroscopically detectable tumors (B) per Rip1Tag2 mouse treated for 3 weeks with nintedanib or vehicle control starting at the age of 9 weeks (pooled analysis of 3 independent experiments). Vehicle: n=15 mice, nintedanib: n=20 mice. Statistical analysis by Mann-Whitney *U* test; ***, P < 0.001. (C) Tumor nodules (arrows) in the pancreas of nintedanib-treated mice are barely detectable, because they are less frequent and of whitish color as compared to more frequent and red-colored tumors in vehicle-treated Rip1Tag2 mice. Scale bar, 2mm. (D) Survival trial of nintedanib treatment starting at the age of 10 weeks and 2 days. Median survival: vehicle group: 24 days on treatment, nintedanib group: 55 days on treatment. Vehicle n=16 mice, nintedanib n=15 mice. Log-rank test; P < 0.001.

Most anti-angiogenic drugs are known to mediate their anti-tumor activity by increasing apoptosis rather than inhibiting proliferation [255]. Consistently, cCasp3 IF staining revealed that the strong reduction of MVD was accompanied by an increase of tumor cell apoptosis in nintedanib-treated tumors as compared to controls (Figure 2B). This finding is supported by the increased levels of double-strand breaks as detected by TUNEL assay (Figure S1B) and the lack of a change in tumor cell proliferation as determined by pH3 staining (Figure S1C). These data suggest that the anti-tumor effect of nintedanib is mainly caused by increased tumor cell apoptosis triggered by the strong reduction of MVD. A direct effect of nintedanib on tumor cells is rather unlikely, since treatment of cultured insulinoma cells derived from Rip1Tag2 mice only reduced tumor cell numbers at high nintedanib concentrations (IC50 =

1.891µM) – levels that are not reached when treating mice daily with 50mg/kg [70, 103] (Figure S1D).
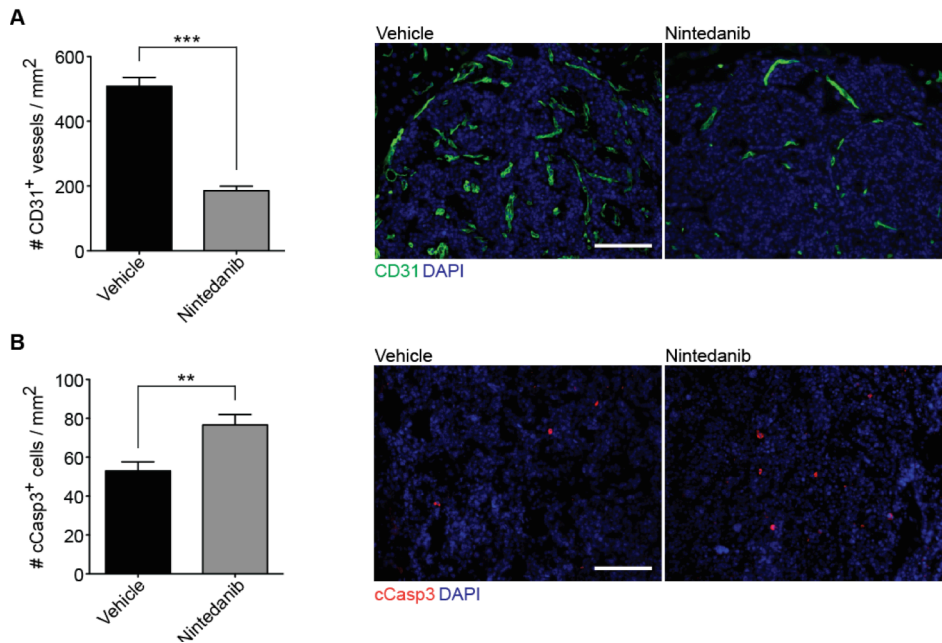
Figure 2. Nintedanib reduces microvessel density and induces apoptosis.
(A, B) Microvessel density (A) and apoptosis rate (B) of 3 weeks nintedanib-treated Rip1Tag2 tumors starting from 9 weeks of age were assessed by immunofluorescence staining for CD31 (green) and cCasp3 (red), respectively. Representative immunofluorescence pictures (20x magnification) are shown. Values were obtained by counting the number of vessels or apoptotic cells per area of each microscopic field of view. Bar graphs display means ± SEM and statistical analysis was performed using an unpaired Student *t* test. Vehicle: n=4 mice, nintedanib: n=7 mice. **, $P < 0.01$; ***, $P < 0.001$. Scale bars, 100µm.

3.2.4.3   Nintedanib-treated tumor blood vessels display a mature phenotype

Nintedanib not only inhibits signaling of VEGFRs and FGFRs, both important receptor families for vascular sprouting and therefore neovessel formation, but also targets PDGFRs [103]. Endothelial cell-derived PDGF-B attracts perivascular cells by binding to PDGFRβ expressed by them, and perivascular cells subsequently cover the abluminal surface of the vessel tube to mediate vessel stability and functionality [161]. Interestingly, the targeting of the perivascular cell coverage in addition to inhibiting endothelial cell sprouting has led to a beneficial anti-tumor effect [104]. We thus examined the phenotype of the tumor blood vessels present after 3 weeks of nintedanib treatment.
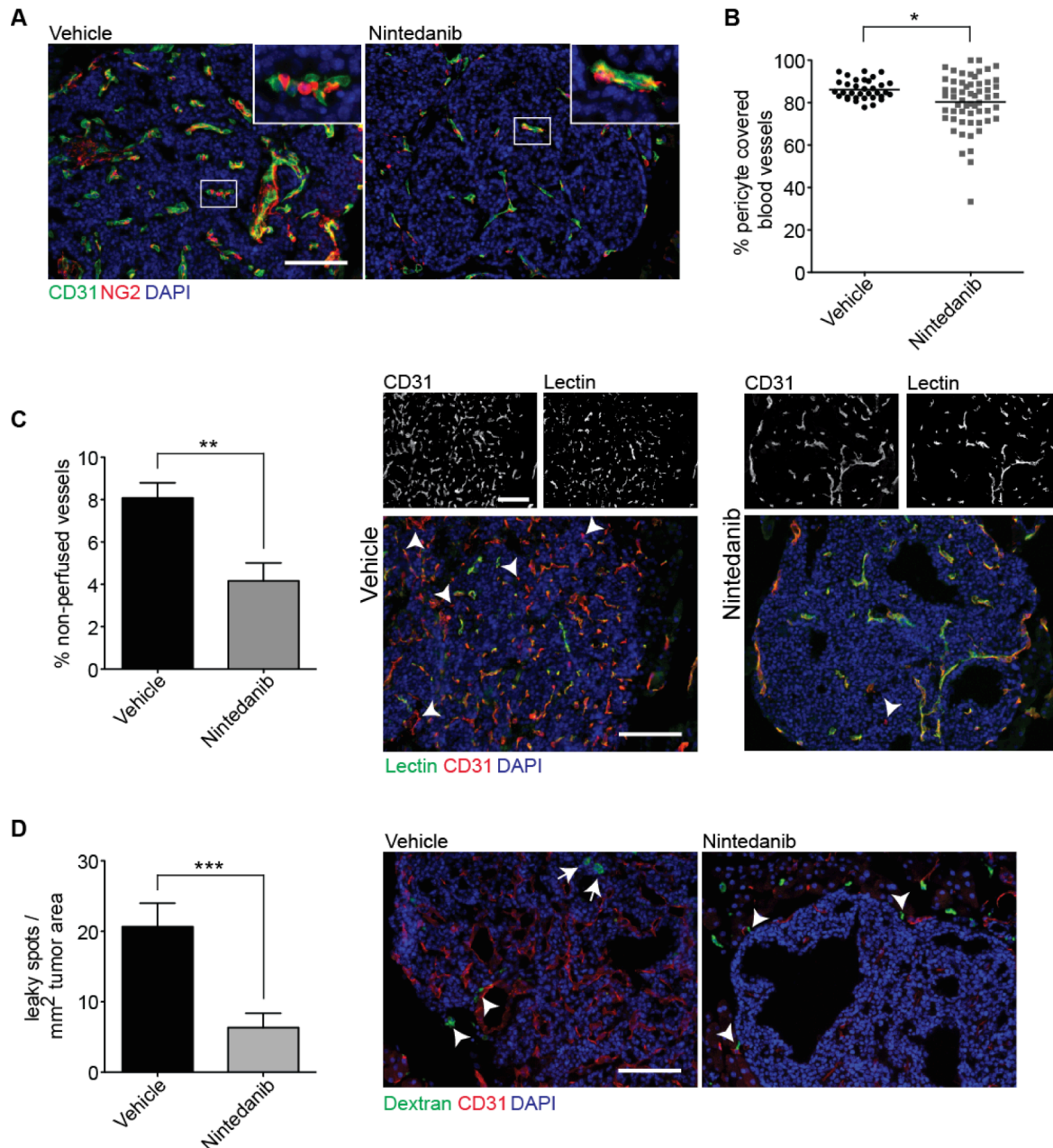
Figure 3. Blood vessels resisting nintedanib treatment display a mature phenotype and retain their function.

(A) Rip1Tag2 mice were treated with nintedanib for 3 weeks starting at 9 weeks of age. Representative images (20x magnification) of an immunofluorescence staining of pancreatic sections for tumor blood vessels (CD31, green), perivascular cells (NG2, red) and cell nuclei (DAPI, blue) are shown. Scale bars, 100µm. (B) Quantification and analysis of the relative localization of NG2^{+} perivascular cells to CD31^{+} blood vessels revealed in nintedanib-treated tumors a slightly reduced NG2^{+} perivascular cell-coverage of the remaining blood vessels. The percentage of perivascular cell-covered blood vessels are displayed per each field of view. Vehicle: n=4 mice, nintedanib: n=7 mice. Scale bars, 100µm. (C) Blood vessel patency was assessed by i.v. injection of Fluorescein-labeled Lectin (green) and immunofluorescence co-staining for CD31 (red) and cell nuclei (DAPI, blue). CD31^{+} blood vessels without signs of Lectin signal were compared to the total number of vessels per field of view and displayed as mean ± SEM. Representative images (20x magnification) are shown as single channels in gray scale and merged. Arrowheads point towards blood vessels without perfusion. Scale bars, 100µm. (D) Blood vessel leakiness was analyzed by injecting Fluorescein labeled Dextran (70kDa) i.v. Quantification and representative immunofluorescence images of Fluorescein-labeled Dextran (70kDa; green) and CD31+ blood vessels (red) are shown. Cell nuclei are visualized by DAPI staining (blue). The bar graph indicates the number of Dextran-positive intratumoral leaky spots per tumor area. Data are displayed as mean ± SEM per field of view.

Arrows point towards intratumoral leaky spots and arrowheads towards leaky spots along the tumor border (quantification not shown). Vehicle: n=6 mice, nintedanib: n=7 mice. Scale bar, 100µm. Statistical analysis was performed using an unpaired Student *t* test (B-D); *, P < 0.05; **, P < 0.01; ***, P < 0.001.

Perivascular cell coverage was assessed by staining for the perivascular cell marker NG2 [161]. Quantification of NG2 staining revealed that nintedanib strongly reduced the total number of NG2$^+$ perivascular cells per field of view (Figure 3A, Figure S2A). Moreover, while in vehicle-treated control tumors almost all perivascular cells found attached to vessels, with the loss of MVD upon nintedanib treatment an increased fraction of perivascular cells is found without contact to vessels (Figure 3A, Figure S2B). Still, the few blood vessels in nintedanib-treated tumors appeared to be substantially covered by perivascular cells and displayed a mature phenotype (Figure 3A, B). We thus tested the functionality of the treatment-resisting blood vessels by intravenously injecting Fluorescein- labeled Lectin shortly before sacrificing the animals. While in the vehicle-treated tumors only a minority of blood vessels was non-functional (~8%), nintedanib treatment further reduced the amount of non-functional vessels (~4%) (Figure 3C).

One important hallmark of the aberrant phenotype of tumor blood vessels is the increased leakiness leading to increased interstitial fluid pressure and thus reduced intratumoral delivery of chemotherapeutic agents [198, 326]. We have assessed blood vessel leakiness by intravenously injecting Fluorescein-labeled Dextran (70kDa) into vehicle and nintedanib-treated animals. Leaky spots, i.e. Fluorescein-labeled Dextran in the abluminal compartment of blood vessels identified by CD31 staining, were mainly detected at the tumor border. The quantification of leaky spots at the tumor border did not reveal a significant difference between vehicle and nintedanib-treated mice (data not shown). Interestingly though, nintedanib treatment reduced the amount of leaky spots in the tumor center (Figure 3D). Finally, we determined the consequences of the strong reduction in MVD observed in nintedanib-treated tumors on tumor oxygenation by pimonidazole staining. Three weeks of nintedanib treatment significantly increased the number of tumors with hypoxic areas and the hypoxic area fraction of hypoxic tumors (Figure S3A – C). However, approximately 85% of nintedanib-treated tumors did not display any signs of hypoxia, further indicating that nintedanib-resistant vessels are mature and fully functional. Tumor hypoxia has often been causally linked with the induction of local tumor invasiveness [267]. Interestingly therefore, hypoxia in nintendanib-treated insulinoma was often found close to clearly non-invasive tumor borders (Figure S3D).

In summary, nintedanib treatment leads to a strong reduction in the total amount of NG2$^+$ perivascular cells. Importantly, the blood vessels that survive nintedanib treatment are

63

patent and, thus, the strong reduction in MVD causes hypoxia only in a minority of tumors.

3.2.4.4   Tumor lymphangiogenesis is not affected by nintedanib treatment

In vitro kinase assays have shown that nintedanib inhibits VEGFR-3 at a concentration comparable to the concentration needed to inhibit VEGFR-2 signaling [70]. Although VEGFR-3 is expressed on blood vessel tip cells with substantial functions in blood vessel sprouting [191], its classical role is attributed to mediating lymphangiogenesis. Since the expression of VEGF-C, the cognate ligand of VEGFR-3, in tumor cells of Rip1Tag2;Rip1VEGF-C double-transgenic mice leads to increased tumor lymphangiogenesis and facilitates lymphogenic metastatic spreading, the inhibition of tumor lymphangiogenesis may represent an interesting therapeutic opportunity [382]. On the other hand, Sennino and colleagues reported that anti-angiogenic treatments of Rip1Tag2 mice increased tumor lymphangiogenesis and lymphatic metastasis [368].

To assess whether nintedanib affects tumor lymphangiogenesis in Rip1Tag2 transgenic mice, we first analyzed peritumoral lymphatic coverage of tumors of Rip1Tag2 mice treated with nintedanib for 3 weeks. Insulinoma were identified by insulin positivity and lymphatic vessels were visualized by immunofluorescent staining against LYVE-1. Insulinoma of 12 weeks old Rip1Tag2 mice were only rarely covered by lymphatic vessels, and this coverage was not influenced by nintedanib treatment (Figure 4A). We then investigated whether nintedanib affected peritumoral lymphatic coverage in the highly lymphangiogenic tumors of Rip1Tag2;Rip1-VEGF-C mice. Surprisingly, nintedanib treatment did not reduce the high lymphatic coverage of tumors in these mice (Figure 4B). From these data we conclude that nintedanib does not affect tumor lymphangiogenesis in this mouse model.
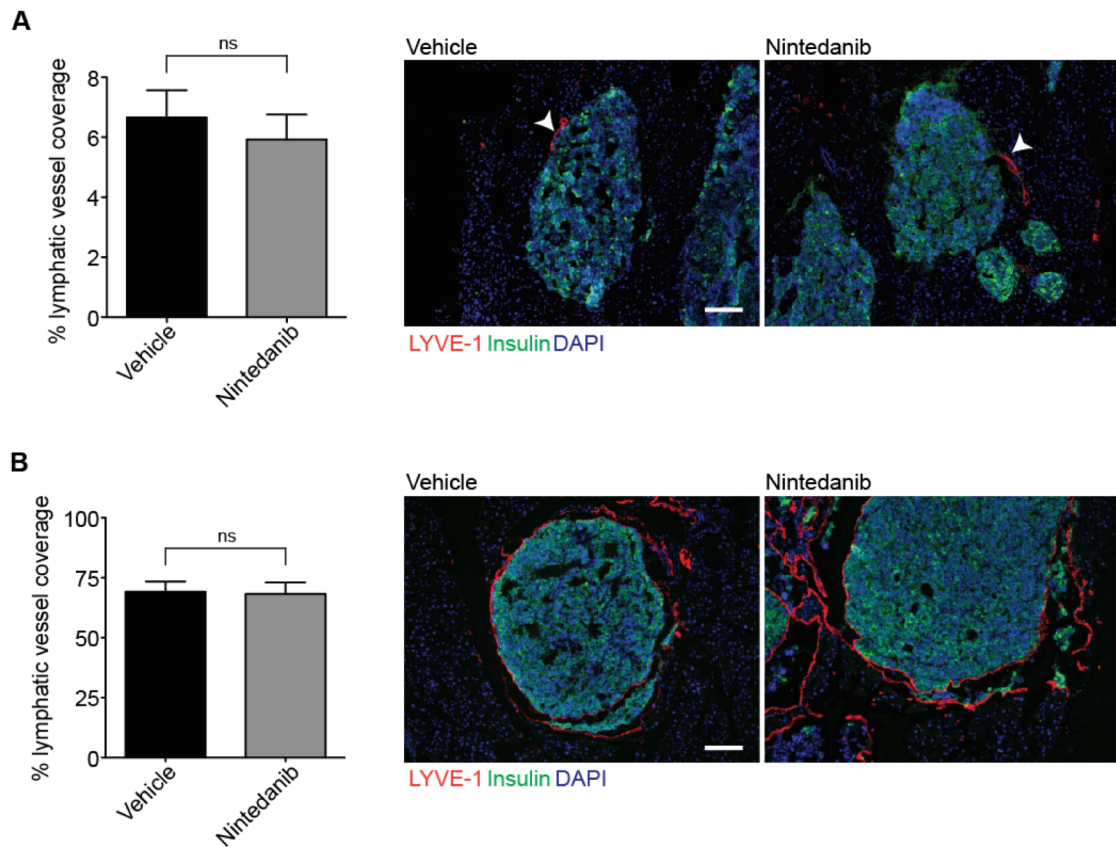
Figure 4. Tumor lymphangiogenesis is not affected by nintedanib treatment.
(A, B) The percentage of LYVE-1^{+} lymphatic endothelium (red, arrowheads) covering the perimeter of insulin-positive β-cell tumors (insulin, green) stained by immunofluorescence was quantified in Rip1Tag2 (A) and Rip1Tag2;Rip1-VEGF-C (B) mice treated for 3 weeks with nintedanib or vehicle control starting at 9 weeks of age. DAPI staining visualizes cell nuclei (blue). Representative microphotographs are shown (10x magnification). Bar graphs represent mean lymphatic tumor coverage per tumor ± SEM. Statistical analysis was performed using an unpaired Student *t* test. A, Vehicle: n=4 mice, nintedanib: n=7 mice; B, n=3 mice for each group. Scale bars, 100µm.

3.2.4.5   Nintedanib does not induce tumor invasiveness and metastasis

Recent reports have suggested that anti-angiogenic substances, such as sunitinib, can increase local invasiveness and lymph node and liver metastasis in Rip1Tag2 transgenic mice and other mouse models of cancer, raising major concerns about the use of anti-angiogenic therapies in patients [267, 270, 364]. We therefore analyzed the effect of different nintedanib treatment regimens on local invasiveness and distant metastasis by histological grading of hematoxylin and eosin-stained pancreas sections (see Material and Methods and Figure S1A) [388]. In the 3-week nintedanib treatment regimen initiated at 9 weeks of age, we could neither detect a significant increase in the percentage of micro-invasive lesions (IC1) nor an increase in macro-invasive lesions (IC2) (Figure 5A). In addition, this treatment regimen did not lead to an increase in local lymph node and liver metastases as detected by

staining for SV40 T antigen, the oncogene expressed by β-tumor cells in Rip1Tag2 transgenic mice (Figure 5B, C). Of note, in all of the mice analyzed, liver metastasis exceeding 10 cells per cross section were rarely observed and were restricted to a few mice (data not shown). To rule out a transient and reversible increase of local tumor invasiveness, we initiated treatment at around 9 weeks of age and analyzed pancreata after 5 days of nintedanib treatment. This treatment regimen was sufficient to reduce MVD and tumor volume at borderline significance, yet it also did not increase local tumor invasiveness (Figure S4A - C).
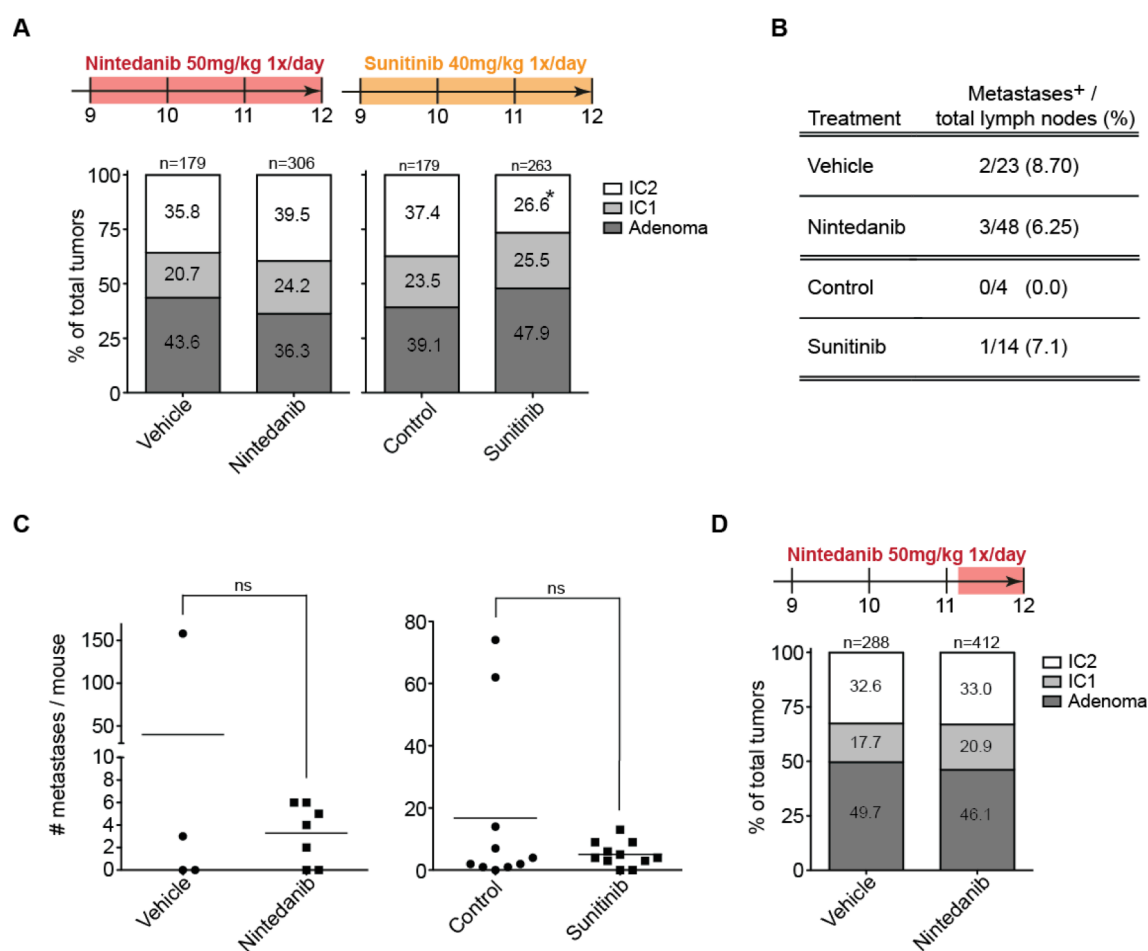
Figure 5. Nintedanib and sunitinib do not induce tumor invasiveness and metastasis.

(A) Tumors of Rip1Tag2 mice treated for 3 weeks with nintedanib or sunitinib in two separate experiments starting at 9 weeks of age were classified into any of the 3 categories as indicated by the percentages of the tumors inside the bar graphs and the numbers of total tumors per experimental group, which are displayed on top of the bars. Vehicle: n=6 mice, nintedanib: n=9 mice, data of two independent experiments was pooled. Control: n=10 mice, sunitinib: n=11 mice. Statistical analysis was performed using Fisher's exact test; *, P < 0.05. (B) Pancreatic lymph node metastases were analyzed in 23 vehicle-treated (10 mice) and 48 nintedanib-treated (14 mice), and in 4 control-treated (10 mice) and 14 sunitinib-treated (11 mice) lymph nodes. Fisher`s exact test; P = 0.6252 (nintedanib treatment), p = 1 (sunitinib treatment). (C) Metastasis to the liver was analyzed on 9 histological liver sections per mouse of vehicle-treated (4 mice) and nintedanib-treated (7 mice), and in control-treated (10 mice) and sunitinib-treated (11 mice) mice. Mann Whitney *U* test. (D) Grading of tumor stages in Rip1Tag2 mice treated for 5 days with nintedanib or vehicle control initiated at 11 weeks of age. Vehicle: n=16 mice, nintedanib: n=18 mice; pooled data of 3 independent experiments are shown.

A meaningful assessment of a potential pro-metastatic effect of compounds prolonging overall survival in clinical trials is often hampered by the latency of metastasizing tumor cells. We therefore asked whether the survival benefit achieved by nintedanib treatment would be paralleled by increased liver metastasis when analyzing vehicle and nintedanib-treated groups at their endpoints. Although nintedanib treatment increased survival by more than 4 weeks, the number of liver metastases per mouse was not increased compared to vehicle-treated mice (Figure S5).

Since treatment with nintedanib for 3 weeks was initiated at an intermediate stage of tumorigenesis, the possibility remained that nintedanib treatment initiated at late stage of Rip1Tag2 tumorigenesis may instead increase local invasiveness. However, treatment with nintedanib for five days initiated at a late tumor stage (11 weeks of age) did not induce local invasiveness, while a substantial reduction in MVD with a significant reduction in tumor volume was observed (Figure 5D, Figure S6A, B).

3.2.4.6   Sunitinib does not induce tumor invasion and metastasis

Although several publications have shown increased invasiveness and metastasis upon anti-angiogenic treatments in the Rip1Tag2 mouse model of PNET [267, 270, 364], this issue remains controversial, and solid data reporting similar findings in human clinical trials are lacking [379]. In particular, it is not known whether the pro-invasive phenotype observed in some preclinical cancer models can be attributed to inhibition of the VEGF-A/VEGFR-2 axis alone, and is therefore applicable to all VEGF pathway inhibitors or whether it is a consequence of increased tumor hypoxia caused by multi-target tyrosine-kinase inhibitors such as sunitinib [267, 270, 364, 365]. To specifically address this question, we analyzed the local invasiveness of Rip1Tag2 tumors treated with the anti-angiogenic small molecule tyrosine-kinase inhibitor sunitinib, which has previously shown to be especially efficient in enhancing tumor invasiveness and metastasis in the Rip1Tag2 mouse model [267, 363]. Interestingly, although a 3-week sunitinib treatment effectively reduced MVD and primary tumor growth (Figure S6C, D), lymph node and liver metastasis were not increased (Figure 5B, C). In contrast, sunitinib slightly reduced the rate of carcinoma classified as IC2 (Figure 5A). Similarly, a 5-day sunitinib treatment at early stage of tumorigenesis reduced MVD and primary tumor volumes compared to control treated mice, but did not affect tumor invasiveness (Figure S4A- C).

3.2.4.7   Blocking VEGFR 1-3 signaling does not induce local tumor invasiveness

To further characterize the general response patterns to different anti-antiogenic TKI in

Rip1Tag2 mice, we performed therapy studies with PTK787/ZK222584 (PTK/ZK) which mainly inhibits VEGFR 1-3 and PDGFR signaling (26). We treated Rip1Tag2 mice starting from 9 weeks of age with PTK/ZK (100mg/kg) for 3, 4, 5 or 6 weeks, whereas the control treatment group was treated for 3 weeks only, to avoid preterm death. Prolonged PTK/ZK treatment efficiently reduced MVD and had varying effects on tumor volumes (Figure S7A, B). Interestingly, we did not observe revascularization even in the 5 and 6 weeks treatment cohorts. None of the PTK/ZK treatment groups displayed any sign of increase local tumor invasiveness compared to the control cohort, even though the prolonged treatment provided additional time for the tumors to progress (Figure 6A). On the contrary, 3 and 6 weeks PTK/ZK treatment rather reduced the percentage of macro-invasive (IC2) lesions. Similar to the nintedanib treatment we assessed whether 5 days of PTK/ZK treatment initiated at late tumor stage (11 weeks of age) would increase tumor invasiveness. Although we could not detect any difference in the percentage of macro-invasive tumors between the PTK/ZK and the control treated cohort, there was a shift towards an increased percentage of micro-invasive lesions in PTK/ZK treated mice (Figure 6B). To further follow up and validate these results, we analyzed the entrapment of amylase-positive cells of the exocrine pancreas within insulin-positive tumors by immunofluorescence staining as has been previously described [364]. Tumors entrapping amylase-positive cells are an indicator of macro-invasiveness (Figure 6C). In concordance with the histological grading, 5 days PTK/ZK treatment initiated at late tumor stage (11 weeks of age) also did not significantly alter the percentage of tumors entrapping cells of the exocrine pancreas, despite strongly reducing MVD and tumor volume (Figure 6C, Figure S7C, D). PTK/ZK treatment initiated at an early tumor stage (9 weeks of age) for five days rather reduced local invasiveness (Figure S4C). In addition, treating Rip1Tag2;Rip1-VEGF-C mice with PTK/ZK for 3 weeks did also not increase local tumor invasiveness (Figure 6D).

Based on these data, we conclude that targeting tumor angiogenesis in Rip1Tag2 transgenic mice by a variety of therapy regimen with the multi-kinase inhibitors nintedanib, sunitinib or PTK/ZK efficiently represses tumor angiogenesis, but does not increase the incidence of invasive tumors or metastasis.
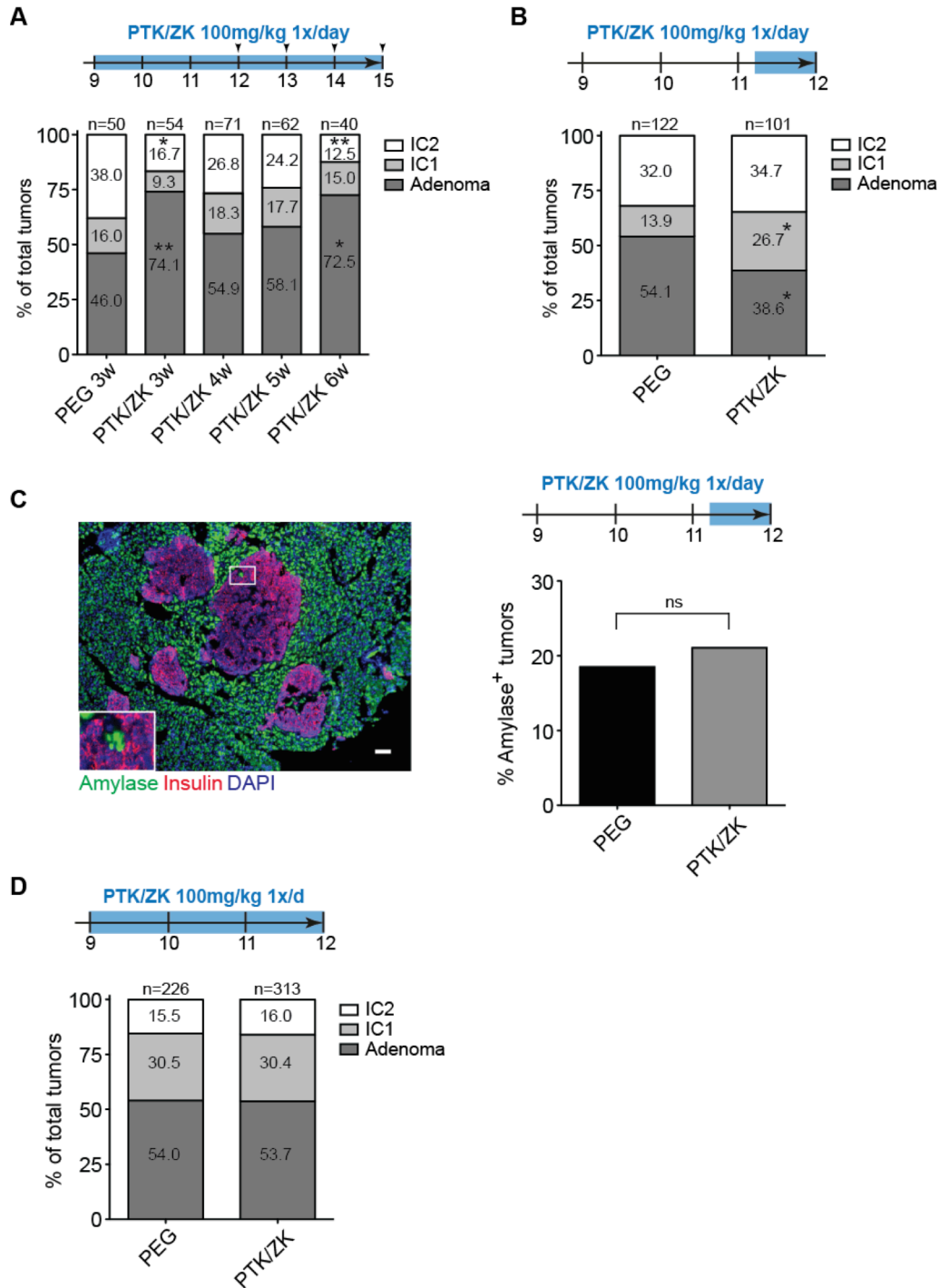
Figure 6. Analysis of local tumor invasiveness upon various PTK/ZK treatment regimens.
(A) Rip1Tag2 mice were treated for 3, 4, 5 and 6 weeks with PTK/ZK starting at 9 weeks of age or for 3 weeks with PEG as control group. PEG: n=5 mice, PTK/ZK: n=3-5 mice per group. Tumor stages were graded and quantified as described in Figure S1A. (B) Tumor grading of tumors of Rip1Tag2 mice treated with PTK/ZK for 5 days between the age of 11 and 12 weeks. Tumor stages were graded as described in Figure S1A. N=5 mice per group. Data of 2 independent experiments were pooled. (C) The extent of insulin-positive tumors (red) entrapping α-amylase-positive cells of the exocrine pancreas (green) was quantified by immunofluorescence staining of the tumors of Rip1Tag mice treated for 5 days at 11 weeks of age as described in panel (B). Scale bar, 100µm. (D) Rip1Tag2;Rip1-VEGF-C mice were treated with PTK/ZK for 3 weeks starting at 9 weeks of age, and tumor stages were graded as described in Figure S1A. PEG: n=7 mice, PTK/ZK: n=8 mice.
Fisher's exact test (A-D); *, P < 0.05; **, P < 0.01.

3.2.5 Discussion

Based on numerous promising results from preclinical cancer models, the strategy of targeting tumor blood vessels and thus reducing the amount of oxygen and nutrients available to tumors has been translated with great enthusiasm into clinical practice [389]. In clinical trials and routine therapy most anti-angiogenic substances have increased progression-free survival, yet they have failed to substantially prolong overall survival in a variety of solid tumor types [287, 297]. As an exception, treatment of patients with advanced PNET with the anti-angiogenic TKI sunitinib has raised the possibility that this group of cancer is particularly sensitive to anti-angiogenic therapy [64]. At the same time, this clinical trial reproduced the beneficial effect observed in preclinical experiments targeting both endothelial- and perivascular cells with sunitinib in the Rip1Tag2 mouse model of PNET [104, 267]. These and other data have proven the Rip1Tag2 model highly predictive in translating findings from the bench to the bedside [258, 265, 266].

In the present study, we have performed an in depth evaluation of the broad- spectrum anti-angiogenic small-molecule TKI nintedanib in the Rip1Tag2 preclinical mouse model of PNET. Nintedanib, which mainly inhibited VEGF, PDGF and FGF tyrosine kinase receptors and SRC non-receptor tyrosine kinase [70], exerted a strong anti-angiogenic effect in the Rip1Tag2 transgenic mouse model of neuroendocrine carcinoma of the pancreas which resulted in reduced tumor volumes and increased animal survival. Nintedanib extensively reduced microvessel density and tumor volume. Interestingly though, despite nintedanib's inhibitory action on perivascular cells, the blood vessels that remained were mature, tightly covered by perivascular cells, well perfused and showed reduced intratumoral leakiness. Although the vasculature in the placebo-treated group was

already well perfused and only rarely showed signs of intratumoral leakiness, prolonged (3 week) nintedanib treatment led to further blood vessel normalization with only a marginal increase of tumor hypoxia. Since blood vessel normalization is associated with enhanced delivery of chemotherapeutic agents into tumors [198, 326], nintedanib should not only be further evaluated for its own anti-cancer effect but also for a potential synergistic function by enhancing the intratumoral delivery of anti-cancer agents. Nintedanib has been shown well tolerated in the treatment of IPF and cancer patients [71, 72] and, hence, it should be clinically tested on patients with PNET and other angiogenic cancer types in combination with conventional chemotherapy. In addition, nintedanib could be used when tumors become refractory to therapies targeting mainly the VEGF-A/VEGFR2 axis by FGF signaling-mediated revascularization – as it has been previously shown for brivanib in the Rip1Tag2 mouse model [253]. Brivanib is an anti-angiogenic TKI displaying a similar target spectrum as nintedanib; both compounds are inhibiting FGFR signaling in addition to VEGFR and

PDGFR signaling.

Surprisingly, nintedanib did not affect tumor lymphangiogenesis in Rip1Tag2 mice as well as in Rip1Tag2 mice in which tumor lymphangiogenesis was induced by tumor cell-specific expression of VEGF-C (Rip1Tag2;Rip1-VEGF-C double-transgenic mice). In concordance with these findings, we have previously shown that the anti-angiogenic TKI PTK/ZK, mainly blocking VEGFRs 1-3, was also not able to inhibit established and ongoing tumor lymphangiogenesis in the Rip1Tag2;Rip1-VEGF-C model despite a substantial reduction of VEGFR-3 phosphorylation [255]. These data indicate that VEGF-C-induced tumor lymphangiogenesis may eventually rely on factors other than VEGF-C and that pathways not targeted by nintedanib and PTK/ZK are at play. These observations warrant further investigations.

Previous work has raised concerns that anti-angiogenic therapy might increase tumor invasiveness and distant metastasis in the Rip1Tag2 model [267, 270, 363, 364, 366]. Some work attributed the invasiveness-promoting effect to a general feature of anti-angiogenic drugs [267, 364], presumably by inducing a hypoxia-driven EMT. In contrast and consistent with our findings, a recent report shows that nintedanib not only repressed primary tumor growth of xenotransplantated NSCLC and exocrine pancreas carcinoma by reducing vessel density, maturation and perfusion but also repressed metastatic dissemination [111]. Moreover, others have observed increased tumor aggressiveness only with drugs that in addition to the VEGF-A/VEGFR-2 axis also targeted perivascular cells, such as sunitinib [365]. To contribute to this important discussion, we not only analyzed potential changes in invasiveness induced by the broad spectrum TKI nintedanib and sunitinib, but also when angiogenesis was inhibited by mainly targeting VEGFRs and PDGFRs with PTK/ZK. In our Rip1Tag2 mice, nintedanib, sunitinib and PTK/ZK did not substantially increase local invasiveness, which stands in contrast to what has been reported by others [267, 270, 363-366]. Supporting our findings is the fact that in cancer patients solid data is lacking that shows an increased invasiveness and metastasis induced by anti-angiogenic therapies, possibly with the exception of glioblastoma multiforme [390]. In addition, it has been shown that sunitinib treatment of metastatic renal cell carcinoma did not adversely alter the patients' clinical outcome [379]. An alternative explanation for this apparent discrepancy has been discussed previously [365]: Rip1Tag2 mice have been bred in isolation between different laboratories for approximately two decades which may have led to genetic drifts resulting in altered susceptibilities to the induction of tumor invasion by anti-angiogenic therapies. The delineation of the mechanisms driving this discrepancy will be part of exciting future research which may lead to the discovery of novel factors and pathways determining the susceptibility

to cancer metastasis, induced by changes in the tumor microenvironment.

In summary, our preclinical data together with the previous reports of successful clinical applications in patients strongly encourage the evaluation of nintedanib treatment as a novel therapeutic strategy in PNET patients with advanced disease.

3.2.6 Materials and Methods

Mice

The generation and characterization of Rip1Tag2 transgenic mice has been reported elsewhere (16). Mice were kept in a C57Bl/6 genetic background. Starting from week 9 of age, mice were fed with food pellets supplemented with 60% glucose (Provimi Kliba AG) to counteract detrimental hypoglycemia caused by excessive insulin production. All animal experiments were performed according to the guidelines and legislation of the Swiss Federal Veterinary Office (SFVO) and the Cantonal Veterinary Office, Basel-Stadt, Switzerland, under licence Nrs. 1878 and 1908.

Therapy studies

Both female and male Rip1Tag2 transgenic mice were treated as indicated in the respective figure legends, starting from 9-10 weeks of age (early stage disease) or from 11 weeks of age (late stage disease). PTK/ZK222584 (PTK/ZK; provided by Novartis Pharma) was dissolved in polyethylene glycol 300 (PEG300, Sigma) and administered daily by oral gavage at 100mg/kg body weight. Nintedanib (provided by Boehringer Ingelheim) was dissolved in Hydroxyethylcellulose Natrosol 0.5% (vehicle treatment; Boehringer Ingelheim) and administered daily by oral gavage at 50mg/kg body weight. Sunitinib L-malate (LC Laboratories) was formulated in carboxymethylcellulose vehicle as described elsewhere (control treatment; ref [267]) and administered daily by oral gavage at 40mg/kg body weight. Total tumor volume per mouse was extrapolated by measuring the diameter (d) of single macroscopic tumors, employing the formula Volume = $4/3*\pi*(d/2)3$ and summing up the volumes of individual tumors per mouse. In the survival study, mice were euthanized by CO_2-suffocation prior to death due to hypoglycemia, according to defined termination criteria. The termination criteria were based on an activity score (normal activity = score 0; wiggling/reduced activity = 2; still/hunchback/poor general condition = 3) and blood glucose levels (>2.1 mmol/l = score 0; 1.1-2.0 mmol/l = 1; 0.7-1.0 mmol/l = 2; <0.7 mmol/l = 3) measured using the blood glucose meter Contour® Next (Bayer). Mice were euthanized when reaching a total score of 4 or if presenting with score 3 in one of the two criteria.

Hypoxia and vessel functionality

To detect hypoxic tumor areas, pimonidazole HCl (Hypoxyprobe Omni Kits, Hypoxyprobe, Inc.) at 60mg/kg was injected intraperitoneally 2 hours prior to euthanizing the animals. Reduced pimonidazole in hypoxic tumor regions was visualized by immunofluorescence staining with a rabbit anti-pimonidazole antisera (Hypoxyprobe Omni Kits, Hypoxyprobe, Inc.). Leaky blood vessels were detected by injecting 250µg fluorescein labeled dextran (70kDa; Life technologies, D-1822) in 200µl PBS intravenously via the tail vein. After a circulation time of 5 minutes, terminally anaesthetized mice were first perfused via the left cardiac ventricle with phosphate-buffered saline (PBS) and subsequently with PBS/ 4% paraformaldehyde (PFA). For the detection of patent blood vessels, 100µg of fluorescein labeled lycopersicon esculentum (tomato) lectin (Vector Laboratories, GL-1171) was injected in 100µl PBS intravenously via the tail vein. After a circulation time of 4 minutes, terminally anaesthesized animals were perfused with PBS/4% PFA followed by PBS via the left cardiac ventricle.

Tissue preparation for histology

For Hematoxilin & Eosin (H&E), immunohistochemistry (IHC) and immunofluorescence (IF) staining, organs (pancreas and liver) were isolated, fixed overnight in PBS/4% PFA at 4°C, dehydrated with ethanol/xylene and subsequently embedded in paraffin. For IF stainings, pancreata were fixed during 2 hours in PBS/4%PFA and cryopreserved in PBS/20% sucrose overnight, both at 4°C. Pancreata were embedded, snap frozen in OCT freezing solution (Thermo Scientific) and stored at -80°C. Macroscopic images of whole dissected pancreata were acquired using a Nikon D5000 camera with AF-S Micro Nikkor 105mm f/2.8D lens.

Immunohistochemistry and metastasis analysis

For the detection of liver and lymph node metastases, 5µm thick PFA-fixed paraffin-embedded liver and pancreas sections were deparaffinized and antigen-retrieval was performed in a pressure cooker (PrestigeMedical) in 10mM Na-Citrate buffer (pH 6.0). IHC stainings were conducted using Dako EnVision plus kit (Dako) according to the manufacturer's advices. Metastatic tumor cells were indentified by staining with an antibody against SV40 Large T antigen (rabbit polyclonal IgG, Santa Cruz, sc-20800, 1:50 dilution) and were counterstained with hematoxylin before mounting with Cytoseal™ XYL (Thermo scientific). 9 serial liver sections per mouse were analyzed with each section 75µm apart. The whole liver was embedded to ensure a comprehensive analysis of all liver lobes. Intravascular metastases were excluded. Clearly SV40 Large T antigen positive parenchymal

single cells were included in the analysis. For the detection of pancreatic lymph node metastases, 1 section per lymph node was analyzed.

Double-strand DNA breaks associated with apoptotic and non-apoptotic cell death were visualized using a TUNEL assay (In Situ Cell Death Detection Kit, POD; Roche) according to the manufacturer`s recommendations, using Proteinase K pretreatment. The staining was developed with 3-amino-9-ethylcarbazole (AEC, Vector Labs) and briefly counterstained with hematoxylin. Light microscopy images were obtained with an AxioVert microscope (Leica Microsystems) or with a Zeiss Axio Observer (Zeiss).

Immunofluorescence

8µm thick cryosections were dried for 30 minutes at room temperature (RT), 5 minutes rehydrated in PBS, permeabilized in PBS/0.1% Triton X-100 during 20 minutes and blocked with PBS/5% normal goat serum (NGS; Sigma). As an exception, cCasp3 stainings were blocked with PBS/20%NGS. All primary antibodies were diluted in PBS/5%NGS. The following antibodies and dilutions were used: rat anti-CD31 (BD Pharmingen, 550274, 1:50), rabbit anti-NG2 (Chemicon, AB5320, 1:100), guinea-pig anti-insulin (Dako, A0564, 1:200), rabbit anti-α-amylase (Sigma, A8273, 1:100), rabbit anti-cCasp3 (Cell Signaling, 9664, 1:50), rabbit anti-pH3 (Millipore, 06-570, 1:200), rabbit anti-LYVE-1 (RELIATech, 103-PA50S/0412P02-2, 1:200). Positive staining was visualized by incubating the specimen during 1 hour with secondary antibodies against the respective species of the corresponding first antibody, labeled with either Alexa488, Alexa568 or Alexa633 (Molecular probes; 1:200 in PBS/5%NGS). Nuclei were stained with DAPI (Sigma) and slides were mounted with Dako mounting medium (Dako). Fluorescence images were acquired with a Leica DMI 4000 or a Nikon Diaphot 300 microscope.

In Figure S4A, IF staining against CD31 was performed on 5µm thick PFA-fixed paraffin-embedded pancreata (PFFPE). The tissue was deparaffinized, rehydrated in PBS and antigen retrieval was performed with PBS/0.1% proteinase K (Fluka) for 20 minutes at 37°C. Endogenous peroxidase was quenched with 3% H2O2, washed in PBS and blocked with PBS/5% NGS for 30 minutes at RT. Primary antibody incubation (rat anti-CD31; Bachem, T-2001, 1:50) and the subsequent staining procedure was performed as described for immunofluorescence staining.

Histopathological grading

H&E stainings of 5µm thick, PFFPE pancreas sections was performed as described [391]. Histopathologic analysis, i.e. grading, was conducted on H&E stained paraffin sections

in a blinded manner. Grading was performed as previously described [388]. In brief, tumors were categorized into either non-invasive insulinoma with smooth tumor borders (adenoma), into tumors with no more than 1-2 microinvasions (IC1), or into macro-invasive carcinomas (IC2) including rare anaplastic carcinomas (Figure S1A). All tumors per experimental group were pooled and percentages of the respective grade are indicated.

2×10^4 primary insulinoma tumor cells/well were seeded in a 96-well plate 3 days (day -3) prior to the addition of nintedanib dissolved in DMSO at different concentrations (day 0). At day +2, nintedanib and medium was replaced. At day +4, cells were fixed with 4% PFA/PBS, blocked and permeabilized with 0.1% BSA and 0.1% Triton X-100/PBS. In order to identify intact cells, nuclei and the microtubule cytoskeleton were stained with Hoechst and a rat anti- tubulin (YL1/2) antibody (Santa Cruz, sc-53029, 1:1000) respectively, followed by the incubation with an anti-rabbit Alexa488 labeled secondary antibody (Molecular Probes; 1:400). Images were acquired employing an Operetta High Content Imaging System (PerkinElmer; Objective 20xWD; non-confocal acquisition).

Statistical methods

Data were analyzed and graphs were generated with GraphPad Prism 6 (GraphPad Prism Software Inc.) or R version 2.15.1 (The R Project for Statistical Computing).

3.2.7 Supplementary data
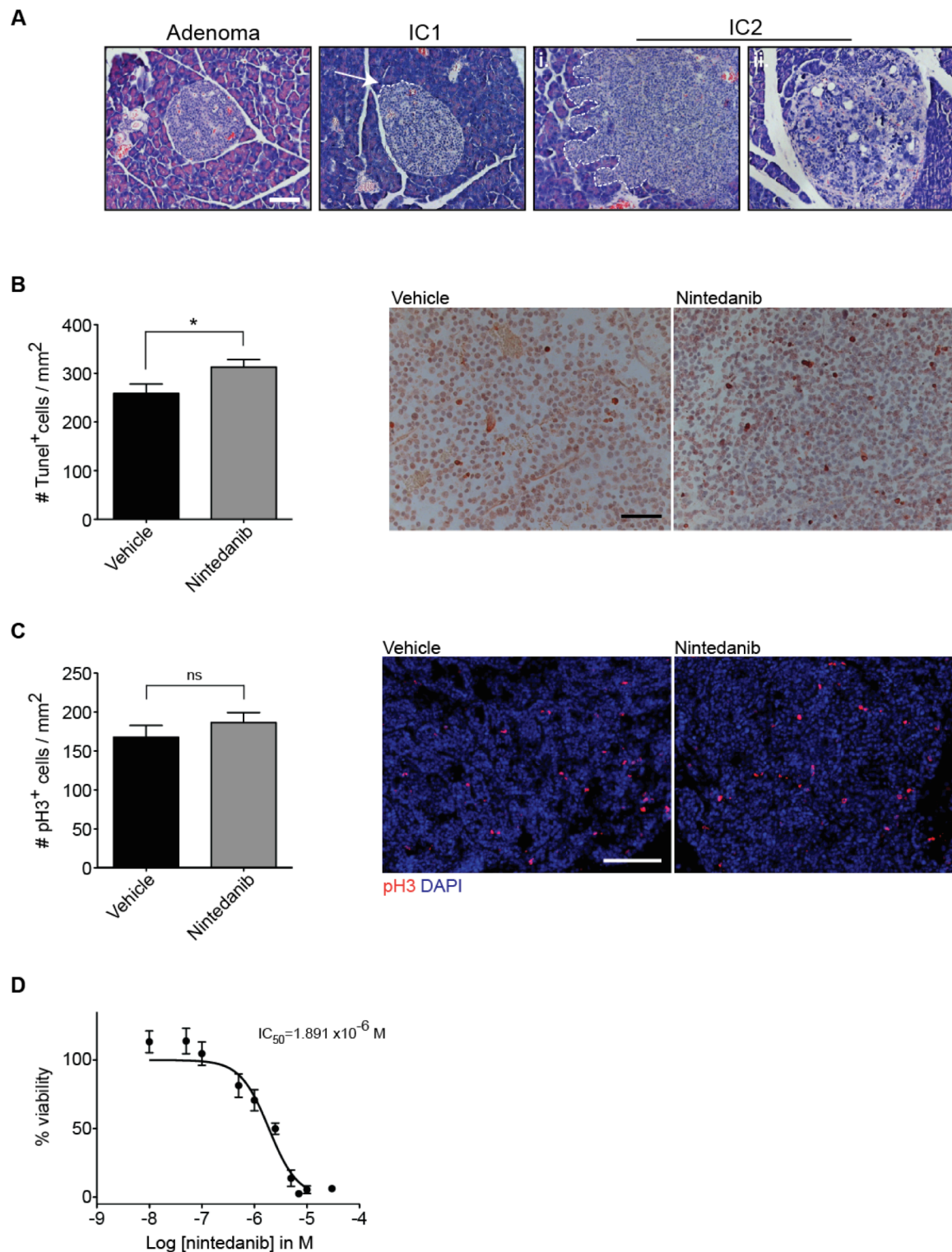
Figure S1. Nintedanib increases tumor cell apoptosis yet does not affect tumor cell proliferation.
(A) Representative microphotographs of hematoxylin and eosin stained sections of the various stages of tumor progression in Rip1Tag2 transgenic mice. Shown are sections of non-invasive adenoma with smooth tumor borders (Adenoma), microinvasive carcinoma with 1-2 invasive protrusions into the surrounding exocrine pancreas (dashed line) (IC1), and macro-invasive (dashed line; i) and anaplastic carcinoma (ii) (IC2). Scale bar, 100μm. (B) The number of cells with double-strand DNA breaks indicating apoptotic and non-apoptotic cell death

was analyzed by Tunel assay. Representative microphotographs are shown, and the number of Tunel-positive cells per area and field of view was determined as mean ± SEM. N=2 mice per group. Scale bar, 50µm. *, P < 0.05. (C) The number of dividing cells was determined by immunofluorescence staining of pH3. Representative microphotographs are shown, and pH3-positive cells per area and field of view were counted and displayed in a bar graph as mean ± SEM. Vehicle: n=4 mice, nintedanib: n=7 mice. Scale bar, 100µm. Statistical analysis was performed employing an unpaired Student *t* test (B, C). (D) Primary insulinoma tumor cells were treated for 4 days with nintedanib in vitro. The number of intact cells/well was determined and displayed per nintedanib concentrations. 3 independent experiments in triplicates were performed and shown as mean ±SEM for each nintedanib concentration. Graphical representation was achieved calculating a non-linear regression of the normalized response allowing a variable slope over the logarithmic inhibitor concentration. IC50 = 1.891 x 10-6 M.
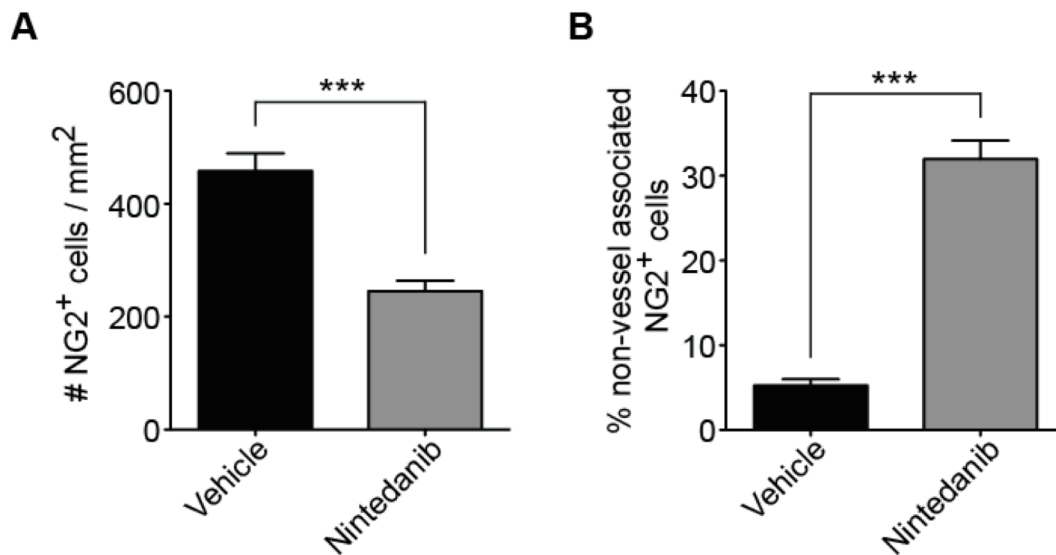
Figure S2. Blood vessels resisting nintedanib-treatment display a mature phenotype and retain their function.
(A, B) Quantification and analysis of the relative localization of NG2$^+$ perivascular cells to CD31$^+$ blood vessels revealed in nintedanib-treated tumors a reduction of total NG2+ perivascular cells per area (A) and an increased percentage of NG2$^+$ perivascular cells not associated with blood vessels (B). Values are displayed as counts per area of each field of view. Statistical analysis was performed using an unpaired Student *t* test; ***, P < 0.001. Vehicle: n=4 mice, nintedanib: n=7 mice.
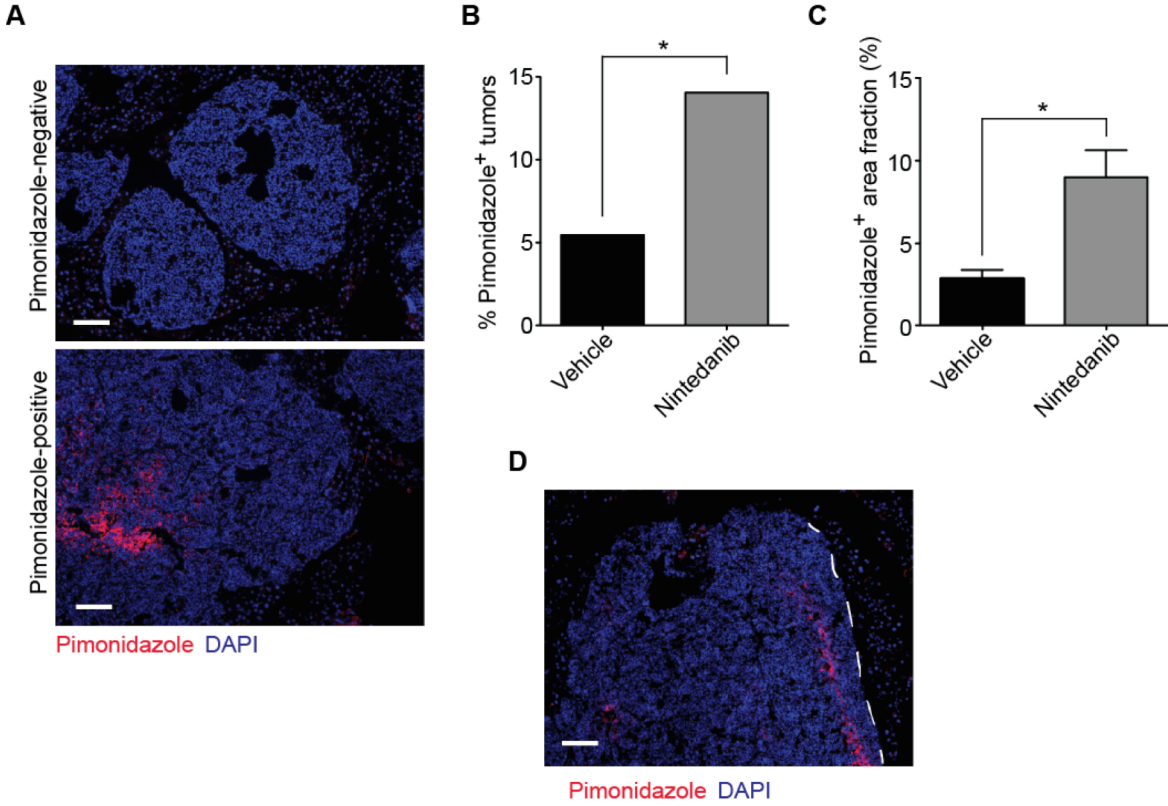
Figure S3. Nintedanib induces hypoxia in a proportion of tumors.

(A) Representative immunofluorescence images of pimonidazole-positive area fractions of tumors representing tissue hypoxia. Scale bar, 100µm. (B, C) Quantification of the percentages of tumors with any signs of hypoxia compared to the total number of tumors per experimental group (B) and of the pimonidazole-positive (red) tumor area fractions of hypoxic tumors (C). Cell nuclei are visualized by DAPI staining (blue). Data are displayed as mean ± SEM. Vehicle: n=6 mice, nintedanib: n=7 mice. P-values were calculated using a Fisher's exact (B) and an unpaired Student *t* test (C); *, P < 0.05. (D) A representative immunofluorescence image of a pimonidazole-positive hypoxic area close to the non-invasive tumor border (dashed line) is shown. Scale bar, 100µm.
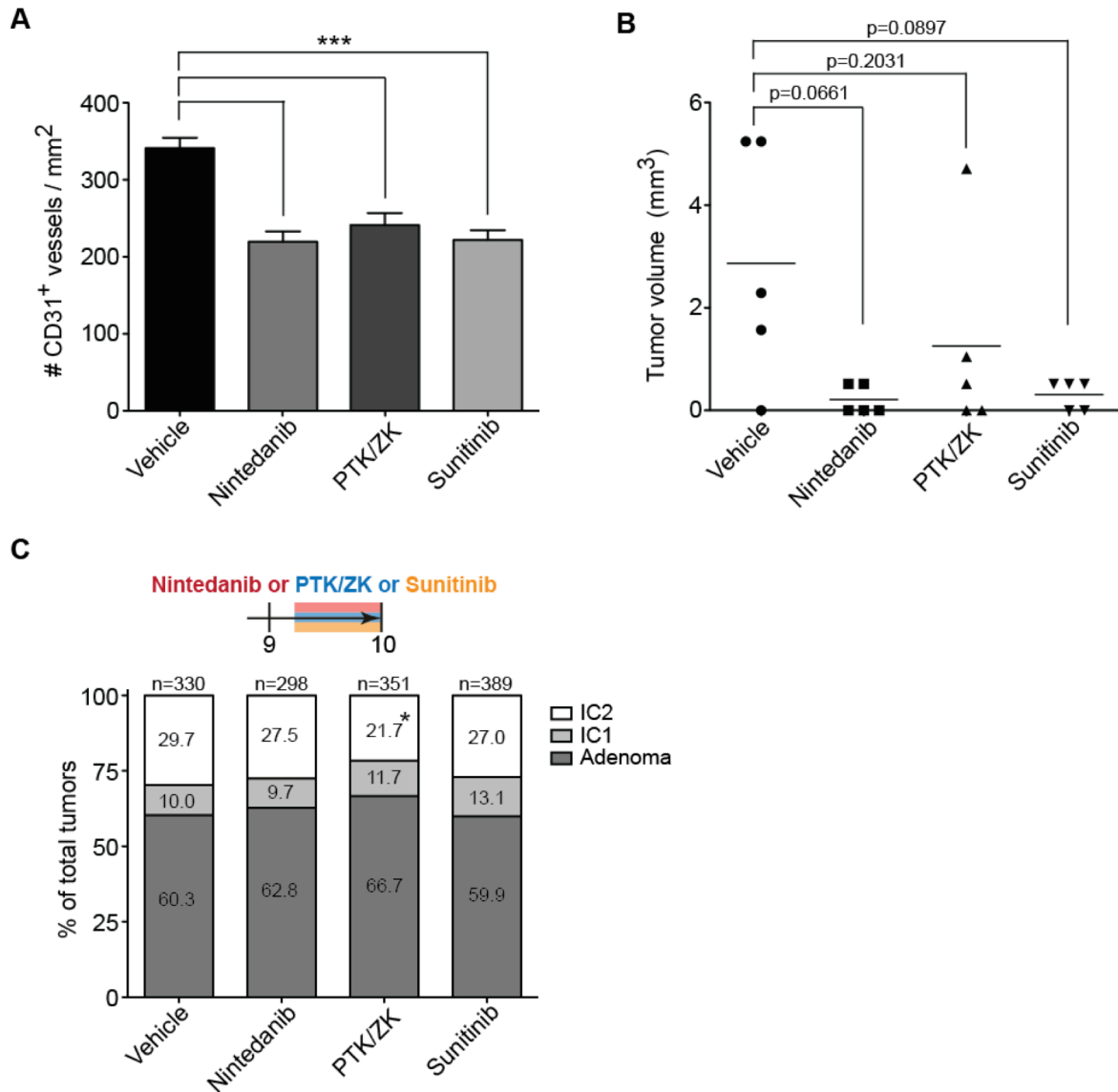
Figure S4. Nintedanib, PTK/ZK and sunitinib treatment reduce MVD and tumor volume and do not induce tumor invasiveness.

(A, B) A 5-day nintedanib PTK/ZK or sunitinib-treatment was initiated in 9 weeks old Rip1Tag2 mice, and blood microvessel density, as determined by CD31 immunofluorescence staining per field of view (A), and tumor volumes (B) were quantified. N=5 mice per group. P-values were calculated employing an unpaired Student t test (A) and a Mann-Whitney U test (B) respectively; ***, $P < 0.001$. (C) Grading of tumor stages in Rip1Tag2 mice treated for 5 days with nintedanib, PTK/ZK, sunitinib or vehicle control initiated at 9 weeks of age (as described in panels B, C). N=5 mice per group. Fisher`s exact test; *, $P < 0.05$.
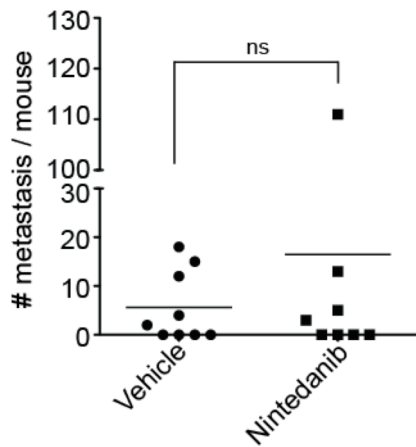
Figure S5. Prolonging survival by nintedanib does not increase liver metastasis.
Mice were treated with nintedanib or vehicle control open end and euthanized before they succumbed to hypoglycemia or other tumor-related complications (survival trial). Livers were screened for metastasis by immunohistochemical staining for SV40 Large-T antigen. Nine sections per liver were analyzed. Vehicle: n=9 mice, nintedanib: n=8 mice. Statistical analysis was performed employing a Mann-Whitney U test.
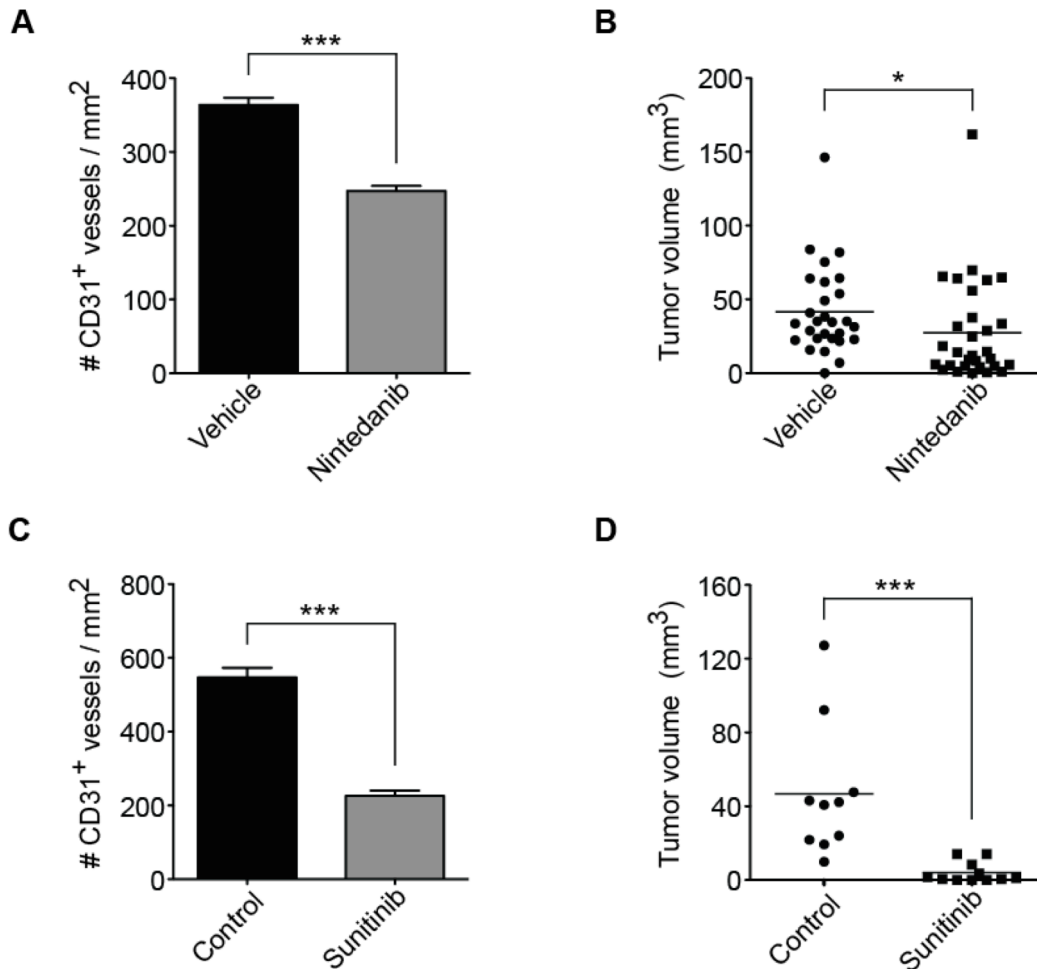
Figure S6. Nintedanib and sunitinib treatment reduce MVD and tumor volumes.
(A - D) Rip1Tag2 mice were treated with nintedanib for 5 days starting at the age of 11 weeks (A, B) or with sunitinib for 3 weeks starting at the age of 9 weeks (C, D). Tumor microvessel density was determined by CD31 immunofluorescence staining per field of view (A, C), and tumor volumes (B, D) were quantified. N=10 mice per group for (A). (B) pooled data of 5 independent experiments are displayed; vehicle: n=28 mice, nintedanib: n=30 mice. (C, D) control: n=10 mice, sunitinib: n=11 mice. P-values were calculated by unpaired Student *t* test (A, C) or Mann-Whitney *U* test (B, D). *, P < 0.05; ***, P < 0.001.
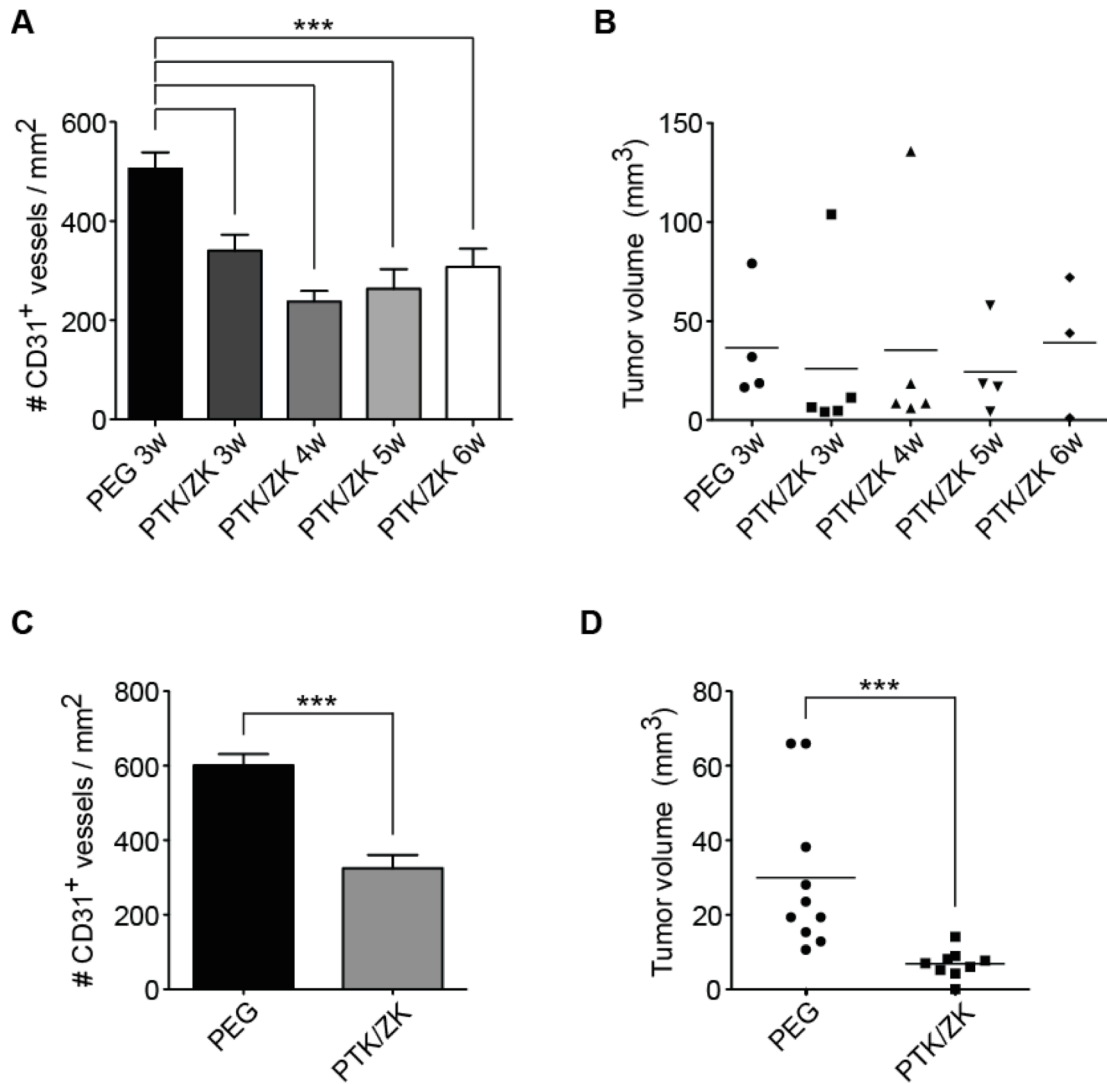
Figure S7. PTK/ZK treatment reduces MVD and tumor volume.
(A – D) 9 weeks old Rip1Tag2 mice were treated with PTK/ZK for 3-6 weeks (A, B) or for 5 days starting at the age of 11 weeks (C, D). Tumor microvessel densities were determined by CD31 immunofluorescence staining per area of each field of view and displayed as mean ± SEM (A, C). Tumor volumes are represented in (B) and (D), respectively. (A, B) PEG: N=4 mice, PTK/ZK: N=3-5 mice per group. (C) one representative experiment is shown. (D) 3 independent experiments were pooled; PEG: N=10 mice, PTK/ZK: N=9 mice. Statistical analysis was performed using an unpaired Student *t* test (A, C) or Mann-Whitney *U* test (B, D). ***, P < 0.001.

3.3 Targeting metabolic symbiosis to overcome resistance to anti-angiogenic therapy

Laura Pisarsky[1*], Ruben Bill[1*], Ernesta Fagiani[1], Ryan William Goosen[1], Jörg Hagmann[1], and Gerhard Christofori[1]

[1]Department of Biomedicine, University of Basel, 4058 Basel, Switzerland

* These authors contributed equally to this work

- submitted -

3.3.1 Summary

Despite the approval of several anti-angiogenic therapies, clinical results remain unsatisfactory, and transient benefits are followed by rapid tumor recurrence. Here, we demonstrate potent anti-angiogenic efficacy of the multi-kinase inhibitor nintedanib in a mouse model of breast cancer. However, after an initial regression, tumors resume growth in the absence of active tumor angiogenesis. Gene expression profiling of tumor cells reveals a metabolic reprogramming towards anaerobic glycolysis. Indeed, combinatorial treatment with a glycolysis inhibitor (3PO) or an mTOR inhibitor (rapamycin) efficiently inhibits tumor growth. Moreover, tumors establish metabolic symbiosis, illustrated by the differential expression of MCT1 and MCT4, monocarboxylate transporters active in lactate exchange in glycolytic tumors. Accordingly, ablation of MCT4 expression surmounts the adaptive resistance to anti-angiogenic therapy.

3.3.2 Significance

Anti-angiogenic therapy has shown only limited success in breast cancer patients. Here we show that the inhibition of glycolysis or the ablation of MCT4, a lactate/H^+ symporter associated with poor prognosis in triple-negative breast cancer patients, overcomes resistance to anti-angiogenic therapy in a mouse model of breast cancer. Hence, targeting metabolic symbiosis may be an attractive avenue to avoid resistance development to anti-angiogenic therapy in patients.

3.3.3 Introduction

An imbalance between pro and anti-angiogenic factors inducing the formation of new blood vessels from a preexisting vasculature (angiogenesis) has been described as a hallmark of cancer [392]. It has been proposed that targeting angiogenesis might plausibly reduce intra-tumoral levels of oxygen and nutrients, resulting in tumor starvation and thus in reduced tumor growth [167], and anti-angiogenic therapies were rapidly translated with great expectations from preclinical cancer models to clinical practice [146, 393, 394]. For example, the discovery of VEGF-A and its receptors and their identification as a rate-limiting factors for normal and pathological angiogenesis has led to the development of bevacizumab (Avastin[®]), a humanized monoclonal antibody targeting VEGF-A [389, 393]. While some cancer types, such as colorectal [242], renal cell [63] and PNETs [64], have shown encouraging responses to this therapeutic strategy, numerous other cancer types, in particular breast cancer, seem to be poorly responsive to anti-angiogenic regimens. Indeed, metastatic breast cancer patients treated with standard chemotherapy plus bevacizumab have only benefited from 1-2

months of PFS, and the rapid onset of resistance evidently prevented any OS benefit [286, 395, 396].

These data underline the importance of deciphering the molecular mechanisms underlying intrinsic or adaptive resistance to anti-angiogenic therapy. When blocking the VEGF-A signaling axis in preclinical models, e.g. with bevacizumab, tumors escape by activating alternative pro-angiogenic signaling pathways including FGFs, PDGFs, Bv8/prokineticin, and IL-17 [162, 270, 333, 334, 351]. In order to counteract the activation of these alternative pro-angiogenic pathways, several multikinase inhibitors and other anti-angiogenic drugs, targeting VEGF-dependent and independent pro-angiogenic signaling pathways, are currently in clinical use or in clinical trials. For example, sorafenib, a multikinase inhibitor targeting RAF, VEGFRs 1-3, PDGFRα and β, c-KIT and FLT-3, is currently used for the treatment of hepatocellular carcinoma, and sunitinib, blocking VEGFR 1-3, PDGFRα/β, c-KIT and FLT-3, is employed for the treatment of renal cancer. Both therapies show significant anti-tumor efficacy in preclinical tumor models and in cancer patients; however, they also suffer from resistance development based on thus far unknown mechanisms [64, 267]. Transient benefits are rapidly followed by tumor recurrence, sometimes associated with drug resistance and heightened tumor invasiveness [243, 267, 297, 298, 333].

Nintedanib (formerly known as BIBF-1120) is an even wider-spectrum angiokinase inhibitor targeting VEGFR 1-3, PDGFα/β, and FGFRs (FGFR) 1-4, as well as FLT-3 and SRC family kinases [70]. Nintedanib has recently shown promising results in pre-clinical models of lung cancer, ductal adenocarcinoma of the pancreas and PNET [111, 397]. Furthermore, nintedanib has demonstrated excellent tolerance and potent activity in a phase I clinical trial in early HER2-negative breast cancer [120] and in a phase III study in combination with chemotherapy in NSCLC [71].

We have therefore assessed the effects of nintedenab in mouse models of cancer. We report that tumors treated with nintedanib or sunitinib do not revascularize during the development of therapy resistance. Instead, the cells located in avascular areas escape the lack of oxygen by shifting their metabolism towards a hyperglycolytic state and by producing lactate, while the cells localized in the vicinity of blood vessels utilize the lactate for oxidative phosphorylation. The data establish metabolic symbiosis [398, 399] as an alternative route to develop resistance to anti-angiogenic therapy in mouse models of breast cancer and of insulinoma. Notably, interference with glycolysis or disruption of metabolic symbiosis reinstalls nintedanib's efficacy in repressing tumor growth.

3.3.4 Results

3.3.4.1 Py2T tumors develop evasive resistance to anti-angiogenic therapy

Nintedanib is a potent angiogenesis inhibitor that represses endothelial cell proliferation and induces their apoptosis (EC_{50} < 10nM). However, its direct effect on tumor cells is rather limited [70]. A stable murine breast cancer cell line (Py2T) established from a breast tumor of an MMTV-PyMT transgenic mouse [400] displayed an EC_{50} of 8μM *in vitro* which is above the pharmacologically achievable concentration in mice [70, 103] (Figure S1A). To study the tumor suppressive efficacy of nintedanib *in vivo*, Py2T cells were orthotopically implanted into the mammary fat pad of immune-competent syngeneic FVB/N female mice. When the tumors reached a volume of 15-20 mm^3, a tumor size where the angiogenic switch had already taken place (Figure S1B), daily treatment with nintedanib was initiated (50 mg/kg, p.o.). During the first week of treatment (short term treatment; ST), tumor volumes as well as tumor weights in nintedanib-treated animals were significantly reduced (Figure 1A, B). This nintedanib-responsive phase was associated with decreased cell proliferation and increased apoptosis (Figure 1C-F). However, beyond one week of treatment tumors escaped this therapeutic effect and showed an enhanced tumor growth with increased cell proliferation and reduced apoptosis, as observed after three weeks of treatment (long term treatment; LT) (Figure 1A, C-F). Together, the data indicate that Py2T breast cancer cells can escape nintedanib treatment despite its broad range of inhibitory activities.

3.3.4.2 Evasive resistance is not associated with tumor revascularization

Resistance to anti-angiogenic therapy has been reported to be associated with tumor revascularization. For example, VEGF inhibition leads to the activation of alternative pro-angiogenic signaling pathways, such as the FGF/FGFR axis [270]. Because nintedanib inhibits the major pro-angiogenic pathways, we investigated whether angiogenesis had been reactivated in Py2T tumors, thereby escaping nintedanib treatment. Intriguingly, we did not observe any revascularization in the nintedanib-refractory tumors: microvessel density was found decreased both after ST and LT nintedanib regimen, indicating a potent and stable anti-angiogenic effect of nintedanib, even in a phase of drug-refractory exponential tumor growth (Figure 1A, 2A-C). Immunofluorescence co-staining for CD31 and cCasp3 revealed increased apoptosis in endothelial cells after ST and LT nintedanib treatment, demonstrating the sustained anti-angiogenic efficacy of nintedanib even after LT treatment (Figure 2D and Figure S2A).

Next, we asked whether the tumor growth response pattern and sustained suppression of angiogenesis were nintedanib-specific or rather reflected a common denominator of broad-spectrum anti-angiogenic TKI. To this end, we performed a head-to-head comparison between nintedanib and sunitinib in the Py2T cell transplantation breast cancer model. Nintedanib and sunitinib-treated Py2T tumors displayed comparable tumor weights at the experimental endpoint as well as similar reductions in microvessel density after LT treatment (Figure S2B-D).

pH3/DAPI

cCasp3/DAPI
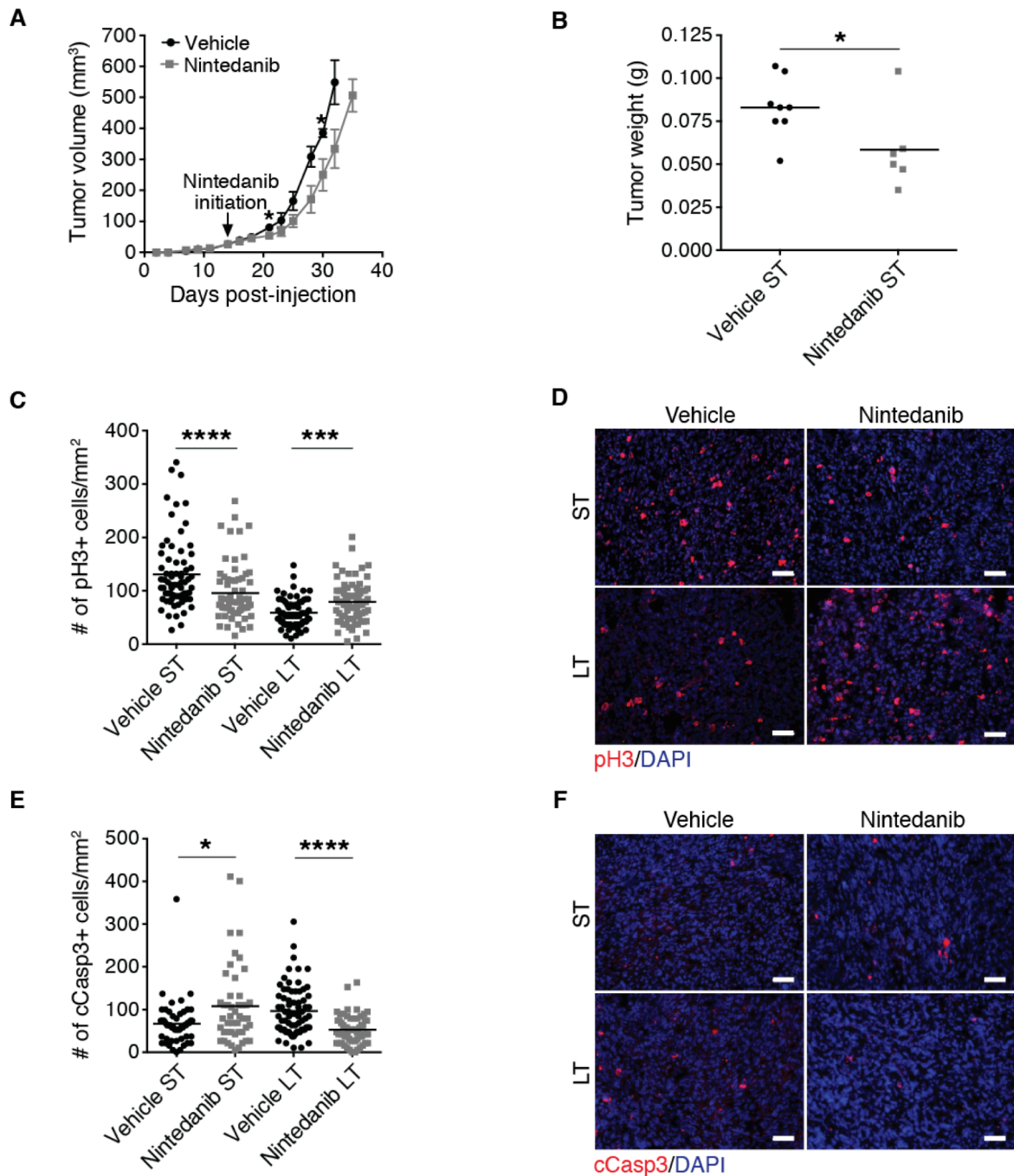
Figure 1. Evasive resistance to anti-angiogenic therapy with nintedanib in the Py2T transplantation mouse model of breast cancer.
Py2T cells were implanted into the mammary fat pad of FVB/N mice, and treated with nintedanib (50mg/kg daily p.o.) or vehicle control from day 14 after tumor cell injection, when tumors were first palpable. (A) Primary tumor growth was monitored by assessing tumor volumes over the time of therapy. Values represent mean ± SEM. N=13 mice per group. (B) Tumor weights were determined after 7 days of nintedanib short-term (ST) treatment. N=6-8 mice per group. (C-F) Cell proliferation (C, D) and the incidence of apoptosis (E, F) were quantified by immunofluorescence staining for pH3 (red) and cCasp3 (red), respectively, of tumor sections from short-term (ST) and long-term (LT) vehicle or nintedanib-treated mice. Representative immunofluorescence microscopy pictures are shown in D and F. DAPI is used to visualize cell nuclei. Values represent the number of pH3 positive (C) and cCasp3 positive (E) cells per area of each microscopic field of view. N=5-8 mice per group. Statistical significance was calculated using Mann–Whitney U test. *, $P < 0.05$; ***, $P < 0.001$; ****, $P < 0.0001$. Scale bars, 50μm.

We next assessed whether Py2T tumors compensate for the lack of blood vessels with increased pericyte coverage. Pericytes promote the maturation and stabilization of blood vessels through PDGFR signaling and thus influence the responsiveness to anti-angiogenic therapy [401]. Interestingly, despite its inhibitory activity on PDGFR signaling, nintedanib did not affect pericyte coverage of blood vessels resisting nintedanib treatment (Figure 2E and Figure S2E). However, the remaining blood vessels showed a significant reduction in their perfusion, as highlighted by the injection of fluorescence-labeled lectin (Figure 2F and Figure S2F). Consistent with decreased tumor perfusion, pimonidazole staining revealed a significant increase in tumor hypoxia not only in the ST-treated, nintedanib-responsive tumors but also in the LT-treated, nintedanib-resistant tumors (Figure 2G, H). These data demonstrate a potent anti-angiogenic activity of nintedanib and suggest a new mechanism of therapy resistance by which tumors escape anti-angiogenic therapy in the absence of any revascularization.

3.3.4.3   *Tumor cells become hyperglycolytic to survive hypoxia*

To investigate the molecular mechanisms underlying the resistance against nintedanib treatment, we isolated by flow cytometry endothelial and tumor cells from nintedanib-treated and untreated tumors at different time points of resistance development. To facilitate the isolation of tumor cells, Py2T cells were transduced with a retroviral construct expressing a truncated, non-functional form of murine CD8α [402]. A CD45$^-$CD8α^+ population could only be identified in Py2T-CD8α^+ tumors and not in wild-type Py2T tumors (Figure S3A). After ST (1 week) and LT (3 weeks) treatment with nintedanib, CD45$^-$CD8α^+ tumor cells and CD45$^-$CD8α^-CD31$^+$podoplanin$^-$ endothelial cells were sorted by flow cytometry (Figure S3B-D), and changes in gene expression were assessed by DNA oligonucleotide microarray analysis. Surprisingly, endothelial cell gene expression profiles between ST and LT nintedanib-treated tumors did not markedly differ, mainly reflecting endothelial cells undergoing apoptosis (data not shown).

In contrast, the gene expression analysis of isolated tumor cells revealed a marked difference between untreated and treated groups. Due to the small sample size in the treatment groups, no significant differences were found using the standard p-value cutoff < 0.05 and fold change (FC) cutoff > 1.5. We therefore performed a less stringent set of analysis using no p-value cutoff combined with a range of FC cutoff values (FC = 1.2 to 1.7).
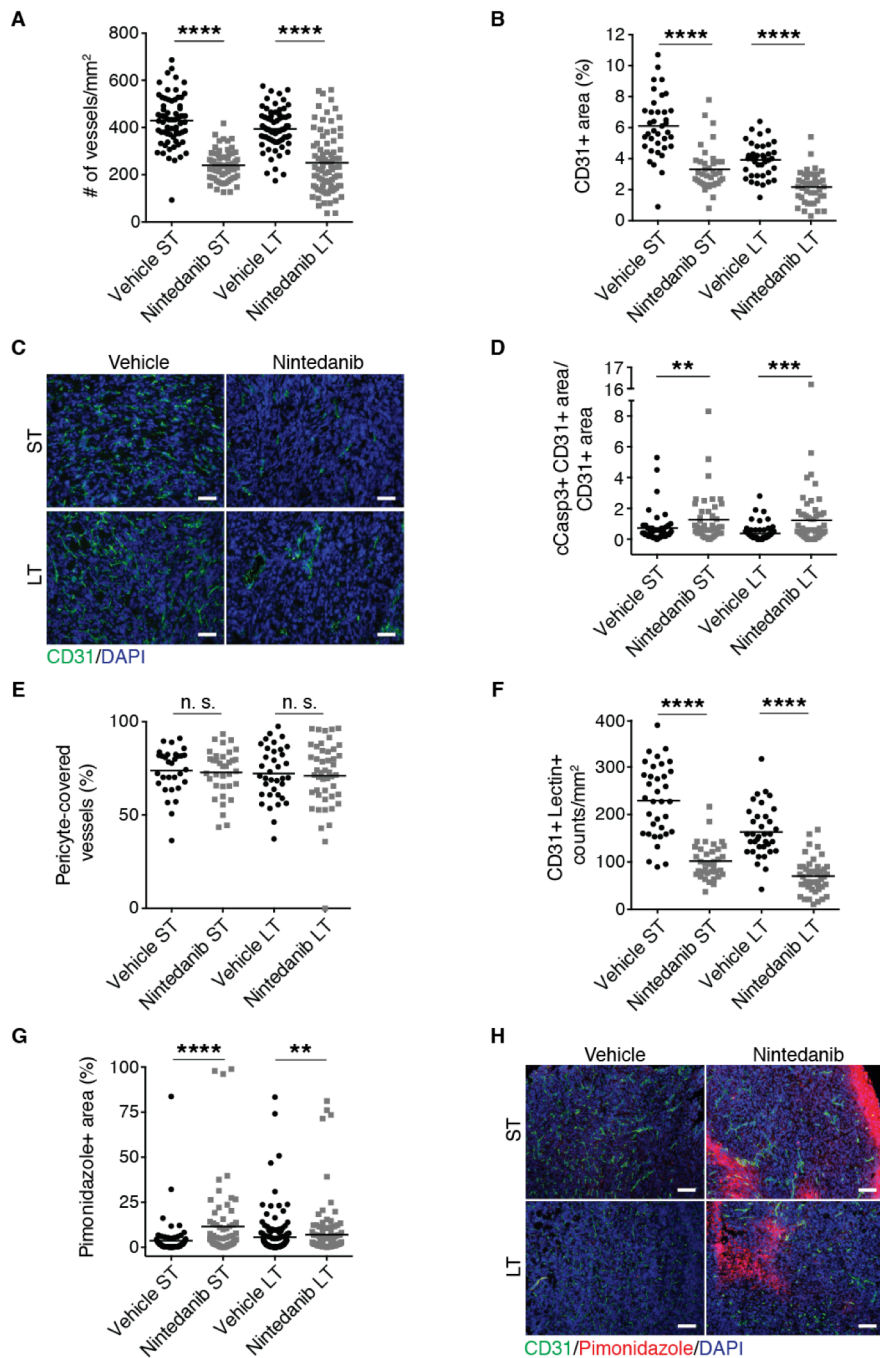
Figure 2. Tumor revascularization is not responsible for the resistance against nintedanib therapy in Py2T tumors.
(A-C) Microvessel densities (A) and CD31-positive area fractions (B) were quantified in Py2T tumors from mice treated for 1 week (ST) or 3 weeks (LT) with vehicle or nintedanib. Representative images of immunofluoresecence stainings of tumor sections from ST and LT vehicle or nintedanib-treated mice with antibodies against CD31 are shown (C; green). DAPI was used to visualize cell nuclei. Scale bars, 50µm. (D) Quantification of endothelial cell apoptosis by immunofluorescence co-staining for cCasp3 and CD31 in tumors from ST and LT vehicle or nintedanib-treated mice. (E) Quantification of the percentage of CD31-positive blood vessels that were in contact with NG2-positive perivascular cells in Py2T tumors from ST and LT vehicle or nintedanib-treated mice. (F) The functionality of blood vessels was assessed by i.v. injection of FITC-Lectin into Py2T tumor-bearing mice following ST or LT vehicle or nintedanib-treatment. Patent, perfused blood vessels were identified by immunofluorescence staining for CD31 and detection of FITC-Lectin and quantified by counting of CD31 and lectin double-positive blood vessels. (G) Hypoxic areas were identified and quantified by immunofluorescence staining for pimonidazole adducts in Py2T tumors from ST and LT vehicle or nintedanib-treated mice. (H) Representative pictures of the immunofluorescence co-staining for pimonidazole adducts (red) and CD31 (green) on histological sections of tumors from ST and LT vehicle or nintedanib-treated mice. DAPI staining visualizes cell nuclei. Scale bars, 100µm. Each dot represents the number of counts per area of microscopic field of view, and means are displayed. N = 6-8 mice per group. Statistical significance was calculated using Mann–Whitney *U* test. **, $P < 0.01$; ***, $P < 0.001$; ****, $P < 0.0001$.

The genes resulting from the comparison between LT nintedanib-treated and untreated tumor cells were subjected to KEGG-pathway analysis which showed an enrichment of metabolic pathways (Figure 3A and S3E), in particular glycolysis. Gene Set Enrichment Analysis (GSEA) [403] also showed an enrichment of glycolysis gene expression, especially when comparing the gene expression profiles of LT vs. untreated tumor cells, yet also when comparing ST vs. untreated tumor cells (Figure 3B). Glycolysis gene-enrichment also became evident when the gene expression profiles associated with a core set of glycolytic enzymes were visualized using a heat map. Indeed, hierarchical clustering almost perfectly clustered the three different treatment conditions (Figure 3C), and the mean expression of a core set of glycolytic enzymes was significantly upregulated between both LT and ST vs. untreated tumor cells (Figure 3D). The nearly significant difference between the ST and LT treatment groups, suggested that the increase in the expression of glycolytic enzymes was a gradual process already starting a few days after treatment initiation. Indeed, quantitative RT-PCR analysis confirmed the upregulated expression of most of the glycolytic enzymes assessed upon both ST and LT nintedanib treatment (Figure 3E, F). We suspect that the "nearly significant differences" observed in gene expression of tumor cells isolated from total tumors may be explained by heterogeneity in tumor cell phenotypes.

Pimonidazole/Glut1/DAPI
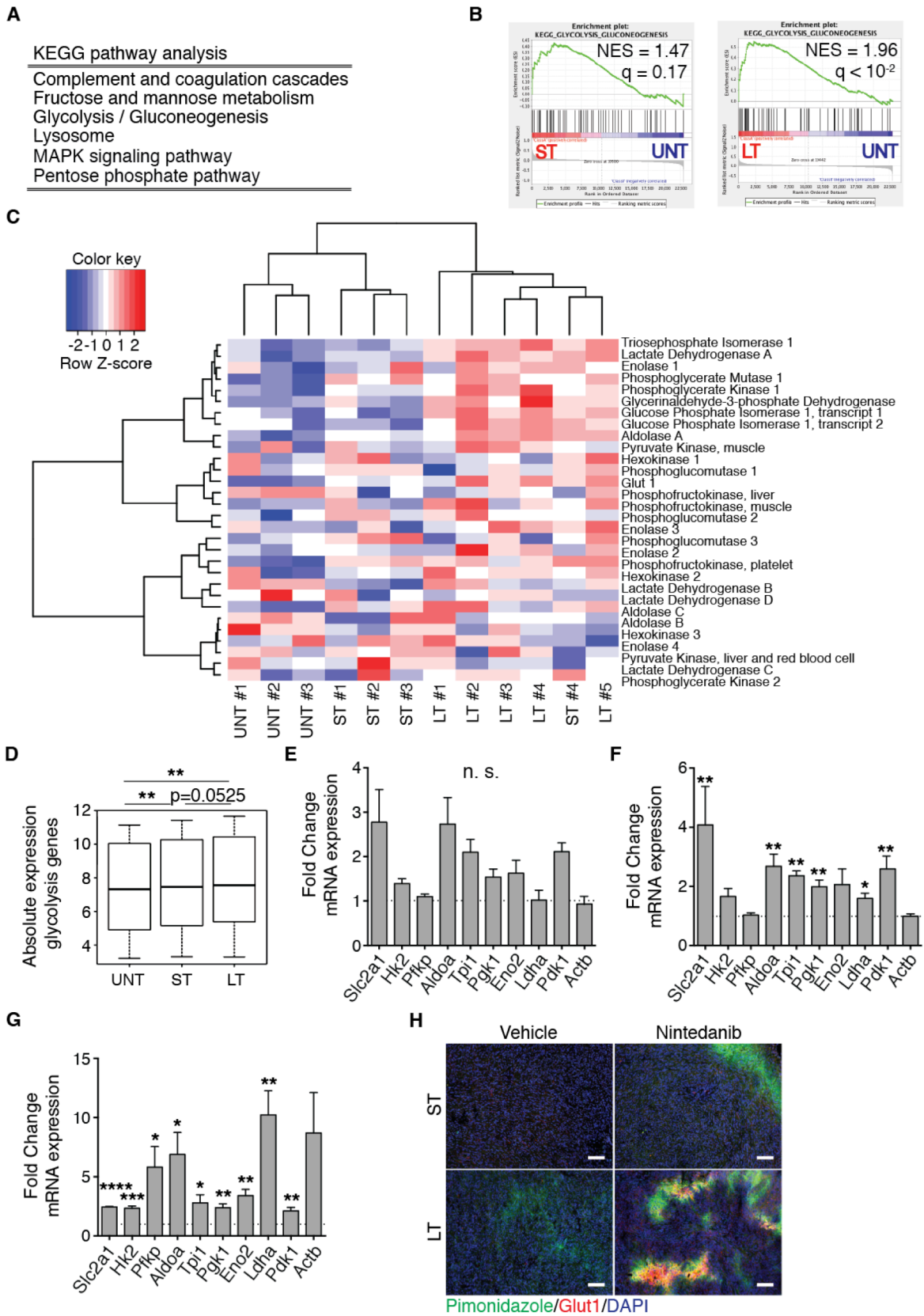
Figure 3. Py2T tumor cells become hyperglycolytic during nintedanib treatment.
(A) Differential gene expression between flow cytometry-isolated LT nintedanib and vehicle-treated tumor cells was assessed using no p-value cutoff combined with a range of fold change cutoff values from 1.2-1.7. The resulting list of differentially expressed genes was subjected to KEGG pathway analysis. KEGG pathways appearing >2 are listed. (B) Gene set enrichment analysis (GSEA) between gene expression profiles of either ST or LT nintedanib and vehicle-treated tumor cells and a set of KEGG defined genes related to glycolysis/gluconeogenesis are shown. Shown are the normalized enrichment score (NES) and the FDR q-value. (C, D) A set of core glycolysis enzymes was used to perform hierarchical clustering (C) of gene expression profiles derived from LT and ST nintedanib and vehicle-treated controls and their median absolute expression values (log2) per experimental group (D) are shown. (E, F) Expression of different glycolysis-related transcripts in ST (E) and LT (F) nintedanib-treated tumors analyzed by quantitative RT-PCR. Data are normalized to vehicle-treated tumors. Shown are mean ± SEM. N = 4 mice per group. Statistical significance was calculated using Mann–Whitney *U* test. n. s.: non significant; *, $P < 0.05$; **, $P < 0.01$. (G) Expression of different glycolysis genes in Py2T cells cultured in hypoxic conditions analyzed by quantitative RT-PCR. Data are normalized to cells cultured in normoxic conditions. Shown are means ± SEM. N = 4. Statistical significance was calculated using Student *t* test. *, $P < 0.05$; **, $P < 0.01$; ***, $P < 0.001$; ****, $P < 0.0001$. (H) Representative microphotographs of immunofluorescence co-stainings for pimonidazole and Glut1 on histological sections of tumors from ST and LT vehicle or nintedanib-treated mice. DAPI is used to visualize cell nuclei. Scale bar, 100µm.

Because nintedanib-treated tumors exhibited enhanced hypoxia compared to size-matched vehicle-treated tumors (Figure 2G, H), we hypothesized that hypoxia could be a determinant of tumor cell heterogeneity and a direct inducer of the glycolytic shift. As expected, when compared with normoxic cultures, Py2T cells cultured for 3 days in hypoxic conditions (1% O_2) exhibited a significantly increased expression of the ten glycolysis-related transcripts analyzed (Figure 3G). Consistent with this result, immunofluorescence microscopy analysis revealed an increased expression of the hypoxia-regulated glucose transporter Glut1 in the hypoxic areas of LT nintedanib-treated tumors (Figure 3H).

Together, the data suggest a metabolic adaptation to anti-angiogenic therapy, in which hypoxic tumor cells shift to a hyperglycolytic state to survive and proliferate with reduced oxygen and nutrient supply.

3.3.4.4   *Glycolysis inhibition overcomes resistance to anti-angiogenic therapy*

Since nintedanib treatment promotes a metabolic shift towards glycolysis, we tested whether glycolysis inhibition might overcome the observed resistance to this anti-angiogenic therapy. mTOR, among many other cell growth-promoting functions, is a well-known inducer of glycolysis [404], and a previous study reported that the combination treatment of bevacizumab and BEZ235, a mTOR inhibitor, led to significant efficacy in a breast cancer model [405]. We here investigated the effect of the mTOR inhibitor rapamycin in combination with nintedanib. Indeed, rapamycin significantly delayed tumor growth by itself, yet showed an additive effect when used in combination with nintedanib (Figure S4A, B).

The small molecule 3PO inhibits the glycolytic activator PFKFB3 in endothelial cells [236]. Its combined activity as a glycolysis and endothelial cell inhibitor made it a prime

compound to overcome glycolysis-induced resistance to anti-angiogenic therapy [237]. While single treatment with nintedanib significantly repressed tumor growth in Py2T-transplanted mice, single treatment with 3PO only marginally delayed it (Figure 4A, B). Notably, the combined treatment with nintedanib and 3PO showed an additive effect on tumor growth inhibition. Importantly, the additive effect achieved by combining nintedanib with 3PO was not mediated by an additive anti-angiogenic effect, since the microvessel densities between the nintedanib single and the nintedanib plus 3PO combination treatment were not significantly altered (Figure 4C). Collectively, these results suggest that the inhibition of glycolysis is one avenue of overcoming resistance to anti-angiogenic therapy with multikinase inhibitors.

3.3.4.5   Targeting metabolic symbiosis delays resistance development

Considering the highly glycolytic phenotype of nintedanib-treated tumor cells, we further analyzed lactate production in Py2T tumors. Unexpectedly, total lactate production was not increased in nintedanib-treated tumors compared to vehicle-treated tumors (Figure S5A). This observation may be explained by a fast metabolic utilization of lactate. The alternation between highly hypoxic, glycolytic areas and normoxic areas in the nintedanib-treated tumors (Figure 3H), together with comparable levels of lactate between nintedanib and vehicle-treated tumors, suggests the establishment of lactate-based metabolic symbiosis [400]. In such symbiosis, hypoxic glycolytic cells use glucose to produce high levels of lactate that is rapidly exported through monocarboxylate transporter 4 (MCT4), mainly a lactate exporter. Oxidative cells located in perfused areas express MCT1, mainly a lactate importer, allowing them to take up lactate and directly fuel their Krebs cycle. Because these cells do not rely on glycolysis, glucose can bypass them and diffuse to hypoxic areas, where it is taken up by glycolytic cells expressing high levels of hypoxia-induced GLUT1 to produce lactate [399].
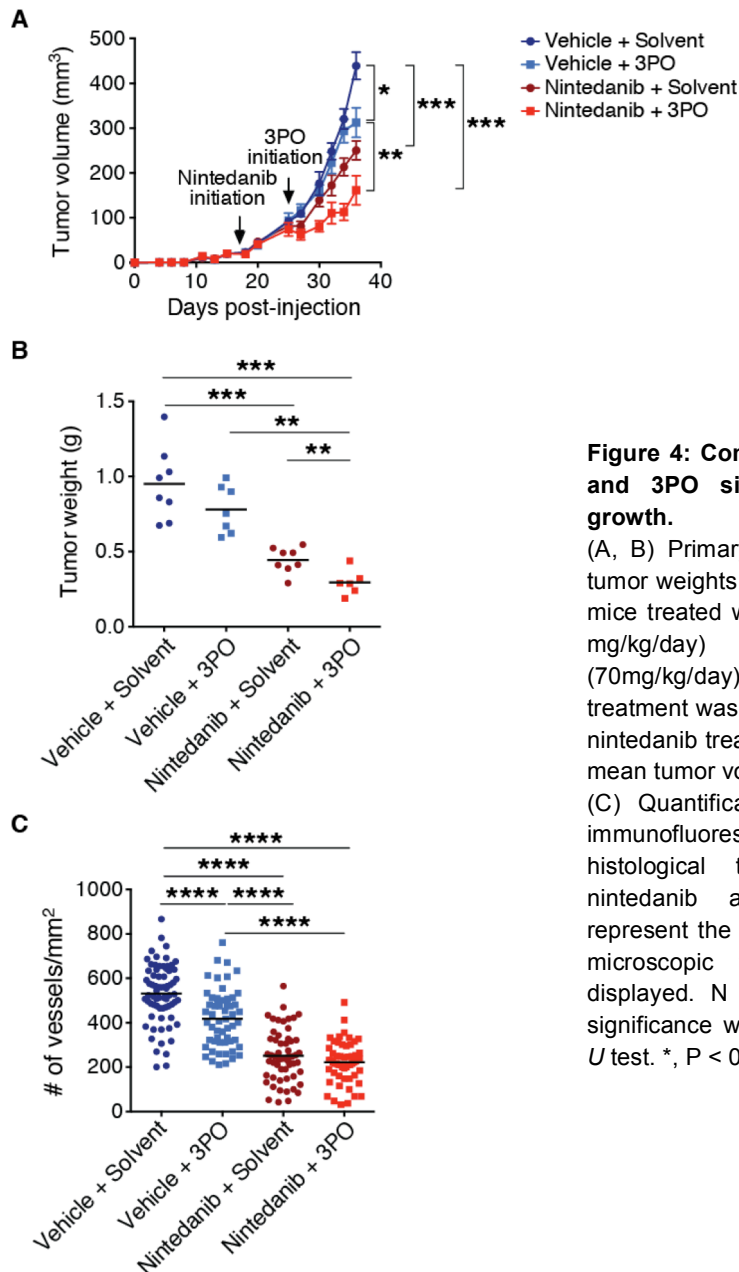
Figure 4: Combined treatment with nintedanib and 3PO significantly delays Py2T tumor growth.

(A, B) Primary tumor growth over time (A) and tumor weights at the experimental end point (B) of mice treated with either vehicle or nintedanib (50 mg/kg/day) in combination with 3PO (70mg/kg/day) or solvent are shown. 3PO treatment was initiated 8 days after the initiation of nintedanib treatment. In (A), data are displayed as mean tumor volumes ± SEM.

(C) Quantification of microvessel densities by immunofluorescence staining for CD31 on histological tumor sections from long-term nintedanib and 3PO-treated mice. Values represent the number of counts per each area of microscopic field of view and means are displayed. N = 6-8 mice per group. Statistical significance was calculated using Mann–Whitney U test. *, $P < 0.05$; ***, $P < 0.001$; ****, $P < 0.0001$.

We assessed the establishment of metabolic symbiosis during the development of resistance against nintedanib-mediated anti-angiogenic therapy in the Py2T transplantation model of breast cancer. Immunofluorescence staining for MCT1 and MCT4 demonstrated a diffuse baseline expression of MCT1 that stayed unchanged during nintedanib treatment, whereas MCT4 was highly expressed in non-vascularized areas of LT nintedanib-treated tumors and to a lesser extent in ST-treated tumors (Figure 5A and Figure S5B, C). Similar results were observed in sunitinib-treated tumors (Figure S5D).

To determine whether the inhibition of metabolic symbiosis could overcome the development of resistance against anti-angiogenic therapy, we generated Py2T cell lines that were devoid of MCT4 by the expression of short hairpin RNAs against MCT4 (shMCT4 #1-5). Py2T shMct4 cell lines #1, #2, #4 and #5 displayed decreased MCT4 expression (also known as Solute carrier 16 a3; *Slc16a3*), notably when Py2T cells were cultured in hypoxic conditions (Figure S5E). shMCT4 #2 and shMCT4 #5 Py2T cell lines were selected for tumor transplantation experiments. The loss of MCT4 expression in shMCT4 significantly retarded tumor growth as compared to shCtrl cells, even in the absence of any nintedanib treatment (Figure 5B). Notably, treatment of shMCT4-transplanted mice with nintedanib led to an additive effect in repressing tumor growth kinetics and final tumor weights (Figure 5B and 5C). However, after this further delay in tumor growth, shMCT4 tumors resumed growth. Immunofluorescence staining for CD31 did not reveal any increase in microvessel density in nintedanib-treated shMCT4 tumors, excluding an escape route by revascularization (Figure 5D). Instead, we observed an increase of MCT4 expression both at the protein and mRNA level in nintedanib-treated shMCT4 tumors, suggesting that cells with poor shRNA-mediated knockdown efficiency developed a selective growth advantage and elicited tumor recurrence (Figure S5F, G).

To assess the generality of our findings, we analyzed microvessel densities and MCT4 expression in tumors of Rip1Tag2 transgenic mice that have been treated with nintedanib [380]. The Rip1Tag2 transgenic mouse model of pancreatic neuroendocrine carcinoma is highly sensitive to anti-angiogenic therapies. It has been instrumental for compound testing and their subsequent successful translation to the treatment of patients with PNETs [258]. In this experiment, nintedanib treatment was initiated at 10 weeks of age, which prolonged median survival from 24 days in control-treated animals to 55 days in nintedanib-treated animals. However, similar to the Py2T breast cancer model, Rip1Tag2 mice also developed resistance to nintedanib therapy and did not display any revascularization in therapy-refractory tumors (Figure 5E). MCT4 expression in tumors was also only found after prolonged nintedanib treatment (Figure 5F).
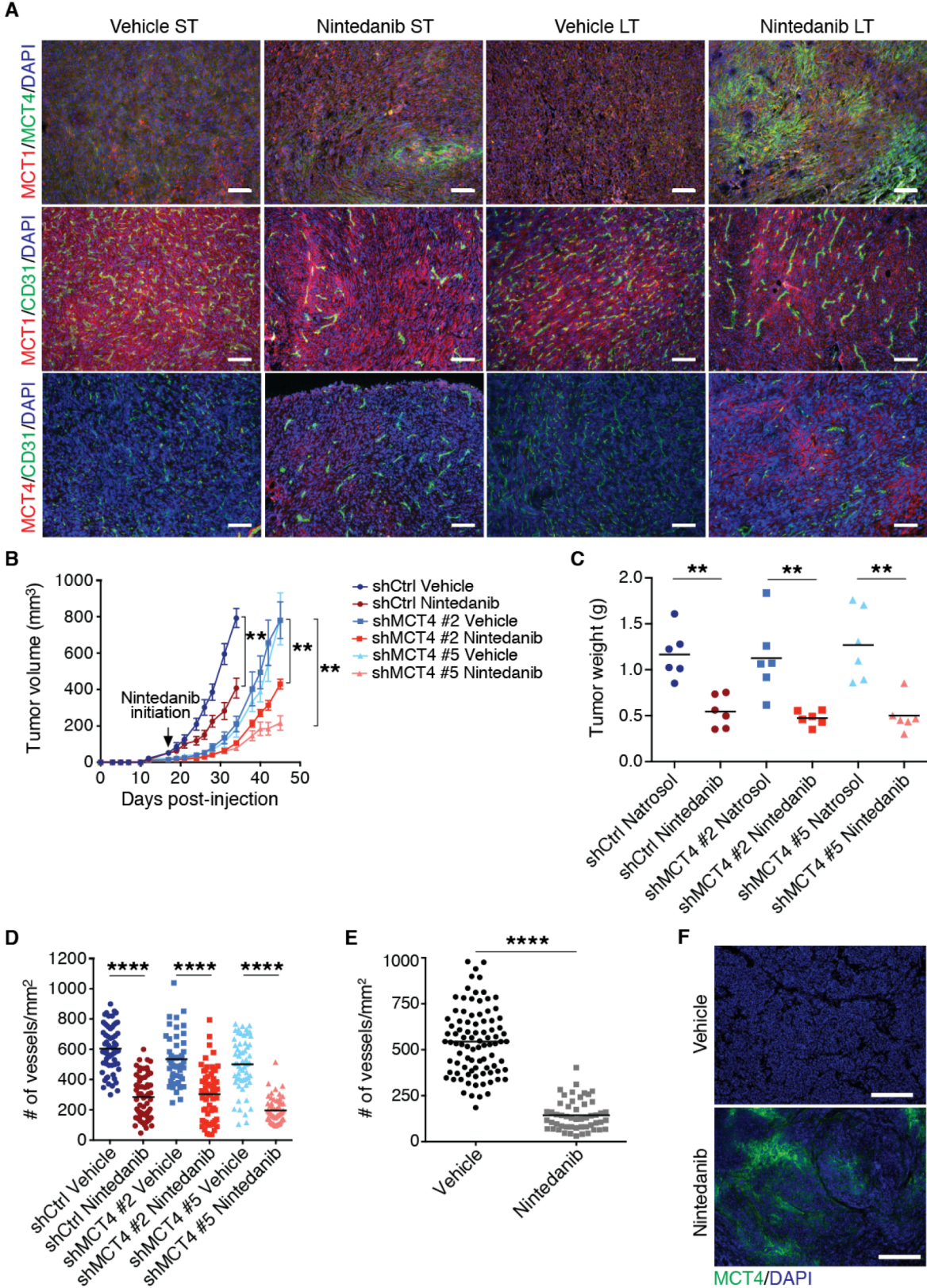
Figure 5. Targeting metabolic symbiosis in combination with nintedanib treatment significantly delays tumor growth.
(A) Representative pictures of combinatorial immunofluorescence staining for MCT1, MCT4 and CD31 on histological sections of tumors from mice treated with either vehicle or nintedanib (50 mg/kg/day) are shown, as indicated. DAPI was used to visualize cell nuclei. Scale bars, 100µm. (B, C) Primary tumor growth (B) and terminal tumor weights (C) of mice following orthotopic injection of Py2T shCtrl or Py2T shMCT4 #2 and #5 cell lines treated with either vehicle or nintedanib (50 mg/kg/day) have been quantified. The time points for animal

96

sacrifice were chosen for all three cell lines individually such that all the tumors of the corresponding vehicle-treated groups were size matched. In (B), mean ± SEM is depicted. (D) Quantification of microvessel densities by immunofluorescence staining for CD31 on Py2T shMCT4 tumors from LT vehicle or nintedanib-treated mice. N = 6 mice per group. Statistical significance was calculated using Mann–Whitney U test. ****, P < 0.0001. (E, F) Shown are microvessel densities (E) and representative immunofluorescence stainings for MCT4 (F) in tumors of Rip1Tag2 transgenic mice treated for 3 weeks (LT) with nintedanib. DAPI was used to visualize cell nuclei. N = 8-9 mice per group. Scale bars, 200µm. Statistical analysis was performed using unpaired Students t test (E).

Taken together, these data show that anti-angiogenic resistance can occur via the establishment of metabolic symbiosis and that interfering with metabolic symbiosis can overcome resistance to anti-angiogenic therapy with a multikinase inhibitor.
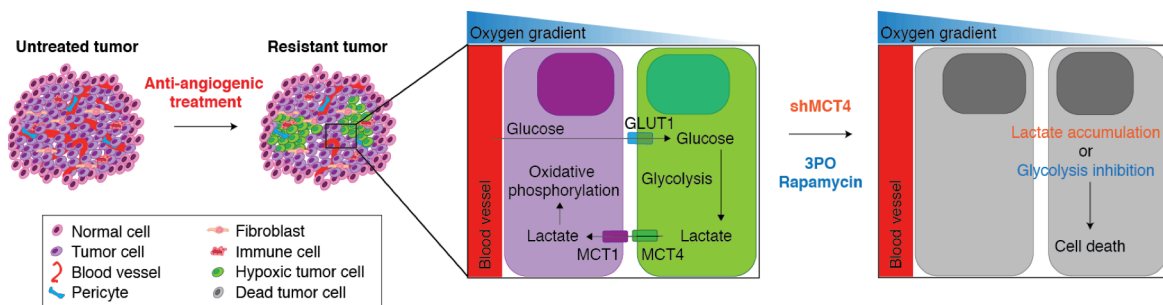
Figure 6. Targeting metabolic symbiosis overcomes resistance to anti-angiogenic therapy.
Anti-angiogenic therapy induces hypoxia and reduces the supply of nutrients. In order to survive in this harsh environment, tumor cells shift their metabolism towards a hyperglycolytic state and establish metabolic symbiosis: tumor cells in hypoxic areas upregulate glycolysis, increase lactate production and export lactate via MCT4 to maintain their intracellular pH on a constant level. On the other hand, lactate is taken up by tumor cells in more oxygenated regions of the tumor and is directly fueling the citric acid cycle and thus oxidative phosphorylation. As a consequence, tumor cells in normoxic tumor regions reduce glucose consumption, which increases its diffusion distance. Reducing MCT4 expression levels (shMCT4) or inhibition of glycolysis (3PO) or mTOR signaling (rapamycin) disrupts this homeostatic interplay and decreases tumor growth.

3.3.5 Discussion

In this and in the accompanying paper by Hanahan and colleagues (Allen et al., submitted), we report the intriguing finding that a glycolytic shift underlies the development of resistance to anti-angiogenic therapy involving potent multi-kinase inhibitors. Notably, in response to the efficient repression of tumor angiogenesis, tumors compartmentalize into hypoxic regions at a distance from blood perfusion and into normoxic regions in the vicinity of mature and functional blood vessels. The hypoxic tumor cells exhibit high glucose uptake by the elevated expression of GLUT1 and they efficiently generate and export lactate by the high expression of the lactate exporter MCT4. Conversely, the normoxic tumor cells take up the lactate produced by the hypoxic tumor cells and oxygen from nearby blood vessels and

fuel both into oxidative phosphorylation (Figure 6). Such aspect of metabolic intra-tumoral heterogeneity is portrayed by the concept of metabolic symbiosis [399].

Here, we have analyzed the efficacy of the angiokinase inhibitors nintedanib and sunitinib in a preclinical mouse model of breast cancer and in the Rip1Tag2 transgenic mouse model of insulinoma (pancreatic neuroendocrine cancer). Treatment of Py2T tumor-bearing mice and of Rip1Tag2 mice with the angiogenesis inhibitors has lead to a significant therapeutic response, characterized by increased tumor and endothelial cell apoptosis, decreased tumor cell proliferation and reduced tumor size. However, despite nintedanib's and sunitinib's potent anti-angiogenic activities in the experiments reported here, the treated tumors rapidly escape the therapy. Evasive resistance to anti-angiogenic therapy has previously been reported to rely partially on the redundancy of pro-angiogenic growth factors leading to tumor revascularization [333, 334, 351]. Intriguingly, the nintedanib and sunitinib-resistant tumors do not show any evidence of revascularization. Rather, with the reduction in tumor perfusion, hypoxia is increased in resistant tumors, and microarray gene expression analysis reveals a metabolic shift to glycolysis in the resistant tumor cells. Indeed, glycolysis and glucose transport-related genes are well known targets of hypoxia-induced cellular adaptations [406], and glycolysis induction has been recently described in response to VEGF-inhibitors [407, 408].

The tumor cells' shift to glycolysis as a mechanism underlying resistance against anti-angiogenic therapy offers the opportunity of defeating therapy-resistance by interfering with glycolysis. Indeed, in this report and in the accompanying report by Hanahan and colleagues (Allen et al., submitted), combination therapy involving angiokinase inhibitors with rapamycin, an mTOR inhibitor that represses glycolysis [409], or 3PO, a glycolytic flux inhibitor [236, 410] surmounts resistance to treatment. However, combination treatment of nintedanib with 2-deoxyglucose, a competitive inhibitor of the production of glucose-6-phosphate from glucose [411], did not delay tumor growth, most likely due the fact that we have been unable to supply the very high concentrations of 2-deoxyglucose in tumors that would be pharmacologically active (data not shown). Dichloroacetate (DCA), a drug inhibiting pyruvate dehydrogenase kinase and thus promoting glucose oxidation over glycolysis by increasing the pyruvate flux into mitochondria [412], also has not shown any effect on tumor growth (data not shown). Hence, the pharmacological targeting of glycolysis in the context of anti-angiogenic therapy may be more complex than anticipated.

Along these lines, despite a clear hypoxia-response pattern to nintedanib therapy, high-throughput metabolomic analysis has failed to show any significant differences in the

central carbon metabolism between nintedanib LT and untreated tumors (data available upon request). In addition, surprisingly few metabolites are significantly changed between these two experimental conditions when considering the dramatic reduction in microvessel densities. Importantly though, the high throughput metabolomic analysis has not given critical information about metabolic flux, and flux analysis will be required to delineate the changes in metabolic pathways, when tumor cells are confronted with experimentally induced acute or chronic hypoxia. Notably, a recent investigation of metabolic changes in tumors after cessation of sunitinb or sorafenib therapy has revealed a metabolic shift to lipid synthesis, and blockade of lipidogenesis has inhibited tumor regrowth [413].

Regions with higher oxygen partial pressure metabolize lactate produced in hypoxic areas and thus increase the diffusion capacity of oxygen and glucose. Indeed, increased expression of MCT4 has been correlated with poor prognosis in melanoma and breast cancer [414, 415]. Accordingly, shRNA-mediated ablation of MCT4 expression in Py2T tumors treated with nintedanib show significantly delayed tumor growth. The critical function of MCT4 in metabolic symbiosis is also illustrated by the fact that a longer period of nintedanib treatment of shMCT4 knockdown tumors selected for outgrowth of revertant MCT4-expressing Py2T tumor cells. Our data therefore suggest that i) despite the broad range activities of the multi-kinase inhibitor nintedanib, tumors can still escape treatment; ii) nintedanib and sunitinib resistance does not occur via tumor revascularization but is induced by a metabolic shift towards hyperglycolysis and the establishment of metabolic symbiosis; iii) nintedanib and sunitinib treatment should be used in combination with glycolysis/metabolic symbiosis inhibitors for long-term efficacy (Figure 6). Notably, the very recent development of specific MCT4 inhibitors may open interesting therapeutic opportunities [416].

In conclusion, the data presented here and in the accompanying report by Hanahan and colleagues (Allen et al., submitted) underscore the variety of evasive responses to anti-angiogenic and likely to other targeted therapies. The establishment of metabolic symbiosis adds not only another level of complexity but also a number of novel drugable targets to the design of combinatorial therapies. The results also emphasize the importance of intra-tumoral heterogeneity as therapy response, in particular with regard to oxygen and nutrient availability. Such heterogeneity likely masks critical adaptation mechanisms when performing cross-sectional analysis without spatial resolution.

3.3.6 Experimental Procedures

Mice

FVB/N mice were kept and bred under specific pathogen-free (SPF) conditions. The generation and characterization of Rip1Tag2 transgenic mice has been described elsewhere [246]. All experiments were performed following the rules and legislations of the Cantonal Veterinary Office, Basel-Stadt, Switzerland and the Swiss Federal Veterinary Office (SFVO) under licence numbers 1878, 1907 and 1908.

Cell lines and orthotopic tumor cell transplantation

Py2T murine breast cancer cells were cultured as previously described [400]. 5×10^5 cells were orthotopically injected into the mammary gland number 9 of 7-11 weeks old female FVB/N mice under isoflurane/oxygen anesthesia. Tumor length (l) and width (w) were assessed 3 times per week using a vernier caliper and tumor volume (V) was calculated using the formula $V=0.543*l*w^2$.

Therapy studies

Treatment of Py2T tumor-bearing mice was initiated when tumors reached a measurable size (15-20mm^3) to allow a thorough stratification into experimental groups with similar mean tumor volumes. Nintedanib (kindly provided by Boehringer Ingelheim) was formulated in 0.5% natrosol hydroxyethylcellulose (Boehringer Ingelheim) and administered daily at 50mg/kg body weight (BW) by oral gavage. Rip1Tag2 transgenic mice were treated with the same regimen from 10 weeks of age onwards [380]. Sunitinib L-malate (LC Laboratories) was administered at 40 mg/kg in carboxymethylcellulose daily by oral gavage as described [267]. 3PO (Axon Medchem, 2175) was dissolved in a 10% EtOH, 40% PEG, 50% PBS solution and administered at 70mg/kg daily by i.p. injection. Treatment was initiated at day 8 of nintedanib treatment. Rapamycin was dissolved in 5% PEG 400, 4% EtOH, 5% Tween 20 and administrated at 2 mg/kg three times a week by i.p. injection. Animals of the experimental arms were euthanized by CO_2 (or cervical dislocation for hypoxia studies), either time- or size matched to the control treatment. Primary tumors were dissected and processed for further analyses.

Hypoxia and vessel functionality

To assess functional blood vessel perfusion, 100μg of fluorescein-labeled *Lycopersicon esculentum* (tomato) lectin (Vector Laboratories, GL-1171) was injected into the tail vein. Two minutes later, mice were terminally anaesthetized and five minutes later perfused via the left cardiac ventricle first with cold 4% PFA and subsequently with cold PBS.

To identify hypoxic tumor areas, 60mg/kg pimonidazole-HCl (Hypoxyprobe Omni Kits, Hypoxyprobe, Inc.) dissolved in PBS was injected i.p. 1 hour before euthanizing the animals by cervical dislocation.

Immunofluorescence microscopy

Tumors were fixed in 4% PFA for 2 hours followed by overnight incubation in 20% sucrose to cryopreserve the tissue, both at 4°C. Then, tumors were snap frozen in Tissue-Tek OCT compound (Thermo Scientific) and stored at -80°C. Eight µm thick tumor sections were cut, dried for 30 minutes, rehydrated with PBS, permeabilized with 0.2% Triton X-100 for 20 minutes and blocked with 5% normal goat serum (NGS; Sigma-Aldrich) for 1 hour. As an exception, when performing stainings with anti-cCasp3 antibodies, blocking was performed using 20% NGS. When using a goat primary antibody, sections were blocked with 5% bovine serum albumin. Subsequently, primary and secondary antibodies were diluted in blocking solution and incubated overnight and 1 hour, respectively, at 4°C. Images were acquired with a Leica DMI microscope.

Antibodies used: rabbit anti- cCasp3 (Cell Signaling, 9664, 1:50), rat anti-CD31 (BD Pharmingen, 550274, 1:50), rabbit anti-NG2 (Chemicon, AB5320, 1:100), rabbit anti-pH3 (Millipore, 06-570, 1:200), rabbit anti-pimonidazole (Hypoxyprobe, 1:25), goat anti-MCT1 (Santa Cruz, sc-14917, 1:50), rabbit anti-MCT4 (Santa Cruz, sc-50329, 1:50), goat anti-GLUT1 (Santa Cruz, sc-1605, 1:50). Primary antibody binding was detected by incubating the histological sections with secondary antibodies directed against the respective species of the primary antibodies for 1 hour at room temperature, diluted 1:200 in blocking solution. Secondary antibodies were fluorescently tagged with Alexa 488, Alexa 568 or Alexa 633 (Molecular probes). Subsequently, nuclei were stained with 4′,6-Diamidin-2-phenylindol (DAPI; Sigma-Aldrich; 1:10,000) followed by mounting the slides with Dako mounting medium (Dako).

Flow cytometry

Freshly dissected Py2T primary tumors were immediately minced into small pieces and digested for 30 minutes at 37°C on a bacterial shaker in DMEM (Sigma-Aldrich) supplemented with Nu-Serum Growth Medium Supplement (6%; Corning), DNase I (200 µg/ml; Roche), Dispase II (1.2mg/ml; Roche) and Collagenase D (1.2mg/ml; Roche). To achieve a single cell suspension, the digested tissue was first passed through a 70µm and subsequently through a 40µm cell strainer (Corning). Cells were washed in FACS-buffer (5% fetal bovine serum in PBS; Sigma-Aldrich). Fc-receptors were blocked with an antibody against CD16/CD32 (BioLegend, 101302, 1:100) diluted in FACS-buffer for 30 minutes at

4°C. Then, cells were incubated for 45 minutes on ice with the following antibodies: hamster anti-mouse podoplanin (Hybridoma supernatant clone 8.1.1, 1:10), anti-CD8α-FITC (BioLegend, 100705, 1:150), anti-CD31-APC (BioLegend, 102409, 1:200), anti-CD45-APC-Cy7 (BioLegend, 103116, 1:500). Staining for podoplanin was achieved by subsequently incubating the cells for 30 minutes on ice with an anti-hamster PE-labeled secondary antibody (eBioscience, 12-4112-83, 1:200). Immediately before sorting with a FACSAriaII (BD Bioscience), cells were filtered through a 40µm mesh and propidium iodide (PI) was added to exclude dead cells. Tumor cells were sorted into FACS-buffer by gating on CD8α$^+$/CD45$^-$ cells (Figure S3D). Endothelial cells were directly sorted into the lysis buffer of the Absolutely RNA Nanoprep Kit (Stratagene) by gating on CD31$^+$/CD45$^-$/Podoplanin$^-$ cells (Figure S3D).

RNA isolation

RNA of sorted endothelial cells was isolated using the Absolutely RNA Nanoprep Kit (Stratagene) following the manufacturer's recommendations. RNA of sorted tumor cells was isolated using TRIzol® LS reagent (Ambion®) and RNA Easy Mini Kit (Qiagen). To isolate RNA from whole tumors, previously snap frozen tissues were homogenized in Tri Reagent (Sigma-Aldrich) using a POLYTRON® (Kinematica) and isolated following the manufacturer's recommendations.

Microarray analysis

Total RNA preparations of flow cytometry-sorted tumor and endothelial cells were analyzed using an Agilent 2100 bioanalyzer. Target synthesis was performed using the following suite of kits provided by Nugen (San Carlos, USA): WT-Ovation Pico (Cat# 3300), WT-Ovation Exon (Cat# 2000) and FL-Ovation Biotin V2 (Cat# 4200). The hybridization cocktail (200µl) containing fragmented biotin-labeled target DNA at a final concentration of 25ng/µl was transferred into Affymetrix GeneChip MoEx-1_0-st-v1 (Affymetrix Cat # 900187) and incubated at 45°C on a rotator in a hybridization oven 640 (Affymetrix) for 17 h at 60 rpm. The arrays were washed and stained on a Fluidics Station 450 (Affymetrix) by using the Hybridization Wash and Stain Kit (Affymetrix, Cat# 900720) and the Fluidics Procedure FS450_0001. The GeneChips were processed with an Affymetrix GeneChip® Scanner 3000 7G (Affymetrix). DAT image files of the microarrays were generated using Affymetrix GeneChip Command Console (AGCC, version 0.0.0.676, Affymetrix).

Bioinformatical analysis

All microarray data were preprocessed and analyzed using R (software environment for statistical computing and graphics) version 3.1.0 (2014-04-10) and packages provided by the Bioconductor package library. Raw Affymetrix CEL files were subjected to background correction and normalization using the Robust Multichip Average (RMA) algorithm (rma method, oligo package). Differential gene expression was determined using the limma package (Smyth et al., 2005) with and without a p-value cutoff of 0.05 and a range of fold-change values (FC = 1.2 to 1.7). The results of differential gene expression were used to conduct pathway enrichment analysis provided by The Database for Annotation, Visualization and Integrated Discovery (DAVID) v6.7 [417, 418], with a particular focus on pathways defined in the Kyoto Encyclopedia of Genes and Genomes (KEGG) database.

The background-corrected and normalized gene expression datasets associated with the placebo-treated (UT), 1 week-treated (ST), and 3 week-treated (LT) samples were subjected to Gene Set Enrichment Analysis (GSEA) using GSEA V2.1.0. Three sets of analyses were conducted: ST versus UT, LT versus UT and ST versus LT. In all cases the default run-time arguments were used except for the "Permute" parameter that was set to "gene_set" (in order to accommodate less than 7 samples per class). In addition, analyses were conducted against the "MoGene_1_0_st.chip" microarray annotation and the following gene set libraries: "c2.cp.kegg.v4.0.symbols.gmt" and "c2.cp.reactome.v4.0.symbols.gmt" [403, 419].

Heat maps were generated using the heatmap.2 method provided by the gplots package. Boxplots were generated using the default boxplot method provided in R and based on the median background corrected and normalized expression value for each gene with respect to all samples within each sample class (UT, ST and LT). Additional statistical analyses were also carried out using GraphPad Prism 6 (GraphPad Prism Software Inc.).

Quantitative RT-PCR

RNA was reverse transcribed using M-MLV reverse transcriptase (Promega) and quantitative PCR was performed using SYBR-green PCR MasterMix (Applied Biosystems) in a StepOne Plus PCR machine (Applied Biosystems). Fold change expression was determined by the comparative Ct method ($\Delta\Delta C_t$) normalized to 60S Ribosomal protein L19 expression. Primers for quantitative PCR are listed in Table S1.

Lactate assay

Lactate concentration was determined on tumor lysate by using the L-Lactate Assay Kit from Abcam (ab65331) following the manufacturer's recommendations.

Lentiviral infection

Lentiviral plasmids containing short-hairpin RNAs #1-5 (shRNA) against mouse MCT4 were purchased from Sigma-Aldrich (Mission Non-Targeting shRNA control vector: SHC002; shMCT4 #1: TRCN0000079653, shMCT4 #2: TRCN0000079654, shMCT4 #3: TRCN0000079655, shMCT4 #4: TRCN0000079656, shMCT4 #5 TRCN0000079657). In order to produce lentiviral particles, HEK293T cells were transfected with the shRNA containing plasmids, the helper vectors pMDL and pREV and the envelope encoding plasmid pVSV using FugeneHD. Virus containing supernatant was conditioned for 2 days, filtered through a 0.45μm filter, gently mixed with Lenti-X Concentrator (Clontech), and followed by an overnight incubation at 4°C and subsequent centrifugation the next day. The virus-containing pellet was resuspended in fresh complete DMEM medium, 8ng/ml polybrene was added and Py2T cells were infected. Successfully transfected cells were selected by puromycin treatment (5μg/ml). Knockdown efficiency was determined by measuring hypoxia-induced (96h, 1% O_2) MCT4 mRNA expression by quantitative RT-PCR.

Statistical analysis

Data analysis and graph generation was performed using GraphPad Prism 6 (GraphPad Prism Software Inc.).

3.3.7   Supplementary data

A

B

15 mm³ tumor

CD31/DAPI
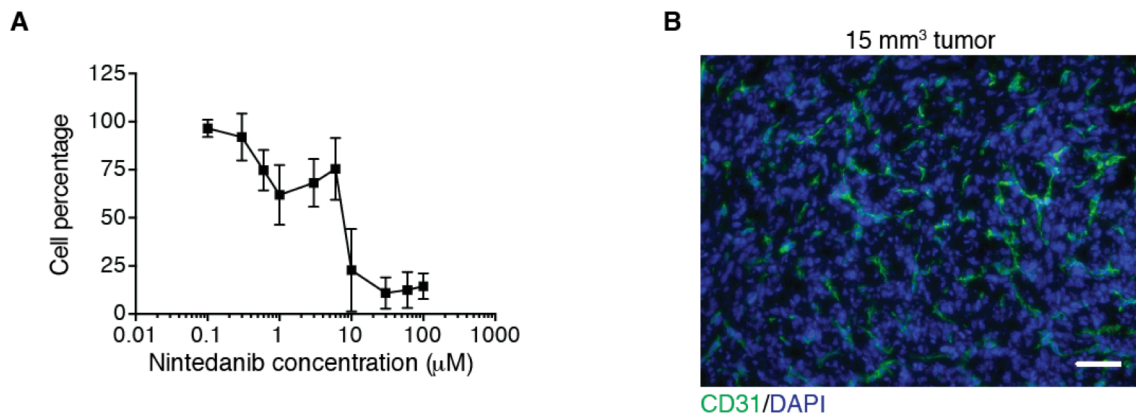
Figure S1. Nintedanib treatment of Py2T cells in vitro.
(A) The inhibitory effect of increasing concentrations of nintedanib after 72 hours of treatment on Py2T tumor cell numbers has been determined by using an MTT assay in vitro. Data are shown as mean cell number normalized to control cells ± SD from three independent experiments. (B) Representative immunofluorescence microphograph showing CD31-positive blood vessels in a tumor with a volume of 15mm3 representing the time point at which treatments were generally initiated. DAPI was used to visualize cell nuclei. Scale bar, 50µm.
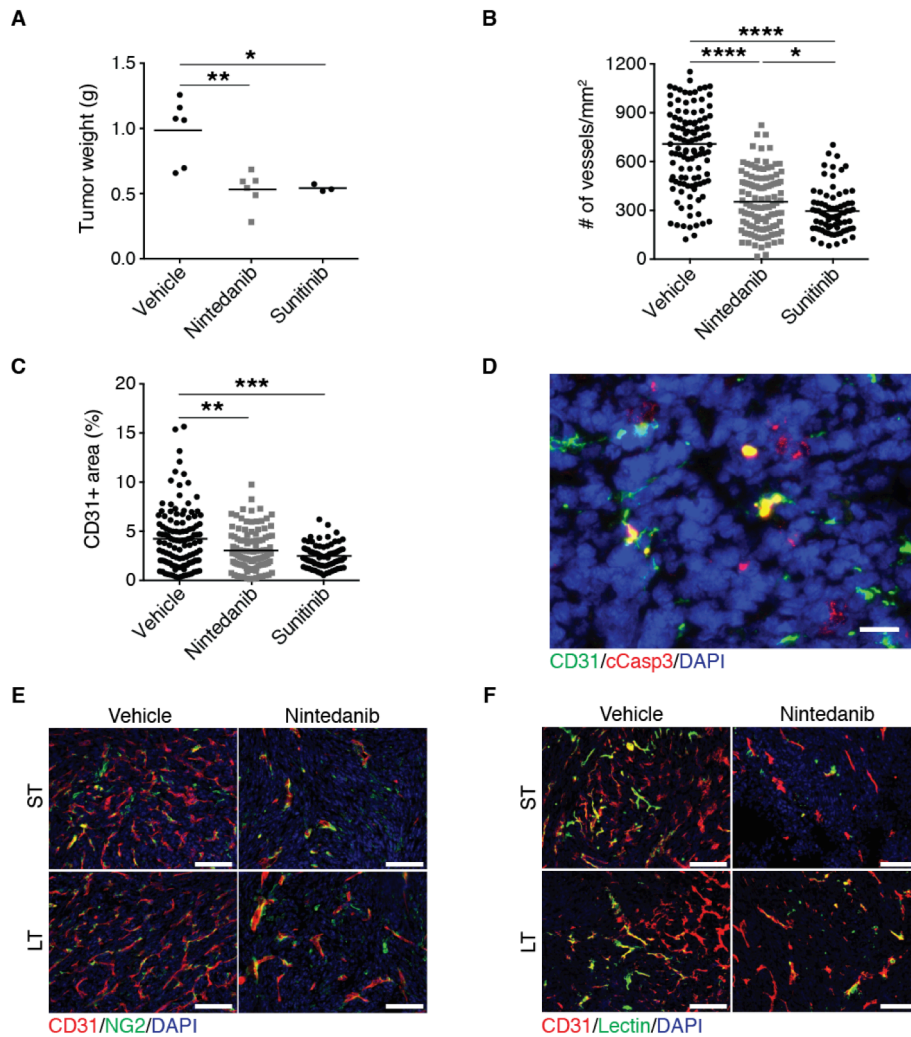
Figure S2. Nintedanib and sunitinib treatments demonstrate potent anti-angiogenic effects.
(A- C) Py2T tumor-bearing mice were treated with nintendanib or sunitinib during 21 days, and mice were sacrificed at day 35 post tumor cell injection. Tumor weights at the experimental end point (A), microvessel densities (B) and CD31-positive area fractions per field of view (C) determined by immunofluorescence staining are shown. N = 3-6 mice per group. Statistical significance was calculated using Mann–Whitney *U* test. *, P < 0.05; **, P < 0.01; ***, P < 0.001; ****, P < 0.0001. (D) Endothelial cell apoptosis (CD31, green; cCasp3, red) is shown on representative immunofluorescence picture of a tumor from a 1 week (ST) nintedanib-treated mouse. DAPI was used to visualize cell nuclei. Scale bars, 20µm.(E) Blood vessel (CD31, red) coverage by perivascular cells (NG2, green) is shown on representative immunofluorescence pictures of tumors from ST and LT vehicle or nintedanib-treated mice. DAPI staining visualizes cell nuclei. Scale bars, 100µm. (F) Blood vessel (CD31, red) perfusion (lectin, green) is shown on representative immunofluorescence pictures of tumors from ST and LT vehicle or nintedanib-treated mice. DAPI was used to visualize cell nuclei. Scale bars, 100µm.
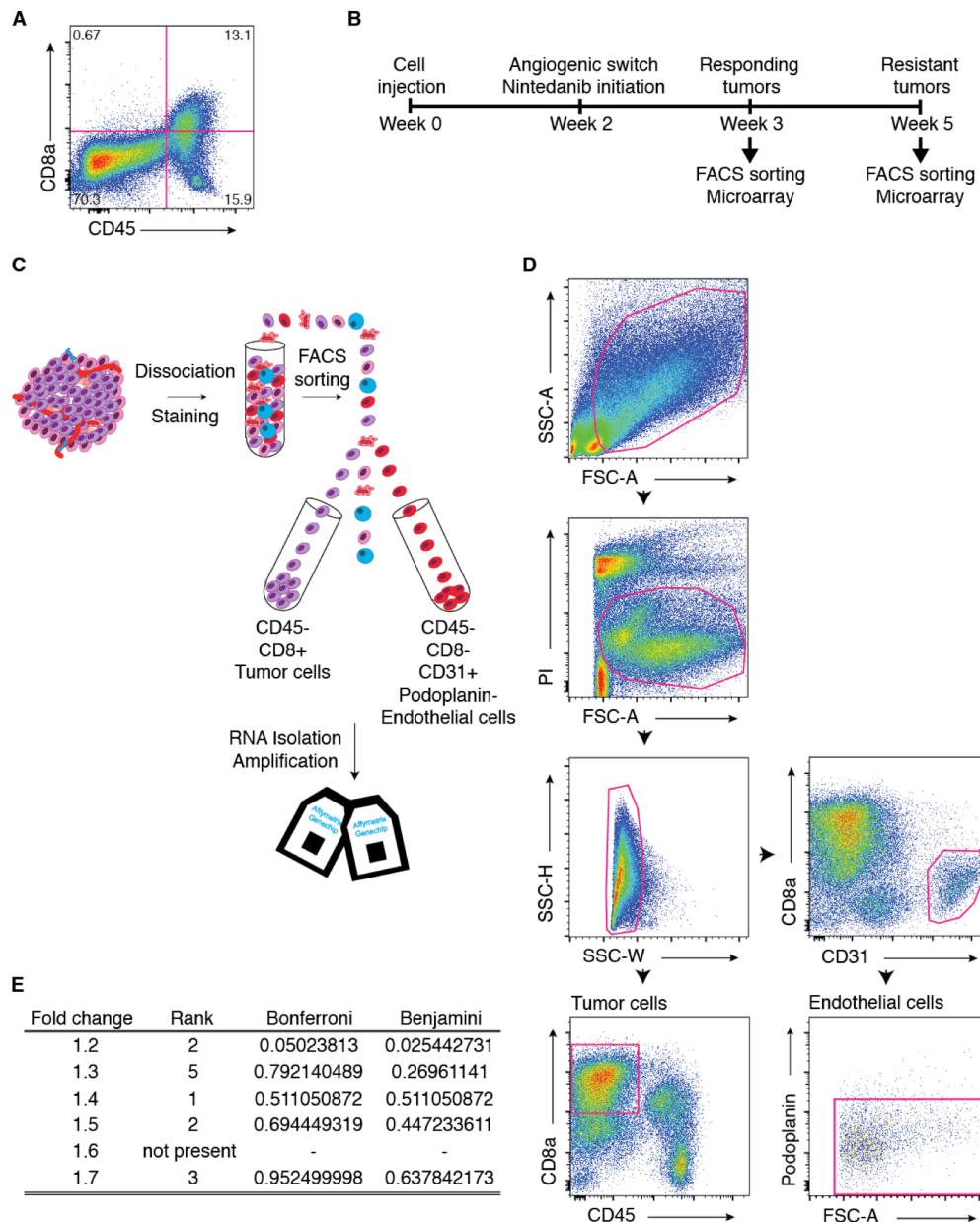
Figure S3. Flow cytometry cell sorting strategy.

(A) Representative flow cytometric analysis of a wild-type Py2T tumor confirming the absence of a CD8α-positive CD45-negative cell population. Relative frequencies of gated populations are shown. (B) Schematic representation of the experimental setup. Py2T-CD8α cells were orthotopically injected into the mammary fat pad of FVB/N female mice. Two weeks later, after the angiogenic switch had occurred, nintedanib (50 mg/kg/day) treatment was initiated. One (ST) or three weeks (LT) after nintedanib initiation, corresponding ST and resistant LT-treated tumors, respectively, were harvested for cell isolation by flow cytometry. (C) Schematic representation of the flow cytometry sorting strategy. Cells from dissociated tumors were separated by flow cytometry: tumor cells were identified by gating on the CD45-CD8α+ population, whereas endothelial cells were identified by gating on CD45-CD8α-CD31+podoplanin- blood vessel endothelial cells. (D) Representative results of cell sorting by flow cytometry. Cells were first gated for forward scatter (FSC) and sideward scatter (SSC), and propidium iodide-positive (PI) dead cells and cell doublets were excluded. Then, tumor cells were sorted by gating on the CD45-CD8α+ population, whereas endothelial cells were sorted by gating on CD45-CD8α-CD31+podoplanin- blood vessel endothelial cells. (E) Differential gene expression between LT nintedanib and untreated tumor cells were assessed using no p-value cutoff combined with a range of fold change cutoff values from 1.2-1.7. KEGG pathway analysis was separately performed for each fold change cutoff and the rank and statistical analysis for the glycolysis pathway are displayed.
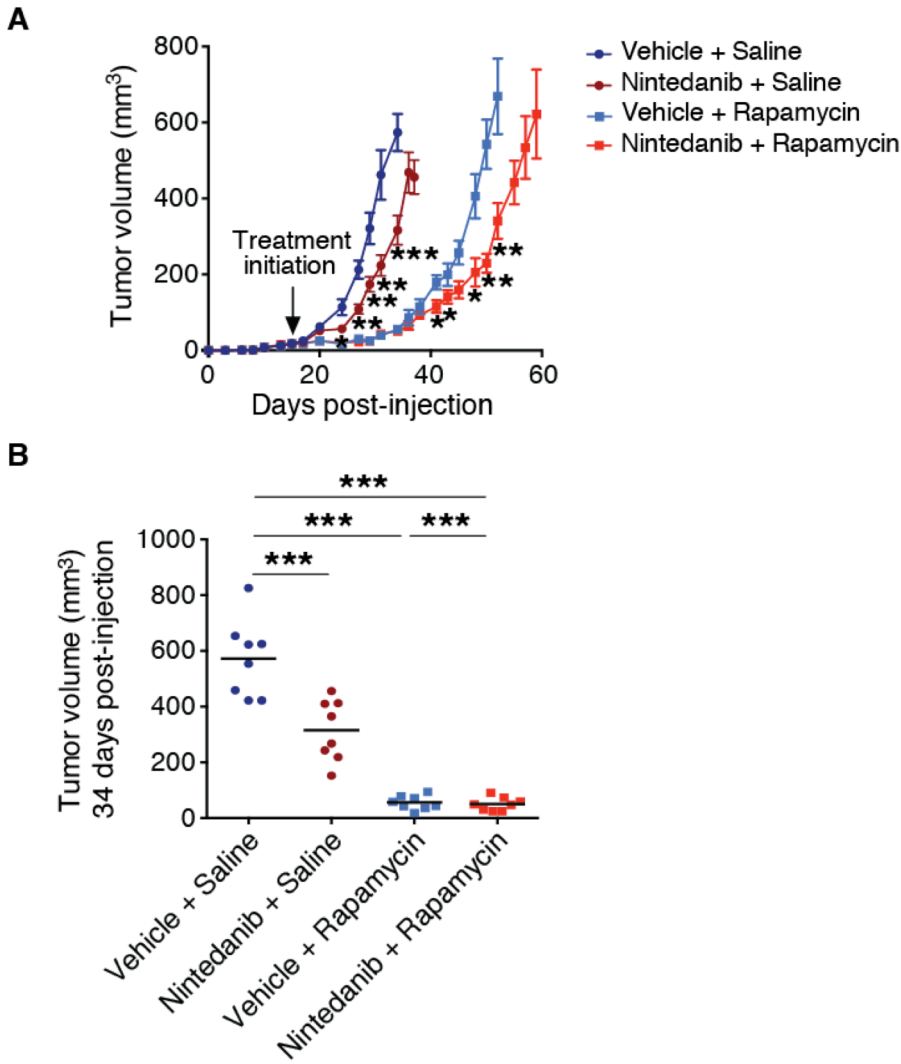
Figure S4. Targeting glucose metabolism with rapamycin in combination with nintedanib significantly delays resistance to anti-angiogenic therapy.
(A) Primary Py2T tumor growth has been determined over time in mice treated with either vehicle or nintedanib (50 mg/kg/day) in combination with rapamycin (2 mg/kg, 3x/week; i.p.) or saline. Values indicated represent mean tumor volume ± SEM. (B) Tumor volumes at day 34 after Py2T tumor cell implantation injection are shown. N = 8 mice per group. Statistical significance was calculated using Mann–Whitney *U* test. *, P < 0.05; **, P < 0.01; ***, P < 0.001.
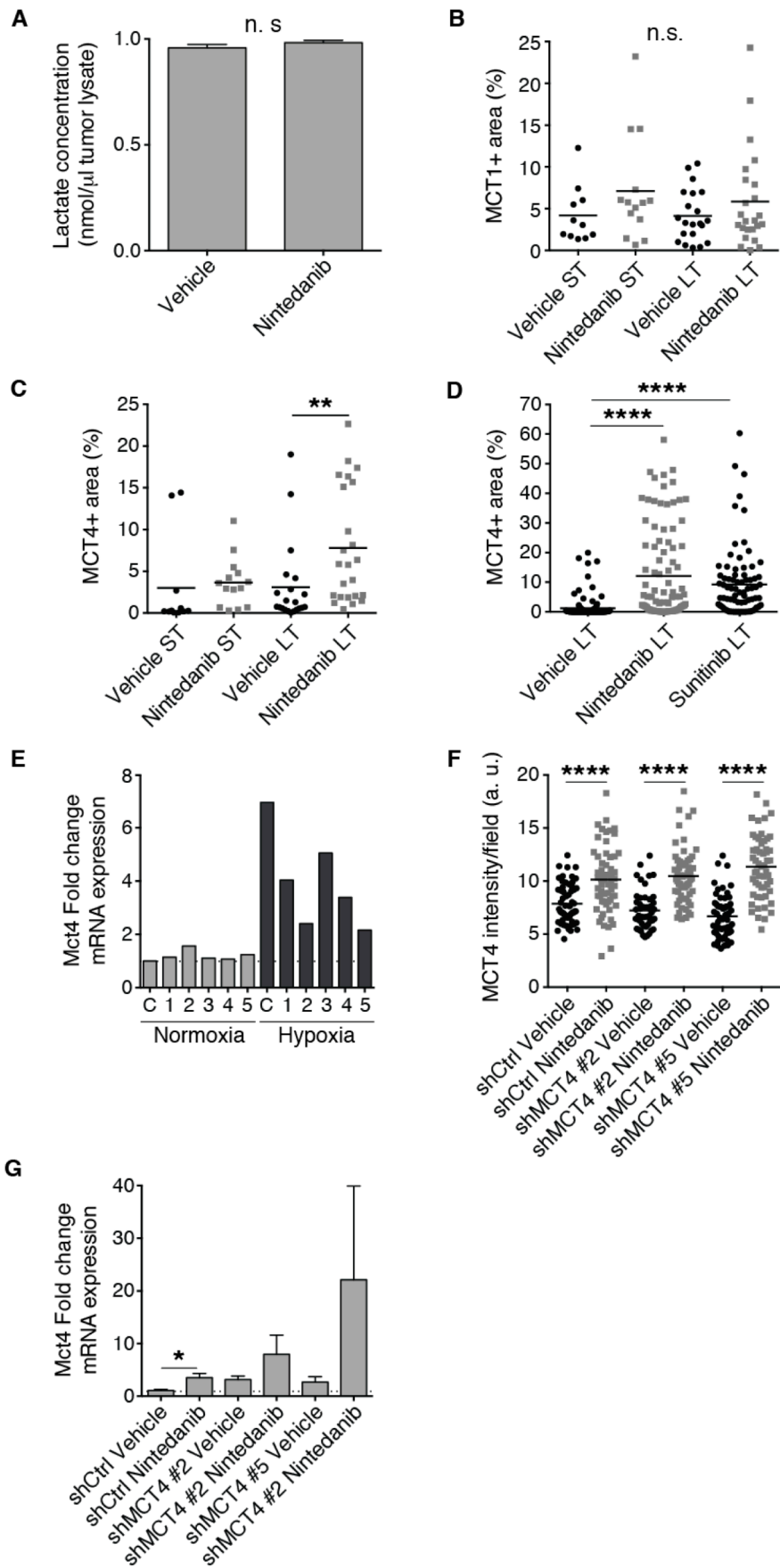
Figure 5. MCT4 is critical for resistance development against anti-angiogenic therapy with nintedanib or sunitinib.

(A) Lactate levels have been quantified in lysates of tumors from LT vehicle or nintedanib-treated mice, and are shown as mean ± SEM. N = 5 mice per group. Statistical significance was calculated using Mann–Whitney U test. n.s, non significant. (B, C) Quantification of MCT1 (A) and MCT4 (B) expression by immunofluorescence staining on histological tumor sections from ST and LT vehicle or nintedanib-treated mice is shown. Mean MCT4 positive area fractions per each field of view are shown. N = 4 mice per group. (D) MCT4 expression in tumors derived from LT vehicle, nintedanib or sunitinib-treated mice was assessed by immunofluorescence staining. Values represent the MCT4-positive area fraction per each field of view. N = 5-6 mice per group. (E) Knockdown efficiency was determined by measuring the MCT4 mRNA expression of shCtrl or shMCT4 Py2T cells cultured in hypoxic or normoxic conditions by quantitative RT-PCR. Data are normalized to shCtrl Py2T cells cultured in normoxic conditions. (F) Quantification of MCT4 expression by immunofluorescence staining on histological sections from shCtrl or shMCT4 Py2T tumors treated either with nintedanib or vehicle is shown. Data displayed represents mean values per each field of view. N = 6 mice per group. (G) MCT4 mRNA expression levels were analyzed by quantitative RT-PCR in shCtrl or shMCT4 Py2T tumors treated with either nintedanib or vehicle, and values are displayed as mean ± SEM. Data are normalized to shCtrl vehicle-treated tumors. N = 3 mice per group. Statistical significance was calculated using Mann–Whitney U test. *, P < 0.05; **, P < 0.01; ****, P < 0.0001.

Primers for qRT-PCR

Name	Sequence (5' - 3')
Glut1 (Slc2a1)	gaccctgcacctcattgg
	gatgctcagataggacatccaag
Hexokinase 2 (Hk2)	gctgaaggaagccattcg
	tcccaactgtgtcatttaccac
Phosphofructokinase, platelet (Pfkp)	gctatcggtgtcctgacca
	actttggcccccgtgtag
Aldolase A (Aldoa)	aaggaagaggttcctctaaagacc
	aatgcggtgagcgatgtc
Triosephosphate isomerase 1 (Tpi1)	ttcgagcaaaccaaggtcat
	ccggagcttctcgtgtactt
Phosphoglycerate kinase 1 (Pgk1)	gaagtcgagaatgcctgtgc
	ccggctcagctttaacctt
Enolase 2 (Eno2)	aacagcgttacttaggcaaagg
	ccaccacggagatacctgag
Lactate dehydrogenase A (Ldha)	ggcactgacgcagacaag
	tgatcacctcgtaggcactg

Pyruvate dehydrogenase kinase 1 (Pdk1)	gttgaaacgtcccgtgct
	gcgtgatatgggcaatcc
β-actin (Actb)	ctaaggccaaccgtgaaaag
	accagaggcatacagggaca
Monocarboxylate transporter 4 (Scl16a3)	gctcacctcctcccttgtg
	ctcttcctcttcccgatgc
60 ribosomal protein L19 (Rpl19)	ctcgttgccggaaaaaca
	tcatccaggtcaccttctca

4 General conclusions and future plans

The rationale behind targeting tumor angiogenesis is based on the hypothesis that tumor cells are "starved to death" when cutting their blood supply. Numerous preclinical and clinical studies have revealed a significant heterogeneous efficacy of anti-angiogenic therapies depending on the tumor type being treated. Whereas PNETs appear to be especially sensitive to this class of drugs, clinical trials in breast cancer patients largely resulted in negative results [64, 287]. In our preclinical studies, we were able to model a similar response pattern. Whereas nintedanib monotherapy increased the survival of PNET bearing Rip1Tag2 mice, nintedanib was able to delay primary tumor growth in breast cancer transplantation models (Py2T and 4T1) for only a few days. Although PNET and breast cancer models responded considerably different to nintedanib monotherapy, mechanisms of resistance might be surprisingly similar. In both tumor types, tumor regrowth (*i.e.* resistance) was not accompanied by revascularization and tumor cell proliferation was sustained in largely avascular tumor regions. These observations suggest a marked adaptability of tumor cells to a rapidly changing availability of oxygen and nutrients. We would like to term this capability with "metabolic plasticity". In resistance to the anti-angiogenic TKI nintedanib, metabolic plasticity signifies the upregulation of anaerobic glycolysis. In oxygen poor situations, glycolysis serves as an important source of ATP. In rapidly proliferating cells however, glycolysis might primarily serve to provide metabolic intermediates in order to generate macromolecules. Furthermore, in hypoxia, instead of entering into the tricarboxylic acid (TCA) cycle, pyruvate is reduced to lactate in order to regenerate the cellular pool of reducing equivalents such as NAD^+. Accumulating lactate has to be exported out of the cells for instance by MCT4 [420]. Indeed, we found upregulation of MCT4 in nintedanib-resistant tumors of breast cancer and Rip1Tag2 mouse models. Importantly, the exported lactate generated in hypoxic areas might not represent a simple waste product, but might be used as a fuel for oxidative metabolism by nearby normoxic areas around remaining blood vessels (*i.e*. metabolic symbiosis). In summary, traditional models explaining resistance to anti-angiogenic therapies are mainly based on mechanisms ensuring reoxygenation – either by revascularization or by migration to locations with higher oxygen saturation (see section 1.4, Figure 5). However, data shown in the present thesis suggest that tumor cells acquire mechanism in order to proliferate in largely avascular tumor areas. Termed metabolic plasticity, we would like to propose a novel paradigm how tumor cells sustain a reduction of the tumor vascularization by anti-angiogenic therapies (Figure 6).

Currently and in the future we are aiming to tackle this metabolic plasticity by combining nintedanib with compounds targeting the identified resistance mechanism. So far, we were able to show additive effects when combining nintedanib with 3PO or rapamycin,

both compounds inhibiting glycolysis. In addition, shRNA mediated knockdown of MCT4 resulted in a marked delay of tumor growth and resistance to nintedanib. Since in this experiment resistant tumors were composed of cells escaping shRNA mediated knockdown, we are currently working on generating Py2T cells deficient for MCT4 employing CRISPR/Cas9 technology. Furthermore, we are in contact with a pharmaceutical company to obtain a novel inhibitor of MCT4.
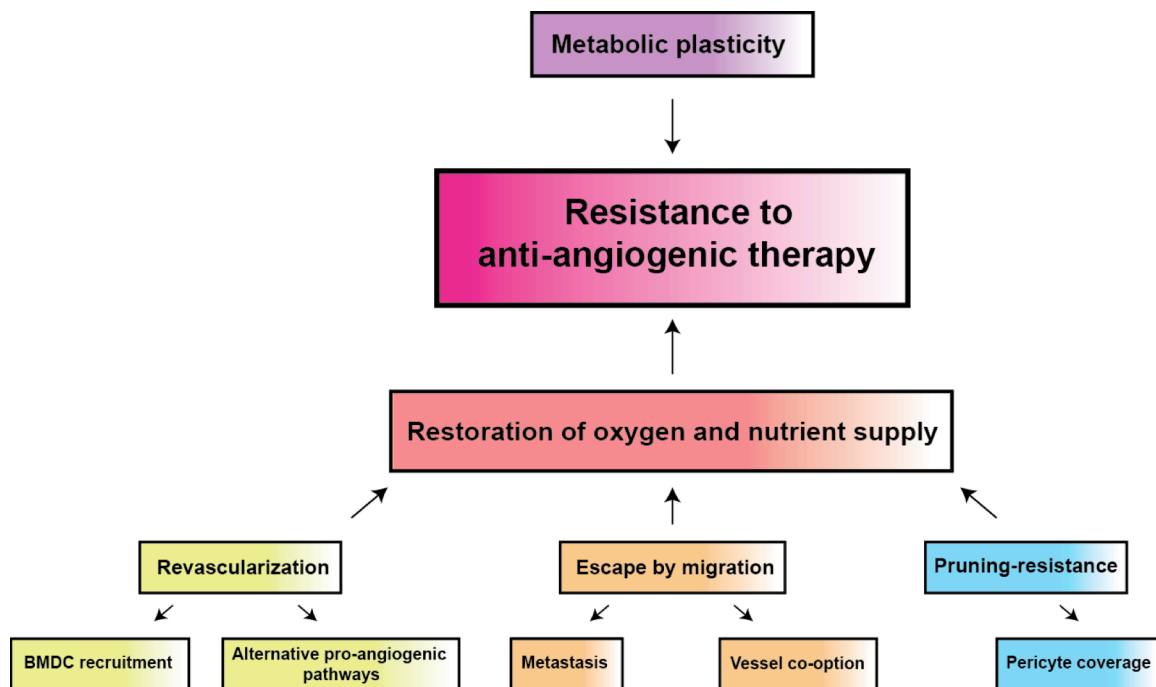
Figure 6. Mechanisms of resistance to anti-angiogenic therapy.
Based on our data, we suggest that the traditional concepts how tumors escape the action of anti-angiogenic therapies should be complemented by the concept of "metabolic plasticity". Tumors resistant to nintedanib treatment displayed a remarkable adaptability allowing them proliferate despite a sustained reduction of MVD and induction of hypoxia. Tumor cells survive these harsh conditions by upregulating glycolysis. Furthermore, lactate produced by glycolytic cells, can potentially be used by cells located in normoxic areas – a mechanism termed "metabolic symbiosis".

Importantly, the knowledge obtained in the preclinical setting by others and us should be tested in patients. Obtaining repeated biopsies from patients before and at different time points during anti-angiogenic therapy would shed light into the question, which mechanism of resistance is actually predominant in the clinical "reality". As our laboratory is part of a European Research Council (ERC) funded consortium ("MERiC" – Mechanisms of Evasive Resistance in Cancer) aiming to unravel mechanisms of resistance to sorafenib in HCC we will have the possibility to validate our findings in preclinical mouse models of HCC and HCC patients.

Besides addressing research questions where the ultimate goal is the translatability into clinics to improve cancer patient care, our model system might serve as an interesting

tool to study the impact of acute and chronic tumor hypoxia (*i.e.* short- and long term nintedanib treatment) on the dynamics of metabolism in tumor cells. By employing the recently established *in vivo* metabolic flux analysis, one might get exciting new insights into metabolic changes induced by altering the tumor microenvironment [421].

Finally, we would like to close the circle and end with a visionary statement by Judah Folkman from 1971: "if anti-angiogenesis is not possible, or even the concept is wrong, the careful consequences may reveal something fundamental" [167]. Almost half a century later, we have seen that anti-angiogenesis is feasible. The concept is correct and provides a powerful therapeutic opportunity in certain cancer types, but clearly not in all. Nevertheless, anti-angiogenesis revealed fundamental insights into metabolic adaptations of cancer cells. Furthermore, it will provide a unique tool to study the consequences of causing acute and chronic hypoxia, and nutrient deprivation in tumors in the context of a living organism – a complexity that is impossible to model even with the most sophisticated *in vitro* approaches.

5 Review

The relevance of EMT in breast cancer metastasis: correlation or causality?

Ruben Bill and Gerhard Christofori

Department of Biomedicine, University of Basel, 4058 Basel, Switzerland

5.1 Abstract

Although major progress has been achieved in treating breast cancer patients, metastatic breast cancer still remains a deadly disease. A full understanding of the process of systemic cancer cell dissemination is therefore critical to develop next generation therapies. A plethora of experimental data points towards a central role of an EMT in the multistep cascade of metastasis formation. However, in patients the data are based on correlative studies, which often, but not always, tie the expression of EMT markers to cancer invasion, metastasis and poor clinical outcome. Moreover, the notion that cancer cells are able to switch between different modes of migration asks for a thorough review of the actual relevance of EMT in cancer metastasis.

5.2 Introduction

The role of an EMT as a fundamental biological mechanism is well established in morphogenic processes of the developing embryo, in wound healing and in organ fibrosis [422-424]. In addition, an EMT is frequently called upon – including by us – as a favored explanation how tumor cells gain migratory and invasive properties in order to leave the primary tumor site, to disseminate throughout the body, and eventually form distant metastases [321, 425, 426]. In the prototypical multistep model of metastasis, the function of EMT is attributed to the initial events, when tumor cells lose their epithelial characteristics to leave the primary tumor, invade into neighboring tissue and enter the blood circulation (Figure 1). An EMT is also thought to support the survival of tumor cells in the blood stream and to promote extravasation at the distant metastatic site [427, 428]. Finally, mesenchymal tumor cells that have undergone an EMT appear to share a variety of hallmarks capabilities with experimentally defined cancer stem cells (CSC; for an in depth review of the link between EMT and CSC see references [422, 429]. Since mesenchymal carcinoma cells are thought to proliferate at reduced rates and since many carcinoma metastases display the same degree of differentiation as their primary tumors, it is thought that mesenchymal, invasive cancer cells undergo a mesenchymal to epithelial transition (MET) after extravasation in distant organs to form overt (macro)metastases [430], [431].

The highly complex process of EMT is busily studied at the molecular level. It appears that EMT (and potentially with it metastasis) does not rely on additional genetic alterations in the cancer cells. Rather complex regulatory circuits involving transcriptional and epigenetic control mediated by distinct "EMT" transcription factors, miRNAs and lncRNAs seem to govern an EMT [428, 432, 433]. Despite or because of the recent insights, it is worthwhile to take a step back and ask to what extent signs of an EMT are detected in primary tumors,

whether an EMT is actually required in the process of metastasis, and to discuss potential alternative models of cancer cell dissemination. Here, we focus on breast cancer, since this cancer type is frequently studied in metastasis research, mainly due to the availability of a variety of valuable transgenic and transplantation mouse models of metastatic breast cancer [434]. In addition, based on the recent molecular classifications of breast cancer subtypes and the identification of a claudin-low subtype exhibiting an EMT gene expression signature, breast cancer specifically qualifies to assess the role of EMT in the metastatic process [435].
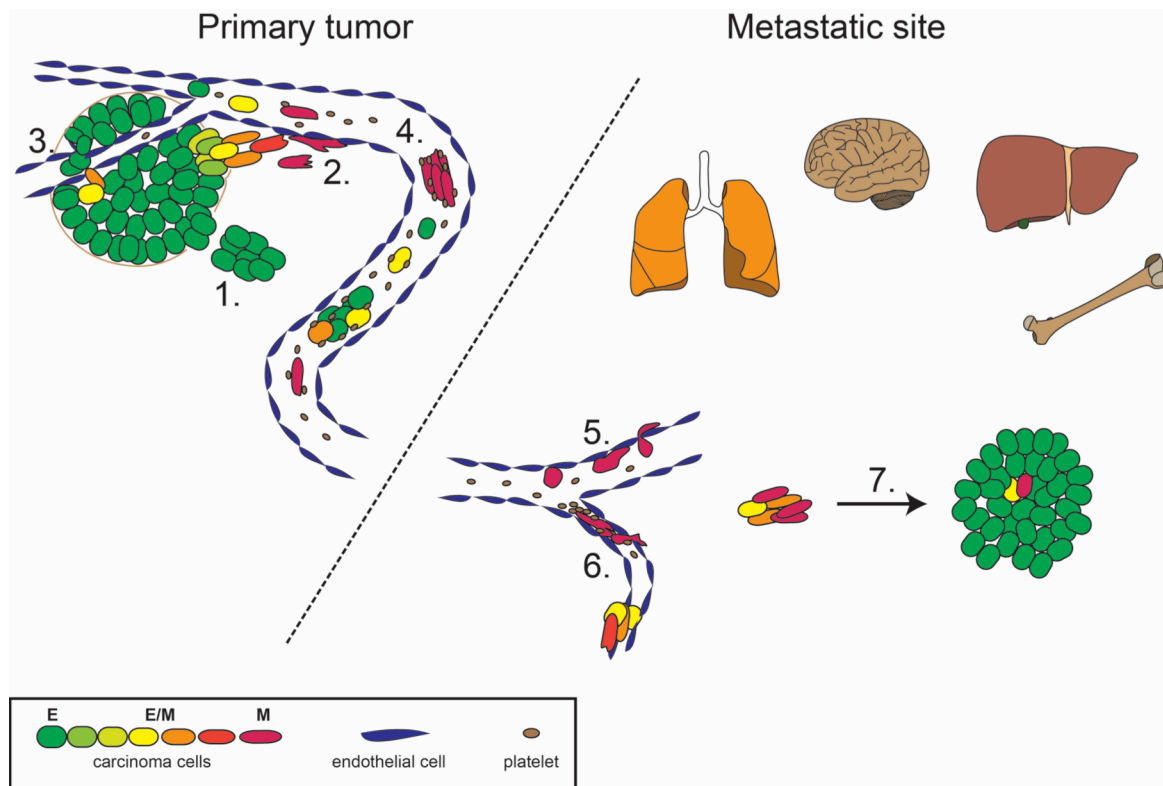
Figure 1. The potential involvement of EMT and MET in the metastatic cascade.
Carcinoma cells reach the systemic circulation by collective invasion (1.) or single-cell migration of EMT-derived mesenchymal cells (2.) into the blood vessels. Alternatively, they can be passively shed (3.) into the blood stream. Circulating tumor cells (CTC), either single cells or CTC-clusters, are found to express predominantly a spectrum of epithelial markers (E), co-express epithelial and mesenchymal markers (E/M) or to express predominantly mesenchymal markers (M; 4.). CTCs are frequently covered by platelets, facilitating carcinoma cell extravasation. At distant organ sites, surviving CTCs are potentially extravasating similar to leukocytes by initial transient contacts, followed by firm adhesion to endothelial cells and subsequent diapedesis and active extravasation, although direct proof for this multistep mechanism is still lacking (5.). CTCs are also physically trapped due to size restriction in small vessels and initiate proliferation inside the vessel lumen (6.). In order to colonize, i.e. to grow from micro- to macrometastases, mesenchymal carcinoma cells may need to undergo an MET (7.). The hematogenous spread of breast cancer cells displays specific tropism to lung, brain, liver and bone.

5.3   EMT and its associated features

Carcinomas, i.e. malignant cancers of epithelial origin, often retain - until a certain state of dedifferentiation - a sheet-like morphology with apico-basal polarity and intact tight and adherens junctions. A prototypical EMT of these cells involves a spectrum of processes having in common the loss of apico-basal polarity and the delocalization of tight and adherens junction proteins, such as E-cadherin, ZO-1, occludins, and claudins. At the same time, they assume a spindle-shaped, mesenchymal-like morphology with upregulated expression of mesenchymal markers, such as N-cadherin, fibronectin and vimentin, and increased migratory and invasive properties [436]. EMT can be easily induced in breast cancer cells in 2D *in vitro* culture, for example by TGFβ or the overexpression of EMT-inducing transcription factors such as TWIST. In addition, EMT-associated migratory and invasive capacities can conveniently be studied *in vitro* by quantifying the efficiency of cells to migrate through porous membranes, either uncoated (for migration) or coated with a layer of extracellular matrix proteins (for invasion) [400, 437]. Although this reductionist approach has provided major mechanistic insights into the principles of EMT and cell invasion, the results cannot be simply extrapolated to the *in vivo* situation in animal models or in patients [438-441]. Studying EMT *in vivo* mostly relies on a retrospective, "snapshot" analysis of surrogate markers for cell migration and invasion and thus lacks critical information on the dynamic changes underlying an EMT process. Migration and invasion *per se* can only be visualized by technically challenging intra-vital life cell imaging techniques in 3D matrices and in living animals [442-444].

5.4   Cell migration, invasion and intravasation

5.4.1   Individual cell migration

Tumor cells migrate either as single cells (individual migration) or as multicellular groups (collective migration) [445, 446]. The characteristics of a special type of cell migration, where cells are aligned in single-cell chains in so called "indian files", will be presented below when discussing the relation of EMT to the lobular histopathologic subtype of breast cancer [440]. Individually migrating cells usually employ mesenchymal traits of migration with integrin-mediated cell-ECM adhesion dynamics characterized by the generation of high traction forces, the use of proteases for ECM cleavage and the formation of focal contacts at sites of integrin clustering [440]. As an alternative, cancer cells may "squeeze" through tissues by amoeboid migration, which is characterized by propulsive cytoplasmic forward flow, the lack of integrin-ECM contacts and the absence of proteolytic cleavage of the ECM. Notably, amoeboid migration is substantially faster than mesenchymal migration [447-449].

In addition, a hybrid amoeboid/mesenchymal phenotype of cancer cells has been described [450]. In a seminal study, the Sixt laboratory has demonstrated that murine leukocytes, which usually utilize integrin-mediated contacts to move on 2D surfaces, do not depend on adhesion to the ECM via integrins when migrating through a 3D environment in an amoeboid-like fashion [451]. In line with this finding, blockade of integrin function induces a so-called mesenchymal to amoeboid transition (MAT) even in cancer cells of solid tumors [452, 453]. Cells induced to undergo an EMT by TGFβ also switch to a faster amoeboid migration mode in experimental conditions of high confinement and the absence of matrix adhesion [447]. Numerous MAT-inducing mechanisms have been identified in the past years, including inhibition of ECM-degrading proteases or of Rac1 activity, induction of RhoA activity, the forced expression of EphA2 or p27, and p53 deficiency [440, 454-459]. These reports may explain why anti-cancer therapies targeting protease or integrin functions have shown disappointing results in clinical trials [244, 459-461].

A novel mechanism of cell extrusion has been recently proposed by which epithelial cells may leave the epithelial sheet [462]. In normal epithelial tissue homeostasis, dying cells are actively extruded apically into the lumen to preserve a tight barrier function. In contrast, oncogenic signaling in transformed cells leads to a basal extrusion of cancer cells. Since in some circumstances cancer cells can cross BM without proteolytic degradation, basally extruded cancer cells might not necessarily leave behind a BM defect [445, 462-465]. Whether a basal extrusion process plays a role in cancer cell dissemination and whether there is functional connection with an EMT will be part of exciting future research [462].

5.4.2 Collective cell migration

Collective cell migration is characterized by the simultaneous movement of a group of cells with intact cell-cell interactions. Depending on their morphological appearance, these collectives can be classified into "clusters", "strands", "tubes" or "sheets" [466]. Collective cell migration is proposed to be a predominant mode of local cancer cell invasion especially in differentiated carcinoma [467]. Leader cells guide the multicellular aggregate by proteolytic degradation of the ECM in the front and by dragging the cells of the inner and trailing edge. Since the leader cells appear to play a dominant role in the movement of these collectives, their characteristics warrant attention – also in relation to EMT. Notably, the importance of a basal epithelial program in the invasive phenotype of locally invading breast cancer has been reported [467]. Leader cells express basal epithelial markers, such as cytokeratin 14 and p63, while lacking evidence for EMT-associated features, such as the loss of E-cadherin function or increased TWIST, SNAIL or vimentin expression. Although a complete EMT seems not obvious in cells leading collectively invading multicellular groups, this does not exclude a

sub-threshold level EMT or intermittent bursts of EMT, as earlier discussed by Friedl and colleagues [445]. In addition to the perception that collective migration is used by epithelial cancer cells, it is also employed by mesenchymal cancer cells [442, 468-470]. In mesenchymal cells, cell-cell contacts are mediated by N-cadherin, a cadherin family member characteristic of a mesenchymal cell phenotype [469, 471].

Similar to what has been described for plasticity of individually migrating cells, collectively migrating cells can eventually leave the group and continue their march individually, by either migrating in a mesenchymal or in an amoeboid mode – the latter is known as collective to amoeboid transition (CAT). Fibrosarcoma and melanoma cell lines preferentially use collective migration in 3D collagen densities (smaller ECM pore sizes), whereas lower collagen densities (bigger ECM pore sizes) induce the break-out of single cells [442], and blocking β_1-integrin induces a CAT in primary melanoma explants [468].

5.4.3 Cancer cell intravasation

Cancer cells can actively enter the systemic circulation employing the migration and invasion modes described above. However, one should be aware of the fact that cancer cells are passively shed into the blood stream at impressively high numbers [472-476]. In addition, not only "how" but also "where" cancer cells enter the blood circulation matters. Most investigations and deliberations on the mechanisms of cancer cell invasion, as individually or collectively migrating cells, are focusing on the invasive front, i.e. the zone of direct contact between the tumor cells and the surrounding desmoplastic stroma [477]. However, tumor cells can disseminate at the stage of carcinoma *in situ* as proposed by the parallel progression model possibly even before the occurrence of an angiogenic switch [478]. The significance of the invasive front might therefore primarily be a surrogate of the intrinsic invasive capacity of a tumor plus having a causal role in the loco-regional spread of cancer cells. On the other hand, tumors are highly vascularized and contain a "highway" of hematogenous spread inside the tumor mass. Indeed, intra-vital imaging has visualized the intravasation of tumor cells within the tumor mass [479]. Interestingly, an EMT drives the expression of a set of pro-angiogenic genes, partially explaining the enhanced tumor-initiating capacity often associated with the EMT process [241, 480]. Based on these findings it appears that an EMT not only renders tumor cells more capable of migrating towards close-by blood vessels, but their pro-angiogenic activities may enable them to "path their own way" into the systemic circulation.

The possibility of switching between different types of cell migration illustrates the large plasticity of cancer cells and the complexity of their therapeutic targeting. The

molecular mechanism underlying the different types of cancer cell migration, the conversion between these different types, the environmental factors promoting this transitions, and the characteristics of the subsets of cells of a given tumor that hold this plasticity still need to be further elucidated. The different modes of cell migration do not seem to be mutually exclusive for a given cell. In a "tuning model", the mode of cell migration is characterized as a continuum and is the result of the integration of physical and biochemical influences of the tissue environment with the genetic and epigenetic makeup of a given cell [466]. Given the emerging picture of intra-tumoral heterogeneity in cancer [481, 482], it is likely that different areas within an individual tumor rely on distinct modes of cell migration and invasion.

5.5   Does an EMT occur in primary tumors?

Carcinomas often elicit a desmoplastic reaction with abundant mesenchymal stroma cells, such as cancer-associated fibroblasts, with predominantly pro-tumorigenic activities [483]. Conventional histopathological analysis can conveniently discriminate between epithelial cancer cells and fibroblasts with their prototypical spindle-shaped morphology. However, once epithelial cancer cells have converted to a mesenchymal morphology by an EMT, they are hardly distinguishable from stromal fibroblasts. Also the marker repertoire of cancer cells changes to a mesenchymal phenotype after undergoing an EMT and, thus, mesenchymal carcinoma cells remain indistinguishable from stromal fibroblasts by molecular or immunohistochemical analyses. Notably, the expression of cytokeratins or epithelial cell adhesion molecules such as EpCAM, which are routinely used to identify tumor cells of epithelial origin, is lost during an EMT [484]. In this context it also should be noted that, in contrast to early embryonic developmental processes, the concept of EMT in malignant tumor progression reflects a transition within the same lineage and does not signify a real conversion of cells of an epithelial lineage to a mesenchymal lineage – a distinction that has brought some controversy into the discussion about the existence of EMT in cancer [441, 485].

5.5.1   EMT in preclinical breast cancer mouse models

Syngeneic and xenogeneic transplantation models of breast cancer cell lines in mice have been extensively used in order to establish a causal relationship between EMT and metastatic dissemination by interfering with critical mediators of EMT, including EMT-inducing growth factor signaling or transcription factor activities [423]. Although transplantation models of primary cancer cells and established cancer cell lines offer important mechanistic insights into the metastatic cascade, there value is limited by the lack of a slow co-evolution of the implanted cancer cells with the host stroma. In the case of

xenografts, the differentiation state of the cells lines used, the lack of an intact immune response, and potential species incompatibilities of growth factor signaling may obscure the processes active in patients [299]. For example, the human breast cancer cell line MDA-MB-231, a frequently used xenograft metastasis mouse model, stably displays mesenchymal traits at baseline, which limits the study of the dynamic processes of an EMT [486]. Hence, to delineate a possible causal role of EMT in breast cancer metastasis we will focus on data derived from transgenic mouse models of breast cancer.

In transgenic mouse models of breast cancer, first lineage-tracing experiments have provided evidence that EMT exists *in vivo*. By genetically tagging tumor cells combined with immunofluorescence analysis of marker expression, Trimboli and colleagues identified carcinoma cells with a loss of E-cadherin and gain of fibronectin expression. Interestingly however, carcinoma cells with signs of EMT were only detected in a c-MYC-driven transgenic mouse model of breast cancer and not in the MMTV-PyMT and MMTV-Neu transgenic mouse models of breast cancer, which are two widely used models to study breast cancer metastasis [487]. In contrast, phospho-SMAD2 and phospho-SMAD3 have been identified in certain areas of MMTV-PyMT tumors as an indicator of active TGFβ signaling, yet the EMT marker status of these tumors has not been assessed [488, 489]. The conditional deletion of p53 in mammary epithelial cells of mice (achieved by Cre recombinase expression under the control of the K14 or WAP promoters, respectively) provoked the formation of some tumors with carcinosarcomatous morphology, with heterogeneous expression for the luminal marker cytokeratin 8 and the basal marker cytokeratin 14, and with increased vimentin expression. Yet, despite the invasive phenotype of the tumors, distant metastasis is a rare event in these models [490, 491]. When CRIPTO-1, a member of the epidermal growth factor-CFC protein family, was conditionally overexpressed in mammary epithelial cells, tumors eventually developed with a latency of 14-18 months in a proportion of multiparous mice. Whereas most lesions displayed a differentiated morphology classified as papillary adenocarcinomas, some tumors contained areas with an EMT phenotype (negative for E-cadherin and positive for N-cadherin, fibronectin, α-smooth muscle actin, vimentin, and SNAIL) [492]. Similarly, conditional overexpression in the adult mammary epithelium of the sine oculis homeobox 1 homolog (SIX1) homeoprotein led to tumors of a variety of different grades of differentiation [493]. A subset of the tumors displayed a sarcomatoid phenotype with the expression of markers suggestive of a complete EMT. In addition, 80% of the non-sarcomatoid tumors showed a partial EMT with areas of E-cadherin loss and nuclear β-catenin accumulation colocalizing with high expression of the Wnt target gene cyclin D1.

For a reality check as to whether transgenic mouse models of breast cancer faithfully recapitulate the patient situation, gene expression profiles of the model tumors have been compared to the gene expression of the various patient breast cancer subtypes (see also below). Whereas tumors of a variety of mouse models displayed a "luminal-like" gene expression profile (the majority of tumors from MMTV-PyMT, MMTV-Neu and WAP-Myc mice), a proportion of model tumors showed either strong expression of mesenchymal features or mixed expression of luminal, basal and mesenchymal signatures (tumors from Brca1$^{fl/fl}$;TgMMTV-Cre;p53$^{+/-}$, WAP-Myc, or DMBA-treated mice) [435].

Taken together, there is convincing evidence that tumor cells bearing a mesenchymal phenotype exist in primary tumors of transgenic mouse models of breast cancer. To assess whether even rare cells with mesenchymal features, which are unable to significantly influence the global gene expression profile of the bulk of a tumor, are present in the metastatic mouse models of breast cancer, appropriate lineage-tracing experiments need to be performed. Such genetic fate mapping of tumor cells combined with immunofluorescence staining for mesenchymal markers has recently identified an EMT as a very early event in a pancreatic ductal adenocarcinoma mouse model [494].

5.5.2 Mechanisms of EMT in mouse models of breast cancer

It is important to note that any evidence for an EMT in a primary tumor does not necessarily allow the conclusion that an EMT is a prerequisite for the metastatic process. To this end, functional studies are needed in which "key EMT players" are genetically manipulated in transgenic mouse models of breast cancer. Subsequent characterization of changes in EMT marker expression in primary tumors and metastatic lesions, the assessment of primary tumor grade and local invasiveness as well as the metastatic burden (typically in the lung) reveals the functional roles of factors of interest in EMT and/or metastasis. Candidates to be assessed could be EMT-inducing cytokines, such as TGFβ, EGF, FGF, and HGF, hypoxia induced by rapid tumor growth or by the pharmacological inhibition of blood vessel angiogenesis (anti-angiogenic therapies), components important for cell-cell contact and cell polarity, and EMT-inducing transcription factors, such as TWIST, SNAIL1/2, and ZEB1/2 [423, 436]. Exciting insights have already been obtained by studying the tumor-promoting role of TGFβ and some of the transcription factors relevant for EMT (see below), yet further studies are needed to identify and distinguish between "simple" markers of an EMT *in vivo* and factors with non-redundant functions during an EMT.

TGFβ, one of the best-studied EMT-inducing cytokines, is produced by both tumor cells and by a variety of cells of the tumor microenvironment. It exerts important effects on

several cell types within a tumor and by canonical, SMAD-dependent and non-canonical, SMAD-independent signaling modulates the expression of a variety of target genes to either exert tumor suppressive functions, such as induction of the cell cycle inhibitor p21 or repression of c-MYC, or tumor-promoting functions by inducing an EMT (for a detailed description of TGFβ signaling and its role in cancer see reference [495]. Consistent with this notion, MMTV promoter-driven mammary epithelial cell-specific expression of TGFβ in the MMTV-Neu model results in primary tumors with higher tumor grades and increased metastatic burden in the lungs. Interestingly, despite the TGFβ-mediated increased local invasiveness, primary tumors still express E-cadherin and do not upregulate the mesenchymal markers vimentin, alpha-SMA and fibronectin [496]. Similarly, overexpression of TGFβ in MMTV-PyMT transgenic mice at late stages of tumor development dramatically increases metastasis to the lungs [497]. In line with the pro-metastatic activities of TGFβ in the MMTV-Neu driven breast cancer mouse model, expression of a constitutive-active TGFβRI promotes the metastatic process, whereas expression of a dominant-negative TGFβRII inhibits lung metastasis [498, 499]. Notably, one of these studies has revealed an important role of TGFβ signaling for tumor cell extravasation rather than for primary tumor invasion and tumor cell intravasation [499].

Encouraging data from a therapeutic point of view comes from experiments where neutralization of TGFβ by a soluble TGFβRII:Fc fusion trap has reduced the incidence of lung metastasis in MMTV-Neu and MMTV-PyMT mice [500]. Since the TGFβRII:Fc trap reduced the number of colony-forming circulating tumor cells (CTCs), the authors suggested a role for TGFβ in intravasation. Alternatively however, CTCs could also come from growing metastases, and the reduction in CTCs may simply reflect the lower metastatic burden. In contrast to these reports, the Moses laboratory has reported a metastasis-promoting effect when attenuating TGFβ signaling in the MMTV-PyMT and MMTV-Neu models by a tumor cell-specific deletion of TGFβRII or the expression of a dominant-negative TGFβRII, respectively [488, 501]. Mechanistically, abrogation of TGFβ signaling in the MMTV-PyMT model results in the recruitment of Gr1$^+$CD11b$^+$ MDSCs, which by secreting MMPs promote invasion of E-cadherin-positive tumor cells [502]. In TGFβ-attenuated MMTV-Neu tumors, increased VEGF-A expression provokes leaky vessels and potentially facilitates cancer cell intravasation [501]. Based on TGFβ's context-dependent and highly complex impact on tumor cells and on cells of the tumor microenvironment, it is not surprising that manipulation of the different components of the TGFβ/TGFβR signaling axis leads to a wide range of sometimes contradictory effects on metastasis formation.

Employing the Rip1Tag2 transgenic mouse model of neuroendocrine carcinoma of the pancreas we have previously shown that abolition of E-cadherin (*Cdh1*)-mediated cell-cell adhesions can be a trigger of tumor invasion and metastasis [503]. Derksen and co-workers have recently reported that the concomitant genetic ablation of *Cdh1* and *Trp53* in mammary epithelial cells of the mouse induces the formation of invasive and metastatic lobular breast carcinomas which, however, do not display features of a complete EMT [490, 491]. These data suggest that, although loss of E-cadherin is sufficient to induce local invasion and distant metastasis, it does not necessarily promote a complete EMT – in contrast to what is observed in cell culture experiments [504, 505]. A characteristic molecular event observed during an EMT is the transcriptional shut-off of the *Cdh1* gene by EMT-inducing transcriptional repressors, such as SNAIL1/2, TWIST1/2, and ZEB1/2 [436]. Accordingly, the inducible expression of TWIST1 and with it the induction of an EMT in the primary tumor site allows the dissemination of tumor cells to distant organs. However, metastatic outgrowth at the distant organs requires the loss of TWIST1 expression and a mesenchymal-to-epithelial transition (MET; see below; [506]. In a mouse model of invasive mammary carcinoma with doxycycline-inducible expression of a constitutive-active version of the Her2/Neu (NeuNT) oncogene, NeuNT-driven tumors completely regress after doxycycline withdrawal and oncogene expression shutdown, yet they display NeuNT-independent recurrence after a latency of several months [507]. Whereas tumors occurring during the initial NeuNT-driven growth phase show extensive lung metastasis but retain an epithelial morphology, the recurring tumors display a SNAIL1-driven mesenchymal phenotype with downregulation of CK8 and E-cadherin and upregulation of vimentin and fibronectin expression. Indeed, the experimental manipulation of a variety of EMT-relevant genes, such as the genes encoding for SNAIL1/2, TWIST1/2, ZEB1/2, FOXC2, SOX4, TEAD2, LHX2, and others, results in a change in breast cancer cell invasion and dissemination and in metastasis formation, evidencing a link between EMT and the disseminating and tumor-initiating capabilities of carcinoma cells [384, 436, 508]. However, a formal proof that metastases are indeed initiated by cancer cells that have ever undergone an EMT is still lacking and will require sophisticated fate-mapping experiments in animal models.

5.6   Extravasation, MET and colonization

5.6.1   Extravasation

Disseminating cancer cells, after having survived the harsh conditions of their travel through the blood stream, have in principle two possibilities how they can form a metastatic nodule in a distant organ: physical trapping in small capillaries of the target organ due to size

restriction and initial proliferation inside the vascular lumen and subsequent disruption of the vessel wall as the metastasis expands [509], or extravasation and subsequent proliferation in the extra-luminal compartment. While the former is difficult to address experimentally without sophisticated intra-vital imaging, the latter is supported by first experimental evidence: similar to the behavior of leukocytes when egressing from blood vessels at inflammatory sites by binding to selectins and subsequent firm adhesion via integrins (tethering, rolling), cancer cells are able to establish weak contacts with endothelial cells *in vitro* [510]. However, in *vivo* evidence for the existence of such initial weak contacts is still missing [511]. Stable contacts of tumor cells to endothelial cells seem to be mediated by adhesion molecules such as members of the integrin-family and CD44 and N-cadherin [511, 512]. Several of these molecules with important functions during transendothelial migration (TEM) are upregulated during an EMT. For example, increased N-cadherin expression and the loss of E-cadherin expression, the cadherin switch, is one hallmark of an EMT [471]. Moreover, EMT-induced integrins on cancer cells can interact with cell adhesion molecules (CAMs) expressed by endothelial cells. Finally, an EMT often leads to the upregulation of enzymes that modify carbohydrate moieties on selectin-binding glycoproteins. On one hand, CD44 isoforms with specific glycosylated residues have been described to mediate initial weak contacts by binding to E-selectin expressed by endothelial cells, whereas on the other hand CD44 plays an important role by mediating firm adhesion to endothelial cells [511]. Notably, human breast cancer cells that have undergone an EMT and resemble breast cancer stem cells are characterized by the expression of high levels of CD44 [513]. In addition, upregulation of TGFβ and VEGF-A by an EMT can enhance permeability of the capillary bed and thereby promote TEM [514, 515]. Hence, the pro-angiogenic phenotype of cancer cells acquired during an EMT does not only promote intravasation by creating a disorganized vessel network in the primary tumor but also may facilitate extravasation at distant sites. The extravasation process involves a crosstalk between the cancer cells and endothelial cells, and leukocytes, platelets and proteins of the coagulation cascade play supportive roles [427, 516]. For example, platelets frequently embrace circulating tumor cells and, by releasing TGFβ, they induce an EMT of cancer cells inside the blood stream and thus increase their extravasation into the lung [427]. Amoeboid cell migration of cancer cells, on the other hand, has also been shown to promote TEM [517]. However, the spatial and temporal contribution of the mesenchymal vs. the amoeboid phenotype during the process of TEM and subsequent crossing of the underlining basement membrane during the process of cancer cell extravasation *in vivo* has to be further investigated.

5.6.2 MET and colonization

If EMT plays an important role in metastasis formation, how comes that carcinoma metastases frequently display a similar degree of differentiation as the primary tumor [431]? One formal possibility has it that EMT is dispensable for intravasation, and cancer cells rather intravasate by collective migration of epithelial cell clusters or by passive shedding into the circulation, promoted by the disorganized and leaky vasculature present in the primary tumor [467, 518]. Another explanation is based on the notion that EMT is a transient/dynamic process conferring high plasticity to cancer cells. Thereby it has been postulated that EMT-derived mesenchymal cells, which are thought to be slowly proliferating cells with cancer stem cell-like properties, are forced to undergo a MET to be able to initiate proliferation [431]. If so, what triggers an MET? Is it simply the lack of EMT-inducing factors in the inhospitable environment of metastatic target organs, or are distinct factors actively promoting MET?

There is a plethora of experimental evidence, supporting the hypothesis that MET in the target organ is required for colonization. One of the earliest reports about the requirement for MET during metastatic outgrowth comes from experiments with a human bladder carcinoma cell line, which by serial passaging in mice gave rise to subclones with increased metastatic potential. Whereas the parental cell line displayed mesenchymal features, the higher metastatic subclones were of epithelial morphology and expressed epithelial markers. However, in contrast to these results by intracardial injection, when the cells were injected orthotopically and all steps of the metastasis cascade had to be successfully completed to form metastases, the mesenchymal parental cell line has shown higher metastatic potential than the epithelial subclones. These results raise the possibility that an EMT plays a critical role in the early steps and an MET in the late steps of the metastatic cascade. Mechanistically, MET can be promoted by increased FGFR-2 expression, interestingly by the mesenchymal-specific splice isoform FGFR-2IIIc [519]. In line with these findings, cells isolated from lung metastases of patient-derived breast cancer xenograft mice (PDX mice) of the basal-like subtype partially lose their aggressiveness compared to the parental tumor cells, accompanied by a more differentiated, MET-like status [520]. A requirement for MET in lung colonization has been further demonstrated by spatially restricting TWIST1 expression to the primary tumor site and preventing its expression during the lung colonization process [506] or by reducing the expression of the EMT-inducing transcription factor PRRX1 [521]. Along these lines, mesenchymal, E-cadherin-deficient breast cancer cells derived from the MMTV-Neu mouse model seed more lung metastases upon orthotopic mammary fat pad injection as compared to epithelial, E-cadherin-expressing cells. However, mesenchymal, E-cadherin-deficient cells are less metastatic as compared to the epithelial cells when injected into the tail vein [480], again supporting a critical role of an EMT in the early and of an MET

in the late stages of metastasis formation. Although TGFβ is a well-characterized inducer of EMT, a recent report has proposed that TGFβ can also induce MET in mesenchymal cancer cells via induction of ID1, which in a dominant-negative manner inhibits TWIST1 activity and increases stem cell-like features of the cells [522]. The same publication proposes the existence of both epithelial and mesenchymal cancer cells with tumor-initiating properties. Indeed, two distinct populations of cancer cells in primary breast cancer patient samples have been identified: an epithelial cell population expressing the enzyme aldehyde dehydrogenase and a mesenchymal cell population characterized as CD44$^+$ CD24$^-$ [523]. In contrast to the reports above underlining the importance of MET in metastatic colonization, recent work has demonstrated that a mesenchymal phenotype with increased β1 integrin and focal adhesion kinase (FAK) activity and increased filopodia formation promotes active lung colonization and metastatic outgrowth of breast cancer cells [510, 524]. Moreover, overexpression of a constitutive-active form of the EMT-inducing transcription factor TEAD2 promotes rather than inhibits lung metastasis formation upon i.v. injection of murine breast cancer cells [508]. Apparently, the fine-tuned cell plasticity and the functional interplay between EMT in earlier stages and MET in the later stages of the metastatic cascade warrants further investigation.

5.6.3 Evidence for EMT in human breast cancers

Breast cancers do not represent a single cancer entity but instead summarize a broad spectrum of different malignant diseases of the breast. Several classification systems are employed in order to provide the optimal treatment regiment for breast cancer patients. Traditionally – and still of great value – breast cancers have been classified according to their morphologic appearance into several histological types. Secondly, immunohistochemical analysis of the estrogen- (ER), progesterone receptors (PR) as well as HER2 expression stratifies patients to anti-hormonal therapy and therapeutics targeting HER2. Since the beginning of this millennium, a new layer of classification has been achieved by the use of gene expression profiling [7, 525].

In the early days, pathologists have developed and employed a highly sophisticated classification system for malignant diseases of the breast based on cancer (cell) morphology. Most invasive breast cancer patients are diagnosed with *invasive breast carcinoma of no special type* (previously termed invasive ductal carcinoma) [526]. Two less frequently observed subtypes, which are interesting with regards to EMT, are *invasive lobular carcinoma* and *metaplastic carcinoma*. *Invasive lobular carcinoma* cells can migrate as so-called "indian files", which is regarded as a single-cell migration mode, although the cells are in close contact to each other at their front and rear [446]. One hallmark of *invasive lobular*

carcinoma is the mutation or reduced expression of E-cadherin. Interestingly, based on gene expression analysis, these tumors were highly prevalent in the luminal A subtype, which is usually characterized by its well-differentiated epithelial morphology [527]. These data, together with the results from the E-cadherin-deficient mouse models of lobular breast carcinoma discussed above [491], contradict the results from *in vitro* experiments demonstrating that a loss of E-cadherin function is sufficient to induce a complete EMT [480, 505].

Metaplastic carcinomas represent - among others - tumors with mesenchymal phenotype and they are typically negative for ER, PR and HER2 expression (i.e. triple-negative). For the nomenclature of the mesenchymal representatives of this subtypes, the terms carcinosarcoma and sarcomatoid carcinoma are often used as synonyms. Interestingly, metaplastic carcinomas are often classified as basal-like or claudin-low (identified based on an EMT-like gene expression signature, see below), they frequently carry mutations of *TRP53* and generally respond less to chemotherapy than other triple-negative breast cancers [486, 528]. Regarding the etiology of their mesenchymal appearance, it is currently unclear if this is due to epigenetic (potentially reversible EMT) or genetic (irreversible EMT) alterations. Other than that, using the term of an EMT to describe the etiology of their mesenchymal morphology implies an epithelial cell as origin, a notion that currently lacks experimental support.

The advent of gene expression profiling has revolutionized the classification systems of cancer in general and of breast cancer in particular and has revealed functional insights into the biological processes underlying breast cancer morphology. Based on gene expression profiling, invasive breast cancers were initially classified into the intrinsic subtypes luminal A, luminal B, HER2-enriched basal-like, and normal breast-like [525, 529]. Later on, these categories were extended by the claudin-low subtype, which with regard to EMT warrants further attention [435, 486].

The claudin-low breast cancer subtype is characterized by the low expression of epithelial markers (E-cadherin, occludin, claudin 3, 4 and 7), luminal markers (cytokeratins 18/19, GATA3), and the receptors ER, PR, HER2 (triple-negative). It is distinct from the closely related triple-negative, basal-like subtype – besides the enrichment of an EMT gene expression signature – by lower expression of proliferation genes [486]. On the other hand, claudin-low tumors display increased expression of genes involved in angiogenesis, cell migration, immune system response (i.e. CXCL12) and extracellular matrix (vimentin), to name but a few. Overall, the gene expression profile of claudin-low tumors suggests an EMT

phenotype with a significant amount of different infiltrating leukocytes [486]. Importantly, several studies have shown that tumors of the claudin-low, but not of the basal-like subtype, are enriched in cancer stem cell/tumor-initiating cell signatures, which is consistent with the finding that EMT and tumor-initiating properties are often shared [422, 486]. Regarding their histopathological appearance, of the tumors classifying as claudin-low most of them classify as *invasive carcinomas not otherwise specified*, while only a minority is characterized as *metaplastic or medullary carcinoma* [486].

If EMT plays an essential role in the process of leaving the primary tumor and entering the systemic circulation, one would assume that the higher the percentage of cells with an EMT phenotype in the primary tumor is, the higher the likelihood of distant metastasis and shorter patient survival will be. However, an EMT signature does not predict breast cancer patient survival [530]. Moreover, claudin-low tumors do not show a worse prognosis than luminal B, HER2-enriched or basal-like - the other subtypes with poor prognosis [486]. These results are rather surprising, since it has been shown for many individual key EMT players, including FOXC1, SOX4, LXH2, PRRX1, and for a signature composed of TGFβ-pathway components and downstream targets that their high expression correlates with poor clinical outcome [384, 425, 521, 530, 531]. An association between lung metastasis relapse and an enrichment of a TGFβ-response signature has only been found in ER$^-$ primary breast tumors but not in ER$^+$ breast tumors, and this signature is not prognostic for metastatic relapse in the liver, bone and brain [515]. In contrast to the lack of prognostic impact on patient survival, several reports have linked tumors of the claudin-low subtype with resistance to chemotherapy, in concordance with the general assumption that cells with an EMT phenotype are intrinsically more refractory to chemotherapy [532]. Along these lines, a gene expression signature representing stromal cells or mesenchymal tumor cells has been associated with a poor response to neoadjuvant chemotherapy [533]. In addition, claudin-low tumors have shown to be less chemosensitive than basal-like tumors [486], and a pathological complete response has been negatively correlated with an EMT signature [530]. Intriguingly, the claudin-low and a cancer stem cell signature are enriched after neoadjuvant treatment with endocrine therapy or chemotherapy compared to pre-treatment conditions [534]. Taken together, it appears that the claudin-low signature *per se* is not an indicator of poor prognosis compared to other aggressive intrinsic breast cancer subtypes, but it seems to be predictive for inferior response to therapy.

Many question remain. For example, similar to the case of metaplastic tumors discussed above, why do certain breast tumors display a mesenchymal gene expression profile? Is it due to genomic alterations resulting in an irreversible EMT or is it rather due to

less stable epigenetic marks or constant EMT-inducing signals of the surrounding tumor stroma? In addition, if the cell of origin of claudin-low tumors is found within the mammary stem cell compartment, the term EMT may be misleading, since the cell of origin never has achieved an epithelial differentiation [535, 536].

Global gene expression profiling of breast cancer samples has critically contributed to the understanding of inter-tumoral heterogeneity; it has provided important information about the predominant intrinsic breast cancer subtypes in the sample analyzed. However, it does not account for the potential co-existence of different tumor cell subpopulations – i.e. intra-tumoral heterogeneity [486]. Apparently, industrious single cell analysis seems required to address the extent and quality of tumor heterogeneity in breast cancer.

To potentially detect rare cancer cells with an EMT phenotype, immunostainings of tumor sections with antibodies against epithelial and mesenchymal markers have been performed. The technical hurdle to distinguish stromal cells from mesenchymal tumor cells in human tumors has recently been elegantly circumvented by performing RNA *in situ* hybridizations (RNA-ISH) on HER2-positive primary breast cancer patient samples concomitantly against HER2 - to identify tumor cells - and against a collection of mesenchymal markers [537]. This approach identified tumor cells expressing mesenchymal markers in these primary tumor samples. In the same study, by using dual-colorimetric RNA-ISH against a pool of epithelial transcripts and a pool of mesenchymal transcripts, they identified biphenotypic cells co-expressing both epithelial and mesenchymal markers in primary breast cancer samples – interestingly, not necessarily at the invasive front – and in draining lymph nodes. Strikingly, the highest percentage of epithelial and mesenchymal double-positive tumor cells is found in the triple-negative subtype known to display a particularly aggressive clinical course [537]. Similarly, it has been reported that cells co-expressing epithelial and mesenchymal markers are predominantly observed in samples of claudin-low and basal-like tumors [486, 538]. These findings clearly show that "partial EMT" (i.e. the co-expression of epithelial and mesenchymal markers) can be observed by histopathological analysis of human breast cancer tissue. Hence, a complete EMT might not be a prerequisite for tumor cell dissemination, consistent with the observation that partial EMT represents a state with higher cell plasticity than a complete EMT [539]. Whether cells with a complete EMT can be identified within the bulk of cancer-associated fibroblasts (CAFs) within the tumor stroma remains unclear. While tumor cell-specific genetic alterations can be found in stromal cells of breast cancers [540, 541], clonal somatic genetic alterations have not been found in CAFs isolated from breast and ovarian cancer stroma [542].

5.7   Lessons learned from circulating tumor cells (CTCs)

The prototypical role of EMT in cancer progression is often described as the initial process of the metastasis cascade, i.e. the gain of migratory and invasive properties allowing cancer cells to leave the primary tumor, to invade into nearby blood vessels and to access the blood circulation – the "highway" of cancer cell dissemination. Hence, the analysis of CTCs in cancer patients might give indirect insights into the state tumor cells are in, when they have reached the blood stream, with the caveat that CTCs can also originate from existing metastases [500]. A growing body of evidence shows that the presence of CTCs in breast cancer patients is not only associated with poor prognosis, but it is also predictive for reduced therapy response. Indeed, CTCs expressing EMT markers, such as TWIST1 and vimentin, have been identified in breast cancer patients [543, 544]. One important caveat screening the literature about CTCs with an EMT phenotype is that the technically highly demanding analysis of CTCs is often biased towards the epithelial phenotype, since conventional CTC capture technologies have been frequently based on epithelial markers, such as EpCAM and cytokeratins, markers that are lost during a complete EMT [537, 545]. A growing panel of new microfluidic CTC-capture devices now allows the isolation of CTCs of the whole spectrum from "fully" epithelial to "fully" mesenchymal tumor cells [518, 537, 546]. Employing these devices, it has been found that the proportion of CTCs expressing various levels of mesenchymal markers is higher in more aggressive breast cancer subtypes and rises during failure of conventional chemotherapy and targeted agents [537]. The detection of CTCs expressing mesenchymal markers and its correlation with parameters of poor clinical outcome in breast cancer patients suggests therefore the importance of EMT in the intravasation process. Alternatively, EMT can also be induced after having reached the blood stream via EMT-inducing factors, such as TGFβ secreted, for example, by platelets that adhere to single-cell CTCs and CTC clusters [427, 518, 537]. This "outside of the primary tumor" induction of EMT may also be functionally important by preventing the CTCs from anoikis and from eradication by chemotherapy and also by supporting extravasation at the distant site.

Although CTC clusters are long known to be important contributors to metastasis formation [472], it has recently been shown that in the breast cancer transplantation models CTC-clusters represent only around 2-5% of CTCs, yet are responsible for approximately half of the lung metastases. This data reveals a dramatically higher metastatic potential of CTC clusters compared to single-cell CTCs – at least in the lung, representing the first capillary bed breast cancer cells encounter when disseminating systemically. CTC clusters are mainly derived from oligoclonal aggregates from the primary tumor rather than being generated by intravascular aggregations or intravascular proliferation [518]. Interestingly,

CTC clusters can co-express epithelial and mesenchymal markers [537], raising the question by which mechanism these oligoclonal clumps have reached the systemic circulation: by collective cell migration or by passive shedding into the circulation in an epithelial state and subsequent (partial) EMT induced by platelet-derived TGFβ, or by induction of EMT within the primary tumor and passive shedding or collective migration of mesenchymal tumor cells into the blood stream? Certainly, the advances in CTC capturing technologies will not only provide important new insights into the biology of cancer cells "en route" from the primary tumor to distant sites [518], but also open new avenues for new strategies to interfere with metastasis formation [547].

5.8   Concluding remarks

There is compelling evidence for the existence of carcinoma cells with a mesenchymal phenotype in human breast cancer as well as in mouse breast cancer models. Sophisticated lineage-tracing experiments as well as novel technologies in single cell analysis will further shed light into the question whether rare EMT-derived mesenchymal cells can be found in the tumor stroma. However, the simple presence of EMT in the primary tumor does not allow the conclusion that EMT is actually required for metastasis. The highly complex multistep metastasis cascade and the transient nature of EMT render it difficult to draw causal conclusions regarding the importance of EMT for metastasis formation in cancer patients. In addition, mesenchymal migration represents just one of multiple migration modes cancer cells can employ to leave tissue boundaries, and therapeutically interfering with mesenchymal migration might activate salvage pathways, such as MAT, or reactivate dormant, mesenchymally disseminated tumor cells by inducing an MET.

The functional manipulation of key EMT players in breast cancer mouse models has provided clear evidence for a causal involvement of EMT-inducing or blocking factors in metastasis. Unfortunately, EMT marker analysis of the primary tumors derived from these functional experiments has been rarely reported, and whether EMT is indeed a prerequisite for metastasis formation remains to be resolved. In addition, the transient nature of EMT adds another layer of complexity to interpreting the data derived from these experiments. While temporal resolution can be achieved by the inducible expression or silencing of genes of interest, spatial resolution as performed by Tsai and co-workers is urgently needed as well [506].

Despite the impressive progress in the past years, we still need to learn about the mechanisms underlying cancer metastasis in mice and men. Animal models that closely

recapitulate the patient situation and the careful design of meaningful clinical studies accompanied with cutting-edge translational research programs will be instrumental to transform cancer from a deadly into a chronic or even curable disease.

6. References

1. Mukherjee, S., *The Emperor of All Maladies: A Biography of Cancer.* 2011, New York: Scribner.
2. Halsted, W.S., *I. The Results of Operations for the Cure of Cancer of the Breast Performed at the Johns Hopkins Hospital from June, 1889, to January, 1894.* Ann Surg, 1894. **20**(5): p. 497-555.
3. Torek, F., *Willy Meyer, M.D., 1858-1932.* Ann Surg, 1933. **97**(1): p. 156-8.
4. Gilman, A. and F.S. Philips, *The Biological Actions and Therapeutic Applications of the B-Chloroethyl Amines and Sulfides.* Science, 1946. **103**(2675): p. 409-36.
5. Jacobson, L.O., C.L. Spurr, and et al., *Nitrogen mustard therapy; studies on the effect of methyl-bis (beta-chloroethyl) amine hydrochloride on neoplastic diseases and allied disorders of the hemopoietic system.* J Am Med Assoc, 1946. **132**: p. 263-71.
6. Farber, S. and L.K. Diamond, *Temporary remissions in acute leukemia in children produced by folic acid antagonist, 4-aminopteroyl-glutamic acid.* N Engl J Med, 1948. **238**(23): p. 787-93.
7. Senkus, E., et al., *Primary breast cancer: ESMO Clinical Practice Guidelines for diagnosis, treatment and follow-up.* Ann Oncol, 2013. **24 Suppl 6**: p. vi7-23.
8. *Comprehensive molecular portraits of human breast tumours.* Nature, 2012. **490**(7418): p. 61-70.
9. *Comprehensive molecular characterization of human colon and rectal cancer.* Nature, 2012. **487**(7407): p. 330-7.
10. Baselga, J., *Treatment of HER2-overexpressing breast cancer.* Ann Oncol, 2010. **21 Suppl 7**: p. vii36-40.
11. Scott, A.M., J.D. Wolchok, and L.J. Old, *Antibody therapy of cancer.* Nat Rev Cancer, 2012. **12**(4): p. 278-87.
12. Smaglo, B.G., D. Aldeghaither, and L.M. Weiner, *The development of immunoconjugates for targeted cancer therapy.* Nat Rev Clin Oncol, 2014. **11**(11): p. 637-48.
13. Sharma, P. and J.P. Allison, *Immune checkpoint targeting in cancer therapy: toward combination strategies with curative potential.* Cell, 2015. **161**(2): p. 205-14.
14. Hodi, F.S., et al., *Improved survival with ipilimumab in patients with metastatic melanoma.* N Engl J Med, 2010. **363**(8): p. 711-23.
15. Robert, C., et al., *Ipilimumab plus dacarbazine for previously untreated metastatic melanoma.* N Engl J Med, 2011. **364**(26): p. 2517-26.
16. Walunas, T.L., et al., *CTLA-4 can function as a negative regulator of T cell activation.* Immunity, 1994. **1**(5): p. 405-13.
17. Brahmer, J.R., et al., *Safety and activity of anti-PD-L1 antibody in patients with advanced cancer.* N Engl J Med, 2012. **366**(26): p. 2455-65.
18. Robert, C., et al., *Nivolumab in previously untreated melanoma without BRAF mutation.* N Engl J Med, 2015. **372**(4): p. 320-30.
19. Topalian, S.L., et al., *Safety, activity, and immune correlates of anti-PD-1 antibody in cancer.* N Engl J Med, 2012. **366**(26): p. 2443-54.
20. Larkin, J., et al., *Combined Nivolumab and Ipilimumab or Monotherapy in Untreated Melanoma.* N Engl J Med, 2015. **373**(1): p. 23-34.
21. Postow, M.A., et al., *Nivolumab and ipilimumab versus ipilimumab in untreated melanoma.* N Engl J Med, 2015. **372**(21): p. 2006-17.
22. Pacini, F., et al., *Thyroid cancer: ESMO Clinical Practice Guidelines for diagnosis, treatment and follow-up.* Ann Oncol, 2012. **23 Suppl 7**: p. vii110-9.
23. Schlumberger, M.J., *Papillary and follicular thyroid carcinoma.* N Engl J Med, 1998. **338**(5): p. 297-306.
24. Horwich, A., et al., *Prostate cancer: ESMO Clinical Practice Guidelines for diagnosis, treatment and follow-up.* Ann Oncol, 2013. **24 Suppl 6**: p. vi106-14.
25. Wu, P., T.E. Nielsen, and M.H. Clausen, *FDA-approved small-molecule kinase inhibitors.* Trends Pharmacol Sci, 2015. **36**(7): p. 422-39.
26. Manning, G., et al., *The protein kinase complement of the human genome.* Science, 2002. **298**(5600): p. 1912-34.
27. Zhang, J., P.L. Yang, and N.S. Gray, *Targeting cancer with small molecule kinase inhibitors.* Nat Rev Cancer, 2009. **9**(1): p. 28-39.
28. Tong, M. and M.A. Seeliger, *Targeting conformational plasticity of protein kinases.* ACS Chem Biol, 2015. **10**(1): p. 190-200.
29. Buchdunger, E., et al., *Inhibition of the Abl protein-tyrosine kinase in vitro and in vivo by a 2-phenylaminopyrimidine derivative.* Cancer Res, 1996. **56**(1): p. 100-4.

30. Demetri, G.D., et al., *Efficacy and safety of imatinib mesylate in advanced gastrointestinal stromal tumors.* N Engl J Med, 2002. **347**(7): p. 472-80.

31. Druker, B.J., et al., *Efficacy and safety of a specific inhibitor of the BCR-ABL tyrosine kinase in chronic myeloid leukemia.* N Engl J Med, 2001. **344**(14): p. 1031-7.

32. Shah, N.P., et al., *Overriding imatinib resistance with a novel ABL kinase inhibitor.* Science, 2004. **305**(5682): p. 399-401.

33. Talpaz, M., et al., *Dasatinib in imatinib-resistant Philadelphia chromosome-positive leukemias.* N Engl J Med, 2006. **354**(24): p. 2531-41.

34. Kantarjian, H., et al., *Nilotinib in imatinib-resistant CML and Philadelphia chromosome-positive ALL.* N Engl J Med, 2006. **354**(24): p. 2542-51.

35. Weisberg, E., et al., *Characterization of AMN107, a selective inhibitor of native and mutant Bcr-Abl.* Cancer Cell, 2005. **7**(2): p. 129-41.

36. Cortes, J.E., et al., *Bosutinib versus imatinib in newly diagnosed chronic-phase chronic myeloid leukemia: results from the BELA trial.* J Clin Oncol, 2012. **30**(28): p. 3486-92.

37. Golas, J.M., et al., *SKI-606, a 4-anilino-3-quinolinecarbonitrile dual inhibitor of Src and Abl kinases, is a potent antiproliferative agent against chronic myelogenous leukemia cells in culture and causes regression of K562 xenografts in nude mice.* Cancer Res, 2003. **63**(2): p. 375-81.

38. Cortes, J.E., et al., *A phase 2 trial of ponatinib in Philadelphia chromosome-positive leukemias.* N Engl J Med, 2013. **369**(19): p. 1783-96.

39. O'Hare, T., et al., *AP24534, a pan-BCR-ABL inhibitor for chronic myeloid leukemia, potently inhibits the T315I mutant and overcomes mutation-based resistance.* Cancer Cell, 2009. **16**(5): p. 401-12.

40. Harrison, C., et al., *JAK inhibition with ruxolitinib versus best available therapy for myelofibrosis.* N Engl J Med, 2012. **366**(9): p. 787-98.

41. Quintas-Cardama, A., et al., *Preclinical characterization of the selective JAK1/2 inhibitor INCB018424: therapeutic implications for the treatment of myeloproliferative neoplasms.* Blood, 2010. **115**(15): p. 3109-17.

42. Vannucchi, A.M., et al., *Ruxolitinib versus standard therapy for the treatment of polycythemia vera.* N Engl J Med, 2015. **372**(5): p. 426-35.

43. Verstovsek, S., et al., *A double-blind, placebo-controlled trial of ruxolitinib for myelofibrosis.* N Engl J Med, 2012. **366**(9): p. 799-807.

44. Changelian, P.S., et al., *Prevention of organ allograft rejection by a specific Janus kinase 3 inhibitor.* Science, 2003. **302**(5646): p. 875-8.

45. van Vollenhoven, R.F., et al., *Tofacitinib or adalimumab versus placebo in rheumatoid arthritis.* N Engl J Med, 2012. **367**(6): p. 508-19.

46. Mok, T.S., et al., *Gefitinib or carboplatin-paclitaxel in pulmonary adenocarcinoma.* N Engl J Med, 2009. **361**(10): p. 947-57.

47. Sirotnak, F.M., et al., *Efficacy of cytotoxic agents against human tumor xenografts is markedly enhanced by coadministration of ZD1839 (Iressa), an inhibitor of EGFR tyrosine kinase.* Clin Cancer Res, 2000. **6**(12): p. 4885-92.

48. Eberhard, D.A., et al., *Mutations in the epidermal growth factor receptor and in KRAS are predictive and prognostic indicators in patients with non-small-cell lung cancer treated with chemotherapy alone and in combination with erlotinib.* J Clin Oncol, 2005. **23**(25): p. 5900-9.

49. Pollack, V.A., et al., *Inhibition of epidermal growth factor receptor-associated tyrosine phosphorylation in human carcinomas with CP-358,774: dynamics of receptor inhibition in situ and antitumor effects in athymic mice.* J Pharmacol Exp Ther, 1999. **291**(2): p. 739-48.

50. Shepherd, F.A., et al., *Erlotinib in previously treated non-small-cell lung cancer.* N Engl J Med, 2005. **353**(2): p. 123-32.

51. Geyer, C.E., et al., *Lapatinib plus capecitabine for HER2-positive advanced breast cancer.* N Engl J Med, 2006. **355**(26): p. 2733-43.

52. Xia, W., et al., *Anti-tumor activity of GW572016: a dual tyrosine kinase inhibitor blocks EGF activation of EGFR/erbB2 and downstream Erk1/2 and AKT pathways.* Oncogene, 2002. **21**(41): p. 6255-63.

53. Wedge, S.R., et al., *ZD6474 inhibits vascular endothelial growth factor signaling, angiogenesis, and tumor growth following oral administration.* Cancer Res, 2002. **62**(16): p. 4645-55.

54. Wells, S.A., Jr., et al., *Vandetanib in patients with locally advanced or metastatic medullary thyroid cancer: a randomized, double-blind phase III trial.* J Clin Oncol, 2012. **30**(2): p. 134-41.

55. Li, D., et al., *BIBW2992, an irreversible EGFR/HER2 inhibitor highly effective in preclinical lung cancer models.* Oncogene, 2008. **27**(34): p. 4702-11.

56.   Miller, V.A., et al., *Afatinib versus placebo for patients with advanced, metastatic non-small-cell lung cancer after failure of erlotinib, gefitinib, or both, and one or two lines of chemotherapy (LUX-Lung 1): a phase 2b/3 randomised trial.* Lancet Oncol, 2012. **13**(5): p. 528-38.

57.   Brose, M.S., et al., *Sorafenib in radioactive iodine-refractory, locally advanced or metastatic differentiated thyroid cancer: a randomised, double-blind, phase 3 trial.* Lancet, 2014. **384**(9940): p. 319-28.

58.   Escudier, B., et al., *Sorafenib in advanced clear-cell renal-cell carcinoma.* N Engl J Med, 2007. **356**(2): p. 125-34.

59.   Llovet, J.M., et al., *Sorafenib in advanced hepatocellular carcinoma.* N Engl J Med, 2008. **359**(4): p. 378-90.

60.   Wilhelm, S.M., et al., *BAY 43-9006 exhibits broad spectrum oral antitumor activity and targets the RAF/MEK/ERK pathway and receptor tyrosine kinases involved in tumor progression and angiogenesis.* Cancer Res, 2004. **64**(19): p. 7099-109.

61.   Demetri, G.D., et al., *Efficacy and safety of sunitinib in patients with advanced gastrointestinal stromal tumour after failure of imatinib: a randomised controlled trial.* Lancet, 2006. **368**(9544): p. 1329-38.

62.   Mendel, D.B., et al., *In vivo antitumor activity of SU11248, a novel tyrosine kinase inhibitor targeting vascular endothelial growth factor and platelet-derived growth factor receptors: determination of a pharmacokinetic/pharmacodynamic relationship.* Clin Cancer Res, 2003. **9**(1): p. 327-37.

63.   Motzer, R.J., et al., *Sunitinib versus interferon alfa in metastatic renal-cell carcinoma.* N Engl J Med, 2007. **356**(2): p. 115-24.

64.   Raymond, E., et al., *Sunitinib malate for the treatment of pancreatic neuroendocrine tumors.* N Engl J Med, 2011. **364**(6): p. 501-13.

65.   Inai, T., et al., *Inhibition of vascular endothelial growth factor (VEGF) signaling in cancer causes loss of endothelial fenestrations, regression of tumor vessels, and appearance of basement membrane ghosts.* Am J Pathol, 2004. **165**(1): p. 35-52.

66.   Rini, B.I., et al., *Comparative effectiveness of axitinib versus sorafenib in advanced renal cell carcinoma (AXIS): a randomised phase 3 trial.* Lancet, 2011. **378**(9807): p. 1931-9.

67.   Demetri, G.D., et al., *Efficacy and safety of regorafenib for advanced gastrointestinal stromal tumours after failure of imatinib and sunitinib (GRID): an international, multicentre, randomised, placebo-controlled, phase 3 trial.* Lancet, 2013. **381**(9863): p. 295-302.

68.   Grothey, A., et al., *Regorafenib monotherapy for previously treated metastatic colorectal cancer (CORRECT): an international, multicentre, randomised, placebo-controlled, phase 3 trial.* Lancet, 2013. **381**(9863): p. 303-12.

69.   Wilhelm, S.M., et al., *Regorafenib (BAY 73-4506): a new oral multikinase inhibitor of angiogenic, stromal and oncogenic receptor tyrosine kinases with potent preclinical antitumor activity.* Int J Cancer, 2011. **129**(1): p. 245-55.

70.   Hilberg, F., et al., *BIBF 1120: triple angiokinase inhibitor with sustained receptor blockade and good antitumor efficacy.* Cancer Res, 2008. **68**(12): p. 4774-82.

71.   Reck, M., et al., *Docetaxel plus nintedanib versus docetaxel plus placebo in patients with previously treated non-small-cell lung cancer (LUME-Lung 1): a phase 3, double-blind, randomised controlled trial.* Lancet Oncol, 2014. **15**(2): p. 143-55.

72.   Richeldi, L., et al., *Efficacy and safety of nintedanib in idiopathic pulmonary fibrosis.* N Engl J Med, 2014. **370**(22): p. 2071-82.

73.   Matsui, J., et al., *E7080, a novel inhibitor that targets multiple kinases, has potent antitumor activities against stem cell factor producing human small cell lung cancer H146, based on angiogenesis inhibition.* Int J Cancer, 2008. **122**(3): p. 664-71.

74.   Schlumberger, M., et al., *Lenvatinib versus placebo in radioiodine-refractory thyroid cancer.* N Engl J Med, 2015. **372**(7): p. 621-30.

75.   Kumar, R., et al., *Pharmacokinetic-pharmacodynamic correlation from mouse to human with pazopanib, a multikinase angiogenesis inhibitor with potent antitumor and antiangiogenic activity.* Mol Cancer Ther, 2007. **6**(7): p. 2012-21.

76.   Motzer, R.J., et al., *Pazopanib versus sunitinib in metastatic renal-cell carcinoma.* N Engl J Med, 2013. **369**(8): p. 722-31.

77.   van der Graaf, W.T., et al., *Pazopanib for metastatic soft-tissue sarcoma (PALETTE): a randomised, double-blind, placebo-controlled phase 3 trial.* Lancet, 2012. **379**(9829): p. 1879-86.

78.   Shaw, A.T., et al., *Crizotinib versus chemotherapy in advanced ALK-positive lung cancer.* N Engl J Med, 2013. **368**(25): p. 2385-94.

REFERENCES

79.   Solomon, B.J., et al., *First-line crizotinib versus chemotherapy in ALK-positive lung cancer.* N Engl J Med, 2014. **371**(23): p. 2167-77.

80.   Zou, H.Y., et al., *An orally available small-molecule inhibitor of c-Met, PF-2341066, exhibits cytoreductive antitumor efficacy through antiproliferative and antiangiogenic mechanisms.* Cancer Res, 2007. **67**(9): p. 4408-17.

81.   Marsilje, T.H., et al., *Synthesis, structure-activity relationships, and in vivo efficacy of the novel potent and selective anaplastic lymphoma kinase (ALK) inhibitor 5-chloro-N2-(2-isopropoxy-5-methyl-4-(piperidin-4-yl)phenyl)-N4-(2-(isopropylsulf   onyl)phenyl)pyrimidine-2,4-diamine (LDK378) currently in phase 1 and phase 2 clinical trials.* J Med Chem, 2013. **56**(14): p. 5675-90.

82.   Shaw, A.T., et al., *Ceritinib in ALK-rearranged non-small-cell lung cancer.* N Engl J Med, 2014. **370**(13): p. 1189-97.

83.   Elisei, R., et al., *Cabozantinib in progressive medullary thyroid cancer.* J Clin Oncol, 2013. **31**(29): p. 3639-46.

84.   Yakes, F.M., et al., *Cabozantinib (XL184), a novel MET and VEGFR2 inhibitor, simultaneously suppresses metastasis, angiogenesis, and tumor growth.* Mol Cancer Ther, 2011. **10**(12): p. 2298-308.

85.   Byrd, J.C., et al., *Ibrutinib versus ofatumumab in previously treated chronic lymphoid leukemia.* N Engl J Med, 2014. **371**(3): p. 213-23.

86.   Herman, S.E., et al., *Bruton tyrosine kinase represents a promising therapeutic target for treatment of chronic lymphocytic leukemia and is effectively targeted by PCI-32765.* Blood, 2011. **117**(23): p. 6287-96.

87.   Wang, M.L., et al., *Targeting BTK with ibrutinib in relapsed or refractory mantle-cell lymphoma.* N Engl J Med, 2013. **369**(6): p. 507-16.

88.   Bollag, G., et al., *Clinical efficacy of a RAF inhibitor needs broad target blockade in BRAF-mutant melanoma.* Nature, 2010. **467**(7315): p. 596-9.

89.   Chapman, P.B., et al., *Improved survival with vemurafenib in melanoma with BRAF V600E mutation.* N Engl J Med, 2011. **364**(26): p. 2507-16.

90.   McArthur, G.A., et al., *Safety and efficacy of vemurafenib in BRAF(V600E) and BRAF(V600K) mutation-positive melanoma (BRIM-3): extended follow-up of a phase 3, randomised, open-label study.* Lancet Oncol, 2014. **15**(3): p. 323-32.

91.   Sosman, J.A., et al., *Survival in BRAF V600-mutant advanced melanoma treated with vemurafenib.* N Engl J Med, 2012. **366**(8): p. 707-14.

92.   Hauschild, A., et al., *Dabrafenib in BRAF-mutated metastatic melanoma: a multicentre, open-label, phase 3 randomised controlled trial.* Lancet, 2012. **380**(9839): p. 358-65.

93.   Flaherty, K.T., et al., *Improved survival with MEK inhibition in BRAF-mutated melanoma.* N Engl J Med, 2012. **367**(2): p. 107-14.

94.   Gilmartin, A.G., et al., *GSK1120212 (JTP-74057) is an inhibitor of MEK activity and activation with favorable pharmacokinetic properties for sustained in vivo pathway inhibition.* Clin Cancer Res, 2011. **17**(5): p. 989-1000.

95.   Long, G.V., et al., *Combined BRAF and MEK inhibition versus BRAF inhibition alone in melanoma.* N Engl J Med, 2014. **371**(20): p. 1877-88.

96.   Finn, R.S., et al., *The cyclin-dependent kinase 4/6 inhibitor palbociclib in combination with letrozole versus letrozole alone as first-line treatment of oestrogen receptor-positive, HER2-negative, advanced breast cancer (PALOMA-1/TRIO-18): a randomised phase 2 study.* Lancet Oncol, 2015. **16**(1): p. 25-35.

97.   Fry, D.W., et al., *Specific inhibition of cyclin-dependent kinase 4/6 by PD 0332991 and associated antitumor activity in human tumor xenografts.* Mol Cancer Ther, 2004. **3**(11): p. 1427-38.

98.   Brown, J.R., et al., *Idelalisib, an inhibitor of phosphatidylinositol 3-kinase p110delta, for relapsed/refractory chronic lymphocytic leukemia.* Blood, 2014. **123**(22): p. 3390-7.

99.   Gopal, A.K., et al., *PI3Kdelta inhibition by idelalisib in patients with relapsed indolent lymphoma.* N Engl J Med, 2014. **370**(11): p. 1008-18.

100. Lannutti, B.J., et al., *CAL-101, a p110delta selective phosphatidylinositol-3-kinase inhibitor for the treatment of B-cell malignancies, inhibits PI3K signaling and cellular viability.* Blood, 2011. **117**(2): p. 591-4.

101. *Compendium, Swiss Drug Reference Book.* 21.08.2015]; Available from: http://www.compendium.ch.

102. Swissmedic. 25.08.2015]; Available from: https://http://www.swissmedic.ch/arzneimittel/00156/00221/00222/00223/00224/00227/00228/index.html?lang=de.

103. Roth, G.J., et al., *Design, synthesis, and evaluation of indolinones as triple angiokinase inhibitors and the discovery of a highly specific 6-methoxycarbonyl-substituted indolinone (BIBF 1120).* J Med Chem, 2009. **52**(14): p. 4466-80.

104. Bergers, G., et al., *Benefits of targeting both pericytes and endothelial cells in the tumor vasculature with kinase inhibitors.* J Clin Invest, 2003. **111**(9): p. 1287-95.

105. Cazzaniga, V., et al., *LCK over-expression drives STAT5 oncogenic signaling in PAX5 translocated BCP-ALL patients.* Oncotarget, 2015. **6**(3): p. 1569-81.

106. Poindessous, V., et al., *EGFR- and VEGF(R)-targeted small molecules show synergistic activity in colorectal cancer models refractory to combinations of monoclonal antibodies.* Clin Cancer Res, 2011. **17**(20): p. 6522-30.

107. Tai, W.T., et al., *Nintedanib (BIBF-1120) inhibits hepatocellular carcinoma growth independent of angiokinase activity.* J Hepatol, 2014. **61**(1): p. 89-97.

108. Stopfer, P., et al., *Pharmacokinetics and metabolism of BIBF 1120 after oral dosing to healthy male volunteers.* Xenobiotica, 2011. **41**(4): p. 297-311.

109. Awasthi, N., et al., *Nintedanib, a triple angiokinase inhibitor, enhances cytotoxic therapy response in pancreatic cancer.* Cancer Lett, 2015. **358**(1): p. 59-66.

110. Kudo, K., et al., *Antitumor activity of BIBF 1120, a triple angiokinase inhibitor, and use of VEGFR2+pTyr+ peripheral blood leukocytes as a pharmacodynamic biomarker in vivo.* Clin Cancer Res, 2011. **17**(6): p. 1373-81.

111. Kutluk Cenik, B., et al., *BIBF 1120 (nintedanib), a triple angiokinase inhibitor, induces hypoxia but not EMT and blocks progression of preclinical models of lung and pancreatic cancer.* Mol Cancer Ther, 2013. **12**(6): p. 992-1001.

112. Huang, R.Y., et al., *Functional relevance of a six mesenchymal gene signature in epithelial-mesenchymal transition (EMT) reversal by the triple angiokinase inhibitor, nintedanib (BIBF1120).* Oncotarget, 2015.

113. Jechlinger, M., et al., *Autocrine PDGFR signaling promotes mammary cancer metastasis.* J Clin Invest, 2006. **116**(6): p. 1561-70.

114. Shirakihara, T., et al., *TGF-beta regulates isoform switching of FGF receptors and epithelial-mesenchymal transition.* EMBO J, 2011. **30**(4): p. 783-95.

115. Porte, J. and G. Jenkins, *Assessment of the effect of potential antifibrotic compounds on total and alphaVbeta6 integrin-mediated TGF-beta activation.* Pharmacol Res Perspect, 2014. **2**(4): p. e00030.

116. Bousquet, G., et al., *Phase I study of BIBF 1120 with docetaxel and prednisone in metastatic chemo-naive hormone-refractory prostate cancer patients.* Br J Cancer, 2011. **105**(11): p. 1640-5.

117. Doebele, R.C., et al., *A phase I, open-label dose-escalation study of continuous treatment with BIBF 1120 in combination with paclitaxel and carboplatin as first-line treatment in patients with advanced non-small-cell lung cancer.* Ann Oncol, 2012. **23**(8): p. 2094-102.

118. Ellis, P.M., et al., *Phase I open-label study of continuous treatment with BIBF 1120, a triple angiokinase inhibitor, and pemetrexed in pretreated non-small cell lung cancer patients.* Clin Cancer Res, 2010. **16**(10): p. 2881-9.

119. Mross, K., et al., *Phase I study of the angiogenesis inhibitor BIBF 1120 in patients with advanced solid tumors.* Clin Cancer Res, 2010. **16**(1): p. 311-9.

120. Quintela-Fandino, M., et al., *Phase I clinical trial of nintedanib plus paclitaxel in early HER-2-negative breast cancer (CNIO-BR-01-2010/GEICAM-2010-10 study).* Br J Cancer, 2014. **111**(6): p. 1060-4.

121. Baselga, J., et al., *Sorafenib in combination with capecitabine: an oral regimen for patients with HER2-negative locally advanced or metastatic breast cancer.* J Clin Oncol, 2012. **30**(13): p. 1484-91.

122. Bergh, J., et al., *First-line treatment of advanced breast cancer with sunitinib in combination with docetaxel versus docetaxel alone: results of a prospective, randomized phase III study.* J Clin Oncol, 2012. **30**(9): p. 921-9.

123. Okamoto, I., et al., *Phase I safety, pharmacokinetic, and biomarker study of BIBF 1120, an oral triple tyrosine kinase inhibitor in patients with advanced solid tumors.* Mol Cancer Ther, 2010. **9**(10): p. 2825-33.

124. Ledermann, J.A., et al., *Randomized phase II placebo-controlled trial of maintenance therapy using the oral triple angiokinase inhibitor BIBF 1120 after chemotherapy for relapsed ovarian cancer.* J Clin Oncol, 2011. **29**(28): p. 3798-804.

125. Wong, H.H., et al., *Prolonged response of relapsed high grade serous ovarian carcinoma to the oral angiokinase inhibitor nintedanib in a patient with a germline BRCA1 mutation.* Gynecol Oncol Case Rep, 2012. **3**: p. 7-10.

126. Reck, M., et al., *A phase II double-blind study to investigate efficacy and safety of two doses of the triple angiokinase inhibitor BIBF 1120 in patients with relapsed advanced non-small-cell lung cancer.* Ann Oncol, 2011. **22**(6): p. 1374-81.

127. Dizon, D.S., et al., *A phase II evaluation of nintedanib (BIBF-1120) in the treatment of recurrent or persistent endometrial cancer: an NRG Oncology/Gynecologic Oncology Group Study.* Gynecol Oncol, 2014. **135**(3): p. 441-5.

128. Droz, J.P., et al., *Randomized phase II study of nintedanib in metastatic castration-resistant prostate cancer postdocetaxel.* Anticancer Drugs, 2014. **25**(9): p. 1081-8.

129. Muhic, A., et al., *Phase II open-label study of nintedanib in patients with recurrent glioblastoma multiforme.* J Neurooncol, 2013. **111**(2): p. 205-12.

130. Norden, A.D., et al., *Phase II trial of triple tyrosine kinase receptor inhibitor nintedanib in recurrent high-grade gliomas.* J Neurooncol, 2015. **121**(2): p. 297-302.

131. *LUME-Ovar 1: Nintedanib (BIBF 1120) or Placebo in Combination With Paclitaxel and Carboplatin in First Line Treatment of Ovarian Cancer; NCT01015118.*

132. Hanna, N., et al., *Lume-lung 2: A multicenter, randomized, double-blind, phase III study of nintedanib plus pemetrexed versus placebo plus pemetrexed in patients with advanced nonsquamous non-small cell lung cancer (NSCLC) after failure of first-line chemotherapy.* J Clin Oncol, 2013. **31**(suppl; abstr 8034 ASCO Annual Meeting).

133. Richeldi, L., et al., *Efficacy of a tyrosine kinase inhibitor in idiopathic pulmonary fibrosis.* N Engl J Med, 2011. **365**(12): p. 1079-87.

134. Reck, M. and A. Mellemgaard, *Emerging treatments and combinations in the management of NSCLC: clinical potential of nintedanib.* Biologics, 2015. **9**: p. 47-56.

135. Cavalli, F., *An appeal to world leaders: stop cancer now.* Lancet, 2013. **381**(9865): p. 425-6.

136. Cavalli, F. and R. Atun, *Towards a global cancer fund.* Lancet Oncol, 2015. **16**(2): p. 133-4.

137. Wicki, A. and J. Hagmann, *Diet and cancer.* Swiss Med Wkly, 2011. **141**: p. w13250.

138. Tanneberger, S., F. Cavalli, and F. Pannuti, *Cancer in Developing Countries: The great challenge for oncology in the 21st century*. 2004.

139. Kantarjian, H., *Chemotherapy drug shortages in the United States revisited.* J Oncol Pract, 2014. **10**(5): p. 329-31.

140. *Shortages of cancer drugs in the USA.* Lancet Oncol, 2011. **12**(4): p. 313.

141. Gogineni, K., K.L. Shuman, and E.J. Emanuel, *Survey of oncologists about shortages of cancer drugs.* N Engl J Med, 2013. **369**(25): p. 2463-4.

142. Gatesman, M.L. and T.J. Smith, *The shortage of essential chemotherapy drugs in the United States.* N Engl J Med, 2011. **365**(18): p. 1653-5.

143. Schmid, S. Article last updated: 25.05.2012 27.08.2015]; Available from: http://www.aargauerzeitung.ch/schweiz/spitaeler-brechen-immer-mehr-chemotherapien-ab-124504385.

144. Fojo, T. and C. Grady, *How much is life worth: cetuximab, non-small cell lung cancer, and the $440 billion question.* J Natl Cancer Inst, 2009. **101**(15): p. 1044-8.

145. Smith, T.J. and B.E. Hillner, *Bending the cost curve in cancer care.* N Engl J Med, 2011. **364**(21): p. 2060-5.

146. Carmeliet, P. and R.K. Jain, *Molecular mechanisms and clinical applications of angiogenesis.* Nature, 2011. **473**(7347): p. 298-307.

147. Ogawa, S., et al., *A novel type of vascular endothelial growth factor, VEGF-E (NZ-7 VEGF), preferentially utilizes KDR/Flk-1 receptor and carries a potent mitotic activity without heparin-binding domain.* J Biol Chem, 1998. **273**(47): p. 31273-82.

148. Takahashi, H., et al., *A novel snake venom vascular endothelial growth factor (VEGF) predominantly induces vascular permeability through preferential signaling via VEGF receptor-1.* J Biol Chem, 2004. **279**(44): p. 46304-14.

149. Carmeliet, P., et al., *Abnormal blood vessel development and lethality in embryos lacking a single VEGF allele.* Nature, 1996. **380**(6573): p. 435-9.

150. Ferrara, N., et al., *Heterozygous embryonic lethality induced by targeted inactivation of the VEGF gene.* Nature, 1996. **380**(6573): p. 439-42.

151. Ferrara, N., *Binding to the extracellular matrix and proteolytic processing: two key mechanisms regulating vascular endothelial growth factor action.* Mol Biol Cell, 2010. **21**(5): p. 687-90.

152. Chung, A.S. and N. Ferrara, *Developmental and pathological angiogenesis.* Annu Rev Cell Dev Biol, 2011. **27**: p. 563-84.

153. Bry, M., et al., *Vascular endothelial growth factor-B in physiology and disease.* Physiol Rev, 2014. **94**(3): p. 779-94.

154. Hagberg, C.E., et al., *Vascular endothelial growth factor B controls endothelial fatty acid uptake.* Nature, 2010. **464**(7290): p. 917-21.

155. Lohela, M., et al., *VEGFs and receptors involved in angiogenesis versus lymphangiogenesis.* Curr Opin Cell Biol, 2009. **21**(2): p. 154-65.

156. Pellet-Many, C., et al., *Neuropilins: structure, function and role in disease.* Biochem J, 2008. **411**(2): p. 211-26.

157. Shibuya, M., *Vascular endothelial growth factor and its receptor system: physiological functions in angiogenesis and pathological roles in various diseases.* J Biochem, 2013. **153**(1): p. 13-9.

158. Fredriksson, L., H. Li, and U. Eriksson, *The PDGF family: four gene products form five dimeric isoforms.* Cytokine Growth Factor Rev, 2004. **15**(4): p. 197-204.

159. Lindahl, P., et al., *Pericyte loss and microaneurysm formation in PDGF-B-deficient mice.* Science, 1997. **277**(5323): p. 242-5.

160. Soriano, P., *Abnormal kidney development and hematological disorders in PDGF beta-receptor mutant mice.* Genes Dev, 1994. **8**(16): p. 1888-96.

161. Armulik, A., G. Genove, and C. Betsholtz, *Pericytes: developmental, physiological, and pathological perspectives, problems, and promises.* Dev Cell, 2011. **21**(2): p. 193-215.

162. Compagni, A., et al., *Fibroblast growth factors are required for efficient tumor angiogenesis.* Cancer Res, 2000. **60**(24): p. 7163-9.

163. Touat, M., et al., *Targeting FGFR Signaling in Cancer.* Clin Cancer Res, 2015. **21**(12): p. 2684-94.

164. Pepper, M.S., et al., *Potent synergism between vascular endothelial growth factor and basic fibroblast growth factor in the induction of angiogenesis in vitro.* Biochem Biophys Res Commun, 1992. **189**(2): p. 824-31.

165. Seghezzi, G., et al., *Fibroblast growth factor-2 (FGF-2) induces vascular endothelial growth factor (VEGF) expression in the endothelial cells of forming capillaries: an autocrine mechanism contributing to angiogenesis.* J Cell Biol, 1998. **141**(7): p. 1659-73.

166. Figg, W. and J. Folkman, *Angiogenesis - An Integrative Approach from Science to Medicine*. 2008: Springer US.

167. Folkman, J., *Tumor angiogenesis: therapeutic implications.* N Engl J Med, 1971. **285**(21): p. 1182-6.

168. Gospodarowicz, D., et al., *Clonal growth of bovine vascular endothelial cells: fibroblast growth factor as a survival agent.* Proc Natl Acad Sci U S A, 1976. **73**(11): p. 4120-4.

169. Esch, F., et al., *Primary structure of bovine pituitary basic fibroblast growth factor (FGF) and comparison with the amino-terminal sequence of bovine brain acidic FGF.* Proc Natl Acad Sci U S A, 1985. **82**(19): p. 6507-11.

170. Shing, Y., et al., *Heparin affinity: purification of a tumor-derived capillary endothelial cell growth factor.* Science, 1984. **223**(4642): p. 1296-9.

171. Senger, D.R., et al., *Tumor cells secrete a vascular permeability factor that promotes accumulation of ascites fluid.* Science, 1983. **219**(4587): p. 983-5.

172. Ferrara, N. and W.J. Henzel, *Pituitary follicular cells secrete a novel heparin-binding growth factor specific for vascular endothelial cells.* Biochem Biophys Res Commun, 1989. **161**(2): p. 851-8.

173. Keck, P.J., et al., *Vascular permeability factor, an endothelial cell mitogen related to PDGF.* Science, 1989. **246**(4935): p. 1309-12.

174. Leung, D.W., et al., *Vascular endothelial growth factor is a secreted angiogenic mitogen.* Science, 1989. **246**(4935): p. 1306-9.

175. Rosenthal, R.A., et al., *Conditioned medium from mouse sarcoma 180 cells contains vascular endothelial growth factor.* Growth Factors, 1990. **4**(1): p. 53-9.

176. Folkman, J., *Angiogenesis: an organizing principle for drug discovery?* Nat Rev Drug Discov, 2007. **6**(4): p. 273-86.

177. Carmeliet, P., *Angiogenesis in life, disease and medicine.* Nature, 2005. **438**(7070): p. 932-6.

178. Rogers, P.A. and C.E. Gargett, *Endometrial angiogenesis.* Angiogenesis, 1998. **2**(4): p. 287-94.

179. Jain, R.K. and P. Carmeliet, *SnapShot: Tumor angiogenesis.* Cell, 2012. **149**(6): p. 1408-1408 e1.

180. Plate, K.H., A. Scholz, and D.J. Dumont, *Tumor angiogenesis and anti-angiogenic therapy in malignant gliomas revisited.* Acta Neuropathol, 2012. **124**(6): p. 763-75.

181. Risau, W., *Mechanisms of angiogenesis.* Nature, 1997. **386**(6626): p. 671-4.

182. Semenza, G.L., *Molecular mechanisms mediating metastasis of hypoxic breast cancer cells.* Trends Mol Med, 2012. **18**(9): p. 534-43.

183. Lamalice, L., F. Houle, and J. Huot, *Phosphorylation of Tyr1214 within VEGFR-2 triggers the recruitment of Nck and activation of Fyn leading to SAPK2/p38 activation and endothelial cell migration in response to VEGF.* J Biol Chem, 2006. **281**(45): p. 34009-20.

184. Bergers, G., et al., *Matrix metalloproteinase-9 triggers the angiogenic switch during carcinogenesis.* Nat Cell Biol, 2000. **2**(10): p. 737-44.

185. Chun, T.H., et al., *MT1-MMP-dependent neovessel formation within the confines of the three-dimensional extracellular matrix.* J Cell Biol, 2004. **167**(4): p. 757-67.

186. Pepper, M.S., *Role of the matrix metalloproteinase and plasminogen activator-plasmin systems in angiogenesis.* Arterioscler Thromb Vasc Biol, 2001. **21**(7): p. 1104-17.

187. Christofori, G., P. Naik, and D. Hanahan, *Vascular endothelial growth factor and its receptors, flt-1 and flk-1, are expressed in normal pancreatic islets and throughout islet cell tumorigenesis.* Mol Endocrinol, 1995. **9**(12): p. 1760-70.

188. Hanahan, D. and J. Folkman, *Patterns and emerging mechanisms of the angiogenic switch during tumorigenesis.* Cell, 1996. **86**(3): p. 353-64.

189. Hellstrom, M., et al., *Dll4 signalling through Notch1 regulates formation of tip cells during angiogenesis.* Nature, 2007. **445**(7129): p. 776-80.

190. Suchting, S., et al., *The Notch ligand Delta-like 4 negatively regulates endothelial tip cell formation and vessel branching.* Proc Natl Acad Sci U S A, 2007. **104**(9): p. 3225-30.

191. Tammela, T., et al., *Blocking VEGFR-3 suppresses angiogenic sprouting and vascular network formation.* Nature, 2008. **454**(7204): p. 656-60.

192. Valtola, R., et al., *VEGFR-3 and its ligand VEGF-C are associated with angiogenesis in breast cancer.* Am J Pathol, 1999. **154**(5): p. 1381-90.

193. Felcht, M., et al., *Angiopoietin-2 differentially regulates angiogenesis through TIE2 and integrin signaling.* J Clin Invest, 2012. **122**(6): p. 1991-2005.

194. Kamei, M., et al., *Endothelial tubes assemble from intracellular vacuoles in vivo.* Nature, 2006. **442**(7101): p. 453-6.

195. Potente, M., H. Gerhardt, and P. Carmeliet, *Basic and therapeutic aspects of angiogenesis.* Cell, 2011. **146**(6): p. 873-87.

196. Bergers, G. and S. Song, *The role of pericytes in blood-vessel formation and maintenance.* Neuro Oncol, 2005. **7**(4): p. 452-64.

197. Baluk, P., et al., *Abnormalities of basement membrane on blood vessels and endothelial sprouts in tumors.* Am J Pathol, 2003. **163**(5): p. 1801-15.

198. Jain, R.K., *Normalization of tumor vasculature: an emerging concept in antiangiogenic therapy.* Science, 2005. **307**(5706): p. 58-62.

199. Ribatti, D., B. Nico, and E. Crivellato, *Morphological and molecular aspects of physiological vascular morphogenesis.* Angiogenesis, 2009. **12**(2): p. 101-11.

200. Kerbel, R.S., *Tumor angiogenesis.* N Engl J Med, 2008. **358**(19): p. 2039-49.

201. de la Puente, P., et al., *Cell trafficking of endothelial progenitor cells in tumor progression.* Clin Cancer Res, 2013. **19**(13): p. 3360-8.

202. Nolan, D.J., et al., *Bone marrow-derived endothelial progenitor cells are a major determinant of nascent tumor neovascularization.* Genes Dev, 2007. **21**(12): p. 1546-58.

203. Shaked, Y., et al., *Therapy-induced acute recruitment of circulating endothelial progenitor cells to tumors.* Science, 2006. **313**(5794): p. 1785-7.

204. Gothert, J.R., et al., *Genetically tagging endothelial cells in vivo: bone marrow-derived cells do not contribute to tumor endothelium.* Blood, 2004. **104**(6): p. 1769-77.

205. Larrivee, B., et al., *Minimal contribution of marrow-derived endothelial precursors to tumor vasculature.* J Immunol, 2005. **175**(5): p. 2890-9.

206. Li, H., W.L. Gerald, and R. Benezra, *Utilization of bone marrow-derived endothelial cell precursors in spontaneous prostate tumors varies with tumor grade.* Cancer Res, 2004. **64**(17): p. 6137-43.

207. Peters, B.A., et al., *Contribution of bone marrow-derived endothelial cells to human tumor vasculature.* Nat Med, 2005. **11**(3): p. 261-2.

208. Zumsteg, A., et al., *Myeloid cells contribute to tumor lymphangiogenesis.* PLoS One, 2009. **4**(9): p. e7067.

209. Burri, P.H. and M.R. Tarek, *A novel mechanism of capillary growth in the rat pulmonary microcirculation.* Anat Rec, 1990. **228**(1): p. 35-45.

210. Caduff, J.H., L.C. Fischer, and P.H. Burri, *Scanning electron microscope study of the developing microvasculature in the postnatal rat lung.* Anat Rec, 1986. **216**(2): p. 154-64.

211. Patan, S., et al., *Intussusceptive microvascular growth: a common alternative to capillary sprouting.* Arch Histol Cytol, 1992. **55 Suppl**: p. 65-75.

212. Djonov, V.G., H. Kurz, and P.H. Burri, *Optimality in the developing vascular system: branching remodeling by means of intussusception as an efficient adaptation mechanism.* Dev Dyn, 2002. **224**(4): p. 391-402.

213. Ribatti, D. and V. Djonov, *Intussusceptive microvascular growth in tumors.* Cancer Lett, 2012. **316**(2): p. 126-31.

214.   Crivellato, E., et al., *Recombinant human erythropoietin induces intussusceptive microvascular growth in vivo.* Leukemia, 2004. **18**(2): p. 331-6.

215.   Gianni-Barrera, R., et al., *VEGF over-expression in skeletal muscle induces angiogenesis by intussusception rather than sprouting.* Angiogenesis, 2013. **16**(1): p. 123-36.

216.   Djonov, V., A.C. Andres, and A. Ziemiecki, *Vascular remodelling during the normal and malignant life cycle of the mammary gland.* Microsc Res Tech, 2001. **52**(2): p. 182-9.

217.   Ribatti, D., et al., *Microvascular density, vascular endothelial growth factor immunoreactivity in tumor cells, vessel diameter and intussusceptive microvascular growth in primary melanoma.* Oncol Rep, 2005. **14**(1): p. 81-4.

218.   Hlushchuk, R., A.N. Makanya, and V. Djonov, *Escape mechanisms after antiangiogenic treatment, or why are the tumors growing again?* Int J Dev Biol, 2011. **55**(4-5): p. 563-7.

219.   Holash, J., et al., *Vessel cooption, regression, and growth in tumors mediated by angiopoietins and VEGF.* Science, 1999. **284**(5422): p. 1994-8.

220.   Kienast, Y., et al., *Real-time imaging reveals the single steps of brain metastasis formation.* Nat Med, 2010. **16**(1): p. 116-22.

221.   Maniotis, A.J., et al., *Vascular channel formation by human melanoma cells in vivo and in vitro: vasculogenic mimicry.* Am J Pathol, 1999. **155**(3): p. 739-52.

222.   McDonald, D.M., L. Munn, and R.K. Jain, *Vasculogenic mimicry: how convincing, how novel, and how significant?* Am J Pathol, 2000. **156**(2): p. 383-8.

223.   Paulis, Y.W., et al., *Signalling pathways in vasculogenic mimicry.* Biochim Biophys Acta, 2010. **1806**(1): p. 18-28.

224.   Seftor, R.E., et al., *Tumor cell vasculogenic mimicry: from controversy to therapeutic promise.* Am J Pathol, 2012. **181**(4): p. 1115-25.

225.   Wagenblast, E., et al., *A model of breast cancer heterogeneity reveals vascular mimicry as a driver of metastasis.* Nature, 2015. **520**(7547): p. 358-62.

226.   Hanahan, D., G. Bergers, and E. Bergsland, *Less is more, regularly: metronomic dosing of cytotoxic drugs can target tumor angiogenesis in mice.* J Clin Invest, 2000. **105**(8): p. 1045-7.

227.   Kerbel, R.S., *A cancer therapy resistant to resistance.* Nature, 1997. **390**(6658): p. 335-6.

228.   Wang, R., et al., *Glioblastoma stem-like cells give rise to tumour endothelium.* Nature, 2010. **468**(7325): p. 829-33.

229.   Ricci-Vitiani, L., et al., *Tumour vascularization via endothelial differentiation of glioblastoma stem-like cells.* Nature, 2010. **468**(7325): p. 824-8.

230.   Pezzolo, A., et al., *Tumor origin of endothelial cells in human neuroblastoma.* J Clin Oncol, 2007. **25**(4): p. 376-83.

231.   Streubel, B., et al., *Lymphoma-specific genetic aberrations in microvascular endothelial cells in B-cell lymphomas.* N Engl J Med, 2004. **351**(3): p. 250-9.

232.   Kulla, A., et al., *Analysis of the TP53 gene in laser-microdissected glioblastoma vasculature.* Acta Neuropathol, 2003. **105**(4): p. 328-32.

233.   Rodriguez, F.J., et al., *Neoplastic cells are a rare component in human glioblastoma microvasculature.* Oncotarget, 2012. **3**(1): p. 98-106.

234.   Cheng, L., et al., *Glioblastoma stem cells generate vascular pericytes to support vessel function and tumor growth.* Cell, 2013. **153**(1): p. 139-52.

235.   De Bock, K., et al., *Role of PFKFB3-driven glycolysis in vessel sprouting.* Cell, 2013. **154**(3): p. 651-63.

236.   Schoors, S., et al., *Partial and transient reduction of glycolysis by PFKFB3 blockade reduces pathological angiogenesis.* Cell Metab, 2014. **19**(1): p. 37-48.

237.   Rivera, L.B. and G. Bergers, *Angiogenesis. Targeting vascular sprouts.* Science, 2014. **344**(6191): p. 1449-50.

238.   Schoors, S., et al., *Fatty acid carbon is essential for dNTP synthesis in endothelial cells.* Nature, 2015. **520**(7546): p. 192-7.

239.   De Bock, K., M. Georgiadou, and P. Carmeliet, *Role of endothelial cell metabolism in vessel sprouting.* Cell Metab, 2013. **18**(5): p. 634-47.

240.   Dvorak, H.F. and I. Gresser, *Microvascular injury in pathogenesis of interferon-induced necrosis of subcutaneous tumors in mice.* J Natl Cancer Inst, 1989. **81**(7): p. 497-502.

241.   Goel, H.L. and A.M. Mercurio, *VEGF targets the tumour cell.* Nat Rev Cancer, 2013. **13**(12): p. 871-82.

242.   Hurwitz, H., et al., *Bevacizumab plus irinotecan, fluorouracil, and leucovorin for metastatic colorectal cancer.* N Engl J Med, 2004. **350**(23): p. 2335-42.

243.   Sennino, B. and D.M. McDonald, *Controlling escape from angiogenesis inhibitors.* Nat Rev Cancer, 2012. **12**(10): p. 699-709.

244.   Coussens, L.M., B. Fingleton, and L.M. Matrisian, *Matrix metalloproteinase inhibitors and cancer: trials and tribulations.* Science, 2002. **295**(5564): p. 2387-92.

REFERENCES

245. Tabatabai, G., et al., *Targeting integrins in malignant glioma.* Target Oncol, 2010. **5**(3): p. 175-81.

246. Hanahan, D., *Heritable formation of pancreatic beta-cell tumours in transgenic mice expressing recombinant insulin/simian virus 40 oncogenes.* Nature, 1985. **315**(6015): p. 115-22.

247. Hanahan, D., E.F. Wagner, and R.D. Palmiter, *The origins of oncomice: a history of the first transgenic mice genetically engineered to develop cancer.* Genes Dev, 2007. **21**(18): p. 2258-70.

248. Christofori, G., P. Naik, and D. Hanahan, *A second signal supplied by insulin-like growth factor II in oncogene-induced tumorigenesis.* Nature, 1994. **369**(6479): p. 414-8.

249. Folkman, J., et al., *Induction of angiogenesis during the transition from hyperplasia to neoplasia.* Nature, 1989. **339**(6219): p. 58-61.

250. Babu, V., N. Paul, and R. Yu, *Animal models and cell lines of pancreatic neuroendocrine tumors.* Pancreas, 2013. **42**(6): p. 912-23.

251. Parangi, S., et al., *Antiangiogenic therapy of transgenic mice impairs de novo tumor growth.* Proc Natl Acad Sci U S A, 1996. **93**(5): p. 2002-7.

252. Inoue, M., et al., *VEGF-A has a critical, nonredundant role in angiogenic switching and pancreatic beta cell carcinogenesis.* Cancer Cell, 2002. **1**(2): p. 193-202.

253. Allen, E., I.B. Walters, and D. Hanahan, *Brivanib, a dual FGF/VEGF inhibitor, is active both first and second line against mouse pancreatic neuroendocrine tumors developing adaptive/evasive resistance to VEGF inhibition.* Clin Cancer Res, 2011. **17**(16): p. 5299-310.

254. Bergers, G., et al., *Effects of angiogenesis inhibitors on multistage carcinogenesis in mice.* Science, 1999. **284**(5415): p. 808-12.

255. Schomber, T., et al., *Differential effects of the vascular endothelial growth factor receptor inhibitor PTK787/ZK222584 on tumor angiogenesis and tumor lymphangiogenesis.* Mol Cancer Ther, 2009. **8**(1): p. 55-63.

256. Gannon, G., et al., *Overexpression of vascular endothelial growth factor-A165 enhances tumor angiogenesis but not metastasis during beta-cell carcinogenesis.* Cancer Res, 2002. **62**(2): p. 603-8.

257. Schomber, T., et al., *Placental growth factor-1 attenuates vascular endothelial growth factor-A-dependent tumor angiogenesis during beta cell carcinogenesis.* Cancer Res, 2007. **67**(22): p. 10840-8.

258. Tuveson, D. and D. Hanahan, *Translational medicine: Cancer lessons from mice to humans.* Nature, 2011. **471**(7338): p. 316-7.

259. Hu, W., et al., *Gene Amplifications in Well-Differentiated Pancreatic Neuroendocrine Tumors Inactivate the p53 Pathway.* Genes Cancer, 2010. **1**(4): p. 360-368.

260. Tang, L.H., et al., *Attenuation of the retinoblastoma pathway in pancreatic neuroendocrine tumors due to increased cdk4/cdk6.* Clin Cancer Res, 2012. **18**(17): p. 4612-20.

261. Zhou, J., et al., *Incidence rates of exocrine and endocrine pancreatic cancers in the United States.* Cancer Causes Control, 2010. **21**(6): p. 853-61.

262. Yao, J.C., et al., *One hundred years after "carcinoid": epidemiology of and prognostic factors for neuroendocrine tumors in 35,825 cases in the United States.* J Clin Oncol, 2008. **26**(18): p. 3063-72.

263. Jensen, R.T. and G. Delle Fave, *Promising advances in the treatment of malignant pancreatic endocrine tumors.* N Engl J Med, 2011. **364**(6): p. 564-5.

264. Oberg, K., et al., *Neuroendocrine gastro-entero-pancreatic tumors: ESMO Clinical Practice Guidelines for diagnosis, treatment and follow-up.* Ann Oncol, 2012. **23 Suppl 7**: p. vii124-30.

265. Yao, J.C., et al., *Everolimus for advanced pancreatic neuroendocrine tumors.* N Engl J Med, 2011. **364**(6): p. 514-23.

266. Chiu, C.W., H. Nozawa, and D. Hanahan, *Survival benefit with proapoptotic molecular and pathologic responses from dual targeting of mammalian target of rapamycin and epidermal growth factor receptor in a preclinical model of pancreatic neuroendocrine carcinogenesis.* J Clin Oncol, 2010. **28**(29): p. 4425-33.

267. Paez-Ribes, M., et al., *Antiangiogenic therapy elicits malignant progression of tumors to increased local invasion and distant metastasis.* Cancer Cell, 2009. **15**(3): p. 220-31.

268. Ahn, H.K., et al., *Phase II study of pazopanib monotherapy in metastatic gastroenteropancreatic neuroendocrine tumours.* Br J Cancer, 2013. **109**(6): p. 1414-9.

269. Phan, A.T., et al., *Pazopanib and depot octreotide in advanced, well-differentiated neuroendocrine tumours: a multicentre, single-group, phase 2 study.* Lancet Oncol, 2015. **16**(6): p. 695-703.

270. Casanovas, O., et al., *Drug resistance by evasion of antiangiogenic targeting of VEGF signaling in late-stage pancreatic islet tumors.* Cancer Cell, 2005. **8**(4): p. 299-309.

271.   ClinicalTrials.gov.

272.   Im, S.A., et al., *Inhibition of breast cancer growth in vivo by antiangiogenesis gene therapy with adenovirus-mediated antisense-VEGF.* Br J Cancer, 2001. **84**(9): p. 1252-7.

273.   Ran, S., et al., *Evaluation of novel antimouse VEGFR2 antibodies as potential antiangiogenic or vascular targeting agents for tumor therapy.* Neoplasia, 2003. **5**(4): p. 297-307.

274.   Zhang, W., et al., *A monoclonal antibody that blocks VEGF binding to VEGFR2 (KDR/Flk-1) inhibits vascular expression of Flk-1 and tumor growth in an orthotopic human breast cancer model.* Angiogenesis, 2002. **5**(1-2): p. 35-44.

275.   Abrams, T.J., et al., *Preclinical evaluation of the tyrosine kinase inhibitor SU11248 as a single agent and in combination with "standard of care" therapeutic agents for the treatment of breast cancer.* Mol Cancer Ther, 2003. **2**(10): p. 1011-21.

276.   Bear, H.D., et al., *Bevacizumab added to neoadjuvant chemotherapy for breast cancer.* N Engl J Med, 2012. **366**(4): p. 310-20.

277.   Earl, H.M., et al., *Efficacy of neoadjuvant bevacizumab added to docetaxel followed by fluorouracil, epirubicin, and cyclophosphamide, for women with HER2-negative early breast cancer (ARTemis): an open-label, randomised, phase 3 trial.* Lancet Oncol, 2015. **16**(6): p. 656-66.

278.   Sikov, W.M., et al., *Impact of the addition of carboplatin and/or bevacizumab to neoadjuvant once-per-week paclitaxel followed by dose-dense doxorubicin and cyclophosphamide on pathologic complete response rates in stage II to III triple-negative breast cancer: CALGB 40603 (Alliance).* J Clin Oncol, 2015. **33**(1): p. 13-21.

279.   von Minckwitz, G., et al., *Neoadjuvant chemotherapy and bevacizumab for HER2-negative breast cancer.* N Engl J Med, 2012. **366**(4): p. 299-309.

280.   Bear, H.D., et al., *The effect on tumor response of adding sequential preoperative docetaxel to preoperative doxorubicin and cyclophosphamide: preliminary results from National Surgical Adjuvant Breast and Bowel Project Protocol B-27.* J Clin Oncol, 2003. **21**(22): p. 4165-74.

281.   Fisher, B., et al., *Effect of preoperative chemotherapy on local-regional disease in women with operable breast cancer: findings from National Surgical Adjuvant Breast and Bowel Project B-18.* J Clin Oncol, 1997. **15**(7): p. 2483-93.

282.   Cortazar, P., et al., *Pathological complete response and long-term clinical benefit in breast cancer: the CTNeoBC pooled analysis.* Lancet, 2014. **384**(9938): p. 164-72.

283.   von Minckwitz, G., et al., *Survival after adding capecitabine and trastuzumab to neoadjuvant anthracycline-taxane-based chemotherapy for primary breast cancer (GBG 40--GeparQuattro).* Ann Oncol, 2014. **25**(1): p. 81-9.

284.   Cameron, D., et al., *Adjuvant bevacizumab-containing therapy in triple-negative breast cancer (BEATRICE): primary results of a randomised, phase 3 trial.* Lancet Oncol, 2013. **14**(10): p. 933-42.

285.   Holmgren, L., M.S. O'Reilly, and J. Folkman, *Dormancy of micrometastases: balanced proliferation and apoptosis in the presence of angiogenesis suppression.* Nat Med, 1995. **1**(2): p. 149-53.

286.   Miller, K., et al., *Paclitaxel plus bevacizumab versus paclitaxel alone for metastatic breast cancer.* N Engl J Med, 2007. **357**(26): p. 2666-76.

287.   Ocana, A., et al., *Addition of bevacizumab to chemotherapy for treatment of solid tumors: similar results but different conclusions.* J Clin Oncol, 2011. **29**(3): p. 254-6.

288.   Crown, J.P., et al., *Phase III trial of sunitinib in combination with capecitabine versus capecitabine monotherapy for the treatment of patients with pretreated metastatic breast cancer.* J Clin Oncol, 2013. **31**(23): p. 2870-8.

289.   Robert, N.J., et al., *RIBBON-1: randomized, double-blind, placebo-controlled, phase III trial of chemotherapy with or without bevacizumab for first-line treatment of human epidermal growth factor receptor 2-negative, locally recurrent or metastatic breast cancer.* J Clin Oncol, 2011. **29**(10): p. 1252-60.

290.   Burstein, H.J., *Bevacizumab for advanced breast cancer: all tied up with a RIBBON?* J Clin Oncol, 2011. **29**(10): p. 1232-5.

291.   Miles, D.W., et al., *First-line bevacizumab in combination with chemotherapy for HER2-negative metastatic breast cancer: pooled and subgroup analyses of data from 2447 patients.* Ann Oncol, 2013. **24**(11): p. 2773-80.

292.   Ratner, M., *Fearful of Avastin's fate, Genentech asks for unusual hearing.* Nat Med, 2011. **17**(3): p. 233.

293.   Barrios, C.H., et al., *Phase III randomized trial of sunitinib versus capecitabine in patients with previously treated HER2-negative advanced breast cancer.* Breast Cancer Res Treat, 2010. **121**(1): p. 121-31.

294.   Robert, N.J., et al., *Sunitinib plus paclitaxel versus bevacizumab plus paclitaxel for first-line treatment of patients with advanced breast cancer: a phase III, randomized, open-label trial.* Clin Breast Cancer, 2011. **11**(2): p. 82-92.

295.   Schwartzberg, L.S., et al., *Sorafenib or placebo with either gemcitabine or capecitabine in patients with HER-2-negative advanced breast cancer that progressed during or after bevacizumab.* Clin Cancer Res, 2013. **19**(10): p. 2745-54.

296.   *Phase III Trial Comparing Capecitabine in Combination With Sorafenib or Placebo in the Treatment of Locally Advanced or Metastatic HER2-Negative Breast Cancer, NCT01234337.*

297.   Ebos, J.M. and R.S. Kerbel, *Antiangiogenic therapy: impact on invasion, disease progression, and metastasis.* Nat Rev Clin Oncol, 2011. **8**(4): p. 210-21.

298.   Singh, M. and N. Ferrara, *Modeling and predicting clinical efficacy for drugs targeting the tumor milieu.* Nat Biotechnol, 2012. **30**(7): p. 648-57.

299.   Francia, G., et al., *Mouse models of advanced spontaneous metastasis for experimental therapeutics.* Nat Rev Cancer, 2011. **11**(2): p. 135-41.

300.   Guerin, E., et al., *A model of postsurgical advanced metastatic breast cancer more accurately replicates the clinical efficacy of antiangiogenic drugs.* Cancer Res, 2013. **73**(9): p. 2743-8.

301.   Gray, R., et al., *Independent review of E2100: a phase III trial of bevacizumab plus paclitaxel versus paclitaxel in women with metastatic breast cancer.* J Clin Oncol, 2009. **27**(30): p. 4966-72.

302.   Miles, D.W., et al., *Phase III study of bevacizumab plus docetaxel compared with placebo plus docetaxel for the first-line treatment of human epidermal growth factor receptor 2-negative metastatic breast cancer.* J Clin Oncol, 2010. **28**(20): p. 3239-47.

303.   Miller, K.D., et al., *Randomized phase III trial of capecitabine compared with bevacizumab plus capecitabine in patients with previously treated metastatic breast cancer.* J Clin Oncol, 2005. **23**(4): p. 792-9.

304.   Brufsky, A.M., et al., *RIBBON-2: a randomized, double-blind, placebo-controlled, phase III trial evaluating the efficacy and safety of bevacizumab in combination with chemotherapy for second-line treatment of human epidermal growth factor receptor 2-negative metastatic breast cancer.* J Clin Oncol, 2011. **29**(32): p. 4286-93.

305.   Gianni, L., et al., *AVEREL: a randomized phase III Trial evaluating bevacizumab in combination with docetaxel and trastuzumab as first-line therapy for HER2-positive locally recurrent/metastatic breast cancer.* J Clin Oncol, 2013. **31**(14): p. 1719-25.

306.   Martin, M., et al., *Phase III trial evaluating the addition of bevacizumab to endocrine therapy as first-line treatment for advanced breast cancer: the letrozole/fulvestrant and avastin (LEA) study.* J Clin Oncol, 2015. **33**(9): p. 1045-52.

307.   von Minckwitz, G., et al., *Bevacizumab plus chemotherapy versus chemotherapy alone as second-line treatment for patients with HER2-negative locally recurrent or metastatic breast cancer after first-line treatment with bevacizumab plus chemotherapy (TANIA): an open-label, randomised phase 3 trial.* Lancet Oncol, 2014. **15**(11): p. 1269-78.

308.   Andre, N., M. Carre, and E. Pasquier, *Metronomics: towards personalized chemotherapy?* Nat Rev Clin Oncol, 2014. **11**(7): p. 413-31.

309.   Browder, T., et al., *Antiangiogenic scheduling of chemotherapy improves efficacy against experimental drug-resistant cancer.* Cancer Res, 2000. **60**(7): p. 1878-86.

310.   Klement, G., et al., *Continuous low-dose therapy with vinblastine and VEGF receptor-2 antibody induces sustained tumor regression without overt toxicity.* J Clin Invest, 2000. **105**(8): p. R15-24.

311.   Kerbel, R.S. and B.A. Kamen, *The anti-angiogenic basis of metronomic chemotherapy.* Nat Rev Cancer, 2004. **4**(6): p. 423-36.

312.   Hao, Y.B., et al., *New insights into metronomic chemotherapy-induced immunoregulation.* Cancer Lett, 2014. **354**(2): p. 220-6.

313.   Folkins, C., et al., *Anticancer therapies combining antiangiogenic and tumor cell cytotoxic effects reduce the tumor stem-like cell fraction in glioma xenograft tumors.* Cancer Res, 2007. **67**(8): p. 3560-4.

314.   Vives, M., et al., *Metronomic chemotherapy following the maximum tolerated dose is an effective anti-tumour therapy affecting angiogenesis, tumour dissemination and cancer stem cells.* Int J Cancer, 2013. **133**(10): p. 2464-72.

315.   Cham, K.K., et al., *Metronomic gemcitabine suppresses tumour growth, improves perfusion, and reduces hypoxia in human pancreatic ductal adenocarcinoma.* Br J Cancer, 2010. **103**(1): p. 52-60.

316.   Mupparaju, S., et al., *Repeated tumor oximetry to identify therapeutic window during metronomic cyclophosphamide treatment of 9L gliomas.* Oncol Rep, 2011. **26**(1): p. 281-6.

317. Lee, K., et al., *Anthracycline chemotherapy inhibits HIF-1 transcriptional activity and tumor-induced mobilization of circulating angiogenic cells.* Proc Natl Acad Sci U S A, 2009. **106**(7): p. 2353-8.

318. Andre, N., et al., *Has the time come for metronomics in low-income and middle-income countries?* Lancet Oncol, 2013. **14**(6): p. e239-48.

319. Jain, R.K., *Normalizing tumor vasculature with anti-angiogenic therapy: a new paradigm for combination therapy.* Nat Med, 2001. **7**(9): p. 987-9.

320. Carmeliet, P. and R.K. Jain, *Principles and mechanisms of vessel normalization for cancer and other angiogenic diseases.* Nat Rev Drug Discov, 2011. **10**(6): p. 417-27.

321. Cooke, V.G., et al., *Pericyte depletion results in hypoxia-associated epithelial-to-mesenchymal transition and metastasis mediated by met signaling pathway.* Cancer Cell, 2012. **21**(1): p. 66-81.

322. Cobleigh, M.A., et al., *A phase I/II dose-escalation trial of bevacizumab in previously treated metastatic breast cancer.* Semin Oncol, 2003. **30**(5 Suppl 16): p. 117-24.

323. Yang, J.C., et al., *A randomized trial of bevacizumab, an anti-vascular endothelial growth factor antibody, for metastatic renal cancer.* N Engl J Med, 2003. **349**(5): p. 427-34.

324. Winkler, F., et al., *Kinetics of vascular normalization by VEGFR2 blockade governs brain tumor response to radiation: role of oxygenation, angiopoietin-1, and matrix metalloproteinases.* Cancer Cell, 2004. **6**(6): p. 553-63.

325. Mazzone, M., et al., *Heterozygous deficiency of PHD2 restores tumor oxygenation and inhibits metastasis via endothelial normalization.* Cell, 2009. **136**(5): p. 839-51.

326. Leite de Oliveira, R., et al., *Gene-targeting of Phd2 improves tumor response to chemotherapy and prevents side-toxicity.* Cancer Cell, 2012. **22**(2): p. 263-77.

327. Maes, H., et al., *Tumor vessel normalization by chloroquine independent of autophagy.* Cancer Cell, 2014. **26**(2): p. 190-206.

328. Franco, M., et al., *Targeted anti-vascular endothelial growth factor receptor-2 therapy leads to short-term and long-term impairment of vascular function and increase in tumor hypoxia.* Cancer Res, 2006. **66**(7): p. 3639-48.

329. Man, S., et al., *Antitumor effects in mice of low-dose (metronomic) cyclophosphamide administered continuously through the drinking water.* Cancer Res, 2002. **62**(10): p. 2731-5.

330. Van der Veldt, A.A., et al., *Rapid decrease in delivery of chemotherapy to tumors after anti-VEGF therapy: implications for scheduling of anti-angiogenic drugs.* Cancer Cell, 2012. **21**(1): p. 82-91.

331. Shrimali, R.K., et al., *Antiangiogenic agents can increase lymphocyte infiltration into tumor and enhance the effectiveness of adoptive immunotherapy of cancer.* Cancer Res, 2010. **70**(15): p. 6171-80.

332. Batchelor, T.T., et al., *AZD2171, a pan-VEGF receptor tyrosine kinase inhibitor, normalizes tumor vasculature and alleviates edema in glioblastoma patients.* Cancer Cell, 2007. **11**(1): p. 83-95.

333. Bergers, G. and D. Hanahan, *Modes of resistance to anti-angiogenic therapy.* Nat Rev Cancer, 2008. **8**(8): p. 592-603.

334. Ferrara, N., *Role of myeloid cells in vascular endothelial growth factor-independent tumor angiogenesis.* Curr Opin Hematol, 2010. **17**(3): p. 219-24.

335. Kopetz, S., et al., *Phase II trial of infusional fluorouracil, irinotecan, and bevacizumab for metastatic colorectal cancer: efficacy and circulating angiogenic biomarkers associated with therapeutic resistance.* J Clin Oncol, 2010. **28**(3): p. 453-9.

336. Fagiani, E., et al., *Angiopoietin-1 and -2 exert antagonistic functions in tumor angiogenesis, yet both induce lymphangiogenesis.* Cancer Res, 2011. **71**(17): p. 5717-27.

337. Machein, M.R., et al., *Angiopoietin-1 promotes tumor angiogenesis in a rat glioma model.* Am J Pathol, 2004. **165**(5): p. 1557-70.

338. Huang, J., et al., *Angiopoietin-1/Tie-2 activation contributes to vascular survival and tumor growth during VEGF blockade.* Int J Oncol, 2009. **34**(1): p. 79-87.

339. Fagiani, E. and G. Christofori, *Angiopoietins in angiogenesis.* Cancer Lett, 2013. **328**(1): p. 18-26.

340. Brown, J.L., et al., *A human monoclonal anti-ANG2 antibody leads to broad antitumor activity in combination with VEGF inhibitors and chemotherapy agents in preclinical models.* Mol Cancer Ther, 2010. **9**(1): p. 145-56.

341. Hashizume, H., et al., *Complementary actions of inhibitors of angiopoietin-2 and VEGF on tumor angiogenesis and growth.* Cancer Res, 2010. **70**(6): p. 2213-23.

342. Rigamonti, N., et al., *Role of angiopoietin-2 in adaptive tumor resistance to VEGF signaling blockade.* Cell Rep, 2014. **8**(3): p. 696-706.

149

343. Kienast, Y., et al., *Ang-2-VEGF-A CrossMab, a novel bispecific human IgG1 antibody blocking VEGF-A and Ang-2 functions simultaneously, mediates potent antitumor, antiangiogenic, and antimetastatic efficacy.* Clin Cancer Res, 2013. **19**(24): p. 6730-40.

344. Crawford, Y., et al., *PDGF-C mediates the angiogenic and tumorigenic properties of fibroblasts associated with tumors refractory to anti-VEGF treatment.* Cancer Cell, 2009. **15**(1): p. 21-34.

345. Bais, C., et al., *PlGF blockade does not inhibit angiogenesis during primary tumor growth.* Cell, 2010. **141**(1): p. 166-77.

346. Fischer, C., et al., *Anti-PlGF inhibits growth of VEGF(R)-inhibitor-resistant tumors without affecting healthy vessels.* Cell, 2007. **131**(3): p. 463-75.

347. Shojaei, F., et al., *Tumor refractoriness to anti-VEGF treatment is mediated by CD11b+Gr1+ myeloid cells.* Nat Biotechnol, 2007. **25**(8): p. 911-20.

348. De Palma, M., et al., *Tie2 identifies a hematopoietic lineage of proangiogenic monocytes required for tumor vessel formation and a mesenchymal population of pericyte progenitors.* Cancer Cell, 2005. **8**(3): p. 211-26.

349. Facciabene, A., et al., *Tumour hypoxia promotes tolerance and angiogenesis via CCL28 and T(reg) cells.* Nature, 2011. **475**(7355): p. 226-30.

350. Curiel, T.J., et al., *Dendritic cell subsets differentially regulate angiogenesis in human ovarian cancer.* Cancer Res, 2004. **64**(16): p. 5535-8.

351. Chung, A.S., et al., *An interleukin-17-mediated paracrine network promotes tumor resistance to anti-angiogenic therapy.* Nat Med, 2013. **19**(9): p. 1114-23.

352. Shojaei, F., et al., *G-CSF-initiated myeloid cell mobilization and angiogenesis mediate tumor refractoriness to anti-VEGF therapy in mouse models.* Proc Natl Acad Sci U S A, 2009. **106**(16): p. 6742-7.

353. Shojaei, F., et al., *Bv8 regulates myeloid-cell-dependent tumour angiogenesis.* Nature, 2007. **450**(7171): p. 825-31.

354. Huang, D., et al., *Interleukin-8 mediates resistance to antiangiogenic agent sunitinib in renal cell carcinoma.* Cancer Res, 2010. **70**(3): p. 1063-71.

355. Sitohy, B., et al., *Tumor-surrogate blood vessel subtypes exhibit differential susceptibility to anti-VEGF therapy.* Cancer Res, 2011. **71**(22): p. 7021-8.

356. Sennino, B., et al., *Sequential loss of tumor vessel pericytes and endothelial cells after inhibition of platelet-derived growth factor B by selective aptamer AX102.* Cancer Res, 2007. **67**(15): p. 7358-67.

357. Helfrich, I., et al., *Resistance to antiangiogenic therapy is directed by vascular phenotype, vessel stabilization, and maturation in malignant melanoma.* J Exp Med, 2010. **207**(3): p. 491-503.

358. Bill, R. and G. Christofori, *The relevance of EMT in breast cancer metastasis: Correlation or causality?* FEBS Lett, 2015. **589**(14): p. 1577-87.

359. Gerber, H.P. and N. Ferrara, *Pharmacology and pharmacodynamics of bevacizumab as monotherapy or in combination with cytotoxic therapy in preclinical studies.* Cancer Res, 2005. **65**(3): p. 671-80.

360. Blouw, B., et al., *The hypoxic response of tumors is dependent on their microenvironment.* Cancer Cell, 2003. **4**(2): p. 133-46.

361. Rubenstein, J.L., et al., *Anti-VEGF antibody treatment of glioblastoma prolongs survival but results in increased vascular cooption.* Neoplasia, 2000. **2**(4): p. 306-14.

362. Norden, A.D., J. Drappatz, and P.Y. Wen, *Antiangiogenic therapies for high-grade glioma.* Nat Rev Neurol, 2009. **5**(11): p. 610-20.

363. Maione, F., et al., *Semaphorin 3A overcomes cancer hypoxia and metastatic dissemination induced by antiangiogenic treatment in mice.* J Clin Invest, 2012. **122**(5): p. 1832-48.

364. Sennino, B., et al., *Suppression of tumor invasion and metastasis by concurrent inhibition of c-Met and VEGF signaling in pancreatic neuroendocrine tumors.* Cancer Discov, 2012. **2**(3): p. 270-87.

365. Singh, M., et al., *Anti-VEGF antibody therapy does not promote metastasis in genetically engineered mouse tumour models.* J Pathol, 2012. **227**(4): p. 417-30.

366. Anderberg, C., et al., *Deficiency for endoglin in tumor vasculature weakens the endothelial barrier to metastatic dissemination.* J Exp Med, 2013. **210**(3): p. 563-79.

367. Ebos, J.M., et al., *Accelerated metastasis after short-term treatment with a potent inhibitor of tumor angiogenesis.* Cancer Cell, 2009. **15**(3): p. 232-9.

368. Sennino, B., et al., *Inhibition of c-Met reduces lymphatic metastasis in RIP-Tag2 transgenic mice.* Cancer Res, 2013. **73**(12): p. 3692-703.

369. Lu, X. and Y. Kang, *Hypoxia and hypoxia-inducible factors: master regulators of metastasis.* Clin Cancer Res, 2010. **16**(24): p. 5928-35.

370. Xian, X., et al., *Pericytes limit tumor cell metastasis.* J Clin Invest, 2006. **116**(3): p. 642-51.
371. Keskin, D., et al., *Targeting vascular pericytes in hypoxic tumors increases lung metastasis via angiopoietin-2.* Cell Rep, 2015. **10**(7): p. 1066-81.
372. Chung, A.S., et al., *Differential drug class-specific metastatic effects following treatment with a panel of angiogenesis inhibitors.* J Pathol, 2012. **227**(4): p. 404-16.
373. Ebos, J.M., et al., *Neoadjuvant antiangiogenic therapy reveals contrasts in primary and metastatic tumor efficacy.* EMBO Mol Med, 2014. **6**(12): p. 1561-76.
374. De Bock, K., M. Mazzone, and P. Carmeliet, *Antiangiogenic therapy, hypoxia, and metastasis: risky liaisons, or not?* Nat Rev Clin Oncol, 2011. **8**(7): p. 393-404.
375. Erler, J.T., et al., *Lysyl oxidase is essential for hypoxia-induced metastasis.* Nature, 2006. **440**(7088): p. 1222-6.
376. Pennacchietti, S., et al., *Hypoxia promotes invasive growth by transcriptional activation of the met protooncogene.* Cancer Cell, 2003. **3**(4): p. 347-61.
377. Conley, S.J., et al., *Antiangiogenic agents increase breast cancer stem cells via the generation of tumor hypoxia.* Proc Natl Acad Sci U S A, 2012. **109**(8): p. 2784-9.
378. Lu, K.V., et al., *VEGF inhibits tumor cell invasion and mesenchymal transition through a MET/VEGFR2 complex.* Cancer Cell, 2012. **22**(1): p. 21-35.
379. Blagoev, K.B., et al., *Sunitinib does not accelerate tumor growth in patients with metastatic renal cell carcinoma.* Cell Rep, 2013. **3**(2): p. 277-81.
380. Bill, R., et al., *Nintedanib is a highly effective therapeutic for neuroendocrine carcinoma of the pancreas (PNET) in the Rip1Tag2 transgenic mouse model.* Clin Cancer Res, 2015.
381. Albrecht, I., et al., *Suppressive effects of vascular endothelial growth factor-B on tumor growth in a mouse model of pancreatic neuroendocrine tumorigenesis.* PLoS One, 2010. **5**(11): p. e14109.
382. Mandriota, S.J., et al., *Vascular endothelial growth factor-C-mediated lymphangiogenesis promotes tumour metastasis.* EMBO J, 2001. **20**(4): p. 672-82.
383. Hager, J.H., et al., *Oncogene expression and genetic background influence the frequency of DNA copy number abnormalities in mouse pancreatic islet cell carcinomas.* Cancer Res, 2004. **64**(7): p. 2406-10.
384. Kuzmanov, A., et al., *LIM-homeobox gene 2 promotes tumor growth and metastasis by inducing autocrine and paracrine PDGF-B signaling.* Mol Oncol, 2014. **8**(2): p. 401-16.
385. *Hypoxyprobe, Inc.* 27.08.2015]; Available from: http://www.hypoxyprobe.com/faq.html.
386. Hunter, K.E., et al., *Identification and characterization of poorly differentiated invasive carcinomas in a mouse model of pancreatic neuroendocrine tumorigenesis.* PLoS One, 2013. **8**(5): p. e64472.
387. Wild, D., et al., *[Lys40(Ahx-DTPA-111In)NH2]exendin-4, a very promising ligand for glucagon-like peptide-1 (GLP-1) receptor targeting.* J Nucl Med, 2006. **47**(12): p. 2025-33.
388. Lopez, T. and D. Hanahan, *Elevated levels of IGF-1 receptor convey invasive and metastatic capability in a mouse model of pancreatic islet tumorigenesis.* Cancer Cell, 2002. **1**(4): p. 339-53.
389. Ferrara, N., et al., *Discovery and development of bevacizumab, an anti-VEGF antibody for treating cancer.* Nat Rev Drug Discov, 2004. **3**(5): p. 391-400.
390. de Groot, J.F., et al., *Tumor invasion after treatment of glioblastoma with bevacizumab: radiographic and pathologic correlation in humans and mice.* Neuro Oncol, 2010. **12**(3): p. 233-42.
391. Wicki, A., et al., *Tumor invasion in the absence of epithelial-mesenchymal transition: podoplanin-mediated remodeling of the actin cytoskeleton.* Cancer Cell, 2006. **9**(4): p. 261-72.
392. Hanahan, D. and R.A. Weinberg, *Hallmarks of cancer: the next generation.* Cell, 2011. **144**(5): p. 646-74.
393. Ferrara, N. and R.S. Kerbel, *Angiogenesis as a therapeutic target.* Nature, 2005. **438**(7070): p. 967-74.
394. Crawford, Y. and N. Ferrara, *VEGF inhibition: insights from preclinical and clinical studies.* Cell Tissue Res, 2009. **335**(1): p. 261-9.
395. Rose, S., *FDA pulls approval for avastin in breast cancer.* Cancer Discov, 2011. **1**(7): p. OF1-2.
396. Kerbel, R.S., *Issues regarding improving the impact of antiangiogenic drugs for the treatment of breast cancer.* Breast, 2009. **18 Suppl 3**: p. S41-7.
397. Awasthi, N., et al., *Nintedanib, a triple angiokinase inhibitor, enhances cytotoxic therapy response in pancreatic cancer.* Cancer Lett, 2014.
398. Porporato, P.E., et al., *Anticancer targets in the glycolytic metabolism of tumors: a comprehensive review.* Front Pharmacol, 2011. **2**: p. 49.

399. Sonveaux, P., et al., *Targeting lactate-fueled respiration selectively kills hypoxic tumor cells in mice.* J Clin Invest, 2008. **118**(12): p. 3930-42.

400. Waldmeier, L., et al., *Py2T murine breast cancer cells, a versatile model of TGFbeta-induced EMT in vitro and in vivo.* PLoS One, 2012. **7**(11): p. e48651.

401. Hellstrom, M., et al., *Role of PDGF-B and PDGFR-beta in recruitment of vascular smooth muscle cells and pericytes during embryonic blood vessel formation in the mouse.* Development, 1999. **126**(14): p. 3047-55.

402. Misteli, H., et al., *High-throughput flow cytometry purification of transduced progenitors expressing defined levels of vascular endothelial growth factor induces controlled angiogenesis in vivo.* Stem Cells, 2010. **28**(3): p. 611-9.

403. Subramanian, A., et al., *Gene set enrichment analysis: a knowledge-based approach for interpreting genome-wide expression profiles.* Proc Natl Acad Sci U S A, 2005. **102**(43): p. 15545-50.

404. Cheng, S.C., et al., *mTOR- and HIF-1alpha-mediated aerobic glycolysis as metabolic basis for trained immunity.* Science, 2014. **345**(6204): p. 1250684.

405. Lindholm, E.M., et al., *Proteomic characterization of breast cancer xenografts identifies early and late bevacizumab-induced responses and predicts effective drug combinations.* Clin Cancer Res, 2014. **20**(2): p. 404-12.

406. Harris, A.L., *Hypoxia--a key regulatory factor in tumour growth.* Nat Rev Cancer, 2002. **2**(1): p. 38-47.

407. Curtarello, M., et al., *VEGF-Targeted Therapy Stably Modulates the Glycolytic Phenotype of Tumor Cells.* Cancer Res, 2014.

408. Kumar, K., et al., *Dichloroacetate reverses the hypoxic adaptation to bevacizumab and enhances its antitumor effects in mouse xenografts.* J Mol Med (Berl), 2013. **91**(6): p. 749-58.

409. Edinger, A.L., et al., *Differential effects of rapamycin on mammalian target of rapamycin signaling functions in mammalian cells.* Cancer Res, 2003. **63**(23): p. 8451-60.

410. Clem, B., et al., *Small-molecule inhibition of 6-phosphofructo-2-kinase activity suppresses glycolytic flux and tumor growth.* Mol Cancer Ther, 2008. **7**(1): p. 110-20.

411. Wick, A.N., D.R. Drury, and T.N. Morita, *2-Deoxyglucose; a metabolic block for glucose.* Proc Soc Exp Biol Med, 1955. **89**(4): p. 579-82.

412. Michelakis, E.D., et al., *Metabolic modulation of glioblastoma with dichloroacetate.* Sci Transl Med, 2010. **2**(31): p. 31ra34.

413. Sounni, N.E., et al., *Blocking lipid synthesis overcomes tumor regrowth and metastasis after antiangiogenic therapy withdrawal.* Cell Metab, 2014. **20**(2): p. 280-94.

414. Ho, J., et al., *Importance of glycolysis and oxidative phosphorylation in advanced melanoma.* Mol Cancer, 2012. **11**: p. 76.

415. Doyen, J., et al., *Expression of the hypoxia-inducible monocarboxylate transporter MCT4 is increased in triple negative breast cancer and correlates independently with clinical outcome.* Biochem Biophys Res Commun, 2014. **451**(1): p. 54-61.

416. Parks, S.K. and J. Pouyssegur, *The Na /HCO Co-Transporter SLC4A4 Plays a Role in Growth and Migration of Colon and Breast Cancer Cells.* J Cell Physiol, 2015.

417. Huang da, W., B.T. Sherman, and R.A. Lempicki, *Systematic and integrative analysis of large gene lists using DAVID bioinformatics resources.* Nat Protoc, 2009. **4**(1): p. 44-57.

418. Huang, D.W., et al., *DAVID Bioinformatics Resources: expanded annotation database and novel algorithms to better extract biology from large gene lists.* Nucleic Acids Res, 2007. **35**(Web Server issue): p. W169-75.

419. Mootha, V.K., et al., *PGC-1alpha-responsive genes involved in oxidative phosphorylation are coordinately downregulated in human diabetes.* Nat Genet, 2003. **34**(3): p. 267-73.

420. Parks, S.K., J. Chiche, and J. Pouyssegur, *Disrupting proton dynamics and energy metabolism for cancer therapy.* Nat Rev Cancer, 2013. **13**(9): p. 611-23.

421. Marin-Valencia, I., et al., *Analysis of tumor metabolism reveals mitochondrial glucose oxidation in genetically diverse human glioblastomas in the mouse brain in vivo.* Cell Metab, 2012. **15**(6): p. 827-37.

422. Nieto, M.A., *Epithelial plasticity: a common theme in embryonic and cancer cells.* Science, 2013. **342**(6159): p. 1234850.

423. Thiery, J.P., et al., *Epithelial-mesenchymal transitions in development and disease.* Cell, 2009. **139**(5): p. 871-90.

424. Kalluri, R. and R.A. Weinberg, *The basics of epithelial-mesenchymal transition.* J Clin Invest, 2009. **119**(6): p. 1420-8.

425. Tiwari, N., et al., *Sox4 is a master regulator of epithelial-mesenchymal transition by controlling Ezh2 expression and epigenetic reprogramming.* Cancer Cell, 2013. **23**(6): p. 768-83.

426. Zheng, H., et al., *PKD1 phosphorylation-dependent degradation of SNAIL by SCF-FBXO11 regulates epithelial-mesenchymal transition and metastasis.* Cancer Cell, 2014. **26**(3): p. 358-73.

427. Labelle, M., S. Begum, and R.O. Hynes, *Direct signaling between platelets and cancer cells induces an epithelial-mesenchymal-like transition and promotes metastasis.* Cancer Cell, 2011. **20**(5): p. 576-90.

428. Tam, W.L. and R.A. Weinberg, *The epigenetics of epithelial-mesenchymal plasticity in cancer.* Nat Med, 2013. **19**(11): p. 1438-49.

429. Scheel, C. and R.A. Weinberg, *Cancer stem cells and epithelial-mesenchymal transition: concepts and molecular links.* Semin Cancer Biol, 2012. **22**(5-6): p. 396-403.

430. Christiansen, J.J. and A.K. Rajasekaran, *Reassessing epithelial to mesenchymal transition as a prerequisite for carcinoma invasion and metastasis.* Cancer Res, 2006. **66**(17): p. 8319-26.

431. Brabletz, T., *To differentiate or not--routes towards metastasis.* Nat Rev Cancer, 2012. **12**(6): p. 425-36.

432. Brabletz, S. and T. Brabletz, *The ZEB/miR-200 feedback loop--a motor of cellular plasticity in development and cancer?* EMBO Rep, 2010. **11**(9): p. 670-7.

433. Yuan, J.H., et al., *A long noncoding RNA activated by TGF-beta promotes the invasion-metastasis cascade in hepatocellular carcinoma.* Cancer Cell, 2014. **25**(5): p. 666-81.

434. Fantozzi, A. and G. Christofori, *Mouse models of breast cancer metastasis.* Breast Cancer Res, 2006. **8**(4): p. 212.

435. Herschkowitz, J.I., et al., *Identification of conserved gene expression features between murine mammary carcinoma models and human breast tumors.* Genome Biol, 2007. **8**(5): p. R76.

436. Tiwari, N., et al., *EMT as the ultimate survival mechanism of cancer cells.* Semin Cancer Biol, 2012. **22**(3): p. 194-207.

437. Yang, J., et al., *Twist, a master regulator of morphogenesis, plays an essential role in tumor metastasis.* Cell, 2004. **117**(7): p. 927-39.

438. Baker, B.M. and C.S. Chen, *Deconstructing the third dimension: how 3D culture microenvironments alter cellular cues.* J Cell Sci, 2012. **125**(Pt 13): p. 3015-24.

439. Doyle, A.D., et al., *Dimensions in cell migration.* Curr Opin Cell Biol, 2013. **25**(5): p. 642-9.

440. Friedl, P. and K. Wolf, *Tumour-cell invasion and migration: diversity and escape mechanisms.* Nat Rev Cancer, 2003. **3**(5): p. 362-74.

441. Tarin, D., E.W. Thompson, and D.F. Newgreen, *The fallacy of epithelial mesenchymal transition in neoplasia.* Cancer Res, 2005. **65**(14): p. 5996-6000; discussion 6000-1.

442. Haeger, A., et al., *Cell jamming: collective invasion of mesenchymal tumor cells imposed by tissue confinement.* Biochim Biophys Acta, 2014. **1840**(8): p. 2386-95.

443. Ahmed, F., et al., *GFP expression in the mammary gland for imaging of mammary tumor cells in transgenic mice.* Cancer Res, 2002. **62**(24): p. 7166-9.

444. Ellenbroek, S.I. and J. van Rheenen, *Imaging hallmarks of cancer in living mice.* Nat Rev Cancer, 2014. **14**(6): p. 406-18.

445. Friedl, P., et al., *Classifying collective cancer cell invasion.* Nat Cell Biol, 2012. **14**(8): p. 777-83.

446. Yilmaz, M. and G. Christofori, *Mechanisms of motility in metastasizing cells.* Mol Cancer Res, 2010. **8**(5): p. 629-42.

447. Liu, Y.J., et al., *Confinement and low adhesion induce fast amoeboid migration of slow mesenchymal cells.* Cell, 2015. **160**(4): p. 659-72.

448. Pankova, K., et al., *The molecular mechanisms of transition between mesenchymal and amoeboid invasiveness in tumor cells.* Cell Mol Life Sci, 2010. **67**(1): p. 63-71.

449. Parri, M. and P. Chiarugi, *Rac and Rho GTPases in cancer cell motility control.* Cell Commun Signal, 2010. **8**: p. 23.

450. Bergert, M., et al., *Cell mechanics control rapid transitions between blebs and lamellipodia during migration.* Proc Natl Acad Sci U S A, 2012. **109**(36): p. 14434-9.

451. Lammermann, T., et al., *Rapid leukocyte migration by integrin-independent flowing and squeezing.* Nature, 2008. **453**(7191): p. 51-5.

452. Zaman, M.H., et al., *Migration of tumor cells in 3D matrices is governed by matrix stiffness along with cell-matrix adhesion and proteolysis.* Proc Natl Acad Sci U S A, 2006. **103**(29): p. 10889-94.

453. Maaser, K., et al., *Functional hierarchy of simultaneously expressed adhesion receptors: integrin alpha2beta1 but not CD44 mediates MV3 melanoma cell migration and matrix reorganization within three-dimensional hyaluronan-containing collagen matrices.* Mol Biol Cell, 1999. **10**(10): p. 3067-79.

454. Berton, S., et al., *The tumor suppressor functions of p27(kip1) include control of the mesenchymal/amoeboid transition.* Mol Cell Biol, 2009. **29**(18): p. 5031-45.

455.   Gadea, G., et al., *Loss of p53 promotes RhoA-ROCK-dependent cell migration and invasion in 3D matrices.* J Cell Biol, 2007. **178**(1): p. 23-30.

456.   Parri, M., et al., *EphA2 reexpression prompts invasion of melanoma cells shifting from mesenchymal to amoeboid-like motility style.* Cancer Res, 2009. **69**(5): p. 2072-81.

457.   Sahai, E. and C.J. Marshall, *Differing modes of tumour cell invasion have distinct requirements for Rho/ROCK signalling and extracellular proteolysis.* Nat Cell Biol, 2003. **5**(8): p. 711-9.

458.   Taddei, M.L., et al., *Mesenchymal to amoeboid transition is associated with stem-like features of melanoma cells.* Cell Commun Signal, 2014. **12**: p. 24.

459.   Wolf, K., et al., *Compensation mechanism in tumor cell migration: mesenchymal-amoeboid transition after blocking of pericellular proteolysis.* J Cell Biol, 2003. **160**(2): p. 267-77.

460.   Lah, T.T., M.B. Duran Alonso, and C.J. Van Noorden, *Antiprotease therapy in cancer: hot or not?* Expert Opin Biol Ther, 2006. **6**(3): p. 257-79.

461.   Stupp, R., et al., *Cilengitide combined with standard treatment for patients with newly diagnosed glioblastoma with methylated MGMT promoter (CENTRIC EORTC 26071-22072 study): a multicentre, randomised, open-label, phase 3 trial.* Lancet Oncol, 2014. **15**(10): p. 1100-8.

462.   Slattum, G.M. and J. Rosenblatt, *Tumour cell invasion: an emerging role for basal epithelial cell extrusion.* Nat Rev Cancer, 2014. **14**(7): p. 495-501.

463.   Liu, J.S., et al., *Programmed cell-to-cell variability in Ras activity triggers emergent behaviors during mammary epithelial morphogenesis.* Cell Rep, 2012. **2**(5): p. 1461-70.

464.   Marshall, T.W., et al., *The tumor suppressor adenomatous polyposis coli controls the direction in which a cell extrudes from an epithelium.* Mol Biol Cell, 2011. **22**(21): p. 3962-70.

465.   Wyckoff, J.B., et al., *ROCK- and myosin-dependent matrix deformation enables protease-independent tumor-cell invasion in vivo.* Curr Biol, 2006. **16**(15): p. 1515-23.

466.   Friedl, P. and K. Wolf, *Plasticity of cell migration: a multiscale tuning model.* J Cell Biol, 2010. **188**(1): p. 11-9.

467.   Cheung, K.J., et al., *Collective invasion in breast cancer requires a conserved basal epithelial program.* Cell, 2013. **155**(7): p. 1639-51.

468.   Hegerfeldt, Y., et al., *Collective cell movement in primary melanoma explants: plasticity of cell-cell interaction, beta1-integrin function, and migration strategies.* Cancer Res, 2002. **62**(7): p. 2125-30.

469.   Shih, W. and S. Yamada, *N-cadherin-mediated cell-cell adhesion promotes cell migration in a three-dimensional matrix.* J Cell Sci, 2012. **125**(Pt 15): p. 3661-70.

470.   Theveneau, E. and R. Mayor, *Cadherins in collective cell migration of mesenchymal cells.* Curr Opin Cell Biol, 2012. **24**(5): p. 677-84.

471.   Cavallaro, U. and G. Christofori, *Cell adhesion and signalling by cadherins and Ig-CAMs in cancer.* Nat Rev Cancer, 2004. **4**(2): p. 118-32.

472.   Fidler, I.J., *The relationship of embolic homogeneity, number, size and viability to the incidence of experimental metastasis.* Eur J Cancer, 1973. **9**(3): p. 223-7.

473.   Hart, I.R., *New evidence for tumour embolism as a mode of metastasis.* J Pathol, 2009. **219**(3): p. 275-6.

474.   Kusters, B., et al., *Micronodular transformation as a novel mechanism of VEGF-A-induced metastasis.* Oncogene, 2007. **26**(39): p. 5808-15.

475.   Liotta, L.A., M.G. Saidel, and J. Kleinerman, *The significance of hematogenous tumor cell clumps in the metastatic process.* Cancer Res, 1976. **36**(3): p. 889-94.

476.   Sugino, T., et al., *Morphological evidence for an invasion-independent metastasis pathway exists in multiple human cancers.* BMC Med, 2004. **2**: p. 9.

477.   Brabletz, T., et al., *Variable beta-catenin expression in colorectal cancers indicates tumor progression driven by the tumor environment.* Proc Natl Acad Sci U S A, 2001. **98**(18): p. 10356-61.

478.   Husemann, Y., et al., *Systemic spread is an early step in breast cancer.* Cancer Cell, 2008. **13**(1): p. 58-68.

479.   Beerling, E., et al., *Intravital microscopy: new insights into metastasis of tumors.* J Cell Sci, 2011. **124**(Pt 3): p. 299-310.

480.   Fantozzi, A., et al., *VEGF-mediated angiogenesis links EMT-induced cancer stemness to tumor initiation.* Cancer Res, 2014. **74**(5): p. 1566-75.

481.   Gerlinger, M., et al., *Intratumor heterogeneity and branched evolution revealed by multiregion sequencing.* N Engl J Med, 2012. **366**(10): p. 883-92.

482.   Patel, A.P., et al., *Single-cell RNA-seq highlights intratumoral heterogeneity in primary glioblastoma.* Science, 2014. **344**(6190): p. 1396-401.

483.   Pavlides, S., et al., *The reverse Warburg effect: aerobic glycolysis in cancer associated fibroblasts and the tumor stroma.* Cell Cycle, 2009. **8**(23): p. 3984-4001.

484.   Paccione, R.J., et al., *Keratin down-regulation in vimentin-positive cancer cells is reversible by vimentin RNA interference, which inhibits growth and motility.* Mol Cancer Ther, 2008. **7**(9): p. 2894-903.

485.   Ledford, H., *Cancer theory faces doubts.* Nature, 2011. **472**(7343): p. 273.

486.   Prat, A., et al., *Phenotypic and molecular characterization of the claudin-low intrinsic subtype of breast cancer.* Breast Cancer Res, 2010. **12**(5): p. R68.

487.   Trimboli, A.J., et al., *Direct evidence for epithelial-mesenchymal transitions in breast cancer.* Cancer Res, 2008. **68**(3): p. 937-45.

488.   Forrester, E., et al., *Effect of conditional knockout of the type II TGF-beta receptor gene in mammary epithelia on mammary gland development and polyomavirus middle T antigen induced tumor formation and metastasis.* Cancer Res, 2005. **65**(6): p. 2296-302.

489.   Giampieri, S., et al., *Localized and reversible TGFbeta signalling switches breast cancer cells from cohesive to single cell motility.* Nat Cell Biol, 2009. **11**(11): p. 1287-96.

490.   Derksen, P.W., et al., *Mammary-specific inactivation of E-cadherin and p53 impairs functional gland development and leads to pleomorphic invasive lobular carcinoma in mice.* Dis Model Mech, 2011. **4**(3): p. 347-58.

491.   Derksen, P.W., et al., *Somatic inactivation of E-cadherin and p53 in mice leads to metastatic lobular mammary carcinoma through induction of anoikis resistance and angiogenesis.* Cancer Cell, 2006. **10**(5): p. 437-49.

492.   Strizzi, L., et al., *Epithelial mesenchymal transition is a characteristic of hyperplasias and tumors in mammary gland from MMTV-Cripto-1 transgenic mice.* J Cell Physiol, 2004. **201**(2): p. 266-76.

493.   McCoy, E.L., et al., *Six1 expands the mouse mammary epithelial stem/progenitor cell pool and induces mammary tumors that undergo epithelial-mesenchymal transition.* J Clin Invest, 2009. **119**(9): p. 2663-77.

494.   Rhim, A.D., et al., *EMT and dissemination precede pancreatic tumor formation.* Cell, 2012. **148**(1-2): p. 349-61.

495.   Massague, J., *TGFbeta signalling in context.* Nat Rev Mol Cell Biol, 2012. **13**(10): p. 616-30.

496.   Muraoka, R.S., et al., *Increased malignancy of Neu-induced mammary tumors overexpressing active transforming growth factor beta1.* Mol Cell Biol, 2003. **23**(23): p. 8691-703.

497.   Muraoka-Cook, R.S., et al., *Conditional overexpression of active transforming growth factor beta1 in vivo accelerates metastases of transgenic mammary tumors.* Cancer Res, 2004. **64**(24): p. 9002-11.

498.   Muraoka-Cook, R.S., et al., *Activated type I TGFbeta receptor kinase enhances the survival of mammary epithelial cells and accelerates tumor progression.* Oncogene, 2006. **25**(24): p. 3408-23.

499.   Siegel, P.M., et al., *Transforming growth factor beta signaling impairs Neu-induced mammary tumorigenesis while promoting pulmonary metastasis.* Proc Natl Acad Sci U S A, 2003. **100**(14): p. 8430-5.

500.   Kim, M.Y., et al., *Tumor self-seeding by circulating cancer cells.* Cell, 2009. **139**(7): p. 1315-26.

501.   Novitskiy, S.V., et al., *Attenuated transforming growth factor beta signaling promotes metastasis in a model of HER2 mammary carcinogenesis.* Breast Cancer Res, 2014. **16**(5): p. 425.

502.   Yang, L., et al., *Abrogation of TGF beta signaling in mammary carcinomas recruits Gr-1+CD11b+ myeloid cells that promote metastasis.* Cancer Cell, 2008. **13**(1): p. 23-35.

503.   Perl, A.K., et al., *A causal role for E-cadherin in the transition from adenoma to carcinoma.* Nature, 1998. **392**(6672): p. 190-3.

504.   Lehembre, F., et al., *NCAM-induced focal adhesion assembly: a functional switch upon loss of E-cadherin.* EMBO J, 2008. **27**(19): p. 2603-15.

505.   Onder, T.T., et al., *Loss of E-cadherin promotes metastasis via multiple downstream transcriptional pathways.* Cancer Res, 2008. **68**(10): p. 3645-54.

506.   Tsai, J.H., et al., *Spatiotemporal regulation of epithelial-mesenchymal transition is essential for squamous cell carcinoma metastasis.* Cancer Cell, 2012. **22**(6): p. 725-36.

507.   Moody, S.E., et al., *The transcriptional repressor Snail promotes mammary tumor recurrence.* Cancer Cell, 2005. **8**(3): p. 197-209.

508.   Diepenbruck, M., et al., *Tead2 expression levels control the subcellular distribution of Yap and Taz, zyxin expression and epithelial-mesenchymal transition.* J Cell Sci, 2014. **127**(Pt 7): p. 1523-36.

509.   Vaage, J. and J.P. Harlos, *Spontaneous metastasis from primary C3H mouse mammary tumors.* Cancer Res, 1987. **47**(2): p. 547-50.

510. Shibue, T. and R.A. Weinberg, *Metastatic colonization: settlement, adaptation and propagation of tumor cells in a foreign tissue environment.* Semin Cancer Biol, 2011. **21**(2): p. 99-106.

511. Reymond, N., B.B. d'Agua, and A.J. Ridley, *Crossing the endothelial barrier during metastasis.* Nat Rev Cancer, 2013. **13**(12): p. 858-70.

512. Shenoy, A.K. and J. Lu, *Cancer cells remodel themselves and vasculature to overcome the endothelial barrier.* Cancer Lett, 2014.

513. Mani, S.A., et al., *The epithelial-mesenchymal transition generates cells with properties of stem cells.* Cell, 2008. **133**(4): p. 704-15.

514. Jean, C., et al., *Inhibition of endothelial FAK activity prevents tumor metastasis by enhancing barrier function.* J Cell Biol, 2014. **204**(2): p. 247-63.

515. Padua, D., et al., *TGFbeta primes breast tumors for lung metastasis seeding through angiopoietin-like 4.* Cell, 2008. **133**(1): p. 66-77.

516. Peinado, H., S. Lavotshkin, and D. Lyden, *The secreted factors responsible for pre-metastatic niche formation: old sayings and new thoughts.* Semin Cancer Biol, 2011. **21**(2): p. 139-46.

517. Borrull, A., et al., *Nanog and Oct4 overexpression increases motility and transmigration of melanoma cells.* J Cancer Res Clin Oncol, 2012. **138**(7): p. 1145-54.

518. Aceto, N., et al., *Circulating tumor cell clusters are oligoclonal precursors of breast cancer metastasis.* Cell, 2014. **158**(5): p. 1110-22.

519. Chaffer, C.L., et al., *Mesenchymal-to-epithelial transition facilitates bladder cancer metastasis: role of fibroblast growth factor receptor-2.* Cancer Res, 2006. **66**(23): p. 11271-8.

520. Bockhorn, J., et al., *Differentiation and loss of malignant character of spontaneous pulmonary metastases in patient-derived breast cancer models.* Cancer Res, 2014. **74**(24): p. 7406-17.

521. Ocana, O.H., et al., *Metastatic colonization requires the repression of the epithelial-mesenchymal transition inducer Prrx1.* Cancer Cell, 2012. **22**(6): p. 709-24.

522. Stankic, M., et al., *TGF-beta-Id1 signaling opposes Twist1 and promotes metastatic colonization via a mesenchymal-to-epithelial transition.* Cell Rep, 2013. **5**(5): p. 1228-42.

523. Liu, S., et al., *Breast cancer stem cells transition between epithelial and mesenchymal states reflective of their normal counterparts.* Stem Cell Reports, 2014. **2**(1): p. 78-91.

524. Shibue, T. and R.A. Weinberg, *Integrin beta1-focal adhesion kinase signaling directs the proliferation of metastatic cancer cells disseminated in the lungs.* Proc Natl Acad Sci U S A, 2009. **106**(25): p. 10290-5.

525. Perou, C.M., et al., *Molecular portraits of human breast tumours.* Nature, 2000. **406**(6797): p. 747-52.

526. Sinn, H.P. and H. Kreipe, *A Brief Overview of the WHO Classification of Breast Tumors, 4th Edition, Focusing on Issues and Updates from the 3rd Edition.* Breast Care (Basel), 2013. **8**(2): p. 149-54.

527. Cancer Genome Atlas, N., *Comprehensive molecular portraits of human breast tumours.* Nature, 2012. **490**(7418): p. 61-70.

528. Weigelt, B., et al., *Metaplastic breast carcinoma: more than a special type.* Nat Rev Cancer, 2014. **14**(3): p. 147-8.

529. Sorlie, T., et al., *Gene expression patterns of breast carcinomas distinguish tumor subclasses with clinical implications.* Proc Natl Acad Sci U S A, 2001. **98**(19): p. 10869-74.

530. Taube, J.H., et al., *Core epithelial-to-mesenchymal transition interactome gene-expression signature is associated with claudin-low and metaplastic breast cancer subtypes.* Proc Natl Acad Sci U S A, 2010. **107**(35): p. 15449-54.

531. Shipitsin, M., et al., *Molecular definition of breast tumor heterogeneity.* Cancer Cell, 2007. **11**(3): p. 259-73.

532. Li, X., et al., *Intrinsic resistance of tumorigenic breast cancer cells to chemotherapy.* J Natl Cancer Inst, 2008. **100**(9): p. 672-9.

533. Farmer, P., et al., *A stroma-related gene signature predicts resistance to neoadjuvant chemotherapy in breast cancer.* Nat Med, 2009. **15**(1): p. 68-74.

534. Creighton, C.J., et al., *Residual breast cancers after conventional therapy display mesenchymal as well as tumor-initiating features.* Proc Natl Acad Sci U S A, 2009. **106**(33): p. 13820-5.

535. Lim, E., et al., *Aberrant luminal progenitors as the candidate target population for basal tumor development in BRCA1 mutation carriers.* Nat Med, 2009. **15**(8): p. 907-13.

536. Prat, A. and C.M. Perou, *Deconstructing the molecular portraits of breast cancer.* Mol Oncol, 2011. **5**(1): p. 5-23.

537. Yu, M., et al., *Circulating breast tumor cells exhibit dynamic changes in epithelial and mesenchymal composition.* Science, 2013. **339**(6119): p. 580-4.

538.   Sarrio, D., et al., *Epithelial-mesenchymal transition in breast cancer relates to the basal-like phenotype.* Cancer Res, 2008. **68**(4): p. 989-97.

539.   Davis, F.M., et al., *Targeting EMT in cancer: opportunities for pharmacological intervention.* Trends Pharmacol Sci, 2014. **35**(9): p. 479-88.

540.   Kurose, K., et al., *Frequent somatic mutations in PTEN and TP53 are mutually exclusive in the stroma of breast carcinomas.* Nat Genet, 2002. **32**(3): p. 355-7.

541.   Moinfar, F., et al., *Concurrent and independent genetic alterations in the stromal and epithelial cells of mammary carcinoma: implications for tumorigenesis.* Cancer Res, 2000. **60**(9): p. 2562-6.

542.   Qiu, W., et al., *No evidence of clonal somatic genetic alterations in cancer-associated fibroblasts from human breast and ovarian carcinomas.* Nat Genet, 2008. **40**(5): p. 650-5.

543.   Aktas, B., et al., *Stem cell and epithelial-mesenchymal transition markers are frequently overexpressed in circulating tumor cells of metastatic breast cancer patients.* Breast Cancer Res, 2009. **11**(4): p. R46.

544.   Kallergi, G., et al., *Epithelial to mesenchymal transition markers expressed in circulating tumour cells of early and metastatic breast cancer patients.* Breast Cancer Res, 2011. **13**(3): p. R59.

545.   Alix-Panabieres, C. and K. Pantel, *Challenges in circulating tumour cell research.* Nat Rev Cancer, 2014. **14**(9): p. 623-31.

546.   Ozkumur, E., et al., *Inertial focusing for tumor antigen-dependent and -independent sorting of rare circulating tumor cells.* Sci Transl Med, 2013. **5**(179): p. 179ra47.

547.   Yu, M., et al., *Cancer therapy. Ex vivo culture of circulating breast tumor cells for individualized testing of drug susceptibility.* Science, 2014. **345**(6193): p. 216-20.

548.   Fagiani, E., et al., *An immature B cell population from peripheral blood serves as surrogate marker for monitoring tumor angiogenesis and anti-angiogenic therapy in mouse models.* Angiogenesis, 2015. **18**(3): p. 327-45.

7. Abbreviations

ALL	acute lymphoblastic leukemia
ANG	angiopoietin
BC	breast cancer
BM	basement membrane
BMDC	bone marrow-derived cells
BRP	bovine retinal pericytes
CAT	collective to amoeboid migration
cCasp3	cleaved caspase 3
CEC	circulating endothelial cell
CK	cytokeratin
CLL	chronic lymphocytic leukemia
CML	chronic myeloid leukemia
CPT1A	carnitine palmitoyltransferase 1
CRC	colorectal cancer
CSC	cancer stem cell
CTC	circulating tumor cell
DAPI	4′,6-Diamidin-2-phenylindol
DAVID	Database for Annotation, Visualization and Integrated Discovery
DCA	dichloroacetate
DFS	disease-free survival
DLL4	delta-like ligand 4
dNTP	deoxyribonucleotide
EC_{50}	half-maximal effective concentration
ECM	extracellular matrix
EGFR	epidermal growth factor receptor
EMA	European Medicines Agency
EMT	epithelial to mesenchymal transiton
EPC	endothelial progenitor cell
EpCAM	epithelial cell adhesion molecule
ER	estrogen receptor
ERC	European Research Council
FAK	focal adhesion kinase
FC	fold change
FDA	Food and Drug Administration
FGF	fibroblast growth factor

FGFR	fibroblast growth factor receptor
FITC	fluoresceinisothiocyanat
FLK-1	fetal liver kinase-1
FLT-1	fms-like tyrosine kinase
FSC	forward scatter
G-CSF	granulocyte colony stimulating factor
GIST	gastrointestinal stroma tumor
GSEA	gene set enrichment analysis
HCC	hepatocellular carcinoma
HGF	hepatocyte growth factor
HIF	hypoxia-inducible factor
HUASMC	human umbilical artery smooth muscle cells
HUVEC	human umbilical vein endothelial cell
IC_{50}	half-maximal inhibitory concentration
IF	immunofluorescence
IGF	insulin-like growth factor
IL	interleukin
IMG	intussusceptive microvascular growth
i.p.	intraperitoneal
IPF	idiopathic pulmonary fibrosis
i.v.	intravenous
KEGG	Kyoto Encyclopedia of Genes and Genomes
LOX	protein-lysin-6-oxidase
LYVE-1	lymphatic vessel endothelial hyaluronan receptor-1
MAT	mesenchymal to amoeboid transition
MCT	monocarboxylate transporter
MDS	myelodysplastic syndrome
MDSC	myeloid-derived suppressor cell
MeRIC	Mechanisms of Evasive Resistance in Cancer
MET	mesenchymal to epithelial transition
MMP	matrix metalloproteinase
MMTV	mouse mammary tumor virus
MPS	myeloproliferative syndrome
MTD	maximum tolerated dose
mTOR	mammalian/mechanistic target of rapamycin
MVD	microvessel density
NG2	neuron-glia antigen 2

NRP	neuropilin
NSCLC	non-small cell lung cancer
PFK-1	phosphofructokinase-1
PFKFB3	phospho-fructokinase-2/fructose-2,6-bisphosphatase 3
PFS	progression-free survival
PDGF	platelet-derived growth factor
PDGFR	platelet-derived growth factor receptor
PDX	patient-derived xenograft
pH3	phospho-histone H3
PHD	prolyl hydroxylase domain protein
PI	propidium iodide
PIGF	placental growth factor
PNET	pancreatic neuroendocrine tumor
p.o.	*per os*
PR	progesterone receptor
PyMT	polyoma middle T
RA	rheumatoid arthritis
(cc)RCC	(clear cell) renal cell carcinoma
RMA	robust multichip average
RT-PCR	reverse transcription polymerase chain reaction
SFVO	Swiss Federal Veterinary Office
SPF	specific pathogen free
SSC	side scatter
TCA	tricarboxylic acid
TEM	transendothelial migration
TGFβ	transforming growth factor-β
TIE	tyrosine kinase with immunoglobulin-like and epidermal growth factor-like domain
TKI	tyrosine kinase inhibitor
UICC	Union for International Cancer Control
VEGF	vascular endothelial growth factor
VEGFR	vascular endothelial growth factor receptor
VPF	vascular permeability factor
WAP	whey acidic protein
2D; 3D	two-dimensional; three-dimensional
3PO	3-(3-pyridinyl)-1-(4-pyridinyl)-2-propen-1-one

8. Summary of the scientific and academic aspects of my thesis

During my MD-PhD, I led a project aimed at the in depth characterization of nintedanib, which is a relatively new anti-angiogenic small molecule tyrosine kinase inhibitor, in the Rip1Tag2 mouse model of pancreatic neuroendocrine tumors. We recently published this work in "Clinical Cancer Research" [380]. In addition, together with Laura Pisarsky, we were investigating mechanisms of resistance to anti-angiogenic tyrosine kinase inhibitors (nintedanib, sunitinib) in a mouse model of breast cancer and in the Rip1Tag2 model. The manuscript of the latter project has been submitted for publication. Furthermore, I was involved in a project that identified an immature B-cell population serving as a surrogate marker in order to monitor tumor angiogenesis and response to anti-angiogenic compounds in several mouse models of cancer [548]. Subsequent to these research articles, I wrote a book chapter describing our routinely used tumor angiogenesis assays in the Rip1Tag2 mouse model. This chapter will be part of an edition of the lab protocol series "Methods in Molecular Biology" on tumor angiogenesis assays.

Furthermore, I am currently investigating the impact of a yet unpublished TKI of focal adhesion kinase (BI853520) on primary tumor growth and the metastatic cascade in several breast cancer mouse models. However, this project is not yet mature enough to be included in the present thesis. Lately, I was involved in the preclinical validation of Rho-Kinase 1 and 2 (ROCK1/2) as a potential metastasis-inhibiting target (Meyer-Schaller et al., manuscript in preparation).

Additionally, I have summarized the current knowledge about the relevance of EMT in the process of breast cancer metastasis published in a review in "FEBS Letters" [358]. Based on discussions I had during the preparation of this review, I have significantly contributed to the design and initiation of a new project in the Christofori laboratory, which aims to decipher the role of EMT in metastasis in different preclinical breast cancer metastasis mouse models involving sophisticated lineage-tracing and fate-mapping approaches.

Last but not least, I was supervising three master students (2 medical and 1 biology student) and I was engaged in teaching of medical students at the Faculty of Medicine of the University of Basel: During four years, I was a tutor in "Problem oriented Tutorials", gave students insights into biomedical research with animals in the context of laboratory visits during the "Wissenschaftsmonats" and I was giving workshops about "nutrition and cancer" on the "Thementag Ernährung".

9.   *Curriculum Vitae*

Personal Information

Name	Bill
First name	<u>Ruben</u> Michael
Nationality	Swiss
Date and Place of Birth	22.08.1985, Meiringen (Switzerland)
Status	not married, 2 children (Leona *2012, Lilja *2015)
Contact	Morillonstrasse 2
	3007 Bern
	Switzerland
	Tel: (+41) 78 663 67 91
	E-mail: ruben.bill@unibas.ch

Education and Professional Training

Nov 2011- present	**MD-PhD studies in Medical-Biological Research**
	Department of Biomedicine
	University of Basel, Switzerland
	Laboratory of Prof. Dr. Gerhard Christofori,
Dec 2011	**Promotion to Dr. med.**
	University of Bern, Switzerland
Fall 2011	**"Eidgenössisches Staatsexamen Humanmedizin"**
Jul 2011	**Master of Medicine**
	University of Bern, Switzerland
Oct 2005- Jul 2011	**Medical studies**
	University of Bern, Switzerland
Jul 2008- Jan 2010	**Medical thesis**
	Theodor Kocher Institute
	University of Bern, Switzerland
	Thesis: The role of PSGL-1 in the immunopathogenesis of experimental autoimmune encephalomyelitis.
Jun 2005	**Matura**
	Gymnasium Hofwil, Münchenbuchsee, Switzerland
2001- 2005	**Gymnasium**
	Hofwil, Münchenbuchsee, Switzerland,
	"Talentförderungsklasse Sport"

Research Experience and Courses

April 2012	**Felasa Course** Category B; LTK Module 1: Introductory course in Laboratory Animal Science
Nov 2010	**Research internship in tumor biology** Department of Biomedicine University of Basel, Switzerland Laboratory of Prof. Dr. Gerhard Christofori,
Sept- Oct 2010	**Research internship in neuro-oncology** University Hospital Zurich, Switzerland Laboratory of Prof. Dr. Michael Weller
Sept- Nov 2009	**Research internship in immunology** Department of Pathology Harvard Medical School, Boston, USA Laboratory of Prof. Dr. Ulrich von Andrian,
Aug- Sept 2007	**Research internship in neuro-immunology** Theodor Kocher Institute University of Bern, Switzerland Laboratory of Prof. Dr. Britta Engelhardt,

Teaching

2012- present	Supervision of master students David Johansson, medical master student Stefanie Tiede, biology master student Philip Schmassmann, medical master student
2012- 2015	Teaching of medical students at the Faculty of Medicine, University of Basel, Switzerland - Problem oriented Tutorial (PoT) - "Thementag Ernährung" - Laboratory visit
Oct 2007- Apr 2009	Teaching assistant in histology courses of first- and second-year medical students at the Faculty of Medicine, University of Bern, Switzerland
Oct- Dec 2007	Tutor of first- year medical students at the Faculty of Medicine, University of Bern, Switzerland

Conferences and Symposia

May 2015	**Scientific Meeting of the Swiss national MD-PhD program** Basel, Switzerland (poster presentation)
May 2015	**European Cancer Center Meeting** Freiburg i. B., Germany (oral presentation)

Jan 2015	**Keystone Symposium Integrating Biology and Tumor Metabolism** Vancouver, Canada (poster presentation)
Sept 2014	**Kinome III Meeting** Basel, Switzerland (poster presentation)
May 2014	**ENBDC workshop** Methods in mammary gland biology and breast cancer Weggis, Switzerland (poster presentation)
March 2014	**Keystone Symposium Tumor Metabolism** Whistler, Canada (poster presentation)
Oct 2013	**MD/PhD-MSc Basel and Zurich joint Retreat** Monte Verità, Switzerland (poster presentation)
May 2013	**European Cancer Center Meeting** Strasbourg, France (poster presentation)
Apr 2013	**NCCR Molecular Oncology Concluding Symposium** Lausanne, Switzerland (poster presentation)
Feb 2013	**Department of Biomedicine Basel PhD winter retreat** Hasliberg, Switzerland (oral presentation)
Jan 2013	**Charles Rodolph Brupbacher Symposium** Zurich, Switzerland
Nov 2012	**Scientific Meeting of the Swiss national MD-PhD program** Solothurn, Switzerland (poster presentation)
Jun 2012	**International Vascular Biology Meeting 2012** Wiesbaden, Germany (poster presentation)
May 2012	**European Cancer Center Meeting** Freiburg i. B., Germany
Nov 2010	**Day of Clinical Research 2010** Department of Clinical Research, University of Bern, Switzerland (poster presentation)
Jun 2009	**Training course neuro-immunology within the COST action Neurinfnet** University of Minho, Braga, Portugal (poster presentation)
Jun 2009	**Researcher Meeting of the Swiss Multiple Sclerosis Society** Interlaken, Switzerland (poster presentation)

Memberships/Fellowships/Awards

2012	"1. Fakultätspreis" of the Faculty of Medicine, University of Bern, for the best Medical thesis

| 2012- 2014 | MD-PhD Fellowship of the Swiss National Science Foundation (3 years) |
| 2008- 2014 | Member of the Swiss Students Foundation (www.studienstiftung.ch) |

Publication List

Bill R, Döring A, Deutsch U, Engelhardt B. 2010. PSGL-1 is dispensable for the development of active experimental autoimmune encephalomyelitis in SJL/J mice. J Neuroimmunol. 2011.

Bill R, Christofori G. 2015. The relevance of EMT in breast cancer metastasis: Correlation or causality? FEBS Letters. 2015. Review article.

Fagiani E, **Bill R,** Pisarsky L, Ivanek R, Rüegg C, Christofori G. An immature B cell population from peripheral blood serves as surrogate marker for monitoring tumor angiogenesis and anti-angiogenic therapy in mouse models. Angiogenesis. 2015.

Bill R*, Fagiani E*, Zumsteg A, Antoniadis H, Johansson D, Haefliger S, Albrecht I, Hilberg F, Christofori G. Nintedanib is a highly effective therapeutic for neuroendocrine carcinoma of the pancreas (PNET) in the Rip1Tag2 transgenic mouse model. Clinical Cancer Research. 2015.

Pisarsky L*, **Bill R***, Ernesta Fagiani, Ryan William Goosen, Jörg Hagmann, and Gerhard Christofori. Targeting metabolic symbiosis to overcome resistance to anti-angiogenic therapy. (*submitted*)

Bill R, Christofori G. The Rip1Tag2 mouse model. Book chapter in Tumor angiogenesis assays, Methods in Molecular Biology, Springer (*in preparation*).

Bill R, Tiede S, Fagiani E, Meyer-Schaller N, Haefliger S, Schmassmann P, Christofori G. Influence of the novel Focal Adhesion Kinase (FAK) Inhibitor BI853520 on breast cancer primary tumor growth and metastasis (*in preparation*).

*equal contribution

10. Acknowledgements

First of all, I would like to thank Prof. Dr. Gerhard Christofori for giving me the great opportunity to perform my MD-PhD thesis in his laboratory. I appreciated his role as a "consultant" rather than simply being "the boss", allowing us to realize that the success of our career lies in our own hands. The freedom to develop new ideas, experiments and even projects enabled us to evolve into independent scientist with a critical view on the research of others and our own. I am convinced that with his tremendous experience and international network, I can get significant advices when it comes to important decisions in my future career.

Secondly, I am grateful to the current and previous members of the Christofori laboratory for technical inputs, critical questions, discussions and fun moments. I thank Dr. Ernesta Fagiani and Laura Pisarsky for fruitful collaborations in my two main projects. In addition, special thanks go to Dr. Maren Diepenbruck, Dr. Lorenz Waldmeier, Dr. Nathalie Meyer-Schaller, Dr. Ryan Goosen and Dr. Robert Ivanek for significant technical support, manuscript revisions and scientific discussions.

What would I have done without Helena Antoniadis, Isabel Galm, Ursula Schmieder, Petra Schmidt, Miranda Brito, Roland Jost, Angelika Offinger, Erika Visscher, Manfred Sieber, Pascal Lorentz and the other members of the Mattenstrasse administrative, infrastructure, IT and animal house staff? Thank you very much!

I am further highly grateful for the help of the students I have supervised: David Johansson, Philipp Granacher, Stefanie Tiede and Philip Schmassmann. Many thanks also to the civil service guys who have supported our laboratory: Patrick Stillhard, Andrea Vettiger and Simon Häfliger.

Furthermore, I would like to thank the members of my PhD committee, Prof. Dr. Markus Affolter and Prof. Dr. Curzio Rüegg for helping to improve my projects.

Many thanks also to my family for their amazing support ever since.

Last but not least and most importantly, dear Claudia, thank you for your love, for taking care of so many things, for being a great mother and understanding when I was treating mice instead of spending time with the family on countless weekends. Leona and Lilja, your smiles often adjusted the focus to the important things in life.